REACTOR CORE MATERIALS

4 MAR 1 6
OSTI 1961

A Quarterly Technical Progress Review

Prepared for U. S. ATOMIC ENERGY COMMISSION by BATTELLE MEMORIAL INSTITUTE

November 1960

VOLUME 3

NUMBER 4

TECHNICAL PROGRESS REVIEWS

To meet the needs of industry for concise summaries of current atomic developments, the Atomic Energy Commission is publishing this series, Technical Progress Reviews. Issued quarterly, each of the reviews digests and evaluates the latest findings in a specific area of nuclear technology and science.

The four journals published in this series are:

Nuclear Safety, W. B. Cottrell, editor, R. A. Charpie, advisory editor, and associates, Oak Ridge National Laboratory

Power Reactor Technology, Walter H. Zinn and associates, General Nuclear Engineering Corporation

Reactor Core Materials (covering solid material developments), R. W. Dayton, E. M. Simons, and associates, Battelle Memorial Institute

Reactor Fuel Processing, Stephen Lawroski and associates, Chemical Engineering Division, Argonne National Laboratory

Each journal may be purchased ($2.00 per year for subscription and individual issues $0.55) from the Superintendent of Documents, U. S. Government Printing Office, Washington 25, D. C. See back cover for remittance instructions and foreign postage requirements.

Availability of Reports Cited in This Review

Unclassified AEC reports are available for inspection at AEC depository libraries and are sold by the Office of Technical Services, Department of Commerce, Washington 25, D. C. Some of the reports cited are not available owing to their preliminary nature; however, the information contained in them will eventually be made available in formal progress or topical reports.

Unclassified reports issued by other Government agencies or private organizations should be requested from the originator.

Unclassified British and Canadian reports may be inspected at AEC depository libraries. British reports are sold by the British Information Service, 45 Rockefeller Plaza, New York, N. Y.; Canadian reports (AECL series) are sold by the Scientific Document Distribution Office, Atomic Energy of Canada, Ltd., Chalk River, Ontario, Canada.

Classified U. S. and foreign reports identified in this journal as Classified may be purchased by properly cleared Access Permit Holders from the Office of Technical Information Extension, U. S. Atomic Energy Commission, P. O. Box 1001, Oak Ridge, Tenn. Such reports may be inspected at classified AEC depository libraries.

REACTOR CORE MATERIALS

A REVIEW OF RECENT DEVELOPMENTS

Prepared for U. S. ATOMIC ENERGY COMMISSION
by BATTELLE MEMORIAL INSTITUTE

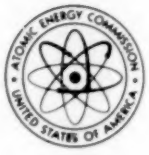

● NOV. 1960

● VOLUME 3

● NUMBER 4

foreword

This issue marks the completion of the third year of publication of *Reactor Core Materials*, one of four Technical Progress Reviews dealing with different areas of nuclear technology. *Reactor Core Materials* is written by staff members of Battelle Memorial Institute, under the auspices of the Office of Technical Information of the U. S. Atomic Energy Commission.

The Review presents the highlights of significant findings which have come to the attention of the writers during the past quarter. Its main intent is to acquaint readers with the existence, nature, and trends of important research programs and publications. Specialists who wish more detailed information are urged to consult the original references.

R. W. DAYTON
E. M. SIMONS
R. W. ENDEBROCK
Battelle Memorial Institute

contents

Foreword

1 I AEC REACTOR MATERIALS HANDBOOK, SECOND EDITION

3 II FUEL AND FERTILE MATERIALS

3 Unalloyed Uranium
4 Alpha-Phase Uranium Alloys
5 Gamma-Phase Uranium Alloys
7 Epsilon-Phase Uranium Alloys
7 Dilute Uranium Alloys
8 Plutonium Alloys
9 Thorium
10 Dispersion Fuels
11 Refractory Fuel and Fertile Materials
15 Basic Studies of Irradiation Effects in Fuel Materials
16 References

19 III MODERATOR MATERIALS

19 Beryllium Metal and Alloys
23 Solid Hydrides
26 References

28 IV NUCLEAR POISONS

28 Rare-Earth Oxide and Boron Control Materials
29 References

30 V CLADDING AND STRUCTURAL MATERIALS

30 Corrosion
35 Metal-Water Reactions
37 Radiation Effects in Nonfuel Materials
42 Selected Mechanical Properties of Cladding and Structural Materials
42 Selected Metallurgical Aspects of Cladding and Structural Materials
44 References

48 VI SPECIAL FABRICATION TECHNIQUES

48 Melting, Casting, Heat-Treatment, and Hot Working
49 Cladding
53 Explosive Forming
55 Welding and Brazing
56 Nondestructive Testing
56 References

59 INDEX, VOLUMES 1–3

Issued quarterly by the U. S. Atomic Energy Commission. Use of funds for printing this publication approved by the Director of the Bureau of the Budget on November 1, 1960.

Section 1

AEC REACTOR MATERIALS HANDBOOK, SECOND EDITION

The chaotic literature of atomic energy is a natural consequence of rapid development in this field. Because published information is scattered so widely, in small bits in numerous reports, researchers have difficulty in keeping abreast of their fields, to the detriment of further progress. The entire series of Technical Progress Reviews, of which this is one part, attempts to alleviate this situation by calling attention to progress being made in several important branches of atomic science. However, these reviews are no substitute for the occasional thorough summing up provided by monographs, books, and the proceedings of the Geneva conferences.

Such publications, when they deal with reactor core materials, have been discussed at some length in these reviews of reactor core materials information because they represent major advances in coordinating atomic energy literature. The recent publication of Volume 1, Reactor Materials, *of the second edition of the* Reactor Handbook *merits discussion because it is the only book which attempts to treat the whole field of reactor materials in any detail.*

For this reason, we have asked Mr. C. R. Tipton, Jr., editor of Volume 1 of the Reactor Handbook, *to review this book for our readers so as to let them know what place it will fill in their libraries. Mr. Tipton's review, which follows, is a special feature of this issue.*

The Editors

Volume I, *Reactor Materials*, of the second edition of the *Reactor Handbook*, made its appearance on booksellers' shelves in June 1960. This volume is the first of a series of four which represent a complete revision and expansion of the original *Reactor Handbook*, which is familiar as one of the Presentation Volumes for the 1955 Geneva Conference. The first edition of the *Reactor Handbook* was sold both commercially and by the Government Printing Office. Although the exact sales figures are not available, it is generally believed that some 30,000 copies of the several volumes were sold.

Considering that a basic requirement for publishing a book is a need, it is obvious that the sales of the first edition of the *Reactor Handbook* indicated not only a need but a general acceptance of the material prepared to fill the need. Because of the clearly indicated utility of the *Reactor Handbook*, and because of the need for updating, it was determined by the USAEC Office of Technical Information and its advisers, the *Reactor Handbook* Review Board (W. H. Zinn, H. Brooks, P. F. Gast, J. P. Howe, S. Lawroski, and M. C. Leverett), that a revised *Handbook* would be a valuable source and reference tool for nuclear scientists and engineers. The recently issued volume is the first result of this decision. The other volumes will be appearing shortly.

In reviewing this first volume, *Reactor Materials*, comments on some of the basic considerations involved in the revision of the *Reactor Materials* volume are in order. In the first edition of the *Handbook*, the materials volume was rather narrowly conceived and limited to normally solid materials. In preparing and planning the revision, it was agreed that all reactor materials (solid, liquid, and gas) would be discussed and that the most useful organizational arrangement would be to group materials according to their functional utilization in a reactor. The *Reactor Materials* volume is made up of seven parts: a general part which covers miscellaneous subjects such as health and safety, zirconium-hafnium separation, D_2O-H_2O separation, etc., and six spe-

cific parts which cover fuel, cladding and structural, control, moderator, coolant, and shielding materials. An appendix covers constitutional diagrams of binary alloy systems.

An objective of the revision was completeness. The editors of the four volumes of the *Handbook* agreed at the outset that each volume should be reasonably self-contained, i.e., capable of being used without recourse to the other volumes. Because of this, one will find material present in Volume I that may also subsequently appear in the other volumes.

Since greater time for preparation was allowed for the second edition, it was possible to have broad author participation. In organizing for the writing effort, every attempt was made to obtain the services of outstanding experts for each major section. The success of this attempt has added greatly to the quality of the presentation. Approximately 140 individuals from over 70 organizations participated in the preparation of the second edition of *Reactor Materials*. In writing the draft of the volume, every attention was to be given to completeness of coverage without regard to classification. It is interesting to note that, by the time the *Handbook* writing was completed and the book was ready for the preliminary phases of publication, the declassification policy was such that only a very minor percentage of the original information was deleted.

Furthering the concept of expert contributors, each part of the book was assigned to an editor. Working with this editor was a Technical Committee constituted to review the individual contributions. These edited and reviewed parts of the book were subsequently reviewed by the *Reactor Handbook* Review Board. Although this review mechanism was time consuming, it did provide the highest possible level of technical excellence for the *Handbook*. In actual elapsed time, approximately $4\frac{1}{2}$ years was required to go from the original point of decision that a revision was desirable to a finished product, a 1207-page volume. The book is an excellent example of good type selection and makeup which, combined with good printing and paper stock and a flexible, leatherlike cover, make a very handsome and readable volume. In this regard the publishers of the book, Interscience Publishers, Inc., deserve special commendation for their efforts.

From the technical point of view, what sort of a book has been produced and what needs will it fill? First and foremost, of course, is the fact that the new edition will more than replace the old one as the only complete source of information on reactor materials. As such, the *Reactor Handbook* is expected to be a most valuable reference book, with the same utility in the field of atomic energy as the *Metals Handbook* has for metallurgy in general.

As to quality, the names of the section authors suffice to guarantee that the treatment was thorough and definitive at the time the sections were written. This uniformly high quality has been attested to by the *Reactor Core Materials* authors, who were asked to review the pertinent sections of the *Handbook* when it appeared.

The only adverse criticism by the *Reactor Core Materials* authors (and this criticism was made only for the *Handbook* articles dealing with the most rapidly advancing areas) was that the most recent information was not included. No apology for this fact appears necessary for two reasons. First, no book on atomic energy can be completely up-to-date. The field is moving too fast for that to be possible. Second, as anyone can testify who has been involved in preparing a book with multiple authors, a very tight time schedule cannot be achieved when the authors work in many laboratories and do their writing as a spare-time effort with their other work taking precedence.

The effects of the delay between writing and publication have been minimized as much as possible by making a final technical check of the galley proofs to delete statements which time had proven to be erroneous. Few such statements were found. Actually, even by today's technology, there are few areas where the *Handbook* treatment would need to be changed greatly. Most of the material is as good today as when it was written, and, as a result, the *Handbook* is the best available reference book on reactor materials, well worth its cost of $36.50.

Finally, it might be mentioned that the past issues of *Reactor Core Materials* more than fill the gap between today's technology and that of about two years ago when the last drafts of *Handbook* sections were completed.

(C. R. Tipton, Jr.)

Section II

FUEL AND FERTILE MATERIALS

Unalloyed Uranium

The metallography of uranium heat-treated in the beta and gamma phases was examined by Robillard.[1] Annealing uranium in the gamma phase followed by cooling at a rate dependent on the annealing temperature causes the formation of substructures different from those resulting from polygonization of alpha uranium. The substructures are indicated by the concentration of impurities on the dislocations induced by the gamma-to-beta transformation. Similar treatment of the uranium–1.4 wt.% chromium alloy, in which the beta phase is stabilized at room temperature, confirms this explanation. In addition to the polygonization substructures, sharp discontinuities can be observed in the network of subboundaries as a fine white edging. The comparison of these discontinuities with the structure revealed by thermal etching *in vacuo* shows that these are traces of grain boundaries of the gamma phase.

Creep measurements on uranium hot rolled in the gamma region were performed by the Russians[2] on rod specimens 10 mm in diameter by 100 mm long, in a lithium atmosphere. The results obtained are shown in Fig. 1. The deformation of uranium subjected simultaneously to thermal cycling and tensile stresses was investigated.[3] In all cases the elongation was greater than that caused by creep in a simple tension test. This occurs even if tensile and thermal-cycling stresses are of opposite sign.

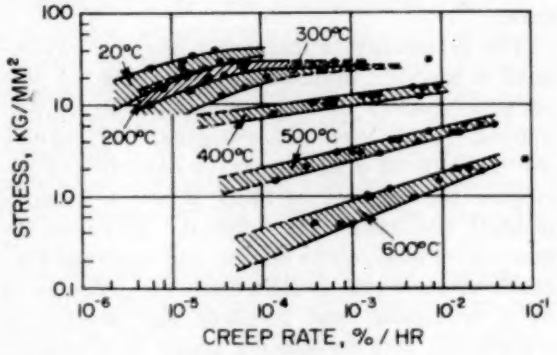

Figure 1—Creep of gamma-rolled uranium versus stress.[2]

In a British study[4] of the effect of the alpha-to-beta transformation on the preferred orientation of alpha uranium, rolled uranium rods were subjected to varying amounts of transformation into the beta phase in a temperature gradient. The results show that the phase change is accomplished by a transformation band of mixed alpha and beta phases passing through each specimen and that the amount of the loss of preferred orientation is a function of the degree of transformation.

Du Pont[5] is using a diffraction technique that utilizes an X-ray orientation parameter, or "growth index," to correlate preferred orientation with irradiation growth. A value of $\gamma_b^* = 114$ per cent elongation/at.% burnup is derived for a highly textured specimen in the form of hot-press-bonded aluminum-clad uranium plate. A dilatometric technique, also devised by Du Pont, makes use of an "orientation coefficient" that is obtained by measuring the thermal expansion just following a reversal in temperature. This procedure avoids extraneous deformation due to grain-interaction effects. A value $\gamma_b = 120$ per cent elongation/at.% burnup was obtained by the dilatometric technique for the aluminum-clad uranium plate. The γ_b values obtained by both the X-ray and the thermal-expansion methods are in good agreement but are considerably less than the value $\gamma_b = 420$ per cent elongation/at.%

*The term γ_b means the effective irradiation growth of an incremental volume of metal in the b-axis direction.

burnup measured for unrestrained single crystals of uranium.

Tensile properties of irradiated uranium carried out on test pieces cut from Calder Hall fuel elements after a 200 to 1100 Mwd/ton exposure have been reported.[6] These tensile tests have produced consistent results, with ultimate tensile strengths between 48,000 and 64,000 psi, and negligible ductility. A small amount of ductility (0.5 per cent) can be restored to the uranium by a prolonged anneal at a temperature high in the alpha range. Thermal cycling between temperatures of about 600 and 250°C causes decreases in density of up to 2 per cent. Microscopic examination shows that the resultant cavity formation is mainly intergranular. The tensile strength is reduced in proportion to the amount of cavity formation.

Hanford[7] has recently published a review of the literature on the release of inert gases from irradiated uranium. Conclusions indicate that there are two kinds of gas release as distinguished by evolution kinetics. One type occurs before gross swelling is evidenced, and the other follows it. Before gross swelling occurs, the gas release is very low, approximately 1 per cent of the total present. The evolution is not described adequately by an equation relating the quantity released directly to the square root of time at temperature. This is evidence that the process of gas release is not diffusion in the classical sense. An evaluation of the available data leads to the conclusion that the condition of the uranium surface is very important in determining release rate and that oxidation enhances gas release. Where gross dimensional changes occur, the gas evolution rate is markedly increased. Thermal cycling increases the release rate and the swelling. The gas release during swelling is of an erratic nature and not amenable to quantitative analysis.

The Israel Atomic Energy Commission has published literature surveys on the following topics: aqueous corrosion of uranium,[8] grain size in uranium,[9] and gamma-to-beta and beta-to-alpha phase transformations in uranium.[10]

(M. S. Farkas)

Alpha-Phase Uranium Alloys

Russian investigators[11] have determined the uranium-germanium phase diagram. The existence of the U_5Ge_3, U_3Ge_4, UGe_2, and UGe_3 compounds was established. A peritectoid compound, U_7Ge, is also believed to exist. The phase diagram is presented in Fig. 2.

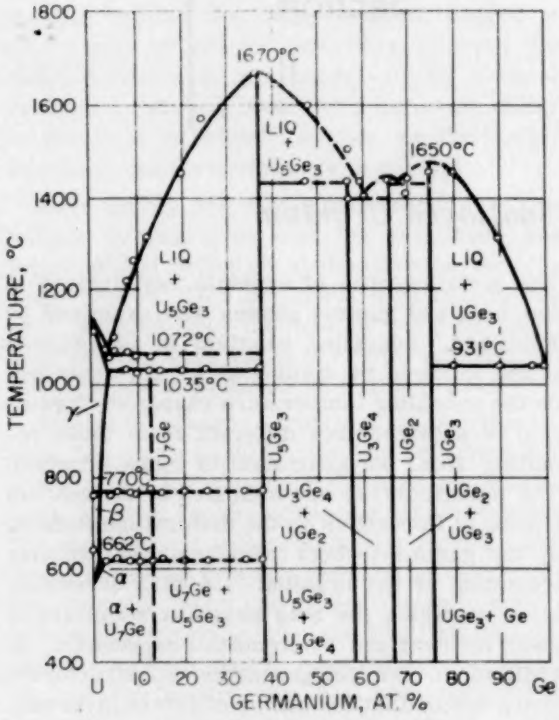

Figure 2—Uranium-germanium phase diagram.[11]

Investigations performed by the French[12] on uranium–0.5 to 4 wt.% molybdenum alloys include (1) isothermal and continuous cooling transformations and (2) equilibrium-diagram determinations. Other studies[13] show that the martensitic phase produced in low molybdenum–uranium alloys has a monoclinic crystal structure.

The feasibility of improving swelling resistance in metallic uranium by increasing the dislocation density is under investigation by Advanced Technology Laboratories.[14] Increasing the density of dislocations is expected to increase the number of sites at which fission-product gas atoms are "pinned," increase the number of gas-bubble nuclei, and increase mechanical strength. Dislocations are introduced by a treatment that involves deformation of metastable beta or gamma phase in uranium-rich alloys, followed by transformation.

Initial results on gamma-stabilized binary alloys containing 2, 3.5, 5, and 7 wt.% molybdenum showed that large plastic reductions are

possible in 5 and 7 wt.% molybdenum alloys at 450°C. The more dilute alloys were relatively difficult to roll. Aging experiments on deformed and undeformed 5 wt.% molybdenum alloys indicate that deformation accelerates the aging process and retards growth of the "pearlitic" eutectoid transformation product. Results with dilute chromium and chromium-molybdenum alloys showed that rolling is possible in the metastable beta phase for a short time at temperatures as low as 450°C. The beta phase is quite hard at lower temperatures, however, and cracking occurs in some alloys at relatively small reductions. Beta-phase deformation of these alloys resulted in no significant hardness increase, although final grain size was reduced appreciably.

The corrosion behavior of irradiated uranium-rich alloys is reported by Argonne.[15] The alloys investigated include uranium–3 wt.% niobium, uranium–3 wt.% niobium–0.5 wt.% tin, uranium–3.8 wt.% silicon (U_3Si), and uranium–2 wt.% zirconium (clad with Zircaloy-2 and diffusion treated). Only the U_3Si and uranium–2 wt.% zirconium alloy specimens retained a significant degree of their preirradiation corrosion resistance.

Irradiation testing of fuels for possible use in the Sodium Reactor Experiment (SRE) has been reported by Atomics International.[16] The irradiated fuel materials examined were (1) alpha-rolled beta-quenched uranium, (2) cast and beta-quenched uranium, (3) cast uranium–2 wt.% zirconium, (4) uranium–1.5 wt.% molybdenum, (5) powder-compacted uranium–1.2 wt.% molybdenum, and (6) extruded and swaged thorium–5.4 wt.% uranium. Maximum fuel burnup was 850 Mwd per metric ton of uranium for the uranium alloys, whereas the thorium alloy received a burnup of 1300 Mwd per metric ton of alloy. Measured fuel control and surface temperatures were 1000 and 850°F, respectively. Fuel-slug dimensions were 6 by ¾ in. in diameter, and the powder compacts were 1 in. long. A résumé of the results of the irradiation is shown in Fig. 3.

The thorium-uranium alloy and the uranium–1.5 wt.% molybdenum alloy appeared to be promising fuels. The burnup and temperature limits of these two materials are not known and merit further experimentation. The powder-compacted uranium–1.2 wt.% molybdenum alloy, the cast uranium–2 wt.% zirconium alloy, and the unalloyed fuels did not appear to be satisfactory for further consideration as sodium graphite reactor fuels in fuel elements requiring good dimensional stability of the fuel material. The cast material appeared to be more stable than the wrought material. (M. S. Farkas)

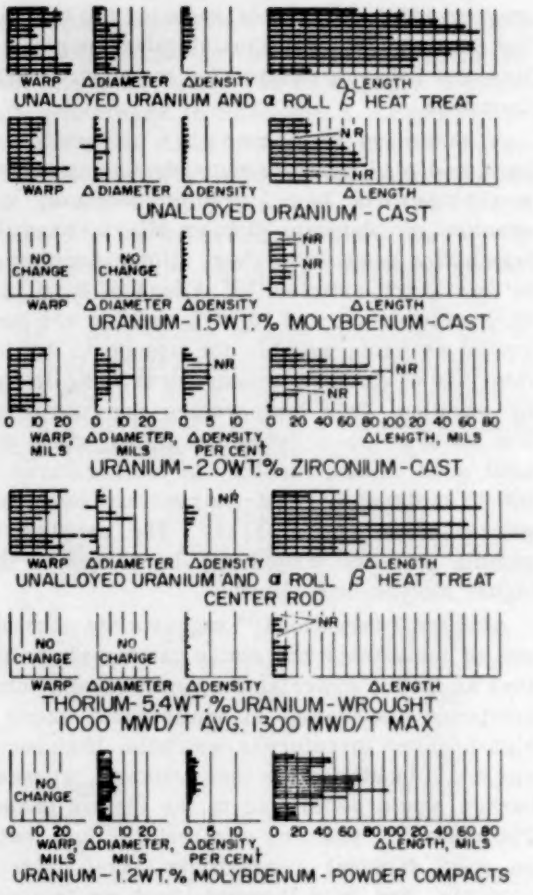

Figure 3 — Summary of individual dimensional changes of alloys irradiated to a maximum burnup of 850 Mwd per metric ton of uranium at a surface temperature[16] of 850°F.

Gamma-Phase Uranium Alloys

A summary has been made of the results of recent French studies[17] on uranium-molybdenum and uranium-niobium alloys. It is pointed out that one may obtain improved corrosion resistance and increased resistance to irradiation swelling through the use of these alloys as compared with unalloyed uranium, but at the expense of reactivity which requires the use of enriched uranium. In order to reduce the enrichment required, ternary alloying and heat-treatment

may provide a means of reducing the total alloy requirements while maintaining the properties and behavior desired for satisfactory performance.

A summary of corrosion properties of bare and clad uranium-molybdenum, uranium-molybdenum base, uranium-niobium, and uranium-molybdenum-niobium alloys and of the irradiation behavior of these alloys is contained in two Dutch articles.[18,19] Alloys of 9 to 13.5 wt.% molybdenum and 10 wt.% niobium are suggested as being suitable for use up to 340°C, their use at elevated temperatures being limited by swelling. This temperature appears to be low for uranium-molybdenum alloys, which exhibit good volume stability to temperatures of 600°C in the absence of neutron-flux-dependent gamma-phase instability. The problem of gamma stability should not be severe in the higher molybdenum alloys.

Atomics International[20] suggests the possible use of metastable and stable gamma-phase alloys as matrix materials for enriched-uranium-compound dispersions in applications where a high-uranium inventory is desirable. High burnups would be attained in the compound, whereas burnup would be limited in the matrix phase. The desirable features of a metallic fuel, such as good thermal conductivity, good neutron economy, and good thermal-shock resistance, are envisaged as being combined with the more desirable high-temperature properties of compound phases.

Samples of rolled uranium–10 wt.% niobium and uranium–7 wt.% molybdenum sheet have been examined at Los Alamos[21] both before and after oxidation to evaluate any epitaxial relation between orientations of the oxide and the underlying metal. Pole figure plots of the base metal were found to be essentially the same for the two alloys, but the oxides showed somewhat different textures.

Uranium-Molybdenum

In a study[19] of the effects of chromium, niobium, rhenium, ruthenium, and zirconium on the gamma-phase stability of uranium-molybdenum alloys, the French found that only zirconium reduced the stability of the gamma phase. The fact that this is the only element of those added which has a larger atomic radius than uranium leads the authors[19] to conclude that metastability arises from contraction of the cubic gamma lattice. The strong tendency for $ZrMo_2$ formation and consequent dealloying of the gamma phase should also be considered. When compared on the basis of reactivity loss associated with the addition, ruthenium is found to be the most effective additive for increasing the incubation period for transformation.

The transformation of the gamma phase in uranium–6 and –10 wt.% molybdenum alloys has been studied[22] using metallographic, hardness, and X-ray diffraction methods. In both alloys, transformation of the gamma phase to alpha uranium and the intermediate U_2Mo phase occurs above 400°C by a nucleation and growth mechanism to yield a pearlitic type structure which is nucleated at the grain boundaries. Below 400°C, transformation occurs by precipitation within the grains. In the 6 wt.% molybdenum alloy, alpha-uranium precipitation precedes ordering of the remaining molybdenum-enriched solid solution, whereas in the 10 wt.% molybdenum alloy, ordering precedes the alpha-phase precipitation.

In another study by the French,[23] similar results are reported. The decomposition of the gamma phase is found to proceed first by the precipitation of alpha uranium which enriches the gamma phase. Formation of U_2Mo occurs when the gamma phase is sufficiently enriched in molybdenum.

A program to perform in-pile resistivity measurements on uranium-molybdenum alloys is reported by Argonne.[24] Initial resistance changes after one-week exposures at 475 to 635°C are given for uranium–5 and –8 wt.% molybdenum alloys. These initial data merely indicate that the experimental arrangement is probably satisfactory.

A Martin report[25] deals with studies designed to lead to the preparation of uranium–10 wt.% molybdenum fuel pellets for use in a fluidized-bed reactor. Nickel plating is being studied as a means of cladding the pellets. Attempts to cast pellets of the fuel alloy were unsuccessful, and emphasis has shifted to a cold-heading process. For this process the alloy is cast in rod form and then swaged into small-diameter pins. The pins are cut into short lengths that are upset in a die to the desired shape. Cracks resulting from the cold-swaging operation are reported, but this problem should be overcome through a proper heat-treatment schedule.

A uranium–10 wt.% molybdenum alloy can withstand contact with stainless steel, without

alloying and melting through the steel by eutectic formation, for longer periods of time than can unalloyed uranium, according to Atomics International.[26] Penetration through a 10-mil-thick stainless-steel jacket is indicated as requiring about 1 and 6 min at 2000 and 1800°F, respectively. The presence of a thin oxide film on the surface of the uranium-molybdenum alloy will substantially lengthen these times.

In a further study[27] of the compatibility of stainless steel, sodium, or NaK bonded to the uranium–10 wt.% molybdenum alloy, no evidence of interalloying between the fuel and type 304 stainless-steel cladding was found after 744- and 2184-hr exposures at 1000°F.

A calculation of the fission-gas yield in the uranium–10 wt.% molybdenum alloy after exposures of 3000 and 7000 Mwd/ton has been performed by Atomics International.[28] Total concentrations of 3.09×10^{19} and 6.78×10^{19} atoms/cm^3, respectively, are calculated. The calculation includes the 15 isotopes of bromine, krypton, iodine, and xenon which are produced in significant amounts.

Epsilon-Phase Uranium Alloys

Uranium-Silicon

An Atomics International report[20] briefly summarizes properties, fabrication, heat-treatment procedures, and irradiation behavior of U_3Si. The need for additional irradiation data to establish the behavior of U_3Si and U_3Si_2 is pointed out. The corrosion and irradiation behavior of uranium-silicon alloys is also summarized in two Dutch articles.[17,18]

The results of X-ray diffraction examination of irradiated uranium-silicon alloys are reported by Chalk River. Material irradiated as heat-treated to yield U_3Si showed no reflections attributable to the U_3Si phase, and material which was alpha uranium and U_3Si_2 prior to irradiation appeared to remain in that condition. A heat-treatment at 400°C for 3 hr produced no change in the patterns obtained. (A. A. Bauer)

Dilute Uranium Alloys

Aluminum-Uranium Alloys

Unalloyed aluminum and binary aluminum-uranium alloys containing 5 and 13 wt.% uranium were studied by Oak Ridge[29] for the purpose of determining the effect of the dispersed UAl_4 on the texture of pure aluminum. As uranium content increased, there was an increase in spread and a decrease in intensity. A random texture did not result from uranium additions. The results can be analyzed in terms of change from a (5, 6, 16) $\langle \bar{1}0, \bar{1}3, 8 \rangle$, near (113) $\langle \bar{3}\bar{4}3 \rangle$, texture in the pure aluminum to a near $\langle 111 \rangle$ fiber texture in the alloy containing 13 wt.% uranium.

As a part of the studies concerned with the effect of ternary additions on the aluminum–35 wt.% uranium alloy, Battelle[30] has determined the 100-hr rupture strength for a series of alloys. These data are reported below:

Type of melt	Alloy (balance Al), wt.%	100-hr rupture strength, psi
Air	35 U	10,100
Air	35 U–2 Sn	8,100
Air	35 U–3 Sn	7,000
Air	35 U–2 Zr	8,600
Air	35 U–3 Zr	7,900
Vacuum	35 U–2 Zr	9,000
Vacuum	35 U–3 Zr	8,700

As can be noted from the above, the binary alloy exhibits the best rupture strength, although the difference between it and the vacuum-melted zirconium alloys is not great enough to be considered significant.

Niobium-Uranium Alloys

The niobium–10 wt.% uranium alloy showed no appreciable deformation at 2200°F after 300 hr under a load of 10,000 psi, according to data obtained at Battelle.[30] However, the specimen broke after 332 hr on test. The ultimate tensile strength of this alloy at 2200°F is as high as 41,000 psi.

Niobium-base binary alloys containing 10 to 60 wt.% uranium showed the presence of a dull black oxide film after a 100-hr exposure to sodium at 1500°F. The alloys containing 40 per cent or more uranium gained weight at a higher rate than did alloys with less uranium. The oxygen content of the alloys seemed to have little effect on the sodium corrosion rate. Similar alloys were exposed to 600°F water for 292 days. Although the material containing 10, 30, 50, and 60 wt.% uranium showed a weight loss,

the 20 and 40 wt.% uranium alloys gained weight. The fabricated 20 wt.% uranium alloy gained up to 0.91 mg/cm^2, and the 40 wt.% uranium alloy gained up to 0.61 mg/cm^2. Zircaloy-2, when tested under similar conditions, gains about 0.30 mg/cm^2.

Tensile tests performed at 800, 1300, 1600, and 1800°F on a niobium–10 wt.% uranium alloy containing 3100 ppm oxygen indicate that the oxygen impurity has its maximum effect around 1600°F. The ultimate tensile strength increases with temperature until it reaches 72,500 psi at 1600°F. At 1800°F the ultimate tensile strength is 52,500 psi.

The electrical resistivity of both the 10 and 20 wt.% uranium alloys increases linearly between 68 and 1800°F. In the case of 10 wt.% uranium alloy, the value at 68°F is 35.9 μohm/cm, whereas at 1800°F the value is 66.3 μohm/cm. Corresponding values for the niobium–20 wt.% uranium alloy are 53.7 and 77.6 μohm/cm. The coefficients of linear expansion for the same two alloys show only moderate deviation from a linear increase between 68 and 1800°F. The values for the low and high temperatures are given below:

Alloy	Expansion, 10^{-6}/°F, at 68 to 200°F	Expansion, 10^{-6}/°F, at 1600 to 1800°F
Nb–10 wt.% U	~4.1	~5.3
Nb–20 wt.% U	~4.2	~5.7

Miscellaneous Alloys

As a part of a study concerned with rhenium-uranium alloys, Ames[31] has investigated the constitutional diagram. An intermediate phase Re_2U was found to be present in the system. This phase melts at 2200 ± 75°C and exhibits an allotropic transformation at 180 ± 2°C. Single-crystal work indicates that the room-temperature structure is orthorhombic or tetragonal. The high-temperature structure is believed to be hexagonal. There is a eutectic reaction between Re_2U and each of the two terminal solid solutions. These occur at 1104 ± 3°C and 2100 ± 60°C with compositions in the neighborhood of 20 and 65 wt.% rhenium, respectively.

Two modifications of the U_2Zr_{17} structure have been noted. One has hexagonal symmetry, and the other has rhombohedral symmetry.

(R. F. Dickerson)

Plutonium Alloys

An Argonne report[24] contains a review of plutonium research conducted there during 1959.

A number of uranium–20 wt.% plutonium–fissium alloys have been studied with emphasis on a uranium–20 wt.% plutonium–10 wt.% fissium alloy. Hardness, density, and solidus temperature for various alloys appear in Table II-1.

Table II-1 PROPERTIES OF URANIUM–20 WT.% PLUTONIUM-FISSIUM ALLOYS[24]

Composition, wt.%	Hardness, R_A	Density, g/cm^3, at room temp.	Solidus temp., °C
75 U–20 Pu–5 Fs	75	17.86 ± 0.02	860 ± 10
70 U–20 Pu–10 Fs	95	17.03 ± 0.02	820 ± 10
65 U–20 Pu–15 Fs	76	16.38 ± 0.02	800 ± 10
75 U–20 Pu–3.5 Fs–1.5 Zr	84	17.72 ± 0.02	
70 U–20 Pu–7 Fs–3 Zr	75	16.84 ± 0.02	
65 U–20 Pu–10.5 Fs–4.5 Zr	73	16.14 ± 0.02	

The compatibility of the uranium–20 wt.% plutonium–10 wt.% fissium alloy with various canning materials is being determined. Diffusion penetration studies of stainless-steel types 347 and 430, zirconium, Zircaloy-2, molybdenum, titanium, tantalum, niobium, and vanadium with the fuel alloy have been conducted at 700 and 800°C for periods of 3, 10, and 30 days. Measurements at 600°C are in progress for periods of 10, 30, and 60 days. The stainless steels formed a molten eutectic at all temperatures studied. No diffusion bond with tantalum was visible at 600 and 700°C. At 794°C a very weak and brittle diffusion bond formed. A very strong diffusion bond was formed with niobium, the diffusion being more than 90 per cent on the niobium side. Zirconium and Zircaloy-2 behaved very similarly, diffusion being more than 95 per cent on the zirconium side. The presence of some cracks in the bond on the fuel alloy side indicated brittleness. The titanium diffusion couple exhibited three bonds which were almost

entirely on the titanium side. Molybdenum formed one very weak and brittle bond, 80 per cent of which was on the fuel alloy side. Mean penetration coefficients obtained from diffusion couples at 694 and 794°C are shown in Table II-2.

Table II-2 MEAN PENETRATION COEFFICIENTS IN DIFFUSION COUPLES OF URANIUM–20 WT.% PLUTONIUM–10 WT.% FISSIUM AND VARIOUS MATERIALS[24]

Canning material	Penetration coefficient, 10^{-12} cm^2/sec, at indicated temp.	
	694°C	794°C
Type 430 S.S.	Molten eutectic formed	Molten eutectic formed
Type 347 S.S.	Molten eutectic formed	Molten eutectic formed
Zirconium	10.76	1239
Zircaloy-2	5.43	640.1
Niobium	16.81	125.8
Tantalum	No diffusion visible	190.7
Titanium	2.71	42.25
Molybdenum	3.24	24.11
Vanadium	No bonding	No bonding

Table II-3 IRRADIATION-INDUCED DIMENSIONAL CHANGES OF ALUMINUM-PLUTONIUM ALLOYS*[32]

Alloy (balance Al), wt.%	Diameter change, in.		Length change, in.	Volume change, %
	Top	Bottom		
5 Pu	0.0028	0.0027	0.0113	2.7–2.8
10 Pu	0.006	0.0025	0.0116	1.1–2.6
15 Pu	0.006	0.0016	0.0090	0.9–1.7
20 Pu	0.0025	0.0026	0.0112	2.5–3.4

*Fuel cores are about 0.5 in. in diameter by 1.98 in. long.

In irradiation experiments the uranium–20 wt.% plutonium–10 wt.% fissium alloy was found to swell excessively at temperatures as low as 400 to 450°C. No improvement was gained by replacing approximately one-third of the fissium with molybdenum or zirconium. However, decreasing the plutonium content to 10 wt.% resulted in significant improvement.

Two cold-rolled zirconium–5 wt.% plutonium specimens and one zirconium–7 wt.% plutonium specimen were irradiated to 1.4 and 1.9 at.% burnup, respectively, at a calculated initial temperature of 530°C. Structure of the alloys should have been a solid solution of plutonium in alpha zirconium. All three specimens elongated by approximately a factor of 3. Their ribbonlike appearance was very similar to that of irradiated pseudocrystals of alpha uranium. Longitudinal surface striations were evident.

Hanford[32] has irradiated aluminum–5, –10, –15, and –20 wt.% plutonium alloys to 0.1 and 0.2 at.% burnup. Dimensional measurements of dejacketed alloy fuel cores which had 0.1 per cent burnup of total atoms appear in Table II-3.

(V. W. Storhok)

Thorium

The solubility of thorium in liquid zinc is reported[31] by Ames as follows:

Temp., °C	Thorium solubility, wt.%
419	0.0026
500	0.022
600	0.19
700	0.99
800	3.79
900	11.12
1000	25.52

The diffusivity of hydrogen in thorium between 300 and 900°C is given by the expression

$$D = 2.92 \times 10^{-3} \exp(-9750/RT)$$

In addition, Ames reports finding two ternary compounds in the thorium-carbon-hydrogen system corresponding to the formulas $ThH_2 \cdot ThC$ and $2ThH_2 \cdot ThC$.

A thorium-nitrogen alloy containing 5.4 wt.% nitrogen was prepared at Battelle[30] by arc melting thorium under nitrogen at 2½ atm pressure. Stoichiometric ThN contains 5.7 wt.% nitrogen.

Smith and Honeycombe[33] found that the ductility of sintered thorium was reduced by nitrogen additions in amounts up to 0.22 wt.%. More than 0.22 wt.% nitrogen interfered with the sinterability of thorium. Massive inclusions of ThN in thorium were observed to tarnish more rapidly than the matrix when exposed to air. The solubility of carbon in thorium was redetermined to be as follows:

Temp., °C	Carbon solubility, wt.%
350	0.2
700	0.3
900	0.4
1100	0.5
1200	0.6
1300	0.8

The dynamic modulus of thorium has been remeasured by Livesey[34] from room temperature to 300°C. At 20°C the modulus was found to be 8.0×10^{11} dynes/cm^2 (11.6×10^6 psi). With increasing temperature, the modulus decreased at a rate of 5.1×10^8 dynes/(cm^2)(°C), or 7400 psi/°C.

Table II-4 EFFECT OF IRRADIATION ON TENSILE PROPERTIES OF THORIUM[36]

Neutron exposure, 10^{20} nvt	Yield strength, 1000 psi	Tensile strength, 1000 psi	Elongation in 2 in., %	Young's modulus, 10^6 psi
0	15.7	25.0	47	11
0	15.4	24.2	37	12
9.9	49.8	56.7	13	12
11.6	49.8	50.8	33	12
34.7		48.8*	0.2*	8*
44.6		55.9*	0.1*	10*
49.9	69.1	75.6	7	9

*These specimens were probably both defective. One is known to have broken outside the gauge section at an oxidized crack.

Further studies by Kneppel[35] of the corrosion behavior of thorium alloys in 500°F water confirm earlier findings by other investigators to the effect that zirconium is the most beneficial alloying addition for improving the corrosion resistance of thorium in water. In 500°F water, thorium alloys containing 5 to 10 wt.% zirconium showed corrosion rates of 25 mg/(cm^2)(hr) as compared with a rate of 150 mg/(cm^2)(hr) for unalloyed thorium. The benefit of this alloy addition is even more pronounced in clad specimens. A specimen of thorium–8.8 wt.% zirconium alloy clad with Zircaloy, which contained an intentional defect, showed only slight cracking of the cladding near the defect after 132 hr in 500°F water. Similar unalloyed, clad thorium specimens failed under similar conditions after only a few hours.

Hanford[36] has canned a series of thorium tensile specimens in NaK and exposed them in the Materials Testing Reactor (MTR) for various lengths of time, presumably at process-water temperatures. The results of tensile tests at room temperature on some of the irradiated specimens are shown in Table II-4. (W. Chubb)

Dispersion Fuels

Mechanical properties of stainless steel–UO_2 dispersion fuel elements were determined at Knolls[37] on specimens fabricated by (1) the cold-binder extrusion and hot-swaging technique, (2) the single hot-extrusion method, and (3) the hot-coextrusion method followed by a second hot extrusion, hot rolling, swaging, or drawing.

Cold-binder material was shown to have very good tensile properties except for ductility. Coarse oxide material has better ductility than fine oxide, both before and after irradiation, as indicated by bend tests. Although low in ductility, test results indicate that dispersion fuel elements of UO_2 clad in stainless steel have fair mechanical properties even after high burnups.

Aluminum-base cores[38,39] have been strengthened by the addition of aluminum-coated fuel-bearing Fiberglas. The Fiberglas contained 38.7 wt.% aluminum and 61.3 wt.% urania glass, RX70, which contains 50 wt.% U_3O_8. Tensile strength of as-hot-pressed, composite cores, parallel to the fibers, ranged from 25,250 psi at 70°F to 18,460 psi at 800°F, with a sharp drop to 6820 psi occurring at 1000°F. The sharp decrease in the strength of aluminum alloys usually occurs near 400°F. The gain in strength observed above in composite cores did not carry over to specimens tested transverse to the fiber direction. The strength decrease in these latter specimens occurred at 400°F.

The effect of dispersions of fine UO_2 particles on the dimensional stability and strength of uranium has been studied by Nuclear Development Corporation of America.[40,41] Various quantities of oxide were added by controlled oxidation of fine uranium-powder particles. The oxidized powders were vacuum hot pressed, or extruded at 1500 to 1700°F. The particle movement during this fabrication breaks off the oxide films to yield the desired dispersion. Analyses of these specimens showed that a large quantity of nitrogen was sometimes associated with the oxygen;

therefore the dispersed phase probably consisted of a $U(ON)_2$ composition. Compositions up to 33 vol.% $U(ON)_2$ consistently resulted in superior dimensional stability over pure uranium upon cycling between alpha and beta phases, 1130 to 1350°F. The duration of each cycle was 15 min, and 20 to 100 cycles were run. Hot bend tests up to 1550°F showed the same trend.

Development and fabrication studies on SM-2 reactor fuel plates at Battelle[42] have progressed to the point where process specifications are being prepared. The irradiation programs with specimens containing 24 to 40 wt.% fully enriched UO_2 and a burnable poison dispersed in a matrix of type 347 stainless steel is continuing. The specimens are to be irradiated with a surface temperature near 700°F to a peak burnup of 40 to 70 at.% of the U^{235}. Specimens in four capsules have been irradiated to estimated burnups of about 40 at.% of the U^{235}. These specimens are now being examined at the Battelle hot cell facility.

A design and fabrication study is being made[42] on instrumented fuel plates. These plates are composed of two half-thickness stainless steel–UO_2 fuel plates and a Zircaloy filler plate. A niobium-foil barrier is used between the Zircaloy and stainless steel to prevent formation of low-melting eutectics during bonding. The entire assembly will be pressure bonded into one unit. Thermocouples will be placed in Zircaloy filler layer on later models.

The Clevite Corporation[43] is attempting to develop procedures which utilize aluminum-coated fuel-bearing Fiberglas as a core material in aluminum-clad fuel elements. Difficulties have been encountered with an uneven core, and corrective fabrication studies are in progress. Fiberglas-reinforced aluminum core material has been produced by consolidation of aluminum-coated Fiberglas by two pressing methods.[44] The hot-pressing operation produced material that had an average density of 98.5 per cent of the theoretical density. Cold pressing followed by hot pressing produced material that had an average density of 99.1 per cent of the theoretical density. Specimens of this material in which the fibers were oriented along the specimen axis exhibited a tensile strength of 25,250 psi at room temperature and maintained a tensile strength of approximately 18,450 psi from 250 to 800°F. (D. L. Keller)

Refractory Fuel and Fertile Materials

Properties and Behavior of Uranium Oxide Fuels

The high-temperature diffusion of Kr^{85} in two uranium oxide powders has been investigated at Bettis.[45] One powder ($UO_{2.004}$) contains 5.6-μ-diameter particles prepared by crushing sintered UO_2. The second powder ($UO_{2.002}$) was prepared by reducing a UO_3 preparation with hydrogen. This latter powder is designated NUR and has a particle diameter of 0.44 μ. Neutron-activated powders were heat-treated several hours at temperatures from 900 to 1500°C, and the Kr^{85} results correlated with the equivalent sphere model. Diffusion coefficients are presented below:

Temp., °C	Diffusion coefficient, cm^2/sec	
	Crushed UO_2	NUR UO_2
900	6.7×10^{-17}	3.9×10^{-18}
1000	1.3×10^{-15}	5.3×10^{-17}
1100	8.3×10^{-15}	7.6×10^{-16}
1200	6.6×10^{-14}	5.3×10^{-15}
1300	2.2×10^{-13}	1.8×10^{-14}
1400	5.9×10^{-13}	1.0×10^{-13}
1500	2.2×10^{-12}	

Activation energies are 65.5 and 73.8 kcal/mole for the crushed UO_2 and the NUR UO_2, respectively. The diffusion coefficients are significantly higher than those reported for xenon by foreign workers and Bettis.

An irradiation loop study of PWR Core 1, UO_2 blanket rods is reviewed fully by Bettis workers.[46] Five Zircaloy-2 rods were irradiated for 300 days at surface temperatures of about 600°F. One of the rods had an intentional defect, a 5-mil hole. All the rods were in good condition after the irradiation. A 1.2-mil diametral expansion occurred in the defective rod. Krypton-85 release from the defective rod was 0.8 per cent. No microstructure changes in the UO_2 other than those associated with the usual high centerline temperatures were observed. The corrosion rate of the Zircaloy-2 was not affected by the irradiation. Hydrogen segregated toward the outer surface of the Zircaloy-2 cladding, but the segregation does

not seriously affect the properties of the cladding.

In a study of the high-temperature compatibility between UO_2 and refractory materials, Gangler et al.[47] have studied 30 metals, oxides, carbides, borides, and nitrides, all having melting points above 4000°F. Short heat-treatments were carried out in vacuum or dry argon. Hafnium carbide, tantalum nitride, and the metals tungsten and tantalum were found to be compatible with UO_2 to its melting point (5000°F). Ditungsten boride, molybdenum carbide, and the metals niobium and molybdenum were found to be compatible with uranium dioxide to their melting points.

As part of a cooperative program between Hanford and Battelle, the effect of fabrication methods and irradiation on the thermal conductivity of UO_2 bodies has been demonstrated.[36] Data are presented in Figs. 4 and 5. As shown in Fig. 5, a large part of the irradiation effect anneals out at relatively low temperature.

A study of the stabilizing influence of oxide additions in uranium oxide is continuing at Battelle.[42] The objectives of this work are (1) to stabilize the fluorite structure of UO_2 under oxidizing conditions and (2) to reduce the volatility of uranium oxide in oxidizing environments at high temperature. In a transpiration study of finely powdered solid solutions of UO_2-La_2O_3, La_2O_3 does not appear to reduce significantly the vaporization of uranium oxide. Work in progress suggests that, in UO_2-La_2O_3 bodies, fuel loss at high temperature may be controlled by the rate of diffusion of uranium in the body.

The general problem of fuel loss in high-temperature UO_2 ceramic dispersions is being studied by a number of workers. Uranium dioxide bodies containing Y_2O_3, ZrO_2, Al_2O_3, La_2O_3, CaO, and CeO_2 are being investigated by the National Bureau of Standards (NBS).[48] High-temperature properties of interest in this latter program include shrinkage, weight loss, structure, and phase composition up to 1800°C.

BeO-UO_2 has been proposed for a number of high-temperature reactor applications. Dense, sintered bodies containing 90 wt.% BeO exhibit excellent structural integrity when heated in air at 700 to 1650°C for long periods.

In an assistance program to Aerojet-General Nucleonics directed toward the development of compact gas-cooled reactors, Battelle[42] is irradiating fully enriched 59 to 44 wt.% BeO-UO_2 pellets in Hastelloy X tubes at surface temperatures of 1450 to 1725°F. After a burnup of 1 to 1.7 at.% of the U^{235}, the pellets were in good condition. Only slight dimensional changes occurred, and there were no apparent microstructural changes in the BeO, UO_2, or Hastelloy X. (W. S. Diethorn)

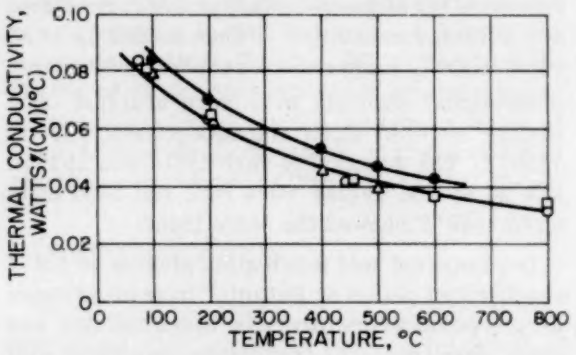

Figure 4 — Dependency of UO_2 thermal conductivity on fabrication method.[36] ●, isostatically pressed UO_2 (93.7 per cent of theoretical density). ○, extruded UO_2 (95.3 per cent of theoretical density). □, extruded UO_2 (87.4 per cent of theoretical density). △, extruded UO_2 (91.9 per cent of theoretical density).

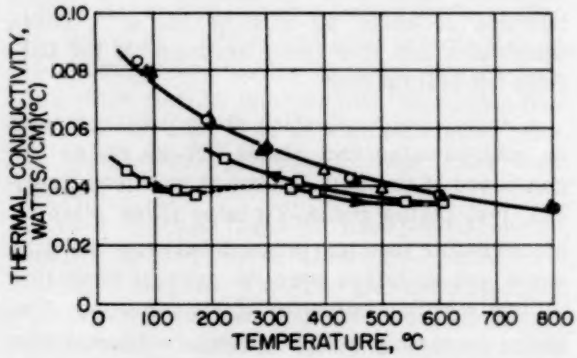

Figure 5 — Irradiation-induced depression and partial annealing recovery of UO_2 thermal conductivity.[36] ○, nonirradiated UO_2 (95.3 per cent of theoretical density). ▲, nonirradiated UO_2 (87.4 per cent of theoretical density). △, nonirradiated UO_2 (91.9 per cent of theoretical density). □, irradiated UO_2 (94.2 per cent of theoretical density), irradiated to 1.16×10^{19} nvt at less than 150°C.

Fabrication of Uranium Oxide Fuels

The process developed by Sylvania-Corning for the pilot-plant fabrication of UO_2 fuel pellets differs markedly from that reported by other sites.[49] Both UO_2 and U_3O_8 were used in the starting powder. Quantities were varied to com-

pensate for lot-to-lot variations in the quality of the ceramic-grade oxide. Pellets pressed at about 8 tsi were sintered at 1300°C for 2 hr in nitrogen, then for 10 min in hydrogen to reduce the U_3O_8 to UO_2. It is reported that a density of 95 to 97 per cent of the theoretical density, a diametral tolerance of ±1 per cent, and a length tolerance of ±1.5 per cent can be maintained in production. The sintered pellets had an oxygen-to-uranium ratio of 1.995 to 2.010 and differed from conventionally prepared pellets only in that the grain size varied from 5 to 9 μ, whereas conventional UO_2, sintered at 1700°C, had a grain size of 18 to 32 μ. Whether this difference would have a significant effect on fission-product retention has yet to be determined. It is reported that the lowered sintering temperature resulted in an appreciable saving in pellet-fabrication costs.

In studies of the sintering of mixtures of UO_2 and PuO_2 at Hanford,[50] it was found that physical mixtures of PuO_2 and PWR-grade UO_2 did not sinter to as high a density as the UO_2 alone. However, the sinterability of a solid solution of up to 10 wt.% PuO_2 in UO_2 was better than the sinterability of the UO_2. (H. D. Sheets)

Properties of Refractory Fuel Other Than Uranium Oxides

The technology of the nuclear carbides is rapidly increasing; a number of laboratories are investigating the stability, corrosion resistance, thermal and electrical conductivity, strength, irradiation behavior, and compatibility of carbides with various high-temperature cladding materials. Two literature reviews[51,52] cover the uranium carbides and their reactions with various groups of elements and compounds. One of the reviews[52] includes published data on the carbides of plutonium and thorium. Thermodynamic data on the reaction of heat-transfer liquids with UC_2 are given in a report by Brewer.[53] Current technological research on carbide fuels is covered in the notes from the second AEC uranium carbide meeting held at Battelle.[54] However, most of these researches have been reported in previous issues of *Reactor Core Materials* and will not be repeated here. During the past quarter, additional data have been compiled on carbide fuel material. Uranium carbide was found[55] to be compatible with niobium-base alloys in 100-hr tests at 1100°C. Battelle[56] has investigated the compatibility of UC with Inconel, mild-steel, stainless-steel (type 304), and zirconium-metal cladding at 800, 900, and 1200°C. Metallographic examination reveals only limited attack of these metals in 100-hr tests at temperatures up to 900°C. However, 24-hr tests at 1200°C resulted in a considerable increase in the depth of penetration. A comprehensive evaluation of the physical properties of uranium carbide and alloys of uranium carbide with other metal carbides is shown in Table II-5.

Rather definite improvements in the physical and chemical properties of UC are obtained by some alloy additions. High-temperature structure studies by Wilson[57] revealed transformation of the tetragonal UC_2 to a cubic CaF_2 type structure at 1820°C. Observed variations in the lattice parameter of the cubic UC_2 indicated a slight decomposition of the dicarbide at extreme temperatures. The variations in the lattice parameter of UC were investigated at Harwell.[58] The lattice parameter first decreases from 4.960 to 4.952 A as the carbon content decreases from 4.8 to 3.8 wt.% and then increases as the carbon content is lowered further in cast material. However, the lattice parameter of the carbide phase in all hypostoichiometric material reverts to the higher value (4.960 A) during a 1300°C anneal.

Additional results on the irradiation behavior of UC are available.[59] Enriched UC castings were evaluated at Atomics International[59] after irradiation in the MTR at 1000 to 1830°F to burnups of 1500 to 14,000 Mwd/ton. The carbide exhibited good dimensional stability, although some cracks formed at the higher burnups. No reaction between the UC and the type 304 stainless-steel cladding was observed. The fission gas released corresponded to that due to recoil. Diffusion coefficients at 1400°C for the fission gas in irradiated UC containing 4.4 to 5.0 wt.% carbon were found by the Canadians to be greater (1.86×10^{-8} cm^2/sec) for the hyperstoichiometric composition than for the hypostoichiometric material (4×10^{-10} cm^2/sec). Work is continuing at Battelle[56] on the diffusion of uranium in UC.

Uranium compounds of interest for reactor fuels which appear most feasible for high-temperature and long burnup application were reviewed at Atomics International.[20] In reference 20 the physical and chemical properties of these compounds are presented, and the nuclear properties are compared. Of the possible

Table II-5 PROPERTIES OF URANIUM-CARBON ALLOYS[56]

Alloy composition, wt.%		As-cast specimens						Specimens annealed 1 hr at 1800°C				
		Rupture stress, psi		Electrical resistivity, μohm-cm	Corrosion rate,* mg/(cm²)(day)			Transverse rupture stress, psi	Electrical resistivity, μohm-cm	Corrosion rate,* mg/(cm²)(day)		
Base	Addition	Transverse	Compressive		Santowax R at 350°C	Water vapor at 45°C	Dry air at 300°C			Santowax R at 350°C	Water vapor at 45°C	Dry air at 300°C
UC_2		12,000		102				6,500	125			
U_2C_3		17,000		55				15,000	45			
U_2C_3	5 Cr_3C_2	28,000	62,000	100	0.92	D		9,000		2.67	D	D
	10 Cr_3C_2	13,000	98,000	150	3.36			11,000	125	3.19	D	
	5 Mo_2C	37,000	108,000	80	+0.011			25,000	85	+0.013	0.68	
	10 Mo_2C	19,000	93,000	92	3.06			16,000	95	5.11		
	5 NbC	14,000	112,000		+0.013	1.38	59.5	22,000	80	+0.013	0.075	
	10 NbC	15,000	138,000	113	3.04			21,000	96	3.44	14.4	
	5 TaC	24,000	94,000	76	0.009			14,000	78	4.68	D	
	5 TiC	22,000	43,000	60	0.003			15,000	54	1.38	4.17	
	10 TiC	43,000	122,000		5.48	0.19	0.0	23,000	55	2.31	1.74	
	5 VC	8,000	42,000	84	1.11			17,000		5.95	33.0	2.77
	10 VC				0.39					8.22	0.11	
	5 WC	17,000	68,000	66	0.513			16,000	67	0.535	1.0	
	10 WC	34,000	99,000	70	0.500			31,000	66	0.535	3.29	
	5 ZrC	27,000	109,000		1.53			19,000		74	0.49	
UC_2	5 Cr_3C_2		69,000		1.55			24,000	82	2.84	D	
	10 Cr_3C_2	1,600	29,000	115	2.30			7,000	125	D	D	
	5 Mo_2C	33,000	68,000	73	0.65			25,000	72	0.65	0.103	
	10 Mo_2C							23,000	115	2.68	11.1	
	5 NbC	34,000	79,000	76				30,000	74	0.35	0.074	
	10 NbC	23,000	94,000	82				16,000	110	0.673	1.72	
	5 TaC	42,000	140,000	88	0.82					0.88		
	10 TaC	23,000	112,000		2.33			36,000		9.16		
	5 TiC		36,000	67	1.15			21,000	63	0.49	D	
	10 TiC				+0.013			21,000	77	0.71	0.17	+0.82
	5 VC	32,000	134,000	74	2.50			29,000	71	2.88	18.2	
	10 VC	11,000	46,000	62	0.553			16,000	70	0.785	43.5	
	5 WC	33,000	87,000	78	0.548			29,000	82	0.706		
	10 WC	28,000	125,000	71	0.361			31,000	68	0.514	0.95	
	5 ZrC	16,000	68,000	91	+0.012			18,000	80	1.41		
	10 ZrC	26,000	92,000	101	0.523			20,000	90	0.745	52.6	
U_2C_3	5 Fe	23,000		140	0.289	D		40,000		0.460		
	5 Mo	26,000	48,000	82	0.361			20,000	86	0.294	34.7	
	5 Nb	6,000	90,000	95	0.278			29,000	82	0.285	6.10	
	5 Ni									0.061	D	
	5 V		67,000		0.267	D		21,000	57	0.592	D	
	5 W	23,000	93,000	70	0.475			23,000	170	0.139	1.11	
	5 Zr	25,000	62,000		1.600	D		6,000		0.855	D	
UC_2	5 Cr							26,000	85	0.640	4.42	D
	5 Fe		38,000		0.448			12,000	124	0.555	D	
	5 Mo		88,000		0.395			23,000	80	0.540	0.209	
	5 Nb	26,000	76,000	73	0.508			19,000	76	0.438	7.00	
	5 Ni	8,000	27,000	143	0.664			19,000	271	0.824	1.31	
	5 Ta		70,000	85	0.560	D		7,000	78	0.608	D	
	5 Ti	18,000		62	0.336			21,000	59	0.376	D	D
	5 V	32,000	06,000	69	0.385	0.23		11,000	93	0.612	0.23	
	5 W	35,000	45,000	77	0.558			31,000	76	0.612	+0.02	
	5 Zr	31,000	62,000	88	0.418	0.284		22,000	80	0.447	42.7	

*D = complete disintegration of specimen.

fuels for the sodium graphite reactor, the monocarbide, mononitride, silicides, boride, phosphide, sulfide, and aluminide of uranium appear most promising.

Plutonium compounds are being investigated at Hanford.[32,60] The stability of PuO_2 in hydrogen at 1500°C was found to be influenced by the oxalate calcining treatment. For calcining temperatures above 500°C, Pu_2O_3 is produced during subsequent hydrogen anneal. Melting PuO_2 in helium, vacuum, or argon resulted in a high-lattice-parameter material, suggesting some decomposition. However, no suboxides were detected by X-ray diffraction analysis. The reactions between PuO_2 and MgO, Al_2O_3, ZrO_2, and stabilized ZrO_2 are being studied. There was no reaction observed between PuO_2 and MgO in 8 hr at 1500°C in hydrogen or helium. In the case of Al_2O_3 and PuO_2, an as yet unidentified reaction occurred. An addition of PuO_2 to ZrO_2 provided dimensional stability to ZrO_2-rich bodies. Reacting PuO_2 with carbon at 1575°C yields Pu_2C_3. The reaction is slow and is believed to proceed by first decomposing PuO_2 to Pu_2O_3 and then reacting with carbon. PuC was obtained by carbon reduction of PuH_3 in vacuum at 1450°C. (D. A. Vaughan)

Fabrication of Ceramic Fuels Other Than Uranium Oxides

The widespread interest in UC as a nuclear fuel continues to be evident from the number of investigators studying methods of preparation and fabrication (references 24, 55, 56, and 61). Oxygen contamination can occur at any of the stages in the operations and is one of the most troublesome aspects of fabricating not only the carbide but other nonoxide uranium fuel compounds. In addition to the common precautions of using inert-atmosphere glove boxes and protection during the handling of materials outside the glove box, sintering conditions have been found to be important. Sintering in vacuum up to 1000°C, followed by sintering to higher temperatures in argon, gives better results than either atmosphere alone.[55] A convenient source of information on the fabrication of UC is provided by a recent review[52] that covers the thermodynamic data relative to UC preparation, the various preparation methods that have been studied, the various fabricating methods available, and handling and storage precautions.

In continued work on fabricating UN, it was found that the commonly used step of denitriding uranium sesquinitride in a vacuum furnace to form the mononitride could be simplified by denitriding in an argon atmosphere[61] at 1450°C. Oxygen pickup during the transfer from the nitriding to the vacuum furnace was avoided in this way.

Studies[61] of the preparation of U_3Si_2 revealed that the compound could be prepared by heating a stoichiometric mixture of the elements contained in a magnesia crucible to 1550°C in an argon atmosphere. The reaction mixture was allowed to cool in the furnace without quenching. The stoichiometric mixture resulted in a slight excess of uncombined silicon in the product. The effects of adding excess uranium to the original reaction mixture or to the reaction product prior to fabrication are under study.[62]

Additional studies of the preparation and fabrication of PuC were reported.[24,63] Methods of controlling the composition and achieving high density have not yet been developed.

(M. J. Snyder)

Basic Studies of Irradiation Effects in Fuel Materials

Metallic Fuels

Excessive anisotropic growth of textured zirconium-rich zirconium-uranium alloys has been observed[64] during neutron irradiation; however, similar effects were not produced by neutron irradiation of textured zirconium-rich zirconium-boron alloys. Based upon theoretical consideration of the data obtained for both types of alloys, Knolls scientists propose that this anisotropic growth in zirconium-uranium is caused by anisotropic precipitation of point defects.

A number of studies are in progress at Hanford[36] directed toward an understanding of the swelling process in the irradiation of uranium. Some of the observations of one aspect of this work (the study of pore size and distribution of gas bubbles in irradiated uranium) are given below. A rod specimen irradiated to 0.25 at.% burnup at an estimated center temperature of 450°C was sectioned into transverse wafers that were annealed for 100 hr at 880°C and then furnace cooled. The following observations were made: (1) in the as-irradiated condition, pores

in the center are larger than those near the periphery; (2) in the as-irradiated condition, the beta-heat-treated structure has been replaced by a strained structure which appears more pronounced at the periphery; (3) the annealing greatly enlarged the pores in the peripheral regions but only slightly in the center; and (4) the annealing, involving phase transformtion, resulted in cracking of the specimen near the core.

Studies of the elongation of hot uranium and of copper in corrosion media (air, nitrogen, and CO_2) have been made by Russian scientists.[65] A mechanism is proposed to explain the dependence of elongation upon temperature, pressure, rod diameter, and surface oxidation.

(F. A. Rough)

Nonmetallic Fuels

Postirradiation studies on fission rare-gas diffusion are continuing at Battelle.[42,56] Xenon-133 diffuses from single crystals of UO_2 with diffusion coefficients between about 1×10^{-19} cm^2/sec at 1200°C and 1×10^{-16} cm^2/sec at 1400°C. Supplementary experiments have shown that, under out-of-pile conditions, iodine diffuses from a surrounding atmosphere into UO_2 with diffusion coefficients between 1.2×10^{-10} cm^2/sec at 1000°C and 4.6×10^{-10} cm^2/sec at 1200°C.

The subject of fission rare-gas reentry into UO_2 under irradiation has been considered at Chalk River.[66] A discussion was presented, relating to possible effects of the diffusion, fission recoil, and knock-on mechanisms on the release and reentry of fission gases. Reliable data to test the hypotheses are still limited. Experiments are in progress at Hanford[32,36] on effects of thermal-neutron irradiation on UO_2 and ThO_2 microstructures and crystal structures. In the exposure range 2.3×10^{16} to 4.4×10^{19} nvt, electron diffraction patterns for UO_2 broadened and became more diffuse. Increasing exposure at 50°C transformed the originally fine-grained films to large-grained dendritic structures. No corresponding effects were observed in ThO_2 specimens. (F. A. Rough)

References

1. A. Robillard, Influence of Heat-Treatment in Beta and Gamma Phases on the Microscopic Structure of Uranium (in French), French Report CEA-1057, 1959.
2. G. Sergeyev and A. Kapstel'tsev, The Creep of Hot Rolled Uranium (Letter to the Editor), *At. Energ.*, 7(6): 558–560 (1959).
3. A. Bochvar et al., Deformation of Uranium Subjected Simultaneously to Thermal Cycles and Tensile Stresses, *At. Energ.*, 8(2): 112–116 (1960).
4. B. R. Butcher and D. Baverstock, The Effect of the Alpha/Beta Phase Transformation on the Preferred Orientation of Alpha Uranium, British Report AERE-R-3217, January 1960.
5. W. R. McDonell, Quantitative Correlation of Irradiation Growth with Preferred Orientation in Uranium, USAEC Report DP-420, E. I. du Pont de Nemours & Company, Inc., May 1960.
6. D. Shaw et al., United Kingdom Atomic Energy Authority, Development and Engineering Group, Sept. 21, 1959. (Unpublished)
7. D. L. Gray, Release of Inert Gases from Irradiated Uranium, a Review of Literature, USAEC Report HW-62639, Hanford Atomic Products Operation, January 1960.
8. Israel Atomic Energy Commission, Literature Survey on Aqueous Corrosion of Uranium and Its Alloys, Its Mechanism, and Its Prevention in Nuclear Reactors, Report LS-40, May 1959.
9. Israel Atomic Energy Commission, Literature Survey on Grain Size in Uranium, Report LS-59, July 1959.
10. Israel Atomic Energy Commission, Literature Survey on Gamma to Beta and Beta to Alpha Phase Transformations in Uranium, Report LS-60, July 1959.
11. V. Lyashenko and V. Bykov, A Study of Uranium-Germanium Alloys (Letter to the Editor), *At. Energ.*, 8(2): 146–148 (1960).
12. J. Lehmann, A Study of Phase Transformation Processes in Uranium–0.5 to 4 wt.% Molybdenum Alloys (in French), French Report CEA-1261, June 9, 1959.
13. J. Lehmann, Characteristics of a Martensitic Phase Obtained in Uranium-Molybdenum Alloys (in French), French Report CEA-1206, April 1959.
14. Advanced Technology Laboratories, Division of American-Standard, Development of Metallic Uranium Fuel Elements of Improved Irradiation Stability, USAEC Report ATL-A-104, Dec. 14, 1959.
15. J. H. Kittel and K. F. Smith, Effects of Irradiation on Some Corrosion-Resistant Fuel Alloys, USAEC Report ANL-5640, Argonne National Laboratory, May 1960.
16. J. L. Ballif et al., Engineering Evaluation of a Mixed Alloy Fuel Element Irradiated at Elevated Temperature in the SRE, USAEC Report NAA-SR-3888, Atomics International, June 1, 1960.
17. G. Cabane, Uranium Alloys with High Amounts of Addition, French Report CEA-1275, 1959.
18. M. J. Brabers, Corrosion Constants of Alloys

with Uranium Base: Parts I and II, *Atoomenergie Haar Toepassingen*, 2: 1–7, 17–20 (January 1960).

19. G. Cabane and G. Donzé, Stabilization of the Gamma Phase in Ternary Alloys with Molybdenum-Uranium Base, *J. Nuclear Materials*, 1: 364–373 (December 1959).
20. N. R. Koenig and B. A. Webb, Properties of Ceramic and Cermet Fuels for Sodium Graphite Reactors, USAEC Report NAA-SR-3880, Atomics International, June 30, 1960.
21. Excerpts from Monthly Progress Reports of LASL, September 1959; UCLRL, September 1959; Mound Laboratory, September 1959; and Hanford Atomic Products Operation, September 1959, USAEC Report WASH-933, May 1960. (Classified)
22. H. Mikăiloff, Study of Transformation by Annealing of the Body-Centered Cubic Gamma Phase of Uranium-Molybdenum Alloys, French Report CEA-1270, June 23, 1959.
23. G. Donzé, X-Ray Diffraction Study of the Gamma Prime Phase Formation in Uranium-Molybdenum Alloys, AEC Translation AEC-tr-4241, 1959.
24. Argonne National Laboratory, Annual Report for 1959, Metallurgy Division, USAEC Report ANL-6099.
25. Martin Co., Nuclear Div., Liquid Fluidized Bed Reactor Study, Second Quarterly Progress Report, USAEC Report MND-LFBR-2304, May 1960.
26. R. S. Neymark, Rate of Alloying of Uranium Alloys with Stainless Steel; Part I, 1800 to 2300°F, USAEC Report NAA-SR-3278, Atomics International, June 1, 1960.
27. R. S. Neymark, Compatibility of Uranium–10 Wt.% Molybdenum with 304 Stainless Steel at 1000°F, USAEC Report NAA-SR-Memo-4943, Atomics International, Feb. 3, 1960.
28. R. H. Davidson, Production of Fission Gas in Uranium–10 Wt.% Molybdenum Fuel Rods, USAEC Report NAA-SR-Memo-3657, Atomics International, Apr. 3, 1959.
29. W. C. Thurber and C. J. McHargue, Deformation Textures on Aluminum-Uranium Alloys, *Trans. Met. Soc. AIME*, 218: 141–144 (February 1960).
30. R. W. Dayton and C. R. Tipton, Jr., Progress Relating to Civilian Applications During March 1960, USAEC Report BMI-1430, Battelle Memorial Institute, Apr. 1, 1960. (Classified)
31. Ames Laboratory, Annual Summary Research Report in Metallurgy for July 1958–June 1959, USAEC Report IS-17, November 1959.
32. F. W. Albaugh, Reactor and Fuels Research and Development Operation Monthly Report for March 1960, USAEC Report HW-64580-A, Hanford Atomic Products Operation, Apr. 15, 1960. (Classified)
33. M. D. Smith and R. W. K. Honeycombe, The Effect of Oxygen, Carbon, and Nitrogen on the Properties of Sintered Thorium, *J. Nuclear Materials*, 1: 345–355 (December 1959).
34. D. J. Livesey, The Variation with Temperature of Young's Modulus for Some Uranium Alloys and for Thorium, Vanadium, and Niobium, *J. Inst. Metals*, 88: 144 (November 1959).
35. D. S. Kneppel, Aqueous Corrosion of Thorium Alloys and Zircaloy-Clad Thorium Alloys, USAEC Report NMI-1226, Nuclear Metals, Inc., Mar. 22, 1960.
36. Hanford Atomic Products Operation, Fuels Development Operation Quarterly Progress Report for April to June 1959, USAEC Report HW-62085, July 15, 1959. (Classified)
37. W. D. Valovage and R. A. Siergiej, Mechanical Properties of Stainless Steel–UO_2 Dispersion Fuel Elements, USAEC Report KAPL-1590, Knolls Atomic Power Laboratory, July 7, 1959.
38. R. H. Baskey, Monthly Progress Report No. 7 for the Period December 1 to December 31, 1959, USAEC Report ORO-246, Clevite Corp., Jan. 7, 1960.
39. R. H. Baskey, Monthly Progress Report No. 8 for the Period January 1 to January 31, 1960, USAEC Report ORO-247, Clevite Corp., Feb. 12, 1960.
40. W. Arbiter, The Preparation and Properties of Dispersion Hardened Uranium Powder Products, Quarterly Technical Report for the Period Ending June 30, 1959, USAEC Report NDA-2112-2, Nuclear Development Corp. of America, July 15, 1959.
41. W. Arbiter, The Preparation and Properties of Dispersion Hardened Uranium Powder Products, Quarterly Technical Report for the Period Ending September 30, 1959, USAEC Report NDA-2112-4, Nuclear Development Corp. of America, Oct. 15, 1959.
42. R. W. Dayton and C. R. Tipton, Jr., Progress Relating to Civilian Applications During May 1960, USAEC Report BMI-1442, Battelle Memorial Institute, June 1, 1960. (Classified)
43. R. H. Baskey, Fuel-Bearing Fiberglas in Aluminum-Base Fuel Elements, Monthly Progress Letter No. 10, March 1 to March 31, 1960, Clevite Corp., Apr. 14, 1960.
44. R. H. Baskey, Fuel-Bearing Fiberglas in Aluminum-Base Fuel Elements, Third Quarterly Progress Report, November 1, 1959, to January 31, 1960, USAEC Report ORO-273, Clevite Corp., Feb. 15, 1960.
45. A. B. Auskern, The Diffusion of Kr^{85} from Uranium Dioxide Powder, USAEC Report WAPD-TM-185, Westinghouse Electric Corp., Bettis Atomic Power Laboratory, February 1960.
46. J. D. Eichenberg et al., Irradiation of UO_2 Fuel Rods: The X-1-L Experiment, USAEC Report WAPD-208, Westinghouse Electric Corp., Bettis Atomic Power Laboratory, April 1960.
47. J. J. Garlyer et al., Uranium Dioxide Compatibility with Refractory Metals, Carbides, Borides, Nitrides, and Oxides Between 3500 and 5000°F,

Report NASA-TN-D-262, National Aeronautics and Space Administration, February 1960.

48. H. S. Parker et al., Fundamental Study of Stable Ceramic Materials, Quarterly Progress Report for October–December 1959, USAEC Report NBS-D-140, National Bureau of Standards, May 23, 1960. (Classified)
49. K. Langrod, Sintering of Uranium Oxide in the Range of 1200–1300°C, *Bull. Am. Ceram. Soc.*, 39(7): 366–369 (July 1960).
50. T. D. Chikalla, Sintering Studies on the System UO_2-PuO_2; Part II, Sinterability, USAEC Report HW-63081, Hanford Atomic Products Operation, Dec. 17, 1959.
51. Louis Silverman, The High Temperature Chemical Reactivities of the Uranium Carbides, USAEC Report NAA-SR-Memo-4269(Rev. 1), Atomics International, Aug. 19, 1959.
52. F. A. Rough and Walston Chubb, An Evaluation of Data on Nuclear Carbides, USAEC Report BMI-1441, Battelle Memorial Institute, May 31, 1960.
53. L. Brewer, Heat-Transfer Fluids for Fuel-Element Cans, USAEC Report AECU-4537, General Atomic Div., General Dynamics Corp., Aug. 4, 1959.
54. Battelle Memorial Institute, Progress in Carbide Fuels (Notes from the Second AEC Uranium Carbide Meeting, held at Battelle Memorial Institute, March 22 and 23, 1960), USAEC Report TID-7589, Apr. 20, 1960.
55. J. J. Finley et al., Columbium-Clad Uranium Carbide Fuel-Element Contract, USAEC Report ORO-266, Union Carbide Metals Co., May 20, 1960.
56. R. W. Dayton and C. R. Tipton, Jr. Progress Relating to Civilian Applications During April 1960, USAEC Report BMI-1434, Battelle Memorial Institute, May 1. 1960. (Classified)
57. W. B. Wilson, High-Temperature X-Ray Investigation of the Uranium-Carbon System, *J. Am. Ceram. Soc.*, 43: 77–81 (February 1960).
58. J. Williams et al., The Variation of Unit Cell-Edge of Uranium Monocarbide in Arc-Melted Uranium-Carbon Alloys, British Report AERE-M-625, February 1960.
59. H. Pearlman, Effects of Radiation on Massive Uranium Monocarbide, USAEC Report NAA-SR-Memo-4631, Atomics International. Dec. 1, 1959.
60. F. W. Albaugh, Reactor and Fuels Research and Development Operation Monthly Report for May 1960, USAEC Report HW-65459-A, Hanford Atomic Products Operation, June 15, 1960. (Classified)
61. K. M. Taylor et al., Synthesis and Fabrication of Refractory Uranium Compounds, USAEC Report ORO-264, Carborundum Co., Mar. 14, 1960.
62. K. M. Taylor et al., Synthesis and Fabrication of Refractory Uranium Compounds, Monthly Progress Report No. 8 for the Period April 1 to April 30, 1960, USAEC Report ORO-276, Carborundum Co., May 10, 1960.
63. J. M. Atwood and W. A. Snyder, Plutonium Recycle Program Annual Report for Fiscal Year 1959, USAEC Report HW-62000, Hanford Atomic Products Operation, Oct. 15, 1959.
64. Knolls Atomic Power Laboratory, Reactor Technology Report No. 12, Metallurgy, USAEC Report KAPL-2000-9, March 1960.
65. I. V. Batenin et al., The Growth of Uranium Rods in Corrosive Gas, *At. Energ.*, 7: 329–332 (October 1959).
66. W. B. Lewis, The Return of Escaped Fission-Product Gases to UO_2, Canadian Report DM-58 (AECL-964), Jan. 21, 1960.

Section III

MODERATOR MATERIALS

Beryllium Metal and Alloys

Most of the present research on beryllium is directed toward overcoming its brittleness at room temperature. This low-temperature brittleness presents the most obvious hindrance to more extended use of the metal as a material of construction. Lagerberg[1] summarized the present views on the brittleness of beryllium in these words:

1. Fracture of single crystals is facilitated by comparatively high slip resistance in combination with limited numbers of deformation modes.
2. The slip resistance may be inherent or caused by impurities. Comparison with deformation modes in other hexagonal metals in relation to the *c/a* ratio gives no information on this point. It is not unlikely that dissolved oxygen gives a slip resistance.
3. Fine-grained metal with suitable texture exhibits ductility in certain directions but will not be able to withstand complicated stress systems.
4. Alloying appears to improve tensile strength in general, whereas ductility remains unchanged or is reduced.
5. It remains to be proved whether the low Poisson's ratio of beryllium is indicative of inherent brittleness.

Refining, Melting, and Casting of Beryllium

Preliminary tests at the Bureau of Mines[2] have demonstrated the possibility of electrorefining beryllium in molten KCl-LiCl-$BeCl_2$ baths. The procedure offers an encouraging route for recovery and purification of beryllium scrap and possibly for production of high-purity metal.

Improvement in the cast structure and improved machinability of the cast beryllium, in comparison with induction-melted vacuum-cast materials, was reported[3] for beryllium melted in an electron-beam furnace. Three-inch-diameter ingots were produced successfully. With a consolidation melt and two remelts, the average vaporization loss was 11.5 per cent per ingot. However, these ingots did not show a significant increase in tensile strength or elongation, nor did they show a significant decrease in metallic impurities. Ingots prepared from Pechiney flake had lower hardness and superior crack-propagation characteristics than any others.

A study[4] of factors influencing grain size in castings was undertaken, and the findings were applied to the production of small beryllium ingots. Decrease in grain size could be obtained by vibration of the mold during casting, when the power input was sufficiently great, and by the addition of certain inoculants, but these means were not additive. Addition of small amounts of rust-colored tantalum nitride (TaN_x), WC, or TiB_2 appeared to nucleate new grains in solidifying beryllium. The addition of 1 at.% germanium prevented the formation of heavy oxide films, significantly improved fluidity of the melt, and promoted finer grain size in the casting (possibly from nucleation induced by the BeO-coated mold wall).

In a similar study[5] it was found that rapid cooling will appreciably reduce the grain size of cast beryllium but that the structure this produces is still of the columnar type.

Ductile beryllium-silver alloys that could be reduced 50 per cent or more by cold rolling were vacuum cast from beryllium containing 1.0 and 1.2 per cent of impurities by adding 14 and 20 at.% of 99.99+ per cent pure silver. These alloys were induction melted in beryllia or alumina crucibles under a reduced pressure of argon. It was reported[6] that rapidly cooled mixtures of these materials consisted of globular beryllium particles in a ductile silver ma-

trix. During rolling, the primary beryllium particles underwent considerable deformation.

Fabrication of Beryllium

The techniques used in Great Britain for hot pressing beryllium and cermet powders, both bare and sheathed, are described in a recent publication.[7] The importance of selecting the proper die materials, lubricants, and temperatures is stressed.

Continued effort at Norair[8] to extrude bare beryllium Z-1 channels from QMV beryllium resulted in the production of an acceptable 14-ft-long extrusion. Salt-bath heating adequately protected the bare beryllium from oxidation, but the problem of a satisfactory extrusion lubricant remains to be solved. Seagle and Bertea[9] reported that extruded and annealed beryllium from electron-beam-melted ingots showed appreciable ductility, both at room temperature and at 400°C, when the rate of melting was slow.

Two reports have become available on The Martin Company's work on structural beryllium. Muvdi writes[10] that hot upsetting was chosen as the most economical process that would yield optimum properties and a good surface finish after making a comparison of beryllium sheet fabricated by five methods. With an upset reduction ratio of 6 : 1, the tensile strength of the sheet produced was about 71,000 psi, and the fatigue strength at 10^7 cycles was approximately 45 per cent of this. The material exhibited appreciable plastic deformation even under biaxial stress conditions. A more complete and detailed report[11] of the process was released by the Air Force. Hot upsetting is a forging process that produces a crystallographic orientation intermediate to the isotropic hot-pressed beryllium and the anisotropic highly worked forms. The structural properties of beryllium sheet made in this way were evaluated by construction of a box beam which was subjected to static, dynamic, and creep tests.

In order to carry out a thorough investigation of beryllium as a capsule material,[12] beryllium tubing was ordered by Oak Ridge from the following vendors: the Pechiney Company of France; the Brush Beryllium Company, who will prepare tubing by four different methods; the Chesterfield Tube Company, Ltd., of Great Britain; and Sylvania-Corning Nuclear Corporation. Nuclear Metals, Inc., has begun a study on the effects of extrusion parameters. Superior Tube Company, American licensee of Chesterfield, will also supply tubes and information on the British process. Meanwhile, Oak Ridge reports that beryllium tubing machined from hot-pressed block by Brush Beryllium appears to have but few and very minor defects in comparison with the extruded tubing that was examined previously.

Joining of Beryllium

Experiments[12] were conducted to determine the suitability of electron-beam welding for the manufacture of beryllium tube-to-end cap joints. Good, leaktight joints were obtained on joining QMV to QMV, but an attempt to join a QMV plug to an extruded tube was unsuccessful.

Also under study[12] are brazing methods and brazing alloys. Preliminary melting-point determinations have been made, and base-metal-wettability tests have been conducted on 15 experimental precious-metal-base alloys. Six of the alloys with melting points between 1000 and 1150°C showed good wetting properties. Leaktight joints have been produced with two of the alloys. Alloys presently undergoing testing are 47 Ti–47 Zr–6 Be, 46 Ti–46 Zr–4 Be–4 V, 45 Ti–45 Zr–10 Fe, and 63 Ti–27 Fe–10 Mo. All these alloys flow well on beryllium without a flux.

Diffusion-bonding studies were continued at Oak Ridge. It was found that partial grain coalescence was obtained after 2 hr at 1100°C and that complete coalescence was obtained after 4 hr at 1100°C. Both types were leaktight. Joints made at 1000°C showed no coalescence and leaked; joints made at 1150°C usually were porous and leaked.[12]

Tests are in progress on the upset welding process developed in Great Britain as another method of joining beryllium caps and tubes.[12]

Brush Beryllium workers suggest[13] that the major factor in attaining high-quality fusion welds in beryllium appears to be the maintenance of a proper thermal equilibrium in the weld zone and that the most critical variable in attaining this is amperage. It appears advisable to use as low an amperage setting as possible. Studies of coated welding rods are in progress.

Physical and Mechanical Properties of Beryllium

The five independent elastic constants of beryllium were determined as a function of temperature with the pulse-echo technique at a frequency[14] of 10 Mc/sec. The values extrapolated to 0°K are $C_{11} = 29.94 \pm 0.06$, $C_{33} = 34.22 \pm 0.12$, $C_{44} = 16.62 \pm 0.05$, $C_{12} = 2.76 \pm 0.08$, $C_{13} = 1.1 \pm 0.05$, in units of 10^{11} dynes/cm^2. Voight averaging and Reuss averaging of the single-crystal elastic constants give excellent agreement because of the small magnitude of the nondiagonal elements, C_{12} and C_{13}. The average data compare favorably with previous data from polycrystalline beryllium.

The lattice parameters of a single crystal of beryllium were determined from observations on a divergent-beam transmission X-ray photograph of the crystal.[15] Diffraction in the crystal leads to a series of deficiency lines on the photographic plate, the geometry of which is determined by the lattice parameters of the crystal and the wavelength of the radiation, but is independent of the exact experimental arrangement. The values obtained were: $a = 2.2866 \pm 0.0006$ A, $c = 3.5833 \pm 0.0009$ A, and $c/a = 1.5671$.

A review of the literature on alloying and other structural modifications and their effect on mechanical properties of beryllium was prepared by Brush Beryllium.[16] Primary consideration was given to mechanical and physical properties of QMV beryllium (both sintered and wrought), beryllium-rich alloys, and structurally modified metal. The fabrication procedures were described, and the methods used to study preferred crystallographic orientation in wrought beryllium were discussed.

The Air Force has set up a new project[17] designed to evaluate the structural properties of beryllium sheet produced by three methods: hot upsetting, hot pressing, and hot pressing followed by bidirectional rolling. Testing will be conducted at room temperature, where the brittleness of beryllium is most critical. On another Air Force project,[18] charts were presented which show that an almost complete set of basic mechanical-property data either is available or is being developed for QMV block and that only biaxial data are missing for cross-rolled beryllium sheet. On the other hand, there are many areas in which basic mechanical properties are not yet available for unidirectionally rolled sheet, hot-upset sheet, and extrusions.

The Russians have produced beryllium metal of very high purity by redistillation of vacuum-cast material.[19] They extruded a vacuum-cast, attritioned, and sintered metal which had a tensile strength of about 28,000 psi at 425°C.

Wikle and Beaver[20] present data which indicate that the ultimate strength of hot-pressed beryllium decreases slowly from room temperature to 600°C and rapidly from there on. Ductility increases above room temperature to a peak at about 450°C and then rapidly decreases. Material that is more ductile at room temperature is also more ductile at the 450°C peak.

Low-load indentation hardness measurements are reported[21] to be markedly dependent on orientation and surface condition. Machining of the beryllium specimens produced a uniform surface layer with a diamond pyramid hardness (DPH) of 300 on both single-crystal and polycrystalline metal. After removal of 0.008 in. by etching, values of 230 DPH were found on the basal plane and 70 DPH on the prism plane of a single crystal. On polycrystalline sheet, large variations in hardness were found, the amount depending on the degree of preferred orientation; in all cases the maximum hardness corresponded to the greatest concentration of basal planes.

In thermal-cycling tests by workers at Oak Ridge,[12] specimens were annealed at 800°C for 2 hr, then heated through 80 thermal cycles at approximately 150°C per minute, and finally subjected to bend tests. A slight densification of the beryllium, especially of hot-pressed blocks, was noted. The cycling temperature ranges were 100 to 400°C, 400 to 700°C, 100 to 700°C, and 100 to 850°C. Tests were made on rod, block, unidirectionally rolled sheet, and cross-rolled sheet. The thermal cycling had no deleterious effect on the mechanical properties.

Canadian stress-rupture tests on beryllium at 400°C* indicated that the time to rupture increased from 47 hr at 30,030 psi to 1236 hr at 29,120 psi. A series of tests on Pechiney beryllium specimens at 620°C produced a plot of time to rupture against stress which was

* W. O. Bennett, Canadian Report AECL-1029, April 1960.

parallel to that obtained from Nuclear Metals' rod, but at a stress 200 to 400 psi lower. The point of inflection occurred at approximately 50 hr on both curves.

The effects of annealing in a vacuum at 900°C for 24 hr and cooling at 2°C per hour were investigated using specimens cut from Nuclear Metals' extruded rod. Although negligible ductility was shown at room temperature after this treatment, at 200 and 300°C remarkably high and consistent values of ductility were obtained. In one case, after annealing, a single peripheral grain appeared to form a continuous case around the specimen.

A burst test was made on a $\frac{1}{2}$-in.-diameter beryllium tube from the United Kingdom. At a temperature of 600°C and a gas pressure of 2400 psi, the whole tube shattered into fragments after approximately 5 min at pressure.

The elevated-temperature mechanical properties of beryllium were reported[22] to be enhanced by forming dispersed-phase alloys. The addition to beryllium of properly dispersed BeO in quantities of 2 to 3 per cent was equivalent to lowering the testing temperature 200° at 1000 to 1350°F. Similarly dispersed intermetallic compounds such as $FeBe_{11}$ resulted in a threefold increase in strength at 1350 to 1650°F when 1.5 to 3 per cent iron powder was blended with beryllium powder prior to fabrication. Tensile and stress-rupture properties of some of these materials were presented along with their oxidation characteristics in 1650°F air and their corrosion behavior in 600°F water relative to unalloyed beryllium.

Nuclear Metals reported[23] that some dispersion-strengthened systems of Be-BeO and Be-Be_2C were formed and tested at temperatures of 1200°F (648°C), 1350°F (732°C), and 1500°F (816°C). The results, presented in a way to permit convenient comparison of the various systems, are associated with certain characteristics of the dispersions. It was found that a 0.3 per cent carbon addition had little effect on rupture life, but a 0.85 per cent carbon addition appeared to increase it markedly. A 1 per cent carbon addition increased the rupture life by a factor of about 4 from 1200 to 1500°F. Oxide additions tended to agglomerate and were, in general, less effective than carbon additions in increasing rupture life. The creep rate at 1200°F decreased rapidly with increased carbon additions over the range of 0.2 to 1.2 per cent carbon.

During the study of grain size at Armour Research Foundation,[4] two thermal arrests were observed upon cooling unalloyed beryllium and all of the alloys except one. For unalloyed beryllium, the first thermal arrest was in the range from 1275 to 1285°C, and the second arrest was 5 to 10°C below the first. This finding, combined with several supporting observations, helps to confirm the previous observation of Martin and Moore[24] that beryllium solidifies in a body-centered cubic structure and then transforms to a close-packed hexagonal structure at 5 to 10°C below the solidification temperature.

Chemical and Thermal Properties of Beryllium

A study of the reactions of beryllium with CO_2 was reported by Oak Ridge.[12] Beryllium powder was held at 700°C for 500 hr at a CO_2 pressure of 1 μ Hg. The rate curve obtained was parabolic and flattened out after approximately 250 hr of exposure. After 500 hr the weight gain was about 0.1 mg/cm^2 of beryllium. X-ray diffraction analysis showed the powder to consist of beryllium and BeO.

The AEC was assigned a patent[25] that was issued to R. G. Townsend on a method of protectively coating beryllium metal. The process consists of etching the metal in acid, briefly immersing the etched beryllium in concentrated nitric acid, immersing in a second solution of sodium zincate, electroplating a thin layer of copper over the beryllium, and finally electroplating a layer of chromium over the copper.

Beryllium Technology

Three electron micrographs[26] showed how a single crystal of beryllium in a rolled polycrystalline sheet was broken up into subcrystalline domains, separated by barriers of dislocations. Numerous dislocations were also present in the subgrains. Another specimen, annealed 30 min at 800°C in a vacuum, showed that most of the dislocations had disappeared. However, a low-density band of dislocations showing a hexagonal pattern still remained. The specimens for these micrographs were prepared by a technique the authors had described previously[27] for producing films about 100 A thick from large polycrystalline samples.

An extensive review[28] of beryllium ores, the metallurgy of beryllium metal, beryllium ox-

ides, and powder metallurgy, with particular reference to nuclear applications, was published by the French. Los Alamos has issued a bibliography[29] that contains 230 references to report literature published between January 1954 and November 1959, describing the properties, metallurgy, and fabrication of beryllium.

(W. Hodge)

Solid Hydrides

Research on zirconium and yttrium hydrides predominates in this subject area, although some data have been published on lithium hydride and barium hydride. Hydrided alloys of zirconium offer promise of greater high-temperature stability for this material. Additional fueled moderator studies have been reported, together with data on hydrogen effects on Zircaloy.

Zirconium Hydride

The phase diagram of the zirconium-hydrogen system at compositions approaching ZrH_2 has been studied at Atomics International.[30] The boundaries of the two-phase beta plus delta hydride region and the single-phase delta hydride region were defined more precisely than in previous investigations. Figure 6 shows the isotherms that were found in the temperature range 550 to 850°C for these regions. A two-phase delta plus epsilon region was observed at room temperature but not at the high temperatures. At elevated temperatures a continuous second-order transition from the cubic delta phase to the tetragonal epsilon phase is postulated. Figure 7 presents these results as a modification of the zirconium-hydrogen phase diagram.

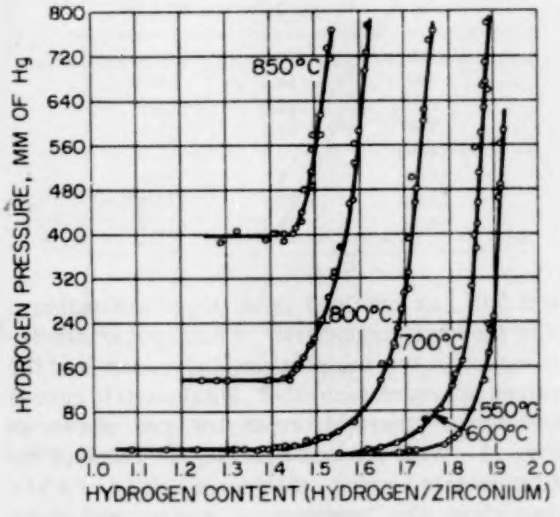

Figure 6 — Pressure-composition isotherms of the zirconium-hydrogen system.[30]

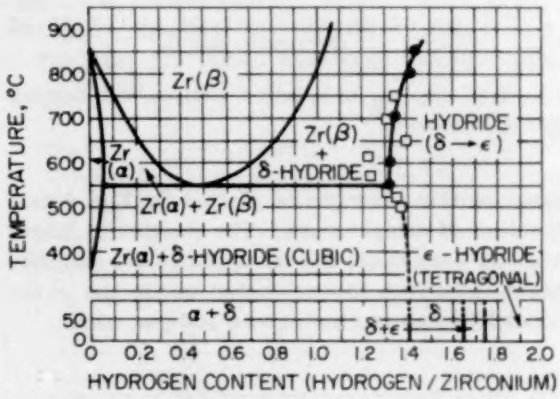

Figure 7 — Modified zirconium-hydrogen phase diagram.[30] □, La Grange et al. ●, Atomics International.

For concentrations of hydrogen in zirconium in the range 50 to 100 ppm, it was observed at General Electric[31] that the hydride phase forms in platelets. The hydride habit planes in zirconium were found to be $\{1\,1\,\bar{2}\,2\}$, $\{1\,0\,\bar{1}\,2\}$, and $\{1\,1\,\bar{2}\,1\}$, which are observed twin planes in the metal. This observation agrees with the fact that precipitated hydride significantly reduces the impact strength of zirconium. Under high-strain-rate loading, the deformation mechanism of twinning becomes increasingly important, and, if hydride is present on the twin planes, cracking may be expected to initiate at the roots of the platelets where high stress concentrations must prevail.

Yttrium Hydride

The known properties of yttrium hydride have been summarized.[32] The density of the hydride as a function of the weight per cent hydrogen is given in Fig. 8. Some slight variations from this curve occur as a result of variations in density of the metal prior to hydriding.

The material is extremely brittle, and short-time tensile properties are very hard to obtain and to evaluate. The problem is further complicated by the fact that the brittle condition exists to temperatures above 2000°F. The ulti-

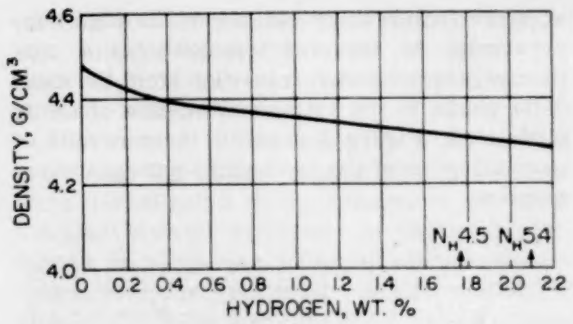

Figure 8— Density of hydrided yttrium with varying hydrogen content.[32]

mate tensile strength is plotted in Fig. 9 as a function of temperature. The scatter is large, and, on occasions, the variation in the data between identical pieces tested under the same conditions has run as high as 100 per cent.

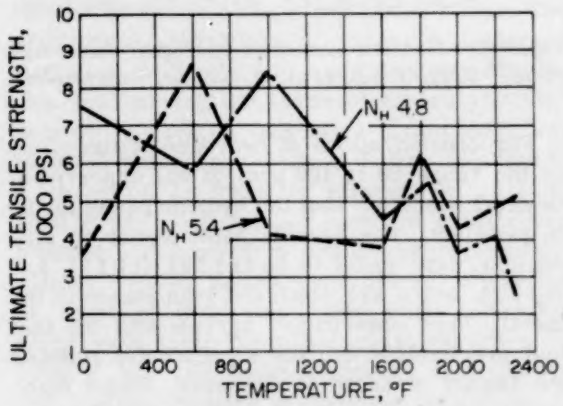

Figure 9— Ultimate tensile strength of hydrided yttrium.[32]

The hardness of yttrium metal is 100 DPH, and the value increases steadily as hydrogen is introduced, until at an N_H of 6 a hardness of 300 DPH is reached. Figure 10 shows the effect of temperature on the hardness of yttrium hydride with an N_H of 4.8 and represents the best estimate from available data. Brittleness of the material also causes scatter in the penetration hardness values.

Creep-rupture data are also influenced by the brittleness of the material, and variations in the impurities in the yttrium metal are believed to cause inconsistencies in the results. Data indicate that the hydride changes very little in creep strength between room temperature and

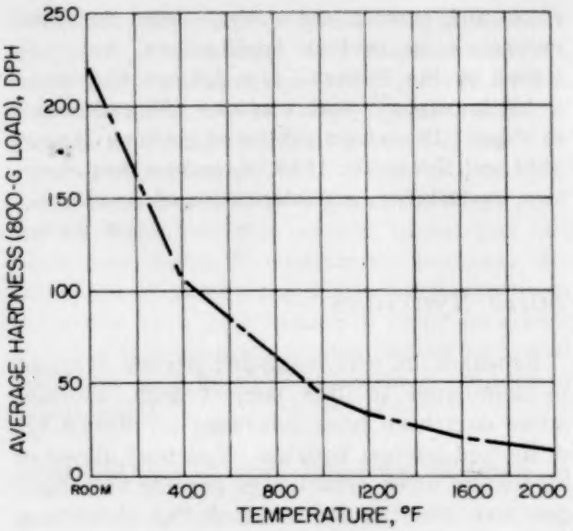

Figure 10— Effect of temperature on hardness of N_H 4.8 hydrided yttrium in argon atmosphere.[32]

2000°F. In general, it possesses good strength and very low ductility. A typical value is a creep rate of 0.005 per cent per hour at 1800°F and 4000 psi for hydride with an N_H of 5.4.

Table III-1 gives the thermal conductivities of hydride samples having N_H values of 4.22 and 5.01, as obtained in an argon atmosphere. The thermal conductivity of both materials decreases as the temperature increases, and the values approach each other. Dilatometric curves for linear thermal expansion are shown in Fig. 11. With yttrium hydride, the slope of the dilatometric curve changes considerably throughout the temperature range, and mean coefficients of expansion can only be specified in narrow temperature ranges.

Table III-1 THERMAL CONDUCTIVITIES OF HYDRIDED YTTRIUM[32]

(Material of N_H 4.22 and 5.01)

Temp., °F	Thermal conductivity, Btu/(hr)(ft)(°F)	
	N_H 5.01	N_H 4.22
200	16.7	34.4
400	14.2	28.8
600	12.0	23.5
800	10.2	18.8
1000	8.8	15.3
1200	8.0	12.9
1400	7.6	11.3
1600	7.3	10.4

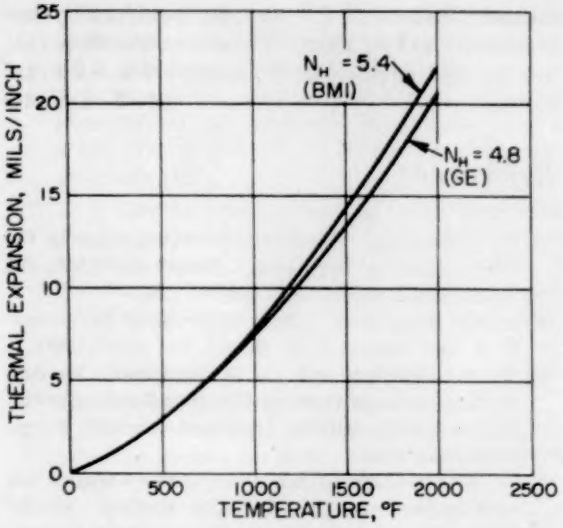

Figure 11—Dilatometric curves for hydrided yttrium.[32]

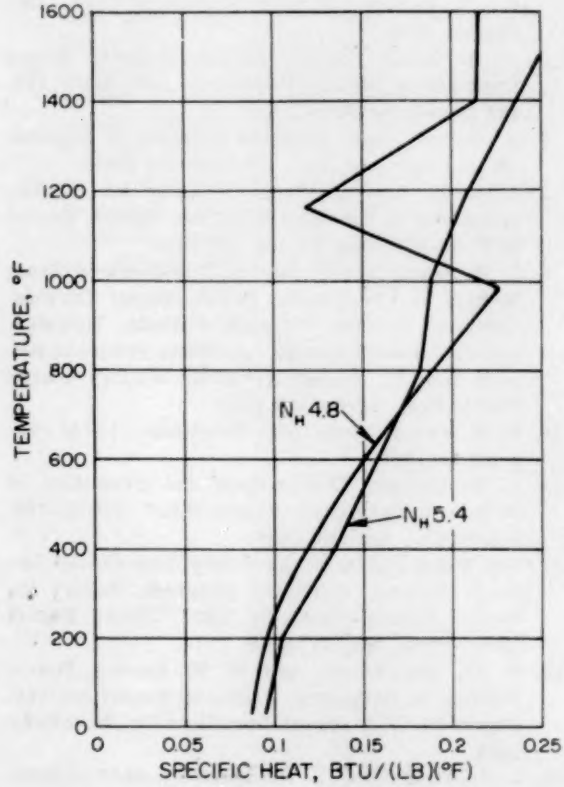

Figure 12—Specific heat versus temperature for hydrided yttrium.[32]

Specific heat measurements have given the only evidence for possible transformations in the yttrium hydride system. Figure 12 shows the instantaneous specific heat values as a function of temperature, and the possibility of a minor transformation is indicated between 600 and 1200°F. In the material with N_H of 4.8, a definite transformation is indicated between 1150 and 1250°F.

Both electrical resistivity and magnetic susceptibility have been examined as possible means for nondestructive determination of the hydrogen content of the hydride. As indicated in Fig. 13, the initial absorption of hydrogen

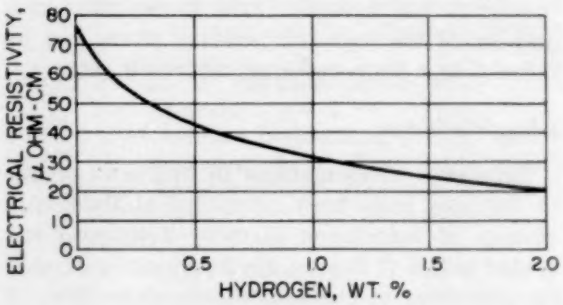

Figure 13—Effect of hydrogen content on electrical resistivity of yttrium.[32]

causes a large drop in resistivity, whereas at concentrations above 1 wt.% hydrogen the resistivity changes little. The magnetic susceptibility varies linearly with hydrogen content, as shown in Fig. 14. Results proved reproducible, with an accuracy of ±0.05 per cent.

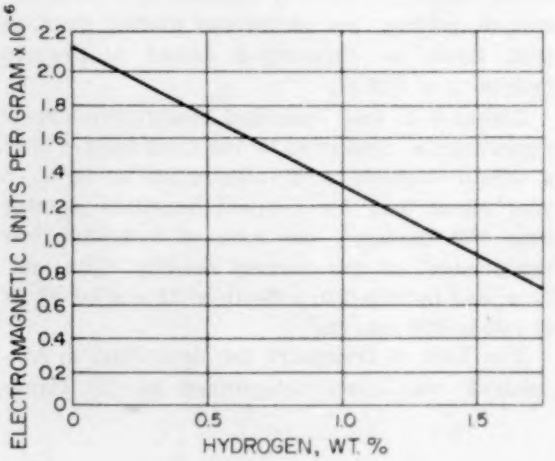

Figure 14—Effect of hydrogen on the magnetic properties of hydrided yttrium.[32]

Barium Hydride

Investigators at Iowa State[33] have studied the barium-hydrogen system and found that the solubility of hydrogen in barium increases from 8 mole % at 300°C to 67 mole % at 950°C. At 950°C the solid solution decomposes peritectically. Liquidus and solidus temperatures increase smoothly from the melting point of barium at 729°C, and extrapolation of the nearly linear liquidus curve indicates a melting point of 1215°C for barium hydride. A phase transformation in barium hydride was detected in the range 500 to 600°C. The X-ray diffraction pattern of the high-temperature phase can be indexed as a body-centered cubic unit cell.

Alloy Hydrides

Extensive investigations of hydrogen pickup in Zircaloy have been conducted at Hanford.[34] Studies of autoclaved Zircaloy-2 coupons hydrided at 500°C in pure dry hydrogen confirmed the proposed mechanism which states that, if the transport of hydrogen through the oxide film is slow, the hydrogen level in the sample builds up uniformly until the solubility limit is reached. At this point the precipitation of the zirconium hydride phase begins and breaks up the oxide surface, allowing rapid attack. However, if the entry of hydrogen at the metal surface is rapid, such as through a scratch in the oxide surface, severe local hydriding occurs. Vapor-blasted Zircaloy-2 surfaces appeared to hydride more readily than etched surfaces, especially at low partial pressures (0.1 mm) of water vapor. Anodizing seemed to reduce hydrogen pickup, but chromium plating over an iron flash on Zircaloy-2 failed to prevent hydriding at 500°C.

Zircaloy-2 was hydrided electrolytically in experiments conducted by the Canadians.* With a dilute sulfuric acid electrolyte at 80°C, it was found that, for current densities greater than 100 ma/cm^2, the rate of hydriding was independent of the current density. The surface was hydrided to a depth of 12 μ after 12 hr at 100 to 200 ma/cm^2.

The heat of transport for deuterium in Zircaloy-2 was also determined by the Canadians.* Values of 6.2 and 6.8 kcal/mole were measured in two runs. The corresponding values for hydrogen lie in the range 5.5 to 6.5 kcal/mole. (H. H. Krause)

* A. Sawatzky, Canadian Report AECL-1046, June 1960.

* A. Sawatzky, Canadian Report CRMet-910, March 1960.

References

1. G. Lagerberg, Metallurgical Viewpoints of the Brittleness of Beryllium, Report NP-8388, AB Atomenergi, Stockholm, Apr. 7, 1960.
2. M. M. Wong et al., Electrorefining of Beryllium, *U. S. Bur. Mines, Rept. Invest. No. 5581* (1960).
3. H. T. Sumsion and C. O. Matthews, Vacuum Melting of Beryllium by Electron Bombardment, Report LMSD-480485, Lockheed Aircraft Corp., December 1959.
4. F. A. Crossley et al., Beryllium Research for Development in the Area of Casting, Report WADC-TR-59-500, Armour Research Foundation, Illinois Institute of Technology, February 1960.
5. P. M. Cohen and R. C. Harris, Beryllium Casting, Phase II, Interim Technical Engineering Report No. 5, Report NP-8552, Beryllium Corp., December 1959.
6. J. B. Cohen, Ductile Beryllium-Silver Alloys Produced by Casting, *Trans. Met. Soc. AIME*, 218: 184 (February 1960).
7. A. Blainey, Hot Pressing Powders in England, *Metal Progr.*, 77: 104–108 (January 1960).
8. Northrop Aircraft Corp., Program for the Development of Extruded Beryllium Shapes, Report NOR-59-491, June 1–Aug. 31, 1959.
9. S. R. Seagle and O. Bertea, The Electron-Beam Melting of Beryllium, Boron, Boron Carbide, Tantalum Carbide, Titanium Carbide, Tungsten, and Zirconium Diboride, Quarterly Progress Report No. 7, Report NP-8279, Mallory-Sharon Metals Corp., February 1960.
10. B. B. Muvdi, Structural Beryllium, *ASTM Preprint 79* (1960).
11. C. J. Giezma, Development and Evaluation of Structural Beryllium, Report WADC-TR-59-349, Martin Co., Apr. 30, 1959.
12. Oak Ridge National Laboratory, Gas-Cooled Reactor Project Quarterly Progress Report for Period Ending March 31, 1960, USAEC Report ORNL-2929, June 21, 1960.
13. B. M. MacPherson and W. W. Beaver, Fusion Welding of Beryllium, Technical Report No. 161, Report NP-8626, Brush Beryllium Co., November 1959.
14. J. F. Smith and C. L. Arbogast, Elastic Constants of Single-Crystal Beryllium, *J. Appl. Phys.*, 31: 99–102 (January 1960).

15. D. R. Schwarzenberger, Accurate Determination of the Lattice Parameters of Beryllium, *Phil. Mag.*, 4(8): 1242–1246 (November 1959).
16. J. G. Klein et al., Development of Wrought Beryllium Alloys of Improved Properties, Report WADC-TR-58-478 (Pt. I), Brush Beryllium Co., February 1959.
17. C. J. Giemza, Evaluation of Structural Beryllium, Progress Report No. 1, Martin Co., Mar. 1, 1960.
18. R. F. Crawford, Monthly Progress Report on Structural Design Data for Beryllium, Report LMSD-312201-1, Lockheed Aircraft Corp., Mar. 8, 1960.
19. G. A. Meerson et al., Beryllium, *Soviet J. At. Energy*, 5(6): 1555–1562 (December 1958).
20. K. G. Wikle and W. W. Beaver, Elevated Temperature Properties of Beryllium, USAEC Report NYO-1114, Brush Beryllium Co., July 15, 1952.
21. N. A. Hill and J. W. S. Jones, The Crystallographic Dependence of Low Load Indentation Hardness in Beryllium, British Report AERE-R-3215, January 1960.
22. Metallurgy Information Meeting, Ames Laboratory, Iowa State College, May 2–4, 1956, USAEC Report TID-7526 (Pt. 7), Oct. 7, 1959.
23. J. Greenspan, Stress-Rupture Properties of Beryllium Containing Carbide and Oxide Dispersions, USAEC Report NMI-1227, Nuclear Metals, Inc., Mar. 23, 1960.
24. A. J. Martin and A. Moore, The Structure of Beryllium with Particular Reference to Temperatures Above 1200°C, *J. Less-Common Metals*, 1(2): 85–93 (April 1959).
25. Protect Beryllium with Electroplate, U. S. Patent 2,901,408, *Electronics*, 33(19): 91 (May 6, 1940).
26. A. Saulnier and P. Mirand, Electron Micrography of Films of Beryllium Reduced from Bulky Specimen—Demonstration of Substructure and Dislocations (in French), *Compt. rend.*, 250: 709 (Jan. 25, 1960).
27. P. Mirand and A. Saulnier, Rapid Method for the Preparation of Thin Metallic Films for Direct Examination with the Electron Microscope, *Compt. rend.*, 246: 1688 (March 1958).
28. Beryllium and Its Products in Industry (in French), *Métallurgie (Paris)*, 92: 19–26 (January 1960).
29. Helen J. Chick, comp., A Bibliography of Report Literature on Beryllium, USAEC Report LAMS-2382, Los Alamos Scientific Laboratory, Nov. 10, 1959.
30. G. G. Libowitz, The Zirconium-Hydrogen System at High Hydrogen Contents, USAEC Report NAA-SR-5015, Atomics International, June 30, 1960.
31. F. W. Kunz and A. E. Bibb, Habit Plane of Hydride Precipitation in Zirconium and Zirconium-Uranium, *Trans. Met. Soc. AIME*, 218: 133–135 (1960).
32. D. S. Parker, Properties of Hydrided Yttrium, USAEC Report APEX-558, General Electric Co., Aircraft Nuclear Propulsion Dept., May 1960.
33. Ames Laboratory, Annual Summary Research Report in Metallurgy for July 1958–June 1959, USAEC Report IS-17, November 1959.
34. F. W. Albaugh, Reactor and Fuels Research and Development Operation Monthly Report for April 1960, USAEC Report HW-64898-A, Hanford Atomic Products Operation, May 1960. (Classified)

Section IV

NUCLEAR POISONS

Rare-Earth Oxide and Boron Control Materials

Dysprosium oxide and dysprosia-based ceramics are being investigated at Knolls.[1] For the two-component systems, alumina, ceria, niobia, urania, and zirconia were blended with Dy_2O_3 and sintered at temperatures of 1600 to 1950°C, except for a few Dy_2O_3-Nb_2O_5 mixtures, which were sintered at temperatures as low as 800°C. Densities varied considerably, ranging from 60.5 per cent of theoretical for a Dy_2O_3-Nb_2O_5 pellet to 99.6 per cent of theoretical for a Dy_2O_3-UO_2 pellet. However, most of the samples were 80 per cent of the theoretical density or more. The following conclusions were reached:

1. Three compounds were observed in the Dy_2O_3-Al_2O_5 system. These appeared in the following molar ratios: the first at 1 : 2, the second at 1 : 1, and the third at 3 : 1.

2. The Dy_2O_3-CeO_2 system had wide solid solubility, no compound formation, and a single sold-solution range extending from 10 to 40 vol.% Dy_2O_3.

3. In the Dy_2O_3-Nb_2O_5 system, one compound, $DyNbO_4$, was observed with undetermined structure, a melting point of 1950°C, and a true density of 5.493 g/cm^3. There was partial solubility of the compound in Dy_2O_3.

4. The Dy_2O_3-UO_2 system had wide solid solubility, and no compound formation was observed. A single face-centered cubic solid-solution range extended up to 70 wt.% Dy_2O_3.

5. The Dy_2O_3-ZrO_2 system had wide solid solubility, and no compound formations were noted. The compositions were one-phase face-centered cubic solid solutions between the limits of 10 to 60 vol.% Dy_2O_3. Below 10 vol.% Dy_2O_3, monoclinic ZrO_2 was found as a second phase; whereas, above 60 vol.% Dy_2O_3, dysprosia solid solution was present as a second phase.

Curves for the thermal expansions of the dysprosia ceramics are shown in Fig. 15. Some

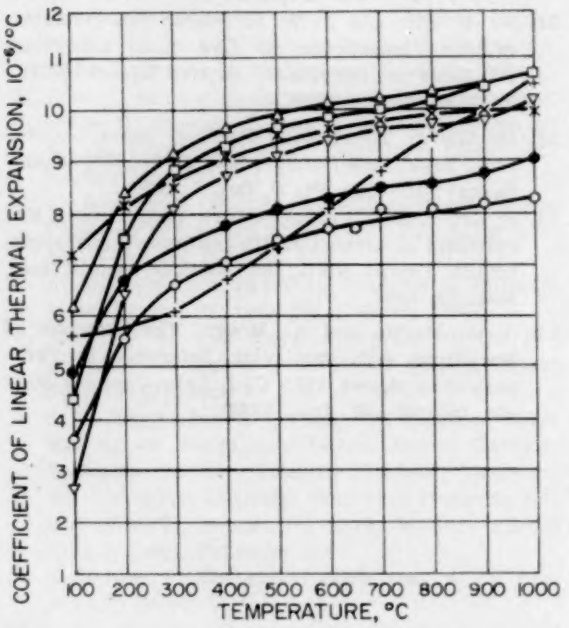

Figure 15 — Thermal-expansion curves for seven dysprosium oxide compositions.[1] Δ, 5 wt.% Dy_2O_3–95 wt.% UO_2. □, 10 vol.% Dy_2O_3–90 vol.% ZrO_2. ×, $Dy_2O_3 \cdot Nb_2O_5$. ∇, 50 vol.% Dy_2O_3–50 vol.% ZrO_2. ●, 50 vol.% Dy_2O_3–50 vol.% CeO_2. ○, $Dy_2O_3 \cdot 2Al_2O_3$. +, 50 wt.% Dy_2O_3–50 wt.% UO_2.

data on the resistance to boiling water are shown in Table IV-1.

Some well-executed and long-needed thermodynamic studies on refractory borides are being conducted at Los Alamos.[2] Leitnaker has used the Knudsen effusion method to determine vapor pressure and calculated thermodynamic

Table IV-1 BOILING-WATER CORROSION TESTS* ON DYSPROSIA-BASED COMPOSITIONS[1]

Composition	Vol.%	Wt.%	Weight change, mg	Dimensional change, mils	
				Length	Diameter
Dy_2O_3-UO_2		5 95	+1.2	−0.1	+0.1
Dy_2O_3-UO_2		50 50	+10.8	−0.1	None
Dy_2O_3-CeO_2	50 50		−2.1	−0.2	−0.7
Dy_2O_3-ZrO_2	50 50		+3.5	−0.3	+0.9
Dy_2O_3-ZrO_2	10 90		+0.1	−0.1	−0.4
$Dy_2O_3 \cdot 2Al_2O_3$			None	None	−0.2
$Dy_2O_3 \cdot Nb_2O_5$			−2.6	None	−0.3

*200-hr test at atmospheric pressure with deionized water, *p*H 6.4; resistivity, 2.5 megohms; *p*H after 200 hr, 7.65.

functions of zirconium diboride. It is interesting to note that he used a tungsten crucible which was compatible with the ZrB_2 at temperatures to 2475°K (~2200°C). Tantalum reacted with the ZrB_2. Leitnaker also observed that water vapor or oxygen will react with ZrB_2 in the temperature range studied (1875 to 2200°C) even at pressures of 10^{-10} atm. Vapor pressures as measured were quite low, e.g., a value of 1.721×10^{-10} atm was obtained for zirconium at 2000°K (1723°C). Some work was also carried out to determine the tantalum-boron phase diagram in the range 0 to 50 at.% boron. The melting point of TaB is estimated to be in excess of 2800°C and that of Ta_3B_2 as 2180°C. The phase Ta_2B is not stable below 2040°C. (G. W. Cunningham)

References

1. Knolls Atomic Power Laboratory, Reactor Technology Report No. 12, Metallurgy, USAEC Report KAPL-2000-9, March 1960.
2. J. M. Leitnaker, Thermodynamic Properties of Refractory Borides, USAEC Report LA-2402, Los Alamos Scientific Laboratory, January 1960.

Section V

CLADDING AND STRUCTURAL MATERIALS

Corrosion

Niobium Corrosion

The transition from parabolic oxidation behavior to linear behavior, which is associated with breakdown of the protective oxide film, has been shown by Oak Ridge[1] to be strongly dependent on the crystallographic orientation of niobium. Oxidation experiments at 400 and 425°C on single-crystal spheres of niobium revealed that oxidation proceeds slower around the (1 0 0) poles than at other orientations. Additional studies showed that the period of protective oxidation was relatively long for specimens of (1 0 0) orientation, whereas specimens of (1 1 0) and (1 1 1) orientation exhibited nonprotective (linear) oxidation after much shorter times.

A second study[2] has shown that several reactions are involved in the successive stages of low-pressure oxidation at 850 to 1200°C. At oxygen pressures of 10^{-5} to 10^{-4} mm, oxygen dissolves in the metal and the reaction behavior is linear, changing to parabolic as diffusion into the metal becomes rate controlling. After saturation of the metal surface with oxygen occurs, intergranular NbO forms and the reaction kinetics become linear. The kinetics then change to parabolic as NbO_2 forms on the surface. At about 10^{-3} mm oxygen pressure, porous Nb_2O_5 forms on top of the adherent NbO_2 and the reaction again becomes linear. The parabolic-to-linear transition as porous Nb_2O_5 forms is the same transition observed at about 400°C in air.

The ignition temperature of niobium in flowing air was determined at General Electric[3] as 1470°C. This is slightly higher than the 1400°C value previously found[4] for ignition in 1 atm oxygen. Coatings may raise the ignition temperature by several hundred degrees.

The reaction of niobium with CO and CO_2 has been shown by General Dynamics[5] to result in contamination hardening of the metal and formation of a carbide case. At 820 to 930°C, carbide formation occurred during 100- to 500-hr exposures in 10^{-4} atm ($CO + 2CO_2$), in 1 atm (helium + 1 vol.% CO), and in 1 atm CO. The weight gains increased as titanium or zirconium was added to the niobium. Carbon monoxide apparently dissociates on reaction with niobium, with oxygen diffusing into the metal and carbon reacting to form a surface carbide layer.

The corrosion resistance of niobium in pressurized water and steam is significantly improved by additions of vanadium, titanium, or zirconium, according to recent Battelle studies.[6,7] Alloys containing 10 at.% vanadium or 25 at.% titanium or zirconium corrode at less than one-tenth the rate of unalloyed niobium in 360°C (680°F) water. The better alloys, such as niobium–28 at.% titanium–6 at.% chromium, corrode slower than Zircaloy-2. General Electric studies[8] on niobium-vanadium alloys confirm their excellent corrosion resistance. The improvement in corrosion resistance appears to be associated with a change in the scale composition from Nb_2O_5 to NbO_2. (W. D. Klopp)

Corrosion of Zirconium

The material properties which limit the useful life of zirconium-base alloys and hafnium in pressurized-water reactors have been critically reviewed by Knolls[9] in the light of theory and experimental data. No limitations on performance are anticipated for presently proposed reactors. However, for long-lived reactors it is foreseen that the limiting factors in the case of zirconium-base alloys are hydrogen pickup and redistribution. For hafnium, the loss in corrosion resistance due to transmutation is probably limiting.

The rate of hydriding of Zircaloy-2 by molecular hydrogen is being studied at Hanford[10] under

conditions which might be experienced in the New Production Reactor (NPR) stack gas if water leaks in and contacts the hot graphite. In dry hydrogen gas at 500°C, a good ZrO_2 autoclave film delays time for hydriding by from 2 to 30 hr. On the other hand, dip coatings of aluminum, lead, zinc, and copper (immersion plate) all failed more rapidly than the autoclave film.

The corrosion behavior in high-temperature water of zirconium-niobium alloys with and without tin is being investigated at several laboratories. Knolls work[11] indicates that best corrosion behavior for a zirconium–2 at.% tin–2 at.% niobium alloy is obtained by annealing for 24 hr at 800°C or by cold rolling 30 per cent after hot rolling at 750°C. Quenching from 950°C was found to be detrimental. This difference in corrosion behavior between quenched and annealed materials is attributed to differences in the epitaxial relation of the oxide to metal resulting from changes in structure.

Chalk River[12] has found that an alloy of reactor-grade sponge containing 2.4 wt.% niobium and quenched from 1000°C evinces about twice the corrosion rate of Zircaloy-2 in 360°C water. Hydrogen pickup, however, was of the same order as that observed for Zircaloy-2. Ternary additions of tin in the range 0.5 to 1.5 wt.% were found to have little or no effect on corrosion properties of the zirconium-niobium alloy at a water temperature of 315°C; whereas tin adversely affected corrosion properties at higher temperatures.

Ternary alloy systems that are being investigated at Nuclear Metals[13] and Argonne[14] for their resistance to 900 and 1000°F steam (600 to 1500 psi) include Zr-Fe-Ni, Zr-Cr-Fe, and Zr-Cr-Ni. In general, the total alloy content is 5 wt.% or less. It would appear that, if properly heat-treated and finished to avoid excessive edge spalling, several alloys show promise of providing satisfactory service for, say, up to two years in 900°F steam and six months in 1000°F steam.

Fretting-corrosion tests under conditions simulating those expected for a single Plutonium Recycle Test Reactor (PRTR) rod with a Zircaloy-2 spider and tube are being conducted at Hanford.[15] On the basis of preliminary studies, the following trends have been noted:

1. With clearances of 5 mils, fretting occurred on the Zircaloy-2 spider and tube in the absence of applied vibration.

2. Oxide films were not effective in preventing fretting.

3. Water velocities between 15 and 30 ft/sec had no significant effect on fretting.

(W. K. Boyd)

Corrosion of Aluminum Alloys

In the field of aluminum alloy corrosion, attention is being focused on the behavior of high-purity materials. The alloys were melted using 99.995 and 99.95 per cent pure aluminum, and they contained from 1.5 to 2.0 wt.% iron with 0.64 to 1.2 wt.% nickel. Data obtained at Hanford[10] in 360°C water show no dependence of base-metal purity in the above range. Penetration rates for both aluminum melting stocks were of the order of 0.2 mil. Similar trends have also been noted at Argonne.[14] Trace amounts of magnesium, zinc, and copper had no effect on corrosion properties. By contrast, however, the Argonne work indicates that silicon in the range of 0 to 0.006 wt.% exhibits a marked adverse effect on corrosion behavior.

The studies at Hanford also have included exposure in steam at 500°C and 1000 psi. All alloys were destroyed in 17 hr. However, the results indicate that resistance increases with the iron content. It is planned to evaluate alloys containing up to 3 wt.% iron.

At Harwell[16] an aluminum–2.5 wt.% nickel alloy was exposed to steam at temperatures from 270 to 500°C for periods up to one week. Up to 350°C, uniform corrosion was the rule. As the temperature was increased to 400°C and above, penetrating attack became very prevalent, and at 500°C considerable specimen growth was noted. It is interesting to note that in these studies the sintered aluminum product (SAP), which was noticeably less resistant than the aluminum–2.5 wt.% nickel alloy at 350°C, was much less susceptible to penetrating attack at 500°C. SAP containing 1 wt.% nickel appears to combine the good resistance of the nickel alloy at low temperatures with the resistance of ordinary SAP to penetrating attack at 500°C. (W. K. Boyd)

The results of a study of the hot-water corrosion of aluminum-iron-nickel alloys were reported recently by French workers.[17] A particular problem in alloys of this system is localized intergranular attack in the mildly corrosive hot-water medium. The French study showed that the addition of about 0.1 wt.% titanium greatly reduced the tendency for localized fissuring in

aluminum-iron-nickel alloys. Zirconium additions behaved similarly but were less effective. The improved behavior was attributed to the ability of titanium to promote better homogeneity of distribution of solute atoms in the matrix. Second-phase dispersion is also benefited by titanium and zirconium additions.

(E. S. Bartlett)

Corrosion of Iron- and Nickel-Base Alloys

A fundamental study of the oxidation behavior of binary iron–0.2 to 10 wt.% chromium alloys was conducted by researchers at Princeton.[18] Kinetic examination of the oxidation process at temperatures from about 1550 to 1850°F showed that no single specific rate law described the behavior observed. Qualitatively, increased oxidation resistance with increasing chromium content was recorded. Since the chromium content in these alloys is lower than that required for spinel formation, modification of the oxidation properties resulted from the effects of chromium dissolved in the basically iron oxide scale.

Inconel, Inconel X, A-nickel, Duranickel, and Monel were exposed, at 1500 and 1700°F for times up to 500 hr, to a dynamic atmosphere activated by the presence of 2×10^{-4} atm of carbon dioxide and carbon monoxide at ratios of 2:1, or less, respectively. This work, carried out at General Dynamics,[5] showed that Inconel and Inconel X are slightly oxidized (films less than 1 mil thick formed during the maximum exposure) under these conditions. High-nickel alloys and Monel were either not corroded or showed only a tarnish film. A-nickel and Monel were significantly decarburized at 1500°F (but not at 1700°F), particularly by the richer (CO_2 rich) gas mixtures; however, Duranickel, despite its higher carbon content, was stable under the test conditions.

A Polish program[19] investigated the absorption of hydrogen in iron, carbon steels, and nickel. For the same hydrogen potential (cathodic evolution from an aqueous solution), it was noted that nickel dissolved much more hydrogen than did the iron-base materials studied.

Screening tests on various potential cladding materials resulted in selection of Hastelloy X, Inconel, and Inconel 702 for continued study in the 99.5 per cent nitrogen–0.5 per cent oxygen, 1750°F, 200-psi atmosphere of the Army Gas-Cooled Reactor Systems Program being studied at Aerojet General.[20] Tests of 5000-hr duration have been completed (10,000-hr service life is expected), and the corrosion results are shown in Table V-1. These data show that Hastelloy X is "reasonable for 5000 hr in the reference gas;

Table V-1 CORROSION OF CLADDING MATERIALS IN 99.5 PER CENT NITROGEN–0.5 PER CENT OXYGEN AT 1750°F, 200 PSI[20]

Exposure time, hr	Average depth of corrosion, mils			
	Hastelloy X	Inconel 702	Inconel	Hastelloy R-235
1000	1	2	No values reported	6
2500		5	No values reported	7
5000	3	10	No values reported	12

and its resistance for 10,000 hr probably is satisfactory." However, of the materials under investigation, only Inconel (which contains no reactive additions) retains good ductility over the design times. Thus mechanical features are also of prime importance in the selection of cladding materials. Other materials currently under investigation are Nichrome V, niobium-modified Nichrome V (poor creep strength will influence the decision for use of these alloys), Inconel 600, Martin "DB" (iron-chromium-aluminum alloys, also low creep strength) alloys, Allegheny Ludlum G-157, Nb–10 Mo–10 Ti (Du Pont D-31), AISI 310, Chromallized Hastelloy X, Inconel 702, and several experimental alloys being produced at Battelle.[21,22]

Investigations to improve the oxidation resistance of iron–25 to 27.5 wt.% chromium alloys with aluminum, yttrium, and rare-earth additions were described by General Electric.[23] Aluminum additions in the range of 2 to 6 wt.% were most effective. Such alloys correspond closely to industrial alloys of the Kanthal or Smith No. 10 type. Minor cerium and gallium additions were observed to be detrimental to oxidation resistance. (Electrical-resistance wire alloys of the nickel-chromium type utilize cerium or misch metal to promote long life in cyclic service, rather than under steady-state conditions, such as studied in the General Electric program.) Yttrium, lanthanum, dysprosium, gadolinium, and erbium additions had moderately beneficial effects on high-temperature oxidation resistance of the iron-chromium-base alloys. Internal oxidation effects were observed in alloys containing yttrium. (E. S. Bartlett)

Corrosion of Refractory and Reactive Metals

Oxidation of tungsten has been the subject of investigations at The Ohio State University[24] and Westinghouse.[25] On the basis of an extensive study, The Ohio State University work reports the existence of three oxide phases:

1. WO_2, stable for short times at low temperatures.
2. $W_{18}O_{49}$ or $W_{20}O_{58}$, blue oxide, characterized by rapid growth to about 10-μ thickness under ordinary pressures.
3. WO_3, porous oxide, stable at all temperatures.

Kinetically, tungsten exhibits parabolic oxidation behavior in the initial stages of oxidation, changing to conform to the linear rate law at an early stage of oxidation at elevated temperatures. Activation energies for the oxidation processes are 35 kcal/gram atom during parabolic oxidation and 36.5 kcal/gram atom in the linear process. The Ohio State University workers concluded that diffusion of oxygen through the blue oxide layer is the rate-controlling mechanism and found that reduced pressures decrease the rate constants by increasing the blue-layer thickness. The maximum temperature investigated at The Ohio State University was 2000°F. Westinghouse workers found that, at low temperatures (less than about 950°F), the reaction was obviously diffusion controlled, but at higher temperatures (up to 2400°F), factors such as localized edge effects, oxide exfoliation, and the volatility of WO_3 complicated the interpretation of weight-change observations. At temperatures above about 2000°F, rapid rates of weight loss were obtained because of the volatility of WO_3.

Ames Laboratory workers investigated the oxidation behavior of yttrium at temperatures[26] from 850 to 1700°F. As noted qualitatively by Martin workers (reported in a previous Review), very rapid oxidation was observed at temperatures in excess of about 950°F. At temperatures below 850°F, oxidation is slight. From 850 to 1110°F, the oxidation process is defined by the $x^n = kt$, where $1 < n < 2$ and the oxidation rate is neither linear nor parabolic. The scale formed at these temperatures is dense and adherent. At higher temperature no single constant-rate process occurred. Cracks develop in the scale at temperatures from about 1110 to 1380°F, and, at still higher temperatures, the oxide is nonadherent and fluffy. At 1470°F a reproducible phenomenon occurs, whereby high initial and final oxidation rates are separated by a period of relatively slow oxidation. A weight-change versus temperature curve plotted for 24-hr exposures showed a maximum weight gain in the region of 1250°F and a minimum at about 1450°F. Hardness measurements, coupled with oxygen determinations, indicated that yttrium contaminates in much the same manner as do the Groups IV-A and V-A metals. This is shown in Table V-2.

Table V-2 OXYGEN CONTAMINATION AND SCALE THICKNESS OF YTTRIUM EXPOSED TO AIR[26] FOR 24 HR

Temp., °F	Approximate oxygen content, ppm	Oxide thickness, mils
(Base)	690	
840	700	0
930	800	1
1026		4
1110	1600	10
1200		21
1290	2400	22
1380	1100	20
1470	1000	
1560	2200	

These data agree with the weight-change observations, indicating less severe oxidation effects in the region of 1350 to 1500°F than at somewhat lower or higher temperatures. No explanation of this effect has been offered.

The effects of neutron-bombardment-induced transmutation of hafnium (used as control material) have been studied at Knolls[9] in reviewing the life expectancy and service efficiency of control rods. Mechanical effects are insignificant, but it appears that the lack of corrosion resistance imparted to hafnium by Ta^{181}, a transmutation product, may be a severe limitation to the life of rods. In 680°F water and in 750°F, 1500-psi steam, simulated alloys of hafnium–0.3 to 2.0 wt.% tantalum, with and without lutetium (another transmutation product), were found to corrode very rapidly at tantalum contents of about 1 per cent or greater. Lutetium appeared to exert a slightly beneficial effect. The mock alloys studied were two-phased, a condition that probably would not exist in alloys resulting from irradiation transmutation. The effects of metallurgical-phase relations upon corrosion behavior may be of some significance.

A bibliographic survey (1) of oxidation investigations of chromium, hafnium, molybdenum, niobium, tantalum, titanium, tungsten, vanadium, and zirconium (and several alloys of these metals) and (2) of properties of the borides, carbides, nitrides, and oxides of these metals has been compiled.[27] This should be of considerable value to persons working with these materials. (E. S. Bartlett)

Corrosion of Silver-Indium-Cadmium Alloy

The silver–15 wt.% indium–5 wt.% cadmium alloy is used as control-rod material in the Yankee reactor primary system. Poor corrosion resistance of this alloy observed during operation led to a laboratory corrosion study[28] of the material. Exposure conditions simulated those encountered during reactor operation: temperature = 600°F, pressure = 2000 psi, and 0.92 per cent boric acid added to the primary water during startup and then bled off. The operating environments studied were lithiated and demineralized water. Corrosion was by intergranular oxidation to a depth of 3 to 4 mils after 700 hr of exposure. Nickel plating of the silver-indium-cadmium alloy prevents intergranular corrosion of the base if the plating is not defective; however, in this study appreciable weight loss was noted in neutral water. Weight-change data are shown in Table V-3.

Table V-3 WEIGHT CHANGES OF BARE AND NICKEL-PLATED SILVER–15 WT.% INDIUM–5 WT.% CADMIUM IN LITHIATED AND NEUTRAL WATER[28] AT 600°F, 2000 PSI

Surface	Environment	Average weight change (after indicated time in hours), mg/dm²					
		135	160	295	541	666	700
Bare	Lithiated water		+14	+49		+207	
Bare	Neutral water	+7.5	+6.5	+21	+60		+69
Nickel-plated	Lithiated water					−13	
Nickel-plated	Neutral water						−180

The weight-gain data do not indicate the severity of the problem since fissure penetration is far greater than is indicated by these figures. The corrosion mechanism has been identified as an oxidation process. In reactor operation it is intended to maintain a finite amount of hydrogen in solution in the primary water to suppress radiolytic oxygen buildup, thereby minimizing the corrosion potential.

During operation, some of the indium in the silver-indium-cadmium alloy is transmuted to tin. To determine the effect of this on the corrosion behavior of the silver–15 wt.% indium–5 wt.% cadmium alloy, specimens of silver–15 wt.% indium–5 wt.% cadmium–0.5 wt.% tin were also exposed to simulated operating environmental conditions. After 700 hr of exposure, a weight gain of 29 mg/dm² was noted. No intergranular corrosion was observed. (E. S. Bartlett)

Corrosion by Liquid Metals

Comprehensive study at Brookhaven and by Babcock and Wilcox workers has firmly established that, at 550°C, the peak temperature of interest to the Liquid Metal Fuel Reactor Experiment (LMFRE), small amounts of magnesium and zirconium are effective inhibitors of corrosion by molten uranium-bismuth alloys. Loop systems fabricated of various ferritic steels can be operated for several thousand hours with negligible corrosion effects. The following characteristics for such systems, derived from pump-loop experiments designed to provide refined studies of behavior, have been established by Brookhaven:[29]

1. High-chromium steels (5 wt.% chromium–0.5 wt.% molybdenum and type 410 stainless steel) are more susceptible to corrosion than low-chromium steels (1.25 wt.% chromium–0.5 wt.% molybdenum and 2.25 wt.% chromium–1 wt.% molybdenum). Of the low-chromium steels, the 2.25 wt.% chromium–1 wt.% molybdenum is the more susceptible.

2. Carbon-steel welds have not shown any corrosion. However, all welds in which type 410 stainless steel is present (joined to 2.25 wt.% chromium–1 wt.% molybdenum, 1.25 wt.% chromium–0.5 wt.% molybdenum, or type 410 stainless steel) are susceptible to corrosion. No attack is exhibited by welds in 2.25 wt.% chromium–1 wt.% molybdenum. The sensitivity of welds to attack is increased in direct relation to surface roughness.

3. Very low-carbon steels (0.10 wt.% or lower) seem to be more susceptible to corrosion than the higher carbon steels.

4. Uranium concentrations can be maintained constant in an EM pumping loop for over 10,000 hr and in a mechanically pumped loop for over 1300 hr of ΔT operation.

Similar uranium-bismuth-loop experiments[30] have been conducted by the Babcock and Wilcox Company. It was found that the heat-treatment of the steel probably has an important effect on corrosion. The effect was rather pronounced in the case of Croloy 2¼, where material normalized and tempered at 975°F exhibited less corrosion than material in the fully annealed state or material normalized and tempered at 1300°F. The comparison here involved a weight loss equivalent to about 0.03 mil/year, as contrasted to a weight loss equivalent to approximately 5 mils/year.

An investigation to determine the susceptibility of beryllium samples to corrosion in a sodium-pumping-loop experiment was conducted at General Electric.[31] The sodium was circulated at a temperature in the 900 to 1000°F range and was gettered by flow through a calcium bath. After slightly over 500 hr of exposure, the samples did not exhibit any evidence of erosion or material loss. However, there was evidence of uniform surface nitriding, presumably as a result of a nitrogen impurity introduced by a method of gettering. This tendency for nitriding is viewed as a potentially serious problem in the direct exposure of beryllium to sodium because of the basic difficulty in controlling the nitrogen contamination in a large-scale sodium flow system. It is of interest to note that the beryllium samples self-welded strongly with each other even though the contact loads involved were low.

An investigation at Oak Ridge[32] was concerned with the compatibility of beryllium with 600, 700, and 800°C NaK. This was a brief materials evaluation for irradiation-capsule service and consisted essentially of the exposure of beryllium cylinders in sealed type 304 stainless-steel capsules. The cylinders were stepped so that liquid-metal-filled annuli of varying thicknesses (2 to 50 mils) existed between a cylinder and the adjacent inner capsule wall. After 500 hr at 800°C, a beryllium cylinder lost the equivalent of 6.2 g/sq in. Analyses of drillings taken from the inner surfaces of the steel capsules indicated appreciable transfer of beryllium into those surfaces; this transfer was highest at regions of minimum annulus thickness.

A report[33] recently issued by Oak Ridge summarizes the results of exposures of various ceramics and cermets in static and tilting-furnace exposures involving 1500°F sodium, lithium, and lead. Figure 16 summarizes the data for various cermets. Figure 8 of the February 1959 issue of *Reactor Core Materials* presents analogous information from the ceramic-materials research at Oak Ridge.

Oak Ridge is also initiating experiments involving corrosion by boiling potassium. Type 316 stainless-steel specimens were exposed in various zones (boiling, vapor phase, condensing, and liquid phase) of a thermal loop in which the potassium was boiling at 1550°F. After 200 hr there was no visible evidence of attack at either the specimen or loop-wall surfaces. Specimens exposed in the vapor region of the hot leg exhibited the greatest weight loss (3.5 mg/cm^2) of any in the system. (J. H. Stang)

Metal-Water Reactions

A number of reports[34–38] covering work performed by the General Electric Vallecitos Atomic Laboratory have been received. These cover an extensive program concerned with metal-water reactions, primarily zirconium-water reactions. A large part of this effort has been theoretical and analytical in nature, although some experimental information is reported.

Studies[34] involving zirconium and Zircaloy-2, which were conducted at temperatures up to 1700°C and water-vapor concentrations up to 30,000 ppm in 1 atm of helium, led to the conclusion that the rate of reaction is controlled by the transport of water vapor through the helium. Good agreement was obtained between experimental results and calculations employing mass-transfer considerations. In the case of zirconium and Zircaloy, under the conditions of these experiments, a surface of reactive metal was continuously exposed because of the rapid diffusion of oxygen into the metal, and no inhibiting film formation was observed.

In another part of the program,[38] experiments established that an excursion in temperature occurred during initial reaction of zirconium with steam and that the amount of increase could be effectively determined by the radiation-pyrometry technique employed. It was found that a measurable temperature rise in the solid might or might not occur, apparently depending on the rate of introduction of the steam.

In an analytical program[35] the various types of equations relating the extent of reaction between a metal and water vapor are reviewed and dis-

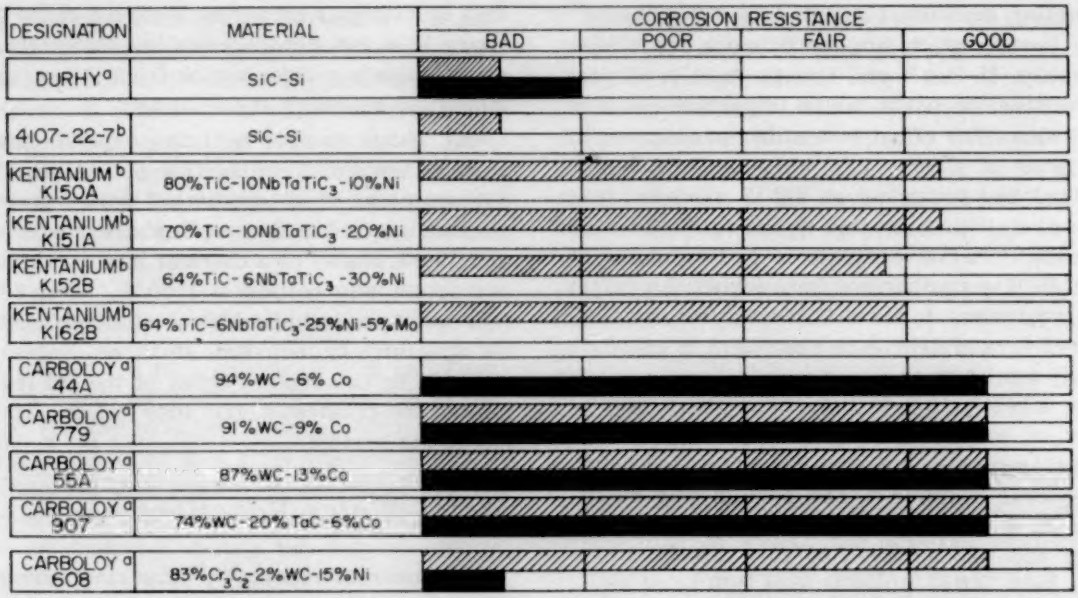

TYPE OF DATA	ARBITRARY CORROSION RATINGS AND DATA RANGE BASES			
	BAD	POOR	FAIR	GOOD
DEPTH OF ATTACK, MILS*	3	2	1	0
WEIGHT CHANGE, %**	6	4	2	0
DIMENSIONAL CHANGE, %	3	2	1	0

* MEASURED IN METALLOGRAPHIC EXAMINATIONS
** DETERMINED BY DIRECT MEASUREMENT AND/OR BY CALCULATIONS BASED ON THE MATERIAL(S) FOUND IN THE TEST MEDIUM BY CHEMICAL ANALYSES

Figure 16—Trends of corrosion resistance of various cermets in sodium and lead[33] for 100 hr at 1500°F. Note: Kentanium is a trade name used by Kennametal, Inc., Latrobe, Pa. Carboloy is a trade name used by the Carboloy Department of General Electric Company, Detroit 32, Mich.

cussed. The origin of the most common relation employed, the so-called parabolic rate law, is shown to be the diffusion process through an oxide film on the surface. Such a law cannot apply to the initial stages of the reaction process before a coherent film has had a chance to form; and, for these conditions, it is postulated that the rate-determining process is the transport of H_2O molecules through the vapor phase. Both an exact formulation combining these two concepts and an empirical representation are presented.

Two additional analyses[36,37] have been reported by General Electric. The first of these is a study of the effect of a chemical reaction between steam and the fuel cladding in a nuclear reactor during a severe loss-of-coolant accident and prior to melting of the cladding. It was concluded that the heat generated by the oxidation of the Zircaloy significantly increases the cladding temperature as soon as the temperature exceeds about 2000°F. This autocatalytic effect causes varying amounts of cladding oxidation prior to melting and a large variation of temperature between the hottest and coolest areas in the core. From the second analysis it is concluded that rapid, violent chemical reaction between metals and water resulting from a temperature excursion in a nuclear reactor can take place only if the metal is molten. The droplet size that can be produced by a nuclear accident remains the outstanding question whose solution is required before the metal-water hazard can be adequately and objectively analyzed. The problem is a difficult one, and no simple approach to its solution appears to be available.

The experimental program at Argonne[39] to determine rates of reaction of molten reactor fuel and cladding materials with water is continuing. The principal laboratory-scale method involves the rapid melting and dispersion of metal wires in a water or steam environment by a surge current from a bank of condensers.

A second laboratory method involves the rapid contact of steam with a crucible containing molten metal. Current results show that solutions obtained by analog modeling and analysis agree with those obtained experimentally.

An excellent review of uranium-water reactions has been published by Hanford.[40]

(A. W. Lemmon, Jr.)

Radiation Effects in Nonfuel Materials

Basic Studies

Corbett and Walker[41] have irradiated copper, silver, and gold at 10°K with 1.5-Mev electrons and measured the changes produced in the electrical resistivity. From these data they infer that the threshold energy for radiation damage is 22 ev for copper, 30 ev for silver, and ≥40 ev for gold. This indicates that the noble metals are not identical as regards radiation damage.

Blewitt et al.[42] have added further experimental evidence to their conclusions that the annealing kinetics of 30 to 50°K peaks in neutron-irradiated copper are difficult to interpret in terms of interstitial migration to vacant lattice sites. Their interpretations of stored-energy-release data would require about five pairs formed per primary displacement (theory suggests 120 pairs); also their deduced value of resistivity, 7 to 12 μohm-cm per at.% pairs, is much higher than the theoretical predictions of 1.5 to 2.0 μohm-cm.

Thompson and Paré[43] have studied the effects of fast-neutron bombardment at temperatures from 90 to 300°K on internal friction and Young's modulus of a high-purity single copper crystal. The results are well described in terms of a simple theory of pinning of dislocations by radiation-induced defects which have migrated from their points of origin. The dislocation pinning rate at 100 to 140°K is about 2.5 per cent of that at room temperature because of the lowered mobility of the thermally sensitive processes. Upon warming to above 260°K, the modulus and decrement change quickly to their "saturation" values, i.e., where the dislocations are completely pinned by defects, presumably because defects "stored" during the low-temperature irradiation become thermally mobile and move to the dislocations.

Damask and Dienes[44] have answered an inference made by Wechsler and Kernohan[45] concerning some of their early work. Damask and Dienes conclude from resistivity annealing, vacancy collapse, activation energies, and relaxation times that the changes in resistivity (as they observed) in alpha brass are associated with changes in short-range order. If the quenched-in vacancy mechanism of Wechsler and Kernohan were valid, they say, an appreciable temperature dependence should be observed during the early stages of irradiation. They observed no temperature dependence over a wide temperature range.

Wechsler and Kernohan[46] reply to the above comments by stating that their position is not to reject an ordering explanation but, on the basis of an analysis of other work and their own, to suggest the possibility of an alternative explanation. They state that experimental evidence is not sufficient at the present time to infer that the decrease in resistivity upon irradiation is due primarily to either a reduction of the number of vacancies or changes in short-range order.

The kinetics of vacancies introduced by tempering platinum wires are discussed by Bacchella et al.[47] The kinetics are of the first order for imperfection concentrations below 10^{-5} or for tempering at low temperatures; they are more complex for higher concentrations or for tempering near the melting temperature. Interpretations on the basis of an activation energy of migration of 1.48 ± 0.09 ev and of the formation of divacancies or of more complicated imperfections at low temperature, the energy of formation and migration of the divacancies, energy of formation of vacancies, and the energy of self-diffusion in platinum are in agreement with the results of Kidson and Ross.

Piercy[48] has claimed that the principal defects remaining in platinum after neutron irradiation (1200 ev at 50°C) were single vacant lattice sites and after quenching (in water from 1600°C) were pairs of vacant lattice sites. After deformation in liquid nitrogen, the defects present were single vacant lattice sites and another type, perhaps interstitials. In all cases the activation energy for motion of the defect was determined from measurements of electrical resistivity. Density, hardness, and X-ray line broadening were measured where applicable.

Thompson[49] reports activation energies for the recovery of neutron-irradiated tungsten. Vacancy migration is reported above 400°C with

an activation energy of 1.7 ev. He advances the general suggestion that vacancies in all metals migrate at about 20 per cent of the absolute melting point (T_m, °K) with an activation energy roughly $5 \times 10^{-4}\ T_m$ ev. Above −170°C, interstitials are released from traps associated with impurity atoms and dislocation lines (between 0.25 and 1.7 ev); below −170°C, the free interstitial was observed to migrate.

Kinchin and Thompson[50] irradiated molybdenum and tungsten with pile neutrons at 30 and −196°C. Processes have been observed with activation energies of 0.25 and 1.3 ev for molybdenum and 0.5 and 1.7 ev for tungsten. A stored-energy release of 0.4 cal/g from 50 to 250°C has also been observed in molybdenum irradiated with 1.3×10^{19} neutrons/cm^2.

A series of transition metals was irradiated near the temperature of liquid nitrogen in the heavy-water pile EL2 at Saclay.[51,52] Measurements of electrical resistance *in situ* were used to compare the changes in resistivity produced by a given number of atomic displacements.

The change in thermal conductivity of superconductors caused by radiation damage has been studied[53] in single crystals of niobium and vanadium, irradiated at 30°C to 10^{18} fast neutrons/cm^2. Measurements were carried out at low temperatures in both superconducting and normal states where conduction is due predominantly to phonons and electrons, respectively. The observed effect on the phonon conductivity indicated an increase in dislocation density, presumably resulting from condensation of mobile interstitials to form either dislocation loops or jogs on existing networks. For niobium and vanadium, respectively, the increase calculated from the conductivity was 3×10^9 and 1×10^{10} dislocation lines per cm^2, compared with an estimated expected increase of 10^9. The change in electron conduction was consistent with the expected vacancy concentration of 10^{-4} due to irradiation.

An increase in the magnetic susceptibility, following neutron irradiation (up to 2.2×10^{19} nvt) at 80°C, of a series of copper-nickel alloys, ranging from 17.22 to 46.5 at.% nickel, and the decrease to their original values after annealing in the temperature range where self-diffusion is significant, were interpreted[54] as radiation-enhanced diffusion of solid-solution alloys toward a true equilibrium with increased local segregation.

A Russian paper[55] reported data on the effect of gamma irradiation on the magnetic properties of Fe_3Al, nickel, and Ni_3Mn, which showed changes in the galvanomagnetic effect and coercive force. The authors suggest that the former effect is associated with formation and relaxation of Frenkel-pair defects and the latter with formation of dislocation loops.

Damask[56] has been granted a patent on the use of electron irradiation to increase the vacancy concentration of metals, alloys, and semiconductors and thereby to enhance diffusion mechanisms which might control physical properties of some materials, such as resistivity or hardness.

Bally and Benes[57] have reported an interesting change in structure of the K-absorption discontinuity of nickel due to neutron irradiation (>0.7 ev).

Silcox and Hirsch[58] have observed dislocation loops in transmission electron micrographs of neutron-irradiated copper. Specimens irradiated to a dose of 6.7×10^{17} nvt at 35°C contain $\sim 3 \times 10^{15}$ defects per cm^{-3}, in the form of small regions of strain (average diameter, 75 A), some of which can be resolved as dislocation loops. At an integrated flux of 5.6×10^{14} and 1.4×10^{20} nvt, respectively, the number of loops increases to 10^{10} to 10^{11} cm^{-2}, with average diameters of ~150 and ~300 A. Their stability and behavior on annealing are as expected for prismatic loops. These were considered to nucleate by collapse of disks of clustered vacancies in the central region of a displacement spike and to grow by migration of vacancies or of vacancy clusters. Radiation hardening anneals out at the same temperature at which the loops disappear by climb.

Young and Noggle[59] have observed slip lines and etch pits at dislocations on a copper crystal hardened by irradiation and deformed by bending. They accounted for the slip lines and subsequent location of dislocations in terms of dislocation interactions. Such dislocation interaction, as observed here, occurs only in hardened crystals.

Thin evaporated films of aluminum supported on a copper grid have been irradiated to 4.4×10^{19} and 5.2×10^{19} nvt (thermal) and examined in the electron microscope.[60,61] Electron-diffraction lines of copper were detected plus, in the first case, $CuAl_2$ and, in the second, an unidentified line, not belonging to $CuAl_2$. The temperature during irradiation was believed to

be less than 60°C; however, irradiation spikes may have caused evaporation of copper onto the film. Another possibility is radiation-enhanced diffusion. A tentative mechanism is proposed whereby copper-vacancy pairs form and permit clustering of copper atoms, giving rise to the observed copper-diffraction lines after 8.4×10^{18} nvt. Continued exposure causes aluminum diffusion into the copper clusters and precipitation of $CuAl_2$.

Mönch and Sander[62] have observed copper films deposited at low temperatures. They report a stored-energy release of 216 cal/mole and a decrease in resistivity of 1.8 μohm-cm in the region 20 to 60°K, which they state is due to a crystallization of highly disordered material between the small crystallites formed during condensation of the film. The stored-energy ratio was 1.9 cal/(g)(μohm-cm) in the region 20 to 60°K, which is in agreement with neutron-bombardment measurements.

Teodorescu and Glodeanu[63] irradiated thin films of nickel at about 10^{16} nvt at roughly 50°C. For irradiation under vacuum they observed an allotropic transformation from face-centered cubic ($a = 3.52$ A) to hexagonal close packed ($a = 2.62$ A; $c = 4.36$ A). Irradiation in oxygen eliminated transformation. The magnetic properties disappeared on irradiation.

Electron-microscope studies[15] of high-purity aluminum foils irradiated to 4.4×10^{19} nvt indicated that twinning occurred at the highest exposure and that zigzag immobile dislocations were present. No dislocation loops were found.

Thin films of carbon and ZrO_2 irradiated in close proximity to fissionable uranium and thorium atoms showed fission damage[10] similar to that observed in thin films of UO_2 and ThO_2, in the form of fission-fragment tracks several microns long by about 150 A wide. Amorphous films of ZrO_2 produced by sputtering and irradiated to 4.4×10^{19} nvt developed crystallinity, the electron-diffraction pattern deviating somewhat from that of cubic ZrO_2.

Analysis[64] of the variation in electrical conductance with isothermal annealing of germanium single crystals irradiated by gamma rays from Co^{60} at −77°C yielded values of 0.765, 0.741, and 1.250 ev, respectively, for the activation energy of direct recombination of vacancy-interstitial pairs, diffusion of interstitials, and diffusion of vacancies.

Microscopic evidence has been obtained,[65] in single-crystal germanium irradiated to an integrated fast-neutron flux up to 10^{13} nvt, of highly strained well-defined regions of structural damage which were interpreted as visual evidence of spike formation.

Whapham and Makin[66] have developed a new theory for the dose dependence of the lattice-hardening component of irradiation hardening which predicts a saturation in hardening at increasingly high doses. It is expected that their formula will apply generally to crystalline solids which deform by slip. They have checked their theory in LiF with 1-Mev electron irradiation and state that the best available data for copper (highest dose so far tested is 10^{20} neutrons/cm^2) is also consistent. Cracking in the LiF samples has also been observed and seems to be of the form suggested by Cottrell for alpha iron.

Inghram and Smoluchowski[67] subjected crystals of NaCl to about 5×10^5 r of Co^{60} gamma radiation at 50°C. Ionic conductivity was measured as a function of temperature with a vibrating-reed electrometer. The decrease in the range 65 to 80°C is presumed to be a direct measure of positive-ion vacancies and fits a consistent bimolecular process rate equation. This confirms the supposition that the change of conductivity reflects the clustering of the positive-ion vacancies with other imperfections at a rate controlled by the diffusion of these vacancies. Above 100°C many of the clusters appear to break up again with an accompanying increase of conductivity. The conducting vacancies appear to be localized in a rather small fraction of the total volume of the crystal.

Results[68] indicate that the low-temperature thermal resistance of LiF after irradiation with doses as low as 4.5×10^{15} neutrons/cm^2 was due largely to clusters of point defects. The thermal resistance passed through a maximum with increasing dose, probably associated with a decrease in the lattice expansion. Similar results are obtained with gamma rays.

In low-temperature annealing of the expansion due to X-ray irradiation-induced defects in LiF, Wiegand and Smoluchowski[69] found that the expansion cannot be caused only by an increased concentration of negative-ion vacancies. They concluded that halogen ion-interstitial pairs are generated by X-ray irradiation of LiF at 90°K and that annealing at 130°K changes the interstitial configuration.

From measurements of the physical expansion and *F*-center coloration of single crystals of

X-ray irradiated NaCl, Rabin[70] obtained estimates of the negative-ion-vacancy concentration in an undoped Harshaw crystal and in a calcium-doped crystal to be $1 \times 10^{16}/cm^3$ and $>6 \times 10^{17}/cm^3$, respectively. The large concentration in the doped sample is not in accord with expectations of charge compensation and the law of mass action.

Arnold and Compton[71] have made observations of the 205-mμ absorption produced in 0.0636-cm-thick alpha Al_2O_3 using fast electrons of various energies. They estimate threshold energies by assuming that the absorption is produced by defects caused by lattice displacement. They conclude that the data do not allow an unequivocal attribution of the effects to either aluminum or oxygen displacements. Estimates are also given for the oscillator strength corresponding to the two possibilities considered.

The fission-fragment damage in neutron-irradiated Al_2O_3 and $ZrSiO_4$ containing UO_2 dispersant was indicated[72] by the disappearance of the grain boundaries and the peaks of the X-ray diffraction profile. Al_2O_3 showed, at the same time, a 30 per cent increase in volume. It was suggested, as a result of calculations which indicated that only a small proportion of the atoms are displaced directly by the fission fragments through elastic or other processes, that the fragments act indirectly to distort the lattice anisotropically. The authors claim that cubic ceramic materials appear to be less susceptible to this type of damage.

Void formation and helium-gas release have been studied[73] in pure aluminum (<0.02 per cent lithium) irradiated with 10^{18} nvt thermal neutrons to produce helium by (n,α) reaction. An encapsulated specimen diffusion annealed 94 hr at 575°C showed, by mass-spectrometer analysis, that less than 3 per cent of the total helium content was released, corresponding to an apparent diffusivity of only 2.4×10^{-10} cm^2/sec. Metallographic examination revealed bubble formation primarily at subgrain and grain boundaries, as suspected from the low diffusivity result.

Compton and Arnold[74] discuss various processes by which lattice atoms are displaced by incident fast electrons. In addition to considering displacements due to the incident electrons, expressions are developed for the fraction of atoms displaced by fast-moving atoms and fast secondary electrons, both of which are generated initially by the incident electron. A discussion of thermal spikes is also given.

Brown and Goedecke[75] have calculated the cascade of displaced atoms in metals induced by high-energy radiation. A screened coulombic interaction was chosen for the determination of defect production, and the problem was treated stochastically on an IBM 650 for several different models. The models used were those of Kinchin and Pease, Seitz and Harrison, and Vineyard. The results indicate that the number of displacements produced by primaries of energy well above the threshold is insensitive to the interaction potential between atoms, provided a stochastic treatment is valid. The nature of the cascade, however, is dependent on the interaction, in that many more collisions take place for soft interactions with most secondaries produced with low energies. These conditions would be pertinent to the geometrical distribution of displaced atoms and hence play a role in the annealing of radiation damage.

A comprehensive review (170 pages, 693 references) on the mechanical properties of irradiated solids has been presented by Levi.[76] After some general considerations on radiation damage, annealing, and experimental techniques, the various mechanical properties of metals and alloys affected by radiation are discussed; special chapters are devoted to uranium and graphite. Work on ionic and covalent crystals and on glasses is also included. An appendix deals briefly with recent papers up to the beginning of 1959. Twelve special tables summarize all the experimental results.

A review of the radiation effects on the noble metals was presented in Geneva[77] in 1958. Studies included the effects on the mechanical properties due to neutron irradiation at liquid-helium temperatures. Sagel[78] has reported a review paper on radiation-damage effects on material properties, and a review article on the effects of reactor irradiation on ceramic materials was given by Clarke.[79] Data on phase changes in irradiated ZrO_2 have been reported elsewhere[80] by Clarke. (C. M. Schwartz)

Effects of Irradiation on Mechanical Properties

The effect of annealing on radiation damage in Zircaloy-2 has been further investigated at Chalk River.[81] Room-temperature tensile tests

were conducted after three different treatments: (1) 9.5×10^{19} fast neutrons/cm^2 at 380°C, (2) 7.7×10^{19} fast neutrons/cm^2 at 280°C, and (3) 9.1×10^{19} fast neutrons/cm^2 at 50°C. Specimens receiving the last two treatments were given isothermal and isochromal postirradiation anneals. The annealed and cold-worked specimens irradiated at 380°C exhibited only a small amount of radiation damage in contrast to the annealed samples irradiated at the lower temperatures. Results on the cold-worked material irradiated at 380°C indicated that the amount of thermal recovery of cold work which occurred during irradiation was virtually identical with that which occurred during a similar out-of-pile heat-treatment. Analysis of the postirradiation annealing data for the 50 and 280°C irradiations revealed that in both cases the hardening annealed out in the range 250 to 400°C, characterized by a single activation of approximately 2 ev.

General Electric[82] has performed tests on Haynes-25 alloy and Inconel X springs irradiated in the compressed condition in an in-pile high-temperature water loop. The loop was operated at 560 to 600°F, and the springs of both materials received integrated neutron fluxes of 5.9 and 42×10^{18} fast neutrons/cm^2. Postirradiation testing and examination revealed no serious deleterious effects resulting from these exposures. It was found that the spring constant increased 5 to 8 per cent and the free length decreased 2 to 3 per cent after exposure. The effect of irradiation on the plastic flow curve was slight, as revealed by three-point bend tests on 0.160-in.-diameter rods irradiated with the springs.

Hanford[10] is studying the radiation-damage recovery for a number of metals, namely, copper, nickel, titanium, zirconium, iron, molybdenum, and type 347 stainless steel, by evaluating tensile properties, microhardness, electrical resistance, and X-ray diffraction spectra after irradiation. These metals were irradiated at up to 4.7×10^{18}, 1.0×10^{19}, and 1.5×10^{20} neutrons/cm^2 in different reactors, and the measurements are being made at Knolls and Hanford. Copper, iron, and titanium were given 1-hr annealing treatments at 25°C increments to 425°C; molybdenum, zirconium, and nickel specimens were given similar treatments to 475°C. Both the hardness and electrical resistance of irradiated copper showed practically no change upon annealing at temperatures up to 150°C. However, pronounced drops in electrical resistance occurred between 25 and 150°C, and hardness recovery occurred at 200°C for titanium specimens. X-ray studies on irradiated titanium showed significant line broadening and some lattice-parameter change. Complete recovery of electrical resistance for zirconium irradiated at 1.5×10^{20} fast neutrons/cm^2 took place at about 475°C, whereas complete recovery for the specimen receiving the lowest exposure was observed at 400°C. Significant hardness recovery was observed above 450°C in zirconium irradiated to 4.7×10^{18} fast neutrons/cm^2. Between 425 and 475°C, little change occurred in the electrical resistance of irradiated nickel and molybdenum. However, the hardness of molybdenum irradiated at 1.5×10^{20} fast neutrons/cm^2 decreased slightly at 450°C. The hardness of both irradiated and unirradiated molybdenum increased markedly between 200 and 375°C but showed little change between 375 and 450°C. Age hardening similar to that observed in irradiated molybdenum above 200°C was observed in unirradiated material solution treated at 1150°C and aged at 500°C for 4.8 to 24 hr. An unirradiated molybdenum specimen and specimens irradiated at 1×10^{17} and 1×10^{18} fast neutrons/cm^2 were prestrained beyond the yield point, annealed for 4 hr at 350°C, and again plastically strained. Strain aging characterized by a return of the yield point was not observed in any of the specimens. However, a small increase in yield strength was observed after annealing. A specimen exposed to 5×10^{18} fast neutrons/cm^2 was brittle and exhibited a cleavage type failure.

For a given integrated flux, there is theoretical evidence[83] that test results obtained in a low-flux reactor will not necessarily be typical of those expected in high-flux environments. For a given metal and temperature, the rate of damage accumulation in a reactor is the difference between the rate of damage production and the rate of damage recovery. When interstitials and vacancies are produced by neutron irradiation in a constant-flux spectrum and recovery occurs by interstitial-vacancy annihiliation, the resulting expression indicates that, at integrated flux levels above about 10^{10} fast neutrons/cm^2, there are about 10 times more displaced atoms at 10^{14} neutrons/cm^2 than at 10^{12} neutrons/cm^2.

(B. C. Allen)

Selected Mechanical Properties of Cladding and Structural Materials

Zirconium Alloys

Creep studies on Zircaloy-2 are being carried on concurrently at Battelle[22] and Hanford.[10,15] These long-term tests at elevated temperatures have indicated that 15 per cent cold-worked material retains its cold-worked properties at 300°C under stressed conditions. However, 45 per cent cold-worked material tested at 400°C shows partial recrystallization after 4000 hr at a stress of 13,000 psi. The creep rate obtained under identical test conditions was higher for 45 per cent cold-worked than for 25 per cent cold-worked Zircaloy-2. The higher creep rate is attributed to recrystallization.

Chalk River workers have studied the stress-relaxation characteristics of Zircaloy-2. Material which had been annealed for 1 hr at 750°C and tested at 13,500 psi and 300°C was found to have relaxed to a stress of 11,300 psi in 300 hr and to 10,900 psi in 600 hr. Other studies made on Zircaloy-2 to determine the amount of recovery of cold work occurring during creep have indicated that, at 300°C, recovery is no greater than that which occurs in the absence of stress.

A comparison of the mechanical properties of Zircaloy-2 and Zircaloy-4 (zirconium–1.2 to 1.7 wt.% tin–0.12 to 0.18 wt.% iron–0.05 to 0.15 wt.% chromium) was made at Bettis.[84] Tensile properties at room temperature and at 500 and 600°F were found to be the same. Duplicate creep tests made by the Canadians on annealed, 13 per cent cold-worked, and 25 per cent cold-worked Zircaloy-2 at 550°F and 13,500 psi are in progress. Total creep strains after approximately 16,000 hr are 0.216, 0.151, and 0.082, respectively.

The tensile properties of two zirconium-base alloys, zirconium–2.5 wt.% niobium and zirconium–2.5 wt.% niobium–1.5 wt.% tin, in the hot-rolled condition and in four cold-worked (10 to 30 per cent) conditions have been measured by the Canadians* at room temperature and at 300°C. These alloys have tensile strengths which are greater than those of Zircaloy-2 at comparable temperatures. Cold working produces a higher strength material. Greatest improvement over Zircaloy-2 is exhibited by the zirconium–2.5 wt.% niobium–1.5 wt.% tin alloy.

Stainless Steels

Studies are continuing at Oak Ridge[32] to investigate the creep of type 304 stainless steel in air, argon, oxygen, nitrogen, hydrogen, carbon monoxide, and carbon dioxide, respectively, at temperatures up to 1700°F. It has been noted that the creep rate is reduced in air and nitrogen because of the strengthening action of a nitride precipitate. Hydrogen affects the creep properties adversely at 1700°F, but data obtained at 1500°F are inconclusive. In tests at 1500 and 1700°F in both CO and CO_2, carburization occurs and causes a reduction in the rupture ductility. Tube burst tests on seamless 0.020-in.-wall type 304 stainless-steel capsules are also being made. The effects of differential pressure, temperature, and environment on time to rupture are being investigated.

General Dynamics[5] is investigating the effect of aging temperatures on room-temperature tensile properties of 430T stainless steel. Annealed specimens and specimens aged at 600, 1000, and 1200°F for 1000 hr had tensile strengths of 71,000 to 76,000 psi and elongations of 21 to 24 per cent. Specimens aged at 800°F exhibited tensile strengths of 104,000 to 106,000 psi and elongations of 13 to 15 per cent.

(F. R. Shober)

Selected Metallurgical Aspects of Cladding and Structural Materials

Aluminum

Workers at the Savannah River Laboratory[85] have determined the thermal conductivity of aluminum-lithium alloys, as shown in Fig. 17.

Work being done on the effect of helium in aluminum at Chalk River* has demonstrated that grain growth and recrystallization are inhibited. This was demonstrated by irradiating aluminum in the cold-worked condition with alpha particles at ambient temperatures to a helium concentration of approximately 0.5 cm^3/cm^3 of aluminum. A postirradiation annealing treatment of 1 hr at

*W. R. Thomas, Zr Alloys for Water-Cooled Power Reactors, Report IAEA FE/20/I-1, May 1960.

*C. E. Ells, in *Can. Mining Met. Bull.*, November 1960.

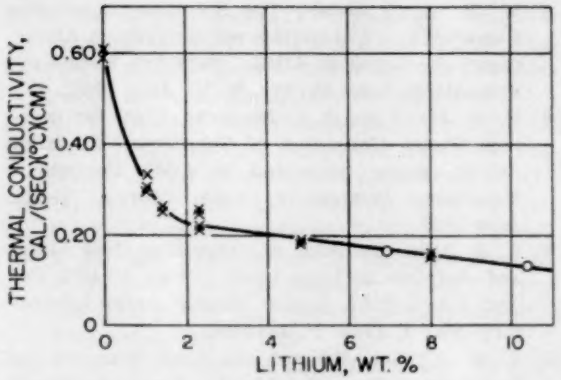

Figure 17—Thermal conductivity of aluminum-lithium alloys.[85] ×, Savannah River. O, C. J. Smithells.

500°C (or less) failed to recrystallize the material in the helium-containing layer.

(J. A. DeMastry)

Chromium

Cooper at Cavendish Laboratory[86] working with the chromium-aluminum system reports that a monoclinic theta phase in the chromium-aluminum system is isomorphous with alpha prime (vanadium-aluminum). The structure was refined, and the interatomic distances are discussed and compared with those in alpha prime (vanadium-aluminum) and with those in two ternary-alloy phases containing chromium and aluminum. (J. A. DeMastry)

Zirconium

Studies being carried out at Chalk River on zirconium-copper-molybdenum and zirconium-niobium alloys are reported. The zirconium–0.5 wt.% copper–0.5 wt.% molybdenum alloy was solution heat-treated in the beta phase at 950°C for 10 min followed by a rapid quench, reduced cold 15 per cent, and then vacuum annealed for 1 hr and 500 hr at 750°C. After the 1-hr anneal, the structure remained unchanged from the as-received material, except that a precipitate originally present was more uniformly distributed. After the 500-hr anneal, two phases were randomly distributed in the alpha-zirconium matrix. One of these had the appearance of an intermetallic compound and could be Zr_2Cu or $ZrMo_2$. In the zirconium–2.5 wt.% niobium alloy, heat-treatments within the temperature range of 650 to 800°C for periods up to 65 hr produced a structure consisting of equiaxed alpha grains mixed with Widmanstätten alpha grains and retained beta zirconium, which indicates that the limits of solubility of niobium in zirconium suggested by Ivanov and Grigorovich (A/CONF.15/P/2046) may be correct.

In a zirconium–2.5 wt.% niobium alloy cold rolled 50 per cent and annealed at 700°C for 4 hr, two phases were identified by X-ray diffraction: a hexagonal phase with lattice parameters $a = 3.231$ A and $c = 5.151$ A and a body-centered cubic beta phase with a lattice parameter of 3.560 A. After the alloy was cold rolled 50 per cent and annealed at 800°C for ½ hr, the same two phases were noted, but the ratio of the amount of cubic to the amount of hexagonal was reduced. The zirconium–2.5 wt.% niobium alloy, heated 10 min at 1000°C (beta phase) and water quenched, showed only broad peaks due to a hexagonal alpha phase. (J. A. DeMastry)

Diffusion Studies

Diffusion in the uranium-zirconium and uranium-nickel systems has been investigated by Müller in Germany.[87] Alloys of uranium–13 at.% zirconium were studied at 1065, 950, and 679°C, and determinations were made of the diffusion coefficients as a function of concentration, the activation energy, and the Kirkendall effect. In the uranium-nickel system, a great number of intermetallic phases exist, and it was found that the nickel atoms diffuse three to six times as fast as the uranium atoms. It is proposed that all diffusion phenomena observed are based on the vacancy-diffusion mechanism. The Kirkendall effect was also studied in uranium-zirconium in all regions by the French.[88] In this study, an inversion effect was observed in the direction of displacement, and the interpretation of this phenomenon is discussed. In the published proceedings[89] of a French conference on solid-state diffusion, studies of the diffusion of the systems of uranium with zirconium, titanium, aluminum, nickel, or oxygen are reported. A considerable portion of the information has been published elsewhere in the literature, but the reader interested in this field will find the studies discussed completely in these proceedings.

Grain-boundary migration in aluminum bicrystals has been investigated by the Germans.[90] The activation energy for the process was determined to be 23 kcal/mole for single-crystal aluminum wires and 44 kcal/mole for polycrys-

talline wires. In the article, models for lattice self-diffusion and grain-boundary self-diffusion are discussed, as well as dependence of migration speeds of grain boundaries on the thickness of the specimen.

Usually all equilibrium phases are formed in a diffusion couple of two metals, but the conditions where this may not occur are discussed in a very interesting paper by Baird.[91] The factors controlling the value of the growth constant for an intermetallic layer are discussed, including the effects of grain-boundary diffusion, oxide films, and pressure.

Studies of the diffusion of niobium with chromium, iron, nickel, molybdenum, and several compositions of stainless steel are being made which utilize an electron-probe microanalyzer.[92] In this research at the Naval Research Laboratory, the intermetallic phases in the diffusion zones have been found for each of the systems. All diffusion couples for the investigation were prepared at 1100°C. It was noted in the study that the couples of niobium-nickel often melted at this temperature, although the eutectic temperature is given as 1175°C in some of the literature. Niobium and molybdenum were miscible at all compositions, and the diffusion coefficient was found to range from 3 to 8×10^{-11} cm^2/sec. This research is being continued.

(D. C. Carmichael)

References

1. R. E. Pawel et al., Formation of Oxide Films on Columbium, paper presented at AIME Columbium Metallurgy Symposium, Lake George, N. Y., June 1960.
2. H. Inouye, Oxidation of Columbium at Low Oxygen Pressures, paper presented at AIME Columbium Metallurgy Symposium, Lake George, N. Y., June 1960.
3. J. W. Clark, Ignition of Columbium and Selected Alloys, paper presented at AIME Columbium Metallurgy Symposium, Lake George, N. Y., June 1960.
4. W. D. Klopp et al., High-Temperature Oxidation and Contamination of Columbium, *Trans. Am. Soc. Metals*, 51: 282 (1959).
5. General Dynamics Corp., Maritime Gas-Cooled Reactor Program, Quarterly Progress Report for the Period Ending June 30, 1959, USAEC Report GA-1099, 1959.
6. D. J. Maykuth et al., Development of Corrosion-Resistant Niobium-Base Alloys, USAEC Report BMI-1437, Battelle Memorial Institute, May 12, 1960.
7. W. D. Klopp et al., The Hot Water Corrosion Resistance of Columbium and Columbium Alloys, paper presented at AIME Columbium Metallurgy Symposium, Lake George, N. Y., June 1960.
8. H. A. Fisch and D. L. Douglass, High-Temperature Steam Corrosion of Columbium-Vanadium Alloys, paper presented at AIME Columbium Metallurgy Symposium, Lake George, N. Y., June 1960.
9. R. J. Allio, Behavior of Zirconium-Base Alloys and Hafnium in Long-Lived Cores, USAEC Report KAPL-2088, Knolls Atomic Power Laboratory, May 5, 1960. (Classified)
10. F. W. Albaugh, Reactor and Fuels Research and Development Operation Monthly Report for March 1960, USAEC Report HW-64580-A, Hanford Atomic Products Operation, Apr. 15, 1960. (Classified)
11. D. L. Douglass and B. E. Dearing, Effect of Heat-Treatment on the Corrosion of Zirconium–2 At.% Tin–2 At.% Niobium, USAEC Report KAPL-2071, Knolls Atomic Power Laboratory, Jan. 20, 1960.
12. S. B. Dalgaard, The Corrosion Resistance of Zirconium-Niobium and Zirconium-Niobium-Tin Alloys in High-Temperature Water and Steam, Canadian Report CRMet-911 (AECL-993), March 1960.
13. J. P. Pimsler, Corrosion of Zirconium Alloys in 900 and 1000°F Steam, USAEC Report NMI-1235, Nuclear Metals, Inc., Mar. 15, 1960.
14. Argonne National Laboratory, Annual Report for 1959, Metallurgy Division, USAEC Report ANL-6099, January 1960.
15. F. W. Albaugh, Reactor and Fuels Research and Development Operation Monthly Report for May 1960, USAEC Report HW-65459-A, Hanford Atomic Products Operation, June 15, 1960. (Classified)
16. N. J. M. Wilkens and J. N. Wanklyn, The Corrosion of Aluminum and Its Alloys in High-Pressure Steam, *J. Inst. Metals*, 88: 134–140 (November 1959).
17. H. Coriou et al., Aluminum-Iron-Nickel Alloys Resistant to Corrosion in Water at High Temperature. Basis for Their Properties—Their Improvement, French Report CEA-1313, 1959.
18. D. Lai et al., Oxidation of Iron-Chromium Alloys, Report AFOSR-TN-60-587, Princeton University, Forrestal Research Center, Feb. 29, 1960.
19. M. Smialowski, The Action of Cathodically Evolved Hydrogen on Iron and Nickel as Special Cases of Corrosion Embrittlement of Metals, *Chem. & Ind. (London)*, No. 35, 1078–1083 (Aug. 29, 1959).
20. Aerojet-General Nucleonics, Army Gas-Cooled Reactor Systems Program, Semiannual Progress Report for July 1 Through December 31, 1959, USAEC Report IDO-28549, Feb. 15, 1960.
21. R. W. Dayton and C. R. Tipton, Jr., Progress Relating to Civilian Applications During April 1960, USAEC Report BMI-1434, Battelle Memorial Institute, May 1, 1960. (Classified)

22. R. W. Dayton and C. R. Tipton, Jr., Progress Relating to Civilian Applications During May 1960, USAEC Report BMI-1442, Battelle Memorial Institute, June 1, 1960. (Classified)
23. E. J. Felten, High-Temperature Oxidation of Iron-Chromium-Base Alloys with Particular Reference to Iron-Chromium-Yttrium Alloys, USAEC Report XDC-60-2-153, General Electric Co., Aircraft Nuclear Propulsion Dept., Feb. 10, 1960.
24. R. Speiser, Research on the Oxidation Behavior of Tungsten, Fourth Quarterly Report, Report AD-226333, The Ohio State University Research Foundation, July 1, 1959.
25. E. A. Gulbransen et al., Oxidation of Tungsten and Tungsten-Based Alloys, Report WADC-TR-59-575, Westinghouse Electric Corp., Research Laboratories, February 1960.
26. O. N. Carlson et al., A Study of the High-Temperature Air Oxidation of Yttrium Metal, USAEC Report IS-115, Ames Laboratory, March 1960.
27. E. A. Cernak, comp., The Oxidation of Chromium, Hafnium, Molybdenum, Niobium, Tantalum, Titanium, Tungsten, Vanadium, Zirconium, and Some of Their Alloys; Properties of Some Borides, Carbides, Nitrides, and Oxides of the Same Metals, Report CNLM-1802-5, Pratt & Whitney Aircraft Div., United Aircraft Corp., Dec. 15, 1959.
28. S. J. Cytron, Corrosion Rate Tests of Yankee Primary System Materials in High-Temperature Dynamic Water, USAEC Report YAEC-153, Westinghouse Electric Corp., Bettis Atomic Power Laboratory, September 1959.
29. Brookhaven National Laboratory, Nuclear Engineering Department Progress Report for May 1–August 31, 1959, USAEC Report BNL-583, April 1960.
30. Babcock and Wilcox Co., Liquid Metal Fuel Reactor Experiment Quarterly Technical Report for April–June 1959, USAEC Report BAW-1170, 1959.
31. W. W. Kendall, Corrosion of Beryllium in Flowing Sodium, USAEC Report GEAP-3333, General Electric Co., Atomic Power Equipment Dept., Jan. 15, 1960.
32. Oak Ridge National Laboratory, Gas-Cooled Reactor Project Quarterly Progress Report for Period Ending March 31, 1960, USAEC Report ORNL-2929, June 21, 1960.
33. W. H. Cook, Corrosion Resistance of Various Ceramics and Cermets to Liquid Metals, USAEC Report ORNL-2391, June 15, 1960.
34. S. C. Furman, Metal-Water Reactions: V. The Kinetics of Metal-Water Reactions. Low Pressure Studies, USAEC Report GEAP-3208, General Electric Co., Vallecitos Atomic Laboratory, July 31, 1959.
35. L. F. Epstein, Metal-Water Reactions: VI. Analytical Formulations for the Reaction Rate, USAEC Report GEAP-3272, General Electric Co., Vallecitos Atomic Laboratory, Sept. 30, 1959.
36. L. F. Epstein, Metal-Water Reactions: VII. Reactor Safety Aspects of Metal-Water Reactions, USAEC Report GEAP-3335, General Electric Co., Vallecitos Atomic Laboratory, Jan. 31, 1960.
37. J. I. Owens et al., Metal-Water Reactions: VIII. Preliminary Consideration of the Effects of a Zircaloy-Water Reaction During a Loss-of-Coolant Accident in a Nuclear Reactor, USAEC Report GEAP-3279, General Electric Co., Atomic Power Equipment Dept., Sept. 30, 1959.
38. S. C. Furman and P. A. McManus, Metal-Water Reactions: IX. The Kinetics of Metal-Water Reactions — Feasibility Study of Some New Techniques, USAEC Report GEAP-3338, General Electric Co., Vallecitos Atomic Laboratory, Jan. 31, 1960.
39. S. Lawroski et al., Chemical Engineering Division Summary Report for July, August, and September 1959, USAEC Report ANL-6068, Argonne National Laboratory, 1959.
40. G. E. Zima, Pyrophoricity of Uranium in Reactor Environments, USAEC Report HW-62442, Hanford Atomic Products Operation, Jan. 22, 1960.
41. J. W. Corbett and R. M. Walker, Threshold Measurements and the Production of Radiation Damage in the Noble Metals, *Phys. Rev.* 117(4): 970–971 (Feb. 15, 1960).
42. T. H. Blewitt et al., Stored Energy of Irradiated Copper, *Phys. Rev. Letters*, 3(3): 132–135 (Aug. 1, 1959).
43. D. O. Thompson and V. K. Paré, Effect of Fast Neutron Bombardment at Various Temperatures upon the Young's Modulus and Internal Friction of Copper, *J. Appl. Phys.*, 31(3): 528–535 (March 1960).
44. A. C. Damask and G. J. Dienes, Neutron-Irradiated Effects in Copper-Aluminum Alloys, *Phys. and Chem. Solids*, 12: 105–107 (1959).
45. M. S. Wechsler and R. H. Kernohan, Neutron-Irradiation Effects on Copper-Aluminum Alloys, *Phys. and Chem. Solids*, 7: 307–326 (1958).
46. M. S. Wechsler and R. H. Kernohan, Reply to the Letter of Damask and Dienes on Neutron-Irradiated Effects in Copper-Aluminum Alloys, *Phys. and Chem. Solids*, 12: 107–109 (1959).
47. G. L. Bacchella et al., Kinetics of Imperfections in Platinum, *Nuovo cimento, Suppl., Series 11*, 3: 435–436 (1959).
48. G. R. Piercy, Point Defects in Platinum, *Phil. Mag.*, 5(51): 201–221 (March 1960).
49. M. W. Thompson, The Damage and Recovery of Neutron-Irradiated Tungsten, *Phil. Mag.*, 5(51): 278–296 (March 1960).
50. G. H. Kinchin and M. W. Thompson, Irradiation Damage and Recovery in Molybdenum and Tungsten, *J. Nuclear Energy*, 6(4): 275–284 (May 1958).
51. P. Lucasson, Low Temperature Irradiation of Transition Metals in an Atomic Pile, *Ann. phys., Series 13*, 4(3–4): 435–488 (March–April 1959).

talline wires. In the article, models for lattice self-diffusion and grain-boundary self-diffusion are discussed, as well as dependence of migration speeds of grain boundaries on the thickness of the specimen.

Usually all equilibrium phases are formed in a diffusion couple of two metals, but the conditions where this may not occur are discussed in a very interesting paper by Baird.[91] The factors controlling the value of the growth constant for an intermetallic layer are discussed, including the effects of grain-boundary diffusion, oxide films, and pressure.

Studies of the diffusion of niobium with chromium, iron, nickel, molybdenum, and several compositions of stainless steel are being made which utilize an electron-probe microanalyzer.[92] In this research at the Naval Research Laboratory, the intermetallic phases in the diffusion zones have been found for each of the systems. All diffusion couples for the investigation were prepared at 1100°C. It was noted in the study that the couples of niobium-nickel often melted at this temperature, although the eutectic temperature is given as 1175°C in some of the literature. Niobium and molybdenum were miscible at all compositions, and the diffusion coefficient was found to range from 3 to 8×10^{-11} cm^2/sec. This research is being continued.

(D. C. Carmichael)

References

1. R. E. Pawel et al., Formation of Oxide Films on Columbium, paper presented at AIME Columbium Metallurgy Symposium, Lake George, N. Y., June 1960.
2. H. Inouye, Oxidation of Columbium at Low Oxygen Pressures, paper presented at AIME Columbium Metallurgy Symposium, Lake George, N. Y., June 1960.
3. J. W. Clark, Ignition of Columbium and Selected Alloys, paper presented at AIME Columbium Metallurgy Symposium, Lake George, N. Y., June 1960.
4. W. D. Klopp et al., High-Temperature Oxidation and Contamination of Columbium, *Trans. Am. Soc. Metals*, 51: 282 (1959).
5. General Dynamics Corp., Maritime Gas-Cooled Reactor Program, Quarterly Progress Report for the Period Ending June 30, 1959, USAEC Report GA-1099, 1959.
6. D. J. Maykuth et al., Development of Corrosion-Resistant Niobium-Base Alloys, USAEC Report BMI-1437, Battelle Memorial Institute, May 12, 1960.
7. W. D. Klopp et al., The Hot Water Corrosion Resistance of Columbium and Columbium Alloys, paper presented at AIME Columbium Metallurgy Symposium, Lake George, N. Y., June 1960.
8. H. A. Fisch and D. L. Douglass, High-Temperature Steam Corrosion of Columbium-Vanadium Alloys, paper presented at AIME Columbium Metallurgy Symposium, Lake George, N. Y., June 1960.
9. R. J. Allio, Behavior of Zirconium-Base Alloys and Hafnium in Long-Lived Cores, USAEC Report KAPL-2088, Knolls Atomic Power Laboratory, May 5, 1960. (Classified)
10. F. W. Albaugh, Reactor and Fuels Research and Development Operation Monthly Report for March 1960, USAEC Report HW-64580-A, Hanford Atomic Products Operation, Apr. 15, 1960. (Classified)
11. D. L. Douglass and B. E. Dearing, Effect of Heat-Treatment on the Corrosion of Zirconium–2 At.% Tin–2 At.% Niobium, USAEC Report KAPL-2071, Knolls Atomic Power Laboratory, Jan. 20, 1960.
12. S. B. Dalgaard, The Corrosion Resistance of Zirconium-Niobium and Zirconium-Niobium-Tin Alloys in High-Temperature Water and Steam, Canadian Report CRMet-911 (AECL-993), March 1960.
13. J. P. Pimsler, Corrosion of Zirconium Alloys in 900 and 1000°F Steam, USAEC Report NMI-1235, Nuclear Metals, Inc., Mar. 15, 1960.
14. Argonne National Laboratory, Annual Report for 1959, Metallurgy Division, USAEC Report ANL-6099, January 1960.
15. F. W. Albaugh, Reactor and Fuels Research and Development Operation Monthly Report for May 1960, USAEC Report HW-65459-A, Hanford Atomic Products Operation, June 15, 1960. (Classified)
16. N. J. M. Wilkens and J. N. Wanklyn, The Corrosion of Aluminum and Its Alloys in High-Pressure Steam, *J. Inst. Metals*, 88: 134–140 (November 1959).
17. H. Coriou et al., Aluminum-Iron-Nickel Alloys Resistant to Corrosion in Water at High Temperature. Basis for Their Properties—Their Improvement, French Report CEA-1313, 1959.
18. D. Lai et al., Oxidation of Iron-Chromium Alloys, Report AFOSR-TN-60-587, Princeton University, Forrestal Research Center, Feb. 29, 1960.
19. M. Smialowski, The Action of Cathodically Evolved Hydrogen on Iron and Nickel as Special Cases of Corrosion Embrittlement of Metals, *Chem. & Ind. (London)*, No. 35, 1078–1083 (Aug. 29, 1959).
20. Aerojet-General Nucleonics, Army Gas-Cooled Reactor Systems Program, Semiannual Progress Report for July 1 Through December 31, 1959, USAEC Report IDO-28549, Feb. 15, 1960.
21. R. W. Dayton and C. R. Tipton, Jr., Progress Relating to Civilian Applications During April 1960, USAEC Report BMI-1434, Battelle Memorial Institute, May 1, 1960. (Classified)

22. R. W. Dayton and C. R. Tipton, Jr., Progress Relating to Civilian Applications During May 1960, USAEC Report BMI-1442, Battelle Memorial Institute, June 1, 1960. (Classified)
23. E. J. Felten, High-Temperature Oxidation of Iron-Chromium-Base Alloys with Particular Reference to Iron-Chromium-Yttrium Alloys, USAEC Report XDC-60-2-153, General Electric Co., Aircraft Nuclear Propulsion Dept., Feb. 10, 1960.
24. R. Speiser, Research on the Oxidation Behavior of Tungsten, Fourth Quarterly Report, Report AD-226333, The Ohio State University Research Foundation, July 1, 1959.
25. E. A. Gulbransen et al., Oxidation of Tungsten and Tungsten-Based Alloys, Report WADC-TR-59-575, Westinghouse Electric Corp., Research Laboratories, February 1960.
26. O. N. Carlson et al., A Study of the High-Temperature Air Oxidation of Yttrium Metal, USAEC Report IS-115, Ames Laboratory, March 1960.
27. E. A. Cernak, comp., The Oxidation of Chromium, Hafnium, Molybdenum, Niobium, Tantalum, Titanium, Tungsten, Vanadium, Zirconium, and Some of Their Alloys; Properties of Some Borides, Carbides, Nitrides, and Oxides of the Same Metals, Report CNLM-1802-5, Pratt & Whitney Aircraft Div., United Aircraft Corp., Dec. 15, 1959.
28. S. J. Cytron, Corrosion Rate Tests of Yankee Primary System Materials in High-Temperature Dynamic Water, USAEC Report YAEC-153, Westinghouse Electric Corp., Bettis Atomic Power Laboratory, September 1959.
29. Brookhaven National Laboratory, Nuclear Engineering Department Progress Report for May 1–August 31, 1959, USAEC Report BNL-583, April 1960.
30. Babcock and Wilcox Co., Liquid Metal Fuel Reactor Experiment Quarterly Technical Report for April–June 1959, USAEC Report BAW-1170, 1959.
31. W. W. Kendall, Corrosion of Beryllium in Flowing Sodium, USAEC Report GEAP-3333, General Electric Co., Atomic Power Equipment Dept., Jan. 15, 1960.
32. Oak Ridge National Laboratory, Gas-Cooled Reactor Project Quarterly Progress Report for Period Ending March 31, 1960, USAEC Report ORNL-2929, June 21, 1960.
33. W. H. Cook, Corrosion Resistance of Various Ceramics and Cermets to Liquid Metals, USAEC Report ORNL-2391, June 15, 1960.
34. S. C. Furman, Metal-Water Reactions: V. The Kinetics of Metal-Water Reactions. Low Pressure Studies, USAEC Report GEAP-3208, General Electric Co., Vallecitos Atomic Laboratory, July 31, 1959.
35. L. F. Epstein, Metal-Water Reactions: VI. Analytical Formulations for the Reaction Rate, USAEC Report GEAP-3272, General Electric Co., Vallecitos Atomic Laboratory, Sept. 30, 1959.
36. L. F. Epstein, Metal-Water Reactions: VII. Reactor Safety Aspects of Metal-Water Reactions, USAEC Report GEAP-3335, General Electric Co., Vallecitos Atomic Laboratory, Jan. 31, 1960.
37. J. I. Owens et al., Metal-Water Reactions: VIII. Preliminary Consideration of the Effects of a Zircaloy-Water Reaction During a Loss-of-Coolant Accident in a Nuclear Reactor, USAEC Report GEAP-3279, General Electric Co., Atomic Power Equipment Dept., Sept. 30, 1959.
38. S. C. Furman and P. A. McManus, Metal-Water Reactions: IX. The Kinetics of Metal-Water Reactions — Feasibility Study of Some New Techniques, USAEC Report GEAP-3338, General Electric Co., Vallecitos Atomic Laboratory, Jan. 31, 1960.
39. S. Lawroski et al., Chemical Engineering Division Summary Report for July, August, and September 1959, USAEC Report ANL-6068, Argonne National Laboratory, 1959.
40. G. E. Zima, Pyrophoricity of Uranium in Reactor Environments, USAEC Report HW-62442, Hanford Atomic Products Operation, Jan. 22, 1960.
41. J. W. Corbett and R. M. Walker, Threshold Measurements and the Production of Radiation Damage in the Noble Metals, *Phys. Rev.* 117(4): 970–971 (Feb. 15, 1960).
42. T. H. Blewitt et al., Stored Energy of Irradiated Copper, *Phys. Rev. Letters*, 3(3): 132–135 (Aug. 1, 1959).
43. D. O. Thompson and V. K. Paré, Effect of Fast Neutron Bombardment at Various Temperatures upon the Young's Modulus and Internal Friction of Copper, *J. Appl. Phys.*, 31(3): 528–535 (March 1960).
44. A. C. Damask and G. J. Dienes, Neutron-Irradiated Effects in Copper-Aluminum Alloys, *Phys. and Chem. Solids*, 12: 105–107 (1959).
45. M. S. Wechsler and R. H. Kernohan, Neutron-Irradiation Effects on Copper-Aluminum Alloys, *Phys. and Chem. Solids*, 7: 307–326 (1958).
46. M. S. Wechsler and R. H. Kernohan, Reply to the Letter of Damask and Dienes on Neutron-Irradiated Effects in Copper-Aluminum Alloys, *Phys. and Chem. Solids*, 12: 107–109 (1959).
47. G. L. Bacchella et al., Kinetics of Imperfections in Platinum, *Nuovo cimento, Suppl., Series 11*, 3: 435–436 (1959).
48. G. R. Piercy, Point Defects in Platinum, *Phil. Mag.*, 5(51): 201–221 (March 1960).
49. M. W. Thompson, The Damage and Recovery of Neutron-Irradiated Tungsten, *Phil. Mag.*, 5(51): 278–296 (March 1960).
50. G. H. Kinchin and M. W. Thompson, Irradiation Damage and Recovery in Molybdenum and Tungsten, *J. Nuclear Energy*, 6(4): 275–284 (May 1958).
51. P. Lucasson, Low Temperature Irradiation of Transition Metals in an Atomic Pile, *Ann. phys., Series 13*, 4(3–4): 435–488 (March–April 1959).

52. P. Lucasson, Low Temperature Irradiation of Transition Metals in an Atomic Pile, *J. Nuclear Energy: Pt. A, Reactor Sci.*, 11(2/4): 108–113 (February 1960).
53. K. D. Chaudhuri et al., The Effect of Radiation Damage on the Thermal Conductivity of Superconductors, British Report AERE-R-3319, April 1960.
54. F. M. Ryan et al., Superparamagnetism, Nonrandomness, and Irradiation Effects in Copper-Nickel Alloys, *Phys. Rev.*, 116: 1106–1112 (December 1959).
55. I. Ya. Dekhtyar and A. M. Shalaev, The Nature of the Imperfections Obtained During the Irradiation of an Alloy Fe_3Al by γ-Rays, *Inzhener.-Fiz. Zhur., Akad. Nauk Belorus. S.S.R.*, 3(2): 78–82 (February 1960).
56. A. C. Damask, Electron Irradiation of Solids (to U. S. Atomic Energy Commission), U. S. Patent 2,911,533, Nov. 3, 1959; also A Comparison of Electron with Neutron Irradiation of Alpha Brass, *Phys. and Chem. Solids*, 4: 177–181 (1958).
57. D. Bally and L. Benes, The K-Absorption Spectrum of Neutron-Irradiated Nickel, *Nuovo cimento*, 14: 1384–1385 (December 1959).
58. J. Silcox and P. B. Hirsch, Dislocation Loops in Neutron-Irradiated Copper, *Phil. Mag.*, 4: 1356–1374 (December 1959).
59. F. W. Young, Jr., and T. S. Noggle, Evidence for Dislocation Reactions in Copper, *J. Appl. Phys.*, 31(3): 604–606 (1960).
60. Excerpts from Monthly Progress Reports of LASL, September 1959; UCLRL, September 1959; Mound Laboratory, September 1959; and Hanford Atomic Products Operation, September 1959, USAEC Report WASH-933, May 1960. (Classified)
61. Hanford Atomic Products Operation, Fuels Development Operation Quarterly Progress Report for April to June 1959, USAEC Report HW-62085, July 15, 1959. (Classified)
62. W. Mönch and W. Sander, Measurements of the Energy of Ordering Defects in Quenched Condensed Copper at Low Temperature, *Z. Physik*, 157(2): 149–158 (1959).
63. I. Teodorescu and A. Glodeanu, Effects of Fast-Neutron Irradiation on Nickel Thin Films, *Phys. Rev. Letters*, 4(5): 231–232 (Mar. 1, 1960).
64. T. Asada et al., Annealing of γ-Ray Damage in Germanium, *J. Phys. Soc. Japan*, 15: 93–94 (January 1960).
65. B. B. Meckel et al., Microscopic Study of Neutron-Irradiated Germanium, *J. Appl. Phys.*, 31(7): 1299 (July 1960).
66. A. D. Whapham and M. J. Makin, The Hardening of LiF by Electron Irradiation, *Phil. Mag.*, 5(51): 237–250 (March 1960).
67. H. S. Inghram and R. Smoluchowski, Ionic Conductivity of γ-Irradiated NaCl, *Phys. Rev.*, 117 (5): 1207–1215 (Mar. 1, 1960).
68. Low-Temperature Thermal Conductivity of LiF Crystal upon Radiation by Thermal Neutrons and Co^{60} γ-Rays, *Bull. inst. intern. froid, Annexe No. 1*, pp. 173–180 (1958).
69. D. A. Wiegand and R. Smoluchowski, Low-Temperature Annealing of Irradiation-Induced Defects in LiF, *Phys. Rev.*, 116: 1069–1080 (December 1959).
70. H. Rabin, X-Ray Expansion and Coloration of Undoped and Impurity-Doped NaCl Crystals, *Phys. Rev.*, 116: 1381–1389 (December 1959).
71. G. W. Arnold and W. D. Compton, Threshold Energy for Lattice Displacement in α-Al_2O_3, *Phys. Rev. Letters*, 4(2): 66–68 (Jan. 15, 1960).
72. R. M. Berman et al., Fission Fragment Damage to Crystal Structures, USAEC Report WAPD-T-1125, Westinghouse Electric Corp., Bettis Atomic Power Laboratory, Feb. 2, 1960.
73. G. T. Murray and G. Pincus, Permeability of Cladding Materials to Inert Gases, USAEC Report MRC-R-156, Materials Research Corp., Apr. 22, 1960.
74. W. D. Compton and G. W. Arnold, Lattice Displacements by Fast Electrons, *J. Appl. Phys.*, 31 (4): 621–625 (April 1960).
75. E. Brown and G. H. Goedecke, Effect of Atomic Interaction Potential on Defect Production in Metals, *J. Appl. Phys.*, 31(5): 932–934 (May 1960).
76. F. A. Levi, Mechanical Properties of Irradiated Solids, *Nuovo cimento, Suppl., Series 12*, 2: 124–294 (1959).
77. D. K. Holmes et al., On the Interpretation of Radiation Effects in the Noble Metals, *Proceedings of the Second United Nations International Conference on the Peaceful Uses of Atomic Energy, Geneva, 1958*, Vol. 6, p. 274, United Nations, New York, 1958.
78. K. Sagel, Changes in Material Properties Induced by Corpuscular and Photon Radiation, *Metall.*, 12: 353–363 (May 1958).
79. F. J. P. Clarke, Effects of Reactor Irradiation on Ceramic Materials, British Report AERE-M-659, April 1960.
80. F. J. P. Clarke, The Effect of Reactor Irradiation on Ceramic Materials, *Angew. Chem.*, 71 (20): 652 (1959).
81. L. M. Howe, The Annealing of Irradiation Damage in Zircaloy-2 and the Effect of High Temperature Irradiation on the Tensile Properties of Zircaloy-2, Canadian Report CRMet-922 (AECL-1024), April 1960.
82. R. L. Mehan, Irradiation of Haynes-25 and Inconel X Compression Springs in High-Temperature High-Pressure Water, *J. Basic Eng.*, 81: 226 (June 1959).
83. D. L. Gray, An Effect of Neutron Flux Level upon Damage Accumulation, USAEC Report HW-61287, Hanford Atomic Products Operation, July 30, 1959.
84. Westinghouse Electric Corp., Bettis Atomic Power Laboratory, Zirconium Highlights, USAEC Report WAPD-ZH-23, March 1960.
85. L. P. Costas, Thermal Conductivity of Aluminum-

Lithium Alloys Containing Up to 8 Wt.% Lithium, USAEC Report DP-463, E. I. du Pont de Nemours & Company, Inc., April 1960.

86. M. J. Cooper, The Structure of the Intermetallic Phase θ (Chromium-Aluminum), *Acta Cryst.*, 13: 257–263 (Mar. 10, 1960).
87. N. Müller, Diffusion in the Systems Uranium-Zirconium and Uranium-Nickel, *Z. Metallk.*, 50: 652–660 (1959).
88. Y. Adda et al., Demonstration and Interpretation of an Inversion Phenomenon in the Direction of Displacement of the Interface in Uranium-Zirconium Diffusion, *Compt. rend.*, 249: 2775–2777 (Dec. 21, 1959).
89. *Symposium on Solid State Diffusion, held at Saclay, July 3, 4, and 5, 1958*, Centre d'Études Nucléaires de Saclay, 1959 (in French).
90. P. Hassen and F. Haessner, Research on Grain-Boundary Migration in Aluminum Bicrystals, *Z. Metallk.*, 51: 101–108 (February 1960).
91. J. D. Baird, The Formation of Intermediate Alloy Layers in the Interdiffusion of Metals, *J. Nuclear Energy: Pt. A, Reactor Sci.*, 11(2/4): 81–88 (February 1960).
92. L. S. Birks and R. E. Seebold, Diffusion of Niobium with Chromium, Iron, Nickel, Molybdenum, and Stainless Steel, Report NRL-5461, Naval Research Laboratory, Mar. 31, 1960.

Section VI

SPECIAL FABRICATION TECHNIQUES

Melting, Casting, Heat-Treatment, and Hot Working

Unalloyed uranium continues to be a material of topical interest because of difficulties experienced in controlling its chemistry and fabrication. In efforts to improve the chemical and metal qualities of unalloyed uranium, National Lead Company of Ohio[1] has been studying the effects of furnace pressure during melting (350 mm, 30 mm, 3 mm, and 3×10^{-2} mm Hg absolute) on the final chemistry of the uranium ingots. Although only a limited number of ingots have been analyzed, the data indicate that (1) at the higher furnace pressures the hydrogen, nitrogen, and oxygen contents of the ingot are higher and the carbon content is lower and (2) it may be practical to control ingot chemistry by controlling the furnace pressures.

The casting of uranium tubes has also received attention. The method presently being studied is the horizontal centrifugal casting technique. Tubes with good surfaces have been obtained with Meehanite mold liners coated with flame-sprayed $MgZrO_3$. The best tubes were obtained in molds rotating at 800 rpm at a metal pouring temperature of 2650°F. It was also noted that the large as-cast grain structure was successfully refined by beta heat-treatments.

The importance of the grain size in subsequent fabrication operations is pointed up by an inquiry currently in progress at Nuclear Metals.[2] Numerous observations have been made which have led to the conclusion that large grain size or large grain "patches" cause rough core-cladding interfaces in a coextruded fuel element. This roughness ultimately requires the imposition of thicker claddings with the accompanying disadvantages in fuel-element operation. In efforts to define the required thickness of fine-grained material sufficiently to overcome the formation of irregular core-cladding interfaces, composite uranium cores made up with fine-grained sleeves and large-grained centers were coextruded in copper. Rods with large-grained centers showed decreasing interface roughness with increasing fine-grained uranium sleeve thickness. However, the rods with the thickest sleeves did not have as smooth an interface as that obtained in reference rods with heavily alpha-worked cores. The effects of the coarse grains were evident even through a thickness of fine-grained uranium about five times the grain diameter of the core material.

In reporting on the results of preliminary studies of vacuum-arc melting and extrusion of tungsten, Foyle et al. of NASA have found[3] that:

1. Sound $1\frac{1}{2}$-in.-diameter ingots could be prepared by consumable-electrode vacuum-arc melting with direct current (electrode positive). The removal of as little as $\frac{1}{8}$ in. from the as-cast surface removed all surface imperfections. Typically, a $\frac{3}{4}$-in. swaged rod could be melted at a rate of 5 lb/min at 23 volts and 3400 amp in a pressure of less than 10 μ. No significant impurity removal was noted, and this lack was attributed to the rapid melting rate.

2. Low-velocity extrusion (94 in./min) could be successfully employed at reduction ratios up to 8:1 at 3100°F if the tungsten was clad in niobium and lubricated. Attempts to extrude unclad tungsten at a reduction ratio of 6:1 and at temperatures up to 3600°F were unsuccessful, even at an extrusion pressure of 150,000 psi.

3. High-velocity-extrusion (150,000 in./min) attempts were successful with unclad tungsten at temperatures of 3000 to 3800°F with reduction ratios of 45:1.

4. No recrystallization occurred in material extruded by the low-velocity process (most severe conditions: 3200°F; reduction ratio 8 : 1). However, complete recrystallization was observed in material extruded by the high-velocity press at 3800°F and a reduction ratio of 45 : 1. Less complete recrystallization was observed in materials extruded at high velocity and at lower temperatures and reduction ratios.

5. There were only slight differences in the ultimate tensile strength at 1000°F (approximately 70,000 psi) of tungsten produced by vacuum-arc casting and low-velocity extrusion, sintering and low-velocity extrusion, and sintering and swaging (commercial rod stock). However, high-velocity extruded tungsten was softer and much lower in tensile strength at 1000°F.

6. At 4000°F a sample of low-velocity extruded, arc-cast tungsten was more ductile than sintered and swaged commercial bar stock. Only a slight loss in strength was noted.

(E. L. Foster)

Cladding

Cladding by Rolling and Swaging

Concentrated interest in the fabrication of rod and tubular elements containing UO_2 by swaging is evident in many recent reports. Efforts to produce a more economical fuel element by simultaneous densification and cladding of various types of UO_2 have yielded significant technical contributions to the art of fabrication of fuel elements by swaging.

Cladding by roll bonding is presently being employed to fabricate advanced fuel systems containing dispersed fuel and distributed poison particles. Initial studies on self-bonding of tungsten by roll cladding appear promising.

The effect of the design of swaging hammers on core density of Zircaloy-2-clad UO_2 fuel elements is being studied at Savannah River.[4] Experiments have shown that swaged oxide densities are about 2 per cent lower for elements prepared with "bump" type hammers rather than with "crown" type hammers. Crown type hammers are being installed for production of tubular fuel elements. It is thought that the 2 per cent lower densities achieved with the bump type hammer resulted from the briefer impact produced by this type of hammer. The forging blow of tne crown hammer dwells on the work about 60 per cent longer per stroke.

Specifications for the preparation of Zircaloy-clad UO_2 by swaging for the 19-rod-cluster fuel element of the Plutonium Recycle Test Reactor have been developed at Hanford.[5] The specifications developed include detail dimensions, materials, fabrication steps, acceptance criteria, and final assembly steps. The elements produced contained UO_2 of 85 per cent of the theoretical density or greater. The rod elements were approximately 0.565 in. in diameter and 90 in. in length after swaging. Reductions of approximately 15 per cent per pass were employed to achieve the desired outside diameter.

Reduction of Zircaloy tubing by drawing is also being investigated. The biggest obstacle to be solved in drawing Zircaloy-2-clad uranium rod elements is the proper lubrication of the hardened steel drawing dies. Copper, plastic films, and solid lubricants are being studied as drawing lubricants for the Zircaloy-2-clad elements.

Stainless-steel-clad UO_2 specimens are being fabricated by swaging for in-pile tests at Savannah River.[6] The test specimens consist of tubes containing fused oxide loaded into an annulus between concentric stainless-steel sheaths. The tubes were loaded with oxide by tapping the tube walls to achieve an initial density of 66 per cent. Tubular elements produced in this manner exhibited excellent sheath surfaces after the swaging operation.

Aluminum-coated fuel-bearing Fiberglas as a core material is being roll clad with aluminum[7] by the Clevite Corporation. During roll cladding, a ripple effect of the fuel-bearing Fiberglas core was observed during the initial studies. This ripple effect is concentrated along the core edges. The Fiberglas core inserts are machined to fit the aluminum frames. This eliminates the edge cracking of the core insert observed during the preliminary roll-cladding studies.

Roll-cladding temperatures of 850, 1000, 1100, and 1150°F were studied. The best results were achieved by rolling at temperatures of 1000 to 1100°F. Total reduction ratios of 4 : 1, 6 : 1, and 8 : 1 with various reductions per pass were used to determine the effect of the roll schedule on rippling of the core and the properties of the resultant fuel plates.

(E. S. Hodge)

Pressure Bonding

The term pressure bonding refers to a process that involves the use of gas pressure at an elevated temperature. In essence, it is a hot-press process that is being utilized for the bonding and joining of reactor components and for the densification of ceramic, cermet, and dispersion fuels.

Solid-phase bonding of niobium and molybdenum has been achieved at Battelle[8–13] by use of a gas-pressure-bonding technique. The study involved the development of a fabrication process for preparing flat-plate, rod, and tubular fuel elements and assemblies. Bonding is achieved at temperatures ranging from 2100 to 2350°F. The most serious problem is associated with the development of compatible materials that can be utilized as spacers during the bonding operation. Graphite-coated molybdenum and Ti-Namel, MgO, molybdenum, UO_2, Vycor, and window glass have been evaluated. Of these materials, UO_2 was found to be least reactive.

The simultaneous densification and cladding of UO_2 fuel by the use of the gas-pressure-bonding process is being investigated by Sylvania-Corning[14,15] and Battelle.[8–13] Sylvania has pressure bonded various grades of UO_2 in the temperature range from 2200 to 2375°F. The optimum density, on the order of 92 to 99 per cent of the theoretical, was achieved with a mixture consisting of 75 per cent coarse fused UO_2 and 25 per cent ceramic-grade UO_2. The work at Battelle was concerned with the evaluation of seven commercial grades of UO_2. By utilization of an ideal rhombohedral packing, cold-pressed compacts with densities up to 85 per cent of the theoretical were produced. Optimum densities were also obtained with a mixture of fused and ceramic grades of UO_2. Helium-permeability tests were conducted on pressure-bonded UO_2 of 95.8 per cent of the theoretical density. The helium flow rate through 1 cm of UO_2 with a 1-mm pressure differential was less than 10^{-10} cm^3/sec, the lowest that could be measured with the technique used.

A Zircaloy-clad flat-plate compartmented UO_2 fuel plate has been designed by Bettis for the PWR Core 2. Both Battelle and Bettis are actively engaged in the development of the gas-pressure-bonding process for the fabrication of these fuel plates. The work conducted by Battelle[16] is summarized in a recent topical report. Specimens of up to 40 in. in length with 330 individual UO_2 fuel compartments have been successfully bonded. Bonding was achieved at 1550°F at 10,000 psi. The individual UO_2 cores were coated with 25 to 40 μ of chromium by vapor deposition or 15 to 40 μ of pyrolytic carbon to prevent reaction with the Zircaloy. Bettis has been conducting a study concerned with an evaluation of the effect of surface treatment of the Zircaloy on subsequent bond characteristics.[17,18] Bettis demonstrated that (1) surface roughness has a pronounced effect — excellent bonds are achieved with very rough surfaces, 190 μin., rms; (2) a metallographic surface finish produces poor bonds; (3) vacuum treatment for 4 hr at 1550°F has an adverse effect; (4) argon-ion bombardment inhibits grain growth at the bond interface; and (5) a fine zirconium oxide film improves bonds of specimens that possess an inherently poor bond.

Cermet fuel materials consisting of 80 vol.% UO_2 in matrices of molybdenum, stainless steel, niobium, and chromium have been densified and clad by the pressure-bonding process.[8–13] The fuels embodying stainless-steel are densified and clad at 2100°F. The refractory cermets have been bonded in the temperature range of 2250 to 2350°F with a pressure of 10,000 psi. Densities up to 95 per cent of the theoretical density have been achieved.

Cladding of uranium with Zircaloy by the pressure-bonding technique is being explored by Hanford and Du Pont. Hanford[19] is evaluating Zircaloy-clad cast uranium tubes bonded by Battelle at 1550°F and 10,000 psi for 4 hr. The fabrication of aluminum-clad uranium tubular fuel elements is being investigated by Du Pont.[20] The process has been optimized, and several process steps have been eliminated to make it economically feasible. (S. J. Paprocki)

Diffusion Bonding

A survey of the field of diffusion bonding has been made by the Defense Metals Information Center.[21] Diffusion bonding with and without the use of intermediate materials is discussed. The various techniques that have been used are described, and their applications to specific materials are discussed in some detail. The report is complete and of considerable general interest.

The diffusion welding of uranium and zirconium is discussed in an Italian publication.[22]

The experimental method used to find more suitable conditions for a good diffusional bonding of uranium and Zircaloy-2 and the results obtained are described. An interpretation of the observed phenomena is also proposed.

(D. C. Carmichael)

Coextrusion

Four variations of the coextrusion process were tried by Nuclear Metals[23] in an effort to develop the most feasible method for fabricating relatively heavy-walled Zircaloy-clad uranium I and E fuel elements with a small inner diameter. The tube specifications were 1.471 ± 0.003 in. in outside diameter and 0.400 ± 0.003 in. in inside diameter, with a 9-ft minimum and an 18-ft maximum length and a cladding thickness of 0.020 ± 0.002 in. A minimum extrusion area reduction of approximately 15:1 was selected to obtain good bonds between the Zircaloy and uranium. The four methods investigated included (1) the conventional floating mandrel, (2) the oversize mandrel, (3) the stationary tipped mandrel, and (4) the filled billet. The best tubes were produced by coextruding directly to size over a conventional floating mandrel.

Studies have been conducted which were aimed at establishing methods and techniques for achieving coextrusions of the following: stainless-steel-clad uranium, magnesium-clad uranium, stainless-steel-clad UO_2, molybdenum-clad UO_2, beryllium-clad uranium, and beryllium-clad uranium having small alloy additions.

Promising samples of two potential types of metal-clad UO_2 rods have been produced by Nuclear Metals.[27] These consist of a stainless-steel-clad UO_2 element which has an invervening layer of graphite about 15 mils thick and a tantalum-clad UO_2 element. UO_2 densities of 10.4 g/cm^3 with oxygen-uranium ratios of less than 2.10 have been obtained; however, the surface smoothness and interface roughness were not as good as those obtained in the usual metal-over-metal coextrusion. A sufficient number of these two types of elements has been produced to demonstrate technical feasibility.

(C. B. Boyer)

Extrusion Cladding

A summary report of work relating to the extrusion cladding of long uranium plates with aluminum indicates that an extrusion speed of 16 in./min will produce a well-bonded element of precise dimensions.[28] The quality of the bonded end seal, which was APM aluminum, was sufficiently high to obviate any need for subsequent welding. As expected, the bond quality depended upon the core preheat temperature and the extrusion speed. As extrusion speeds were increased above 16 in./min, for example, the time allowed for the core to absorb heat from the tools and the preheat station became insufficient to assure good bonding. Thus, at about 30 in./min, only sporadic bonding occurred, and, at 40 in./min, no bonding was observed. On the other hand, a reproducible bond averaging 15,000 psi tensile strength was achieved at an extrusion speed of 16 in./min and a core preheat temperature of 250 to 300°C.

(H. J. Wagner)

Canning

Studies at Argonne[29] show that flat, natural-uranium plates mechanically canned with aluminum sheaths reveal a tendency for thermal contact between cladding and core to diminish as a result of elongation and roughening of the uranium upon irradiation. The assemblies containing beta-quenched uranium showed less damage than those in which material rolled in the high alpha range was used.

A patent has been issued[30] which pertains to a jacketed uranium slug and the process of producing it. In the process, uranium is cast into a molybdenum jacket lined with a bonding layer of nickel.

A fuel element that was developed at the International School of Nuclear Science and Engineering[31] consists of a core composed of a dispersion of U_3O_8 and aluminum powders clad with aluminum. The core powders are mixed and pressed at 25 tsi to form a compact, which is held in the center of a mold by locating pins, and a molten aluminum alloy is poured around it to form the cladding. The cast-clad billet is then hot rolled to a specified thickness and trimmed to size. The fuel element and the techniques used to produce it offer complete containment of fuel material during fabrication with no inherent losses. Also, the cast-cladding technique for canning involves a minimum loss of cladding material.

Studies at Oak Ridge[32] have been concerned with the replacement of helium by a low-

melting-point metal in the annulus between fuel and cladding in elements of the type specified for Cores 1 and 2 of the N.S. *Savannah* reactor. This approach offers a means of minimizing peak fuel centerline temperatures. Current investigations indicate the feasibility of using lead because of (1) its good compatibility with UO_2 and type 304 stainless steel and (2) its availability. Several methods of filling the annulus between the fuel and cladding with lead were investigated. To date, only one method has produced lead bonds of consistent quality. This method involves immersing loaded tubes in a bath of molten lead.

Argonne[33] has succeeded in encapsulating in tight-fitting type 304 stainless-steel cans about 27 kg of alpha-stabilized plutonium in the form of thin, flat, nickel-coated slugs. Nickel was used as a coating for these slugs to protect them against oxidation and to permit their being loaded into the cans outside a glove box. The canned slugs are to be used in the ZPR-III core. (E. G. Smith, Jr.)

Nonelectrolytic Chemical-Plating Techniques

The surfacing of metals for high-temperature-process applications by flame plating, diffusion coating, hot dipping, metallizing, hard surfacing, and cladding is discussed in a recent review.[34]

During studies of the heat-treatment of electroless nickel coatings, Oak Ridge workers[35] found that no microstructural changes occurred below 750°F in coatings of chemically deposited nickel and phosphorus (7 to 10.5 per cent). Above 750°F, precipitation and agglomeration were detected. A maximum hardness (1000 DPH) was found to be independent of phosphorus content and occurred during the formation of an interim lattice from the amorphous structure of the as-deposited plate.

At the U. S. Naval Research Laboratory,[36] oxidation resistance was imparted to samples of niobium by dipping them in liquid zinc. Tests conducted on a sample with an intentional flaw, produced after coating, revealed a moderate hardness increase near the flaw. No indication of oxygen absorption or other embrittlement after 5 hr at 2000°F was observed in the coated metal.

A method of coating plates of sintered UO_2 with beryllium by sandwiching the plate of UO_2 between layers of beryllium powder in a steel can has been developed by the British.[37] The assembly is placed in a die, heated to 1100°C, and pressed to 2000 psi.

Atomics International[38] has presented a useful summary of the literature on vapor-phase plating as applied to the coating of reactor fuel materials.

The successful coating of UO_2 spheres with various metals is described by Nuclear Materials and Equipment Corporation (NUMEC).[39] Chemical immersion followed by electroplating was used to deposit nickel coatings. Chromium coatings were applied by vacuum evaporation, electroplating, and halide-vapor reduction. Copper was applied by chemical immersion and electroplating. Niobium, molybdenum, and tungsten coatings were obtained by hydrogen reduction of the chlorides on particles agitated in the vapor stream by rotation and vibration of the container. Uranium-metal spheres were too reactive to coat by methods that could be used for the UO_2 spheres. Therefore, protective barriers of copper and nickel were applied by electroplating prior to the use of the other methods. The interesting possibility was suggested of forming a fuel-matrix composite by (1) coating the agitated powder and (2) infiltrating the pores with coating material by continuing the reaction in a static bed of the powder.

A subsequent report[40] gives further details on the equipment used to coat −100 +140-mesh UO_2 with niobium in 100- and 300-g lots at rates of 1 and 0.4 μ/hr, respectively. Preliminary experiments on the coating of UO_2 with chromium showed that an undercoat of niobium or nickel was necessary to develop a continuous coating by hydrogen reduction of the chloride. Coatings on bare UO_2 were discontinuous.

In work at Battelle on the coating of nuclear fuel particles by vapor-deposition techniques, the most significant development has been the outstanding fission-product retention of alumina coatings on UO_2.[12,13,41] About 500,000 enriched UO_2 particles, coated with 40 μ of alpha alumina by hydrolysis of Al_2Cl_6 vapor at 1000°C, have been incorporated into a graphite sphere of the type contemplated for the Pebble-Bed Reactor. This fuel element is being operated in the Battelle Research Reactor at a power output of 1.5 kw and a surface temperature of 1360 to 1500°F. Radiation monitoring of helium, swept through the capsule containing the specimen, indicated that only 10^{-7} to 10^{-8} of the volatile fission products generated were being released.

At the end of 64 days, the element had reached a burnup of 2.5 per cent.

The deposition of carbon coatings on UC_2 and ThC_2-UC_2 powders was continued at Battelle. Kinetic data for the formation of pyrolytic carbon from acetylene were obtained.[12] An activation energy of 50 kcal/mole was determined, compared with 90 kcal/mole previously measured for the thermal decomposition of methane. As the result of the much more rapid reaction with acetylene, it is possible to coat 100- to 150-μ particles with pyrolytic carbon at a rate of 20 μ/hr at 1400°C. Owing to the large difference in the coefficients of expansion of pyrolytic carbon and UC_2, the coatings tend to crack when heated to temperatures above the preparation temperature.

The fluidized-bed coating of UO_2 powder with niobium by hydrogen reduction of the chloride vapor is described in detail.[42] More limited information is given on coating with molybdenum, tungsten, niobium, pyrolytic carbon, tantalum, niobium carbide, and niobium-vanadium alloys. (J. M. Blocher, Jr.)

Electroplating

Hanford workers observed[43] that cathodic evolution of hydrogen on nickel-plated fuel elements caused blistering similar to that observed by in-reactor irradiation. The tendency to blister was increased by thermal cycling, but the cause of in-reactor blistering is attributed to atomic hydrogen formed by corrosion or radiation-induced decomposition of water. Blistering of nickel was found[44] to be most severe when the water had a *p*H of 7, much less at *p*H 10, and completely absent at *p*H 4.

Beach and Gurklis[45] have summarized some of the best procedures for electroplating various metals onto the refractory metals. Refractory metals covered are vanadium, niobium, tantalum, tungsten, titanium, molybdenum, and certain alloys of these metals. Procedures for preparation for plating, as well as the plating procedures and postplating treatments, are itemized and discussed.

Huddle and Gibson[46] have patented a method for coating uranium or its alloys. The uranium is heated with a metal or oxide powder mixed with halide or oxyhalide. In one example, uranium was cleaned and dried and immersed in a powdered mixture of beryllium and 25 wt.% $BeCl_2$ and heated to 500°C for 4 hr.

(J. McCallum)

Ceramic Coatings

Uranium dioxide particles, clad with 20 and 50 μ of Al_2O_3 and dispersed in graphite, were heated at 2500°F in helium for periods up to 1000 hr at Battelle.[12,13] Progressive reaction between the graphite and the Al_2O_3 after 500 hr was observed. The 50-μ cladding protected the fuel better than the 20-μ cladding.

A laminated ceramic coating for metal parts has been developed by Knolls.[47] Parts to be coated were cleaned, vapor blasted, and then exposed to $TiCl_4$ vapor. The $TiCl_4$ formed a TiO_2 layer about 1 μ thick on the surface of the part. A coating consisting of 40 per cent Al_2O_3, 20 per cent deionized H_2O, and 40 per cent sodium silicate (water glass) diluted with 50 per cent water was then applied by air-brush spraying. Alternate layers were applied to a total thickness of 10 to 15 μ. The coating is said to be electrically insulating, mechanically strong, and heat resistant.

Hot-pressed composite bodies of $ZrSiO_4$ and ZrB_2 have been prepared which have excellent thermal-shock resistance and oxidation resistance up to 3180°F, according to Carborundum Company.[48] ZrB_2 with either Zr_5Si_3 or $MoSi_2$ have excellent oxidation resistance up to 3540°F.

(B. W. King)

Explosive Forming

The principles of explosive forming and discussions of applications are presented in articles by Williams[49] and Peckner.[50] The characteristics of low and high explosives, the impulsive load, and critical stress and velocity are discussed. The low or deflagrating explosives (e.g., smokeless powder and black powder) are characterized by burning rates of up to hundreds of feet per second and pressures of from 10,000 to 300,000 psi, both of which are dependent on the degree of confinement. High or detonating explosives (e.g., TNT, dynamite, PETN, and RDX) are characterized by a reaction zone that travels through the explosive at velocities of several thousand feet per second. Most high explosives release their energy at a constant rate because of the high speed of reaction, and therefore they will produce a shock front with a pressure of several million pounds per square inch regardless of the confinement. A characteristic of the impulsive load produced by explosive forming is a rapid increase and

decrease of the pressure pulse. This pulse is in the microsecond range for high explosives and in the millisecond range for low explosives, but the total energy released is the same in both cases. Figure 18 is a schematic illustration of a typical time-pressure profile for both a low and a high explosive.

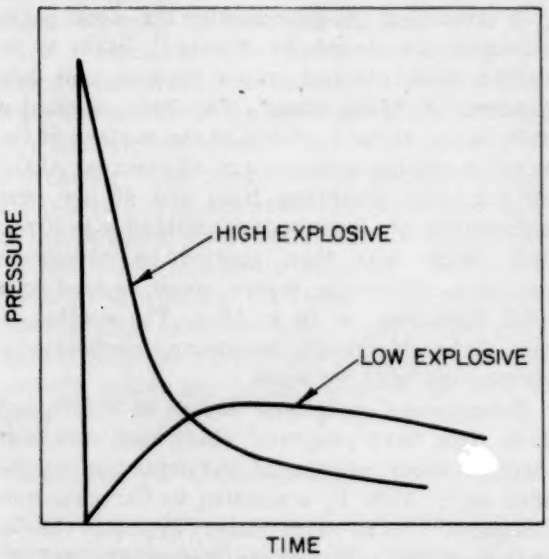

Figure 18—Typical time-pressure profiles for low and high explosives.[49] (Reprinted by permission from the *Journal of Metals*.)

It is possible to vary the pressure pulse generated by the detonation of a high explosive from the abrupt intense pulse to the broader, less intense pulse characteristic of a low explosive. This is accomplished by changing one or more of the following variables: type of charge, charge weight, geometry of charge, standoff distance, or transfer medium. By proper control of these parameters, a wide variety of shapes and strengths of pressure pulse can be obtained. The critical normal fracture stress (that stress required to rupture a specific material) and the critical velocity (that velocity at which permanent deformation will occur on the impacted surface) are of primary concern in explosive forming since these values must be taken into consideration before choosing the explosive parameters to be employed for a particular forming operation.

Water has been found to be an efficient transfer medium in the use of high explosives. It is approximately 30 per cent more efficient than air, it serves to muffle the noise resulting from the detonation, and it minimizes damage to the surface of the workpiece by particles emanating from the explosion. When the amount of deformation required is great or the dimensional tolerances are critical, evacuation of the space between the workpiece and die is necessary.

Different materials have been formed ranging from copper[51] to the refractory metals.[52] The effects of explosive forming on the mechanical properties of several of these materials have been examined. It was found that the increases in hardness, strength, and fatigue limits; the thinning profiles; and the grain deformations obtained were commensurate with the effects resulting from conventional cold-working techniques.

A metal-gathering technique for forming sharp-angle, conical shapes has been developed at the Canadian Armament Research and Development Establishment.[51] Figure 19 shows

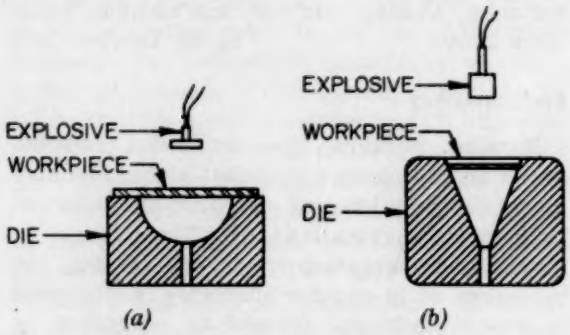

Figure 19—Explosive forming setup for conventional and modified deep-drawing operation.[51] (*a*) Conventional method and (*b*) modified method.

the conventional and new modified setups for explosive deep drawing. A major disadvantage of the conventional process was that, under explosive pressure, the friction between the workpiece and the die prevented the workpiece from flowing into the die. In the modified technique, however, this source of friction was greatly reduced because of the thickening of the workpiece as it accelerated at a high velocity toward the bottom of the die. Hardness and thickness measurements were taken on the shapes formed by this method to determine the mechanics of the forming operation. Results revealed that the forming of the shape was accomplished by two different mechanisms, metal gathering and deep drawing.

A study concerning the explosive welding of similar and dissimilar materials is presently being conducted by National Northern.[53] During the course of this study, attempts will be made to weld explosively such materials as molybdenum, beryllium, B-120VCA titanium, titanium–6 wt.% aluminum–4 wt.% vanadium, and 4340 stainless steel. To date, only tests involving the explosive welding of 4340 stainless steel to itself have been conducted. The data obtained from these tests indicate that, for this material, the more *brisant* explosives will bond more area, a uniform surface roughness will provide better bonding, and certain ratios of explosive weight to standoff distance will produce bonding.

Attempts have been made to prepare ½-in.-diameter by 12-in.-long stainless-steel and Zircaloy-2-clad UO_2 core fuel rods by explosive compaction.[54] Good results were obtained in compacting specimens clad with 0.022-in.-thick mild-steel tubing. Densities of 93 per cent of the theoretical density, measured over a 7-in. rod, were realized with diametral variations of only ±0.003 in. However, it was not possible to duplicate these results with 0.015-in. Zircaloy-2 tubing or with 0.010-in. types 321 and 304 stainless-steel tubing. The more refractory metals behaved erratically. This behavior was ascribed to the inhomogeneity of the stainless-steel material and to the exceedingly large grain size of the Zircaloy-2 material. These assumptions have been corroborated by metallographic examination. Future attempts to compact a fuel rod of these materials will be conducted using a two-step process. A light charge will be used in the first step for the purpose of shrinking the tubing and obtaining a density of approximately 70 per cent of the theoretical density. A heavier charge will be used for the second step to obtain the desired density, and an intermediate anneal will be incorporated between the two steps to remove any residual stresses. (C. C. Simons)

Welding and Brazing

Two new bibliographies of interest to workers in this field are available. One bibliography is restricted to the welding of Zircaloy-2 and contains 40 references on this subject.[55] The second bibliography consists of 850 references on all aspects of welding and brazing.[56]

First reports on the welding of pure yttrium have shown that this metal can be welded easily. Satisfactory tungsten-arc fusion welds and resistance spot welds have been made by personnel at the Albany, Oreg., Bureau of Mines station.[57] Fusion welds were made in sheet 0.02 in. thick; spot welds were accomplished between sheets 0.008 to 0.012 in. thick.

An interesting study of brazing cycles that promote diffusion reactions is reported by Westinghouse.[58] The work was part of the development of joining procedures for assembly of the Yankee Nuclear Power Station fuel-element clusters. Either a nickel-phosphorus alloy or a nickel–13 wt.% chromium–10 wt.% phosphorus alloy was used to braze austenitic stainless-steel tubes into a cluster. Since these alloys are brittle in normal braze thicknesses, the parts were kept at the brazing temperature until the phosphorus (which promotes the embrittlement) could diffuse into the base metal. A typical cycle involved heating to 1850°F for 4 hr. The term "diffusion bonding," used in this report to describe this technique, may lead to some confusion. A new term is needed to distinguish this technique from conventional brazing and diffusion bonding. The conclusions reached in this work are summarized as follows:

1. Preplacement of the brazing alloy as an electroless nickel-phosphorus coating produced the best results.
2. The joint clearance was a critical factor in controlling the final joint properties. A clearance of less than 0.0025 in. was deemed necessary.
3. The tensile strength of joints increased with holding time at temperature.

Beryllium-joining studies are continuing at Oak Ridge,[59] with work now in progress on electron-beam welding, brazing-alloy development, and diffusion bonding. Satisfactory end-cap seals have been made with electron-beam welds on parts machined from bar stock. Results were unsatisfactory when extruded tubing was used. Brazing alloys that are compatible with lithium and that melt between 1000 and 1150°C are being studied for brazing characteristics on beryllium. Some of these alloys have the following nominal compositions:

47 wt.% titanium–47 wt.% zirconium–6 wt.% beryllium

46 wt.% titanium – 46 wt.% zirconium – 4 wt.% beryllium – 4 wt.% vanadium
45 wt.% titanium – 45 wt.% zirconium – 10 wt.% iron
63 wt.% titanium – 27 wt.% iron – 10 wt.% molybdenum

Additional work on diffusion bonding involving cycles such as 1100°C for 2 hr is in progress.

(R. E. Monroe)

Nondestructive Testing

There is interest in the use of Lamb waves where a need exists to measure the thickness of very thin plates, to study bond integrity, to locate laminar type defects very close to the surface of plates, or to inspect very thin-walled tubing. Lamb waves can exist in an infinite series of molds and in two types, symmetrical and asymmetrical. The velocity at which a Lamb wave travels depends upon the thickness of the plate, the material, the frequency of the sound wave, and the mode and type of sound wave. Hanford[60] has made major contributions in the inspection of materials by Lamb waves. Lamb waves have been successfully transmitted over long distances in pipes. They are being used to investigate bond integrity in fuel elements and in the development of a thickness-measuring instrument.

Lambert[61] makes use of the fact that Lamb waves can be generated in thin sections to detect internal unbonded regions. An inspection head containing two ultrasonic transducers is inserted in the tube. One transducer acts as a transmitter, and the other transducer acts as a receiver. The nominal incidence angle using water coupling is 15 deg. The ultrasonic energy from the transmitter produces Lamb waves in the unbonded region which are detected by the receiver. The receiver detects no signal over bonded regions.

Woodward[62] at Savannah River uses what appears to be a similar method to test one side of a clad element. He also reports using the through-transmission method to determine bond integrity, the attenuation of the pulse being a measure of the integrity; but this method cannot indicate on which side of the clad element the unbonding is located.

The minimum size of defect a pulse type inspection unit will detect depends upon the grain size of the metal. Lambert[61] states that it is possible regularly to detect flaws 10 by 30 mils at ¼ in. from the surface in uranium of "relatively small" grain size. Flaws 20 by 20 by 40 mils are detectable in uranium of any grain size. Cracks and fissures smaller than these dimensions are detectable under favorable conditions. Ultrasonic testing techniques at Hanford[63] can detect cracks of 3 mils or greater depth in a 30-mil-wall Zircaloy tube.

(D. Ensminger)

References

1. John W. Simmons, ed., Summary Technical Report for the Period January 1 to March 31, 1960, USAEC Report NLCO-805, National Lead Company of Ohio, Apr. 29, 1960. (Classified)
2. S. Isserow et al., Monthly Progress Report to E. I. du pont de Nemours & Company, Inc., for the Period January 1 to January 31, 1960, USAEC Report NMI-7024, Nuclear Metals, Inc. (Classified)
3. F. A. Foyle et al., Initial Investigation of Arc Melting and Extrusion of Tungsten, Report NASA-TN-D-269, National Aeronautics and Space Administration, March 1960.
4. R. R. Hood and L. Isakoff, comps., Heavy-Water-Moderated Power Reactors, Progress Report for February 1960, USAEC Report DP-475, E. I. du Pont de Nemours & Company, Inc., April 1960.
5. M. K. Millhollen, Specifications for Swaged UO_2 19-Rod Cluster, PRTR Fuel Element Mark I, USAEC Report HW-64359, Hanford Atomic Products Operation, Mar. 15, 1960.
6. R. R. Hood, comp., Heavy-Water-Moderated Power Reactors, Progress Report for March 1960, USAEC Report DP-485, E. I. du Pont de Nemours & Company, Inc., April 1960.
7. R. H. Baskey, Fuel-Bearing Fiberglas in Aluminum-Base Fuel Elements, USAEC Report ORO-277, Clevite Corp., May 10, 1960.
8. R. W. Dayton and C. R. Tipton, Jr., Progress Relating to Civilian Applications During December 1959, USAEC Report BMI-1403, Battelle Memorial Institute, Jan. 1, 1960.
9. R. W. Dayton and C. R. Tipton, Jr., Progress Relating to Civilian Applications During January 1960, USAEC Report BMI-1409, Battelle Memorial Institute, Feb. 1, 1960. (Classified)
10. R. W. Dayton and C. R. Tipton, Jr., Progress Relating to Civilian Applications During February 1960, USAEC Report BMI-1423, Battelle Memorial Institute, Mar. 1, 1960. (Classified)
11. R. W. Dayton and C. R. Tipton, Jr., Progress Relating to Civilian Applications During March 1960, USAEC Report BMI-1430, Battelle Memorial Institute, Apr. 1, 1960. (Classified)

12. R. W. Dayton and C. R. Tipton, Jr., Progress Relating to Civilian Applications During April 1960, USAEC Report BMI-1434, Battelle Memorial Institute, May 1, 1960. (Classified)
13. R. W. Dayton and C. R. Tipton, Jr., Progress Relating to Civilian Applications During May 1960, USAEC Report BMI-1442, Battelle Memorial Institute, June 1, 1960. (Classified)
14. J. L. Zambrow, Quarterly Technical Progress Report for the Period Ending December 31, 1959, USAEC Report SCNC-306, Sylvania-Corning Nuclear Corp., February 1960.
15. J. L. Zambrow, Quarterly Technical Progress Report for the Period Ending March 31, 1960, USAEC Report SCNC-309, Sylvania-Corning Nuclear Corp., May 1960.
16. S. J. Paprocki et al., Further Development of Gas-Pressure Bonding of Zircaloy-Clad Flat-Plate Uranium Dioxide Fuel Elements, USAEC Report BMI-1436, Battelle Memorial Institute, May 11, 1960.
17. Westinghouse Electric Corp., Bettis Atomic Power Laboratory, Pressurized Water Reactor (PWR) Project Technical Progress Report for the Period December 24, 1959, to February 23, 1960, USAEC Report WAPD-MRP-84.
18. Westinghouse Electric Corp., Bettis Atomic Power Laboratory, Pressurized Water Reactor (PWR) Project Technical Progress Report for the Period February 24 to April 23, 1960, USAEC Report WAPD-MRP-85.
19. Hanford Atomic Products Operation, Fuels Development Operation Quarterly Progress Report for April to June, 1959, USAEC Report HW-62085, July 15, 1959. (Classified)
20. Warren W. West, Fluid Pressure Bonding, Part III, USAEC Report DP-462, E. I. du Pont de Nemours & Company, Inc., March 1960. (Classified)
21. R. M. Evans, Notes on the Diffusion Bonding of Metals, Report DMIC-Memo-53 (PB-161203), Defense Metals Information Center, Apr. 20, 1960.
22. G. Perona et al., On the Diffusion Welding of Uranium and Zircaloy-2, *Energia nucleare (Milan)*, 7: 111–120 (February 1960).
23. H. F. Sawyer and A. D. Donaldson, Development of a Method for Fabricating Zircaloy-Clad Uranium Tubes with a Small Inner Diameter and Thick Wall, USAEC Report NMI-4732, Nuclear Metals, Inc., Aug. 21, 1959. (Classified)
24. Reference canceled.
25. Reference canceled.
26. Reference canceled.
27. F. S. Gardner and J. G. Hunt, The Fabrication of Clad Massive UO_2 Fuel Elements by Coextrusion, USAEC Report NMI-2505, Nuclear Metals, Inc., Jan. 14, 1960.
28. A. S. Ferrara, Extrusion Cladding of Plate Fuel Elements, USAEC Report DP-438, E. I. du Pont de Nemours & Company, Inc., February 1960. (Classified)
29. S. H. Paine and W. F. Murphy, Examination of Irradiated Experimental NRU Fuel Rods, USAEC Report ANL-6059, Argonne National Laboratory, November 1959.
30. S. H. Paine, Jacketed Uranium Slugs and Methods, U. S. Patent 2,894,889, July 14, 1959.
31. J. Baird et al., Recent Improvements in the Fabrication of the ISNSE Aluminum Plate Fuel Element, *Trans. Am. Nuclear Soc.*, 2(1): 130–131 (June 1959).
32. Oak Ridge National Laboratory, Maritime Reactor Project Annual Progress Report for the Period Ending November 30, 1959, USAEC Report ORNL-2865, Jan. 25, 1960.
33. Argonne National Laboratory, Annual Report for 1959, Metallurgy Division, USAEC Report ANL-6099, p. 35, 1959.
34. John R. Schley, New Surfacing Methods Vie with Old for High-Temperature Process Applications, *Chem. Eng.*, 67: 184 (Mar. 21, 1960).
35. K. T. Ziehlke et al., Heat Treating Electroless Nickel Coatings, *Metal Progr.*, 77(2): 84 (February 1960).
36. G. Sandoz, Coating of Columbium for High Temperatures, *J. Metals*, 12(4): 340 (April 1960).
37. Leslie Mark Wyatt, Improvements in or Relating to Metal Coatings, British Patent 818,312, Aug. 12, 1959.
38. J. Bodine, Investigation of Vapor-Phase Plating for Cladding Reactor Fuels, USAEC Report NAA-SR-Memo-4140, Atomics International, July 14, 1959.
39. Nuclear Materials and Equipment Corp., Coating of UO_2 Spheres, Coating of Uranium Metal Particles, the Preparation of Dispersions of Coated Particles in Metal Matrices, and Evaluation and Testing of Coated Particles, Final Report for the Period November 15, 1958, to November 14, 1959, USAEC Report NYO-2801.
40. Nuclear Materials and Equipment Corp., The Coating of UO_2 and Uranium Spheres with Various Metals, Quarterly Progress Report for the Period November 16, 1959, to February 15, 1960, USAEC, Report NYO-2804.
41. R. W. Dayton and C. R. Tipton, Jr., Progress Relating to Civilian Applications During June 1960, USAEC Report BMI-1448, Battelle Memorial Institute, July 1, 1960. (Classified)
42. J. M. Blocher et al., Fluidized-Bed Coating of UO_2 Powders with Niobium and Other Elements, USAEC Report BMI-1440, Battelle Memorial Institute, May 25, 1960.
43. Excerpts from Progress Reports of LASL, June 1959; UCLRL, June 1959; Mound Laboratory, June 1959; and Hanford Atomic Products Operation, June 1959, USAEC Report WASH-930, January 1960. (Classified)
44. Excerpts from Progress Reports of LASL, July 1959; UCLRL, July 1959; Mound Laboratory, July 1959; and Hanford Atomic Products Opera-

tion, July 1959, USAEC Report WASH-931, February 1960. (Classified)

45. J. G. Beach and J. A. Gurklis, Procedures for Electroplating Coatings on Refractory Metals, Report DMIC-Memo-35, (PB-161185), Defense Metals Information Center, Oct. 9, 1959.
46. R. A. U. Huddle and A. R. Gibson, Improvement in or Relating to Coating of Uranium Metal and Uranium-Base Alloy, British Patent 829,089, Feb. 24, 1960.
47. Knolls Atomic Power Laboratory, Reactor Technology Report No. 12, Metallurgy, USAEC Report KAPL-2000-9, March 1960.
48. P. T. B. Shaffer, Development of Ultra-Refractory Materials, Summary Report for the Period November 1, 1958, to October 31, 1959, Report AD-228359, Carborundum Co., Nov. 6, 1959.
49. C. P. Williams, Evaluating Explosive Forming, *J. Metals*, 12(1): 33–36 (January 1960).
50. Donald Peckner, High-Energy Rate-Forming Processes: Their Present and Future, *Materials in Design Engineering*, 52(1): 89–96 (July 1960).
51. H. P. Tardif, The Explosive Forming of Conical Shapes by Metal Gathering, Canadian Report CARDE-TM-280/59 (PCC-D46-95-35-08), February 1958.
52. R. L. Wachtell, Explosive Forming of Refractory Metals, Bimonthly Report No. 1 for the Period June 30 to August 31, 1959, Report AD-229174, Chromalloy Corp., Sept. 1, 1959.
53. Vaisl Philipchuck and Frank Bois, Explosive Welding, Progress Report No. 2 for the Period April to June 1960.
54. L. Isakoff, comp., Heavy-Water-Moderated Power Reactors, USAEC Report DP-385, E. I. du Pont de Nemours & Company, Inc., July 1959.
55. G. I. Maughan, comp., Bibliography on Welding of Zircaloy-2, British Report DEGIS-93(R), Jan. 11, 1960.
56. T. H. Davis, comp., Welding and Brazing, USAEC Report TID-3546, February 1960.
57. Northwest Electrodevelopment Experiment Station, Bureau of Mines, Quarterly Metallurgical Progress Report No. 6 for the Period January 1 to March 31, 1960, USAEC Report USBM-U-699, Mar. 31, 1960.
58. P. P. King, The Formation and Statistical Evaluation of Diffusion-Bonded Brazed Joints on Yankee Fuel Subassemblies, USAEC Report YAEC-160, Westinghouse Atomic Power Div., November 1959.
59. Oak Ridge National Laboratory, Gas-Cooled Reactor Project Quarterly Progress Report for the Period Ending March 31, 1960, USAEC Report ORNL-2929, June 21, 1960.
60. D. C. Worlton and C. H. Frederick, Hanford Atomic Products Operation, April–June 1960, unpublished work.
61. T. G. Lambert, The Nondestructive Testing Program for Coextruded Fuel Elements, USAEC Report HW-61775, Hanford Atomic Products Operation, Sept. 7, 1959. (Classified)
62. W. J. Woodward, Savannah River Laboratory, May 25, 1960, unpublished work.
63. F. W. Albaugh, Reactor and Fuels Research and Development Operation Monthly Report for March 1960, USAEC Report HW-64580-A, Hanford Atomic Products Operation, Apr. 15, 1960. (Classified)

Index

VOLUMES 1–3

Included in this issue is a cumulative index for Volumes 1 to 3 of *Reactor Core Materials*. Future indexes for this quarterly will be prepared annually and will appear in the final (Number 4) issue. In this index the bold numbers denote volumes, the numbers in parentheses denote issues, and the other numbers denote pages.

A

Actinium-beryllium alloys, preparation, **3**(3), 31
Alkali halides, effects of pressure on ionic conductivity, **3**(2), 36
  radiation effects, **1**(3), 43; **3**(2), 27
Alkali metal–alkali metal halide systems, phase diagrams, **3**(2), 24
Alloys
  See also Metals and specific alloys
  corrosion resistance to NaK, **1**(3), 37
  diffusion, **2**(4), 33
  oxidation, **3**(2), 35
  pressure bonding, **1**(4), 41
  radiation effects, **3**(3), 1; **3**(4), 38
Alloys (refractory), bibliography, **2**(3), 45
Alnico, graphite diffusion, **1**(3), 24
Alumel, corrosion, **1**(2), 30
Aluminum, cladding interdiffusion, **1**(1), 28
  corrosion by jet impingement, **2**(2), 27–8
  corrosion in, H_2O, **1**(1), 32, 34; **2**(3), 28; **3**(3), 38
    Na, **1**(3), 37
    organic coolant, **3**(1), 35
    polyphenyl, **3**(2), 23
    steam, **1**(1), 32
  corrosion inhibition, **1**(1), 32; **2**(1), 30
  corrosion measurement, **1**(1), 33
  diffusion in Ni, **3**(2), 36
  electrical resistivity, **3**(3), 41
  electron-beam welding, **2**(1), 51
  equilibrium vacancy concentrations, **3**(3), 41
  fabrication of, containing Al-coated fueled fibers, **3**(3), 19–20
  He diffusion, **3**(3), 44
  He effects on grain growth and recrystallization, **3**(4), 42–3
  H_2 effects in oxide film on corrosion, **3**(3), 21–2
  injection casting, **2**(2), 54
  mechanical properties, **3**(3), 32
  nuclear properties, **3**(3), 32
  pressure bonding, **1**(1), 26
  radiation effects, **3**(1), 36–7
  radiation-induced, gas formation, **3**(3), 42
    He release, **3**(4), 40
    void formation, **3**(4), 40
  reaction with H_2O, **2**(1), 33
  reaction with H_2O vapor, **3**(2), 9
  texture, **3**(4), 7
Aluminum (2S)–beryllium couplings, tensile properties, **1**(4), 14
Aluminum (1100), compatibility with UO_2 pellets, **3**(3), 17
  corrosion in H_2O and D_2O, **3**(1), 33
  radiation effects on, hardness, **2**(3), 33
    mechanical properties, **3**(3), 43
    stress relaxation, **2**(3), 33
    tensile properties, **2**(3), 33
Aluminum (2024), explosion-forming effects, **3**(3), 56–7
Aluminum (6061), explosion-forming effects, **3**(3), 56–7
Aluminum (6063), radiation effects on tensile properties, **2**(3), 33
Aluminum (deformed), small-angle X-ray scattering studies, **3**(2), 26
Aluminum (irradiated), annealing kinetics, **3**(2), 26
  dislocation loops, **2**(3), 32
  heating effects, **3**(3), 42
  He injected into, **3**(3), 42
  vacancy formation, **2**(3), 32
Aluminum (M-257), compatibility with UO_2 pellets, **3**(3), 17
Aluminum (molten), reaction with H_2O, **1**(1), 35–6
Aluminum (SAP 865), radiation effects on mechanical properties, **3**(1), 38–9

Aluminum (sintered), corrosion, **3**(4), 31
Aluminum (Zircaloy-2-clad), spontaneous ignition in steam, **3**(2), 23–4
Aluminum alloy (X-8001), corrosion in H_2O, **3**(2), 23
Aluminum alloy extrusions, corrosion, **2**(3), 29
tensile strength, **2**(3), 29
Aluminum alloy fuel rods, coextrusion with Al cladding, **3**(2), 45
Aluminum alloy–niobium–uranium system, diffusion, **2**(3), 16
Aluminum alloys, corrosion inhibition, **2**(1), 30
corrosion protection, **2**(2), 28
H_2 depolarization with Fe and Ni, **3**(3), 22
radiation effects, **2**(1), 43; **3**(1), 38
U diffusion, **3**(3), 44
Aluminum alloys (Ni-coated), corrosion protection, **2**(1), 30
Aluminum-base cores, strengthening with Al-coated fuel-bearing Fiberglas, **3**(4), 10
Aluminum bicrystals, grain-boundary migration, **3**(4), 43–4
Aluminum–boron carbide dispersions, Cu, Mg, Mn, and Ni addition effects on fabricability, **2**(3), 25
description, **1**(4), 18
Aluminum-boron dispersions, properties, **2**(4), 17
Aluminum-boron-manganese dispersion compacts, fabrication, **2**(3), 25
Aluminum–boron monocarbide dispersions, neutron-absorbing properties, **3**(1), 30
Aluminum bromide (liquid), properties, **3**(3), 40
Aluminum-calcium-magnesium system, ternary intermediate phase, **2**(4), 32
Aluminum chloride, properties, **3**(3), 40
Aluminum-chromium alloys, intermetallic structure, **3**(4), 43
oxidation, **2**(4), 22–3
Aluminum-chromium-cobalt-molybdenum-nickel-titanium alloys, B addition effects, **3**(2), 40
heat-treatment effects, **2**(3), 35
melting method effects, **3**(2), 40
Zr addition effects, **3**(2), 40
Aluminum-chromium-iron alloys, **1**(1), 33; **2**(2), 29
See also Hastelloys
annealing effects on structure, **3**(3), 43
corrosion, **3**(3), 39; **3**(4), 32
development for cladding, **3**(3), 38
grain size and oxidation, **3**(2), 34
Mo addition effects, **2**(3), 30, 43
Nb addition effects, **2**(3), 30, 43
oxidation, **2**(1), 29–30; **3**(1), 33; **3**(2), 34
oxidation resistance, **1**(4), 23; **2**(2), 29–30
strength, **3**(3), 45
transition temperatures, **3**(2), 31
Zr addition effects, **2**(3), 30, 43
Aluminum-chromium-iron-nickel-titanium alloys
See Inconel X
Aluminum-chromium-iron-titanium alloys, corrosion in H_2O, **3**(3), 39
Aluminum-chromium-nickel alloys, oxidation kinetics, **2**(2), 29
Aluminum-chromium-nickel-titanium alloys
See Inconel 702
Aluminum-chromium-niobium alloys, oxidation, **2**(1), 28–9; **2**(4), 22–3; **3**(3), 37
Aluminum-chromium-niobium-thorium alloys, oxidation resistance, **1**(3), 34
oxidation weight gain, **1**(3), 34
Aluminum-chromium-niobium-titanium alloys, oxidation, **2**(4), 22–3
Aluminum-chromium-niobium-titanium-zirconium alloys, oxidation, **2**(4), 22–3
Aluminum-chromium-titanium alloys, oxidation, **2**(4), 22–3
Aluminum-chromium-titanium-zirconium alloys, oxidation, **2**(4), 22–3
Aluminum cladding, eddy-current testing, **1**(3), 54
X-ray photometry detection of Al-Si penetrations, **1**(3), 54
Aluminum-copper alloys, annealing effects on electrical resistivity, **3**(1), 36
corrosion in H_2O, **1**(2), 31
corrosion resistance, **1**(3), 34
radiation effects on resistivity and diffusion, **2**(2), 33; **2**(4), 25; **3**(1), 36; **3**(2), 26–7; **3**(4), 37
radiation-induced cold hardening, **3**(2), 26
Aluminum-copper-iron-nickel alloys, corrosion in H_2O, **1**(2), 31
Aluminum-copper-magnesium-tin alloys, corrosion in H_2O, **3**(1), 34
Aluminum-copper-nickel-titanium alloys, corrosion in H_2O, **1**(2), 31
Aluminum-cored fuel elements, swaging of stainless steel and Zircaloy cladding, **3**(1), 49
Aluminum films (Cu-supported), radiation effects, **3**(4), 38–9
Aluminum foils, radiation effects, **3**(4), 39
Aluminum-iron alloy crystal, annealing and radiation effects on diffusion, **3**(3), 41
Aluminum-iron alloys, corrosion, **1**(2), 31; **1**(3), 34; **2**(4), 22; **3**(3), 39
development for roll-bonding use, **2**(4), 42
ductility, **2**(4), 37
oxidation, **2**(3), 43; **2**(4), 22, 37
radiation effects, **2**(4), 25–7; **3**(4), 38
stress-rupture life, **2**(4), 37
tensile properties, **2**(4), 37
thermal-neutron cross sections, **2**(3), 43
Aluminum-iron-nickel alloys, Be addition effects on corrosion, **2**(3), 28–9
corrosion, **2**(2), 28; **3**(4), 31–2
Ti addition effects on corrosion, **2**(3), 28–9; **3**(3), 38
Zr addition effects on corrosion, **2**(3), 28–9; **3**(3), 38
Aluminum-iron-nickel-titanium alloys, corrosion and erosion, **2**(4), 20
Aluminum-iron-nickel-uranium alloy fuel elements, bonding using Si powder, **3**(1), 49
corrosion in H_2O, **3**(2), 4
roll cladding with Al, **3**(1), 48–9

Aluminum-iron-niobium alloys, oxidation, 2(1), 28–9; 3(3), 37
Aluminum-lithium alloys, radiation-induced H^3 formation, 3(3), 42
radiation-induced He formation, 3(3), 42, 44
thermal conductivity, 3(4), 42–3
Aluminum-lithium mixtures, radiation-induced gas formation, 3(3), 23
Aluminum-magnesium alloys, corrosion in $Mg(OH)_2$ inhibited H_2O, 2(4), 23
creep test results, 2(1), 38
erosion in H_2O, 3(2), 23
radiation effects on tensile properties, 3(2), 27
Aluminum-magnesium-manganese-zinc alloys, creep strength, 3(3), 46
Aluminum-magnesium-manganese-zirconium alloys, creep and tensile properties, 2(4), 38
stress-corrosion cracking, 2(4), 23
Aluminum-magnesium-zinc alloys, tensile properties, 3(3), 46
Aluminum-molybdenum-niobium alloys, oxidation, 3(3), 37
Aluminum-molybdenum-uranium alloys, as-cast properties, 2(4), 2
mechanical properties, 3(1), 2; 3(3), 3
metallurgical properties, 3(1), 2; 3(3), 3
thermal-cycling effects on mechanical properties, 3(1), 2
Aluminum-molybdenum-zirconium alloys, aging studies, 1(3), 38
heat-treatment effects on tensile properties, 1(4), 26
tensile properties, 1(3), 38; 1(4), 26; 3(1), 53
transformation temperatures, 2(4), 30
weldability, 3(1), 53
Aluminum-nickel alloys, corrosion, 1(2), 31; 1(3), 34; 2(1), 30; 3(4), 31
intermetallic layer growth, 3(1), 15
Aluminum-nickel diffusion couples, pressure effects, 1(2), 40
Aluminum-nickel system, diffusion in pressure bonding, 1(4), 41
Aluminum-nickel-uranium alloys, diffusion, 2(2), 37–9
ternary eutectic, 3(1), 4; 3(3), 5
Aluminum-nickel-uranium bond, strength and compound formation, 1(4), 6
Aluminum-niobium alloys, existence of NbAl, 3(3), 43
Aluminum-niobium-titanium alloys, oxidation, 3(3), 37
Aluminum-niobium-zirconium alloys, aging studies, 1(3), 38
tensile properties, 1(3), 38
Aluminum oxide, arc spraying, 3(2), 47
bend strength of single-crystal whiskers, 1(3), 26
corrosion resistance, 2(1), 32
dissolution in H_2O, 3(3), 38
radiation effects, 2(4), 11; 3(3), 22; 3(4), 40
reaction with PuO_2, 3(4), 15
thermal expansion, 2(1), 23–4
Aluminum oxide–beryllium oxide, reaction with H_2O vapor, 3(3), 32
Aluminum oxide–beryllium system, high-temperature properties, 1(2), 22
Aluminum oxide–boron carbide dispersions, corrosion in H_2O, 1(3), 32; 2(2), 25
development, 1(2), 26
fabrication of irradiation specimens, 1(3), 31
poison loading, 1(3), 31-2
radiation effects, 1(3), 31; 2(3), 26
Aluminum oxide ceramic, radiation effects, 3(1), 19
Aluminum oxide–dysprosium oxide system, compounds, 3(4), 28
Aluminum oxide–plutonium dioxide mixture, reactions and sintering, 3(3), 21
Aluminum oxide–uranium dioxide dispersions, radiation effects, 3(1), 19; 3(3), 22
Aluminum oxide–uranium dioxide fuel (Zircaloy-clad), pressure bonding, 1(2), 40
Aluminum oxide–uranium dioxide mixtures, density, 1(2), 15
fission-gas release, 1(2), 15
radiation effects, 1(2), 15
Aluminum oxide–uranium dioxide pellets, reaction with Zircaloy-2, 1(3), 19
Aluminum oxide–uranium dioxide system, fabrication, 3(1), 12
ultrahigh-pressure studies, 3(3), 18
Aluminum-plutonium alloy fuel elements, coextrusion with Al cladding, 3(3), 54
swaging of stainless-steel and Zircaloy cladding, 3(1), 49
Aluminum-plutonium alloys, casting, 1(2), 9; 1(4), 39
cold swaging, 1(4), 8
corrosion, 2(2), 9; 3(3), 12, 14
production, 1(2), 8–9; 1(3), 10
radiation-induced dimensional changes, 3(4), 9
roll bonding with Al cladding, 3(3), 15–16
Aluminum-plutonium alloys (Al-clad), radiation effects, 1(2), 9
Aluminum-plutonium alloys (Zircaloy-2-clad), corrosion in H_2O, 3(3), 14
interreaction, 3(3), 14
radiation effects, 1(3), 10; 3(3), 14
Aluminum-plutonium-silicon alloys, radiation effects, 1(2), 9
Aluminum-plutonium-silicon alloys (Zircaloy-2-clad), radiation effects on hardness, 1(3), 10
Aluminum-plutonium-uranium alloys (Zircaloy-clad), bonding evaluation and corrosion in H_2O, 2(3), 7
Aluminum powder alloys, tensile properties, 3(3), 46
Aluminum powder–iron oxide powder mixtures, explosion compaction, 3(2), 49
Aluminum powder metallurgy material, welding, 3(3), 58
Aluminum-silicon alloys, structure, 3(2), 31

Aluminum-silicon spikes, eddy-current detection in fuel-slug jackets, **1**(3), 54
Aluminum-silicon-uranium alloys, fabrication, **1**(4), 5
Aluminum-thorium alloys, casting, **2**(1), 11
constitution, **2**(2), 9–10
eutectics, **2**(2), 10
grain-growth restriction, **2**(4), 6
hot hardness, **2**(4), 6
melting, **2**(1), 11
metallography, **2**(4), 6
precipitation hardening, **3**(1), 8
Aluminum-thorium-uranium alloys, constitution, **1**(2), 7, 10–11
Aluminum-thorium-uranium eutectic, containment by Ta and Y, **1**(4), 25
Aluminum-tin-uranium alloys, casting, **3**(2), 4
corrosion in H_2O, **3**(2), 4
hot hardness, **3**(2), 4
melting, **3**(2), 4
tensile strength, **3**(2), 4
UAl_3-UAl_4 reaction, **3**(2), 4
Aluminum-tin-zirconium alloys, tensile properties, **3**(1), 53
weldability, **3**(1), 53
Aluminum-titanium-vanadium alloys, explosion welding, **3**(4), 55
Aluminum-uranium alloy cored tubes, coextrusion with Al cladding, **2**(2), 51, 53
Aluminum-uranium alloy cores, hot roll bonding with Al (1100), **1**(3), 50
roll cladding with 1100 Al and Al-clad 6061 alloy, **1**(3), 50
Aluminum-uranium alloy extrusion blanks, centrifugal casting, **2**(1), 8
Aluminum-uranium alloy fuel elements, fabrication yield evaluation, **1**(1), 26
hot pressing in Al alloy cans, **3**(2), 46
Aluminum-uranium alloy powder fuel tubes, coextrusion with Al cladding, **2**(3), 51
Aluminum-uranium alloy rods, coextrusion with Cu cladding, **3**(2), 45
Aluminum-uranium alloy shot, production with spinning disk, **2**(1), 8
rod fabrication from, **2**(1), 8
Aluminum-uranium alloy tubes, coextrusion with Zircaloy cladding, **3**(2), 45
Aluminum-uranium alloys, B addition effects, **1**(3), 7; **2**(3), 6
casting, **1**(1), 6–7; **1**(2), 6–7; **1**(3), 48; **2**(2), 7; **3**(1), 48
cladding, **1**(2), 7
coextrusion, **1**(2), 7
composition, **1**(1), 7
corrosion, **1**(1), 7; **1**(3), 7; **3**(2), 4
deformation in textures, **2**(2), 6; **3**(4), 7
diffusion, **1**(1), 7; **3**(4), 43
dip sampling of melt, **2**(1), 7–8
etching, **1**(1), 7
fabrication, **1**(3), 7; **1**(4), 5–6; **2**(2), 48
fuel loading, **2**(1), 7
Ge addition effects, **2**(2), 7
heat-treatment effects on rollability, **3**(1), 4
hot hardness, **3**(2), 4
ignition in air and O_2, **2**(4), 9
intermetallic layer growth, **3**(1), 15
Li addition effects, **2**(3), 6
liquidus temperatures, **1**(4), 6
Mg addition effects on fabricability, **2**(2), 7
microstructure, **3**(2), 4
Pb addition effects on structure, **1**(4), 6
Pd addition effects, **2**(2), 7
physical properties, **1**(3), 7
preparation, **1**(3), 8; **2**(4), 4
pressure effects on interdiffusion, **2**(3), 16
production, **2**(1), 7–8
Pt addition effects on structure, **1**(4), 6
radiation effects, **1**(3), 7
reaction with H_2O vapor, **3**(2), 9
segregation, **2**(1), 7; **2**(2), 47
shot production on spinning disk, **1**(4), 39; **2**(2), 48
Si addition effects, **1**(2), 7; **1**(3), 7; **1**(4), 6; **2**(2), 7; **2**(3), 6–7
Sn addition effects, **1**(3), 7; **1**(4), 6; **2**(3), 7; **2**(4), 3–4; **3**(1), 4; **3**(3), 5; **3**(4), 7
tensile strength, **3**(2), 4
Ti addition effects on UAl_4 formation, **1**(3), 7
UAl_3-UAl_4 transformation kinetics, **3**(1), 4
UAl_3-UAl_4 transformation suppression with Si, Sn, or Zr, **3**(2), 4
Zr addition effects, **1**(3), 7; **2**(2), 7; **2**(3), 7; **2**(4), 3–4; **3**(1), 4; **3**(3), 5; **3**(4), 7
Aluminum–uranium aluminide diffusion couples, UAl_4 growth kinetics, **3**(1), 15
Aluminum–uranium carbide dispersions, chemical reactions, **1**(1), 15; **3**(2), 5
Aluminum–uranium dicarbide dispersion fuel elements, corrosion in H_2O, **3**(2), 5
fabrication, **3**(2), 5
Aluminum–uranium dicarbide system, effects of H_2 on UC_2 stability, **3**(2), 6
Aluminum-uranium diffusion couples, interdiffusion, **3**(1), 13–15
pressure effects, **1**(2), 41
UAl_3 growth, **3**(1), 13–15
Aluminum–uranium dioxide dispersions, chemical reactions, **1**(1), 15; **2**(3), 11
fabrication, **1**(1), 15
swelling, **2**(3), 11
Aluminum–uranium dioxide joints, thermal contact conductance, **2**(1), 13–14
Aluminum–uranium dioxide mixture films, radiation-induced UO_2 redistribution, **3**(2), 8
Aluminum-uranium dispersions, coextrusion with Al cladding, **1**(3), 52
Aluminum-uranium hollow extrusion billets, centrifugal casting, **2**(3), 7
Aluminum–uranium oxide dispersion fuel elements (Al-canned), fabrication, **3**(4), 51

Aluminum–uranium oxide dispersions, chemical reactions, 2(2), 11
development, 1(2), 12–13; 1(3), 14
growth characteristics, 1(2), 13
Aluminum-uranium-zirconium alloys, as-cast properties, 2(4), 2
casting, 3(2), 4
corrosion in H_2O, 1(4), 2–3; 3(2), 4
diffusion, 2(2), 37
hot hardness, 3(2), 4
melting, 3(2), 4
tensile strength, 3(2), 4
thermal-cycling effects on dimensional stability, 3(3), 3
UAl_3-UAl_4 reaction, 3(2), 4
Aluminum-vanadium alloys, constitution, 2(2), 37
Antimony-uranium alloys, constitution, 3(1), 5
Arc melting, crucible cooling with air, 1(1), 25
studies, 1(1), 25
Argon, properties, 3(3), 40
Army Package Power Reactor, control-rod specifications, 1(1), 23
fuel-element fabrication specifications, 1(1), 14

B

Barium-hydrogen system, constitution, 3(4), 26
Barium uranate, preparation, thermal stability, melting point, and reactions with air and He, 2(4), 9
Beryllium, adhesive bonding, 3(2), 13–14
air spectrographic analysis for, 3(3), 31
allotrope, 1(3), 25
alloying effects on mechanical and physical properties, 3(4), 21
annealing effects, 3(4), 22
applications, 1(3), 26; 2(1), 23; 3(3), 29
basal-plane research, 1(3), 24–6
behavior in HNO_3-Pu solution of porous, 3(3), 31
bibliographies, 3(3), 29; 3(4), 23
bolt fabrication, 3(3), 30
braze welding, 3(1), 23
brazing, 3(2), 13–14, 47; 3(3), 30; 3(4), 20, 55–6
brittleness, 1(1), 19; 3(3), 30; 3(4), 19
casting, 2(2), 20; 3(4), 19
coating with Al, 3(3), 29
compatibility with reactor materials, 2(2), 22; 2(4), 15
corrosion, 1(1), 20–1; 1(2), 22; 3(2), 15; 3(2), 24; 3(4), 35
Cr addition effects on tensile properties, 1(3), 24–5
crack propagation, 3(2), 14
Cu addition effects on tensile properties, 1(3), 24–5
density of centrifugally cast, 2(2), 20
determination, 2(2), 22
diffusion bonding, 3(2), 14; 3(3), 30; 3(4), 20, 55–6
dislocations, 3(4), 22
drawing, 3(1), 23; 3(3), 29–30
ductility, 1(2), 20; 3(2), 14; 3(3), 31; 3(4), 20
elastic constants, 2(4), 15; 3(4), 21
electron-beam melting, 3(1), 22; 3(4), 19–20
electron-beam welding, 3(4), 20
electronic structure, 3(3), 31
electroplated coating, 3(4), 22
electrorefining, 3(4), 19
evaporation, 3(3), 31–2
explosion welding, 3(4), 55
extrusion, 3(2), 13; 3(3), 29; 3(4), 20
extrusion cladding, 3(2), 14
fabrication, 1(3), 26; 2(1), 23; 2(2), 22; 3(1), 23; 3(3), 29; 3(4), 23
Fe addition effects on tensile properties, 1(3), 24–5
fission-gas formation, 3(1), 36–7; 3(3), 32
fracture, 2(2), 21; 3(3), 31
fusion welding, 3(1), 23; 3(2), 14; 3(4), 20
grain size, 1(1), 19–20
hazards, 2(1), 23; 2(3), 23; 3(2), 15; 3(3), 32
heat capacity, 3(2), 15
heat effects, 1(4), 14; 3(4), 22
high-temperature allotrope, 1(3), 25
indentation hardness, 3(4), 21
induction-heating effects, 1(4), 14
joining, 1(3), 26; 1(4), 42; 2(4), 15; 3(4), 55–6
joint strength, 1(1), 20
lattice parameters, 3(4), 21
machining, 3(1), 23
melting, 3(1), 22; 3(2), 41; 3(4), 19–20
metallurgy, 3(2), 14; 3(4), 22–3
moderator applications, 1(3), 26
Ni addition effects on tensile properties, 1(3), 24–5
O_2 determination in, 2(3), 23
O_2 source in, 3(3), 31–2
oxide determination, 1(3), 26
phase constitution, 1(2), 22
phase transformation, 1(2), 22; 3(1), 22
plastic deformation, 3(3), 32
plating with Au, 3(3), 31
preparation, 2(1), 23; 3(2), 14
processing, 3(3), 32
production, 1(2), 20–1; 1(3), 24–5; 2(1), 23; 2(2), 21; 2(3), 22–3; 3(4), 21
properties, 2(1), 23; 3(3), 29; 3(4), 23
bend, 3(2), 14
chemical, 3(3), 32
high-temperature, 3(4), 21
mechanical, 2(2), 20; 2(4), 15; 3(3), 32
nuclear, 3(3), 32
physical, 3(3), 32
stress-rupture, 3(4), 21–2
tensile, 1(3), 25; 3(2), 14; 3(4), 21
thermal, 2(3), 23
radiation effects, 1(2), 22; 2(1), 43
radiation-induced gas formation, 2(2), 22; 3(3), 23, 42

Beryllium (Continued)
radiation-induced swelling, 3(3), 32
reaction with CO_2, 3(3), 32; 3(4), 22
reactions with elements, 3(3), 29
roll cladding, 3(2), 14
solid solubility of Fe and Ni in, 3(3), 31
specific heat, 3(2), 15
spectrographic analysis of air for, 3(3), 31
strip and clad composites, 3(1), 22
structural applications, 1(3), 26; 2(1), 23
structural development, 1(3), 26
structural modification effects on mechanical and physical properties, 3(4), 21
structure, 3(2), 14; 3(3), 31
substructure, 3(4), 22
surface condition effects, 3(2), 14
texture, 1(2), 20–1; 2(2), 21–2
thermal arrests, 3(4), 22
thermal conductivity, 3(2), 15; 3(3), 32
thermal cycling, 3(1), 22–3; 3(4), 21
toxicity, 2(1), 23
upset welding, 3(4), 20
vacuum melting, 3(4), 19–20
welding, 2(3), 53; 3(1), 23; 3(2), 14; 3(3), 30, 58; 3(4), 20, 55
wire drawing, 3(1), 23
zone refining, 3(1), 22
Beryllium (cast), grain size, 3(4), 19
He injection effects on expansion behavior, 2(1), 23
ultrasonic grain refinement, 1(3), 24–5
Beryllium (clad), fission-gas retention, 3(3), 32
Beryllium (Cu-jacketed), working, 3(1), 23
Beryllium (irradiated), annealing effects on density, 2(2), 22
behavior of He injected into, 3(3), 42
heating effects, 3(1), 22; 3(3), 42
Beryllium (QMV), work hardening, 3(1), 23
Beryllium (stainless-steel-jacketed), working, 3(1), 23
Beryllium (structural), applications, 1(3), 26; 2(1), 23
development, 1(3), 26; 3(4), 20
evaluation, 3(4), 20–1
mechanical properties, 3(4), 21
Beryllium (wrought), production plant description, 3(3), 29
Beryllium alloys, development, 2(3), 22
ductility, 3(3), 30
intermetallic compound effects on high-temperature strength, 1(1), 20
thermal arrests, 3(4), 22
Beryllium alloys (wrought), development, 1(2), 20
Beryllium amalgam, preparation, 1(2), 21
Beryllium–beryllium carbide dispersions, stress-rupture properties, 3(4), 22
Beryllium–beryllium carbide system, high-temperature properties, 1(2), 22
Beryllium-beryllium couplings, tensile properties, 1(4), 14
Beryllium–beryllium oxide dispersions, stress-rupture properties, 3(4), 22
Beryllium–beryllium oxide system, thermal expansion, 1(2), 22
Beryllium carbide dispersions, development, 1(1), 24
Beryllium carbide–graphite bodies, ceramic coating, 2(4), 44
Beryllium-copper alloys, mechanical properties, 2(3), 22
Beryllium dispersed-phase alloys, corrosion in H_2O, 3(4), 22
high-temperature mechanical properties, 3(4), 22
Beryllium electroplates, production, 3(2), 14
Beryllium extrusions, mechanical properties, 3(2), 13
Beryllium films, preparation, 3(4), 22
Beryllium fuel capsule end closures, fabrication, 2(3), 22
Beryllium ingots, casting, electron bombardment, and melting, 2(2), 20
Beryllium-iron alloys, solid solubility of Fe, 2(2), 21
Beryllium–iron oxide systems, high-temperature properties, 1(2), 22
Beryllium-magnesium alloys, preparation, 2(1), 23
Beryllium monocrystals, plastic properties, 3(3), 31
Beryllium-nickel alloys, high-temperature phase, 3(3), 31
mechanical properties, 2(3), 22
phase diagram, 3(3), 31
phase transformation, 1(2), 22
radiation effects on electrical resistivity, 3(2), 26–7
solid solubility of Ni, 2(2), 21
X-ray diffraction, 1(3), 25
Beryllium-niobium alloys, preparation and properties, 3(1), 23
Beryllium ores, review, 3(4), 22–3
Beryllium oxide, bend strength of single-crystal whiskers, 1(3), 26
compatibility with ceramic fuels, 1(1), 21
corrosion, 1(3), 37; 2(1), 32; 3(1), 23; 3(3), 32
crystal-growth inhibition, 2(1), 24
Beryllium oxide, fabrication, 2(2), 22
mechanical properties, 3(3), 32
nuclear properties, 3(3), 32
radiation effects on thermal conductivity, 3(2), 15
review, 3(4), 22–3
self-diffusion coefficient, 1(3), 26
tensile creep, 2(3), 23
thermal conductivity, 1(4), 15; 3(2), 15
thermal expansion, 2(1), 23–4
Beryllium oxide ceramics, corrosion in liquid Na, 1(4), 15
grain growth, 2(3), 23
Beryllium oxide–thorium dioxide–uranium dioxide system, fusion behavior and grain growth, 2(3), 23

Beryllium oxide–uranium dioxide bodies (sintered), structural integrity, **3**(4), 12
Beryllium oxide–uranium dioxide pellets, radiation effects, **3**(4), 12
Beryllium oxide–uranium dioxide–zirconium dioxide dispersions, properties, **3**(1), 11–12
Beryllium oxide–Vycor dispersions, radiation effects, **1**(1), 23
Beryllium-plutonium alloys, preparation, **1**(4), 7; **3**(3), 31
Beryllium powders, hot pressing, **3**(4), 20
metallurgy review, **3**(4), 22–3
preparation, **1**(2), 21–2
sintering, **2**(2), 21
Beryllium rods, fabrication from Be powder, **3**(2), 13
Beryllium sheet, cracking, **2**(4), 14–15
ductility, **2**(3), 22; **2**(4), 14–15
mechanical properties, **3**(2), 14–15; **3**(3), 29
production, **3**(2), 13
texture, **3**(3), 30–1
true stress–plastic strain relation, **3**(3), 31
Beryllium–silicon dioxide system, high-temperature properties, **1**(2), 22
Beryllium-silver alloys, BeO addition effects on strength, **3**(1), 22
casting, **3**(4), 19–20
cold rolling, **3**(3), 30
ductility, **3**(1), 22
mechanical properties, **2**(3), 22
rolling, **3**(4), 20
Beryllium-sodium system, reactions, **2**(4), 15
Beryllium–stainless steel (type 316) couplings, tensile properties, **1**(4), 14
Beryllium–thorium beryllide dispersions, fabrication, **1**(3), 52
Beryllium-thorium-uranium fuel elements (Be-sheathed), fabrication, **1**(3), 26
Beryllium-tin alloys, mechanical properties, **2**(3), 22
Beryllium tubing, burst testing, **3**(4), 22
capsule material use, **3**(4), 20
inclusions, **3**(3), 30
Beryllium-uranium alloys, preparation, **3**(3), 31
Beryllium–uranium beryllide dispersions, fabrication, **1**(3), 52
Beryllium-yttrium alloys, constitution, **3**(1), 42
preparation, **3**(1), 23
properties, **3**(1), 23
Beryllium-Zircaloy-B alloys (molten), reaction with H_2O, **1**(1), 35
Beryllium-zirconium alloys, preparation and properties, **3**(1), 23
Binary alloys, constitutional diagrams, **3**(4), 2
Bismuth, reactions with metals and liquid metals, **2**(4), 22
Bismuth-lead alloys, specific heat, **3**(2), 15
Bismuth-lead-thorium alloys, constitution, **2**(1), 11
Bismuth-thorium breeder blanket, corrosion, **2**(1), 30
Bismuth-uranium alloys, constitution, **3**(1), 5
corrosion of Ta, **2**(4), 22
Bismuth-uranium alloys (molten), containment by Nb and Y, **1**(4), 25
corrosion of Cr-Mo steel, **2**(2), 31
Bismuth-uranium fuels (molten), corrosion, **2**(1), 30; **2**(3), 31–2
Bonding
See Diffusion, Pressure bonding, and specific metals and alloys
Boral
See Aluminum–boron carbide dispersions
Borides, compatibility with UO_2, **3**(4), 12
properties, **3**(3), 47
utilization as control materials, **3**(3), 35
Borides (refractory), thermodynamic properties, **3**(4), 28–9
Boron, chemistry, **2**(3), 25
corrosion in H_2O, **1**(2), 26
diffusion in Mo, Nb, Ta, Ti, W, and Zr, **2**(2), 37
neutron-absorbing properties, **3**(1), 30
physical properties, **2**(4), 17
purity of commercial, **2**(4), 17
radiation-induced gas formation in materials containing, **3**(3), 23
radiation-induced He release, **3**(3), 35
reactor-control applications, **3**(2), 19
Boron (dispersed), radiation effects, **1**(2), 26
Boron alloy–stainless steel dispersions, fabrication, **2**(2), 26
Boron carbide, bonding, **2**(4), 17
compatibility with stainless steel, **3**(2), 19
corrosion, **1**(2), 26; **1**(3), 32; **2**(1), 32; **2**(2), 25–6
irradiated specimen fabrication, **1**(3), 31
neutron absorption, **3**(1), 30
physical properties, **2**(4), 17
radiation effects, **1**(2), 26
radiation-induced He release, **3**(3), 35
solubility in H_2O, **1**(3), 32
Zircaloy-2 cladding by Cu diffusion bonding, **2**(2), 25
Boron carbide burnable-poison plates, development, **3**(3), 35
Boron carbide cermets, fabrication, **1**(3), 32
Boron carbide control rods (Zircaloy-clad), development, **1**(2), 25–6
Boron carbide–copper dispersions, neutron absorption, **3**(1), 30
roll bonding with stainless steel, **2**(4), 17
Boron carbide–copper dispersions (stainless-steel-clad), fabrication, **2**(4), 17; **3**(1), 29
Boron carbide–silver dispersions, compact production, **2**(1), 27
density, **2**(1), 27
roll cladding with stainless steel (304), **1**(4), 40
Boron carbide sintered pellets (Zircaloy-clad), preparation, **2**(3), 26
Boron carbide–stainless steel dispersions, fabrication, **2**(2), 26

Boron carbide–Zircaloy dispersions, development, **2**(4), 17
extrusion, **2**(3), 25
homogeneity, **2**(3), 25
radiation effects, **2**(3), 26–7
waterlogging effects, **3**(1), 29

Boron carbide–Zircaloy dispersions (clad), salt bath testing, **2**(3), 25–6

Boron carbide–Zircaloy dispersions (irradiated), annealing effects, **2**(3), 26; **2**(4), 17–18

Boron carbide–Zircaloy-2 cermet core strip, coextrusion with Zircaloy-2 cladding, **2**(2), 53

Boron carbide–Zircaloy-2 dispersions, applications, **1**(3), 31
coextrusion, **2**(3), 51–2
radiation effects on corrosion, **2**(2), 25; **2**(4), 17

Boron carbide–zirconium boride dispersions, radiation effects, **2**(3), 26

Boron-chromium compacts, B sintering losses, **3**(2), 19

Boron-chromium-nickel-silicon alloys, corrosion by Na, **3**(3), 40

Boron–chromium oxide compacts, B sintering losses, **3**(2), 19

Boron compounds, chemistry, **2**(3), 25
purity of commercial, **2**(4), 17
solubility in H_2O, **1**(3), 32

Boron control rods, development, **1**(2), 26

Boron-iron alloys, development, **2**(1), 26
phase diagram, **2**(4), 17
radiation effects on electrical resistance, **3**(1), 28

Boron-iron alloys (irradiated), annealing effects on electrical resistance, **3**(1), 28

Boron-iron compacts, B sintering losses, **3**(2), 19

Boron-iron dispersions, development, **2**(1), 26
fabrication specifications, **1**(1), 23

Boron-iron dispersions (austenitic stainless-steel-clad), design, fabrication, and radiation effects, **3**(1), 30

Boron-iron dispersions (Zircaloy-2-clad), fabrication, **2**(2), 25

Boron-nickel cermets, fabrication, **2**(4), 17

Boron-nickel compacts, B sintering losses, **3**(2), 19

Boron–nickel oxide compacts, B sintering losses, **3**(2), 19

Boron-nickel-silicon alloys, corrosion in Na, **3**(3), 40

Boron nitride, compatibility with stainless steel, **3**(2), 19
corrosion resistance to Li, Na, and Pb, **2**(1), 32

Boron nitride–stainless steel dispersions, fabrication, **2**(2), 26

Boron oxide glass–titanium dispersions, development for reactor poison, **2**(1), 27

Boron-silicon compacts, B sintering losses, **3**(2), 19

Boron–silicon dioxide compacts, B sintering losses, **3**(2), 19

Boron–stainless steel alloys, development, **2**(1), 26
radiation effects, **1**(2), 25; **2**(1), 26; **2**(3), 26; **3**(1), 28

Boron–stainless steel alloys (irradiated), annealing effects on electrical resistance, **3**(1), 28

Boron–stainless steel dispersions, development, **2**(1), 26
radiation effects, **1**(3), 31

Boron–stainless steel dispersions (stainless-steel-clad), development, **2**(4), 17

Boron–stainless steel dispersions (Zircaloy-2-clad), fabrication, **2**(2), 25

Boron–stainless steel powder dispersions, radiation effects, **1**(1), 23

Boron–stainless steel–uranium dioxide dispersion fuel plates, B loss control, **3**(2), 19

Boron-tantalum alloys, phase diagram, **3**(4), 29

Boron-titanium-base dispersions (Zircaloy-2-clad), properties and radiation effects, **3**(2), 19

Boron-titanium dispersions, description, **1**(4), 18
extrusion, **3**(2), 19
fabrication, **3**(2), 19
impact properties, **3**(2), 19
radiation effects, **2**(4), 17; **3**(2), 19
radiation-induced internal cracking, **3**(2), 19
tensile properties, **3**(2), 19

Boron-uranium-Zircaloy alloys, radiation effects on dimensions, **2**(3), 8

Boron–uranium–Zircaloy-3 alloys (irradiated), annealing effects on swelling and resistivity, **2**(3), 8

Boron-uranium-zirconium alloys, production, **1**(3), 9
radiation effects, **1**(3), 9; **2**(3), 8; **2**(4), 4–5

Boron-uranium-zirconium alloys (irradiated), annealing effects on swelling, **2**(4), 4

Boron-uranium-zirconium alloys (Zircaloy-3-clad), radiation effects, **1**(2), 7–8

Boron-Zircaloy dispersions, radiation effects, **2**(4), 17

Boron–Zircaloy-2 alloys, radiation effects, **1**(1), 23

Boron-zirconium alloys, phase diagram, **2**(4), 17
radiation effects, **2**(2), 15; **3**(1), 28

Boron-zirconium alloys (irradiated), annealing effects on electrical resistance, **3**(1), 28

Boron-zirconium dispersions, radiation effects, **1**(1), 23; **1**(3), 31

Boron-zirconium dispersions (irradiated), annealing effects, **2**(2), 26

Brass, metallographic effects of explosion shock, **3**(2), 49
radiation effects on electrical resistivity, **3**(4), 37
radiation-induced diffusion in, **2**(2), 32

Brazing
See also specific metals and alloys
alloys, **3**(3), 40, 58

Brazing (Continued)
bibliography, 3(4), 55
for high-temperature service, 3(3), 58
Burnable-poison dispersions, fabrication, 2(2), 25

C

Cadmium, neutron absorption, 3(1), 30
reactor-control applications, 3(2), 19
Cadmium fluoride, neutron absorption, 3(1), 30
Cadmium fluoride–nickel dispersions, neutron absorption, 3(1), 30
Cadmium-indium-silver alloy control rods, diffusion bonding to Ni electroplates, 3(2), 46–7
Cadmium-indium-silver alloys, corrosion, 1(2), 24; 1(3), 29; 1(4), 18; 2(3), 25; 3(4), 34
corrosion protection by plating, 2(1), 26
creep, 1(2), 24; 1(3), 29–31; 1(4), 18; 2(1), 26
development, 2(3), 25
joining to Ti and Zircaloy-2, 1(3), 31
properties, 3(2), 21
creep, 1(4), 18
mechanical, 1(2), 24–5
physical, 1(1), 23
tensile, 1(3), 30
radiation effects, 1(1), 23; 1(2), 24; 1(3), 31; 1(4), 18; 3(4), 34
wear factors against Zircaloy-2, 1(3), 31
welding to Zircaloy-2, 2(2), 25
yield strength, 1(3), 29–31; 2(1), 26
Cadmium-indium-silver alloys (Ni-plated), corrosion in H_2O, 3(4), 34
Cadmium-indium-silver-tin alloys, corrosion in H_2O, 1(3), 29
solid-solution hardening, 1(3), 30
tensile properties, 1(3), 30
yield strength, 1(2), 25
Cadmium-iridium-silver alloys, yield strength, 1(2), 25
Cadmium-iridium-silver-tin alloys, yield strength, 1(2), 25
Calcium boride, radiation effects, 1(2), 26
Calcium fluoride, radiation damage, 2(4), 11
Calcium fluoride–calcium uranate ceramic, radiation effects, 3(1), 19
Calcium fluoride ceramics, radiation effects, 3(1), 19
Calcium fluoride–strontium fluoride ceramic, radiation effects, 3(1), 19
Calcium fluoride–strontium fluoride system, radiation damage, 2(4), 11
Calcium hydride, compatibility with metallic cladding materials, 1(1), 21
thermal conductivity, 1(1), 21
Calcium oxide, radiation effects on crystal properties, 3(3), 22
Calcium oxide–uranium dioxide ceramics, radiation effects, 3(1), 19
Calcium oxide–uranium dioxide–zirconium dioxide ceramics, properties, 3(1), 11
Calcium oxide–uranium dioxide–zirconium dioxide system, fabrication, 3(1), 12
Calcium oxide–zirconium oxide mixtures, radiation-induced amorphism, 3(3), 22
Calcium uranate, preparation and properties, 2(4), 9
Carbides, compatibility with UO_2, 3(4), 12
properties, 3(3), 47
Carbon, diffusion in Mo, Nb, Ta, Ti, W, and Zr, 2(2), 37
solubility in Na, 1(2), 30
Carbon-chromium-uranium system, structure of $UCrC_2$, 3(2), 6
Carbon films, deposition, 3(2), 47
radiation effects, 3(4), 39
Carbon-hydrogen-thorium system, ternary compounds, 3(4), 9
Carbon-molybdenum-titanium-zirconium alloys, recrystallization and rupture stress, 2(4), 41
Carbon-molybdenum-uranium system, compound formation, 1(3), 19
$UMoC_2$ structure, 3(2), 6
Carbon-niobium-uranium alloys, carbide formation, 1(4), 3
Carbon-nitrogen-uranium system, compound formation, 1(3), 19
constitution, 2(1), 14
structure, 1(3), 19
thermal stability, 1(2), 16
Carbon-plutonium system, phase diagrams, 3(3), 8, 11, 21
Carbon-tantalum-uranium system, $UTa_{10}C_4$, 3(3), 20
Carbon-thorium system, constitution, 2(1), 11
Carbon-thorium-uranium system, stability and structure, 2(1), 14–15
Carbon-tungsten-uranium system, compound formation, 1(3), 19
UWC_2 structure, 3(2), 6
Carbon-uranium system, bibliography, 3(3), 20
chemical reactions, 3(3), 20
compounds, 3(3), 20
constitution, 2(4), 2
diffusion, 2(3), 17
H_2 behavior in, 2(4), 2
literature reviews, 3(2), 6; 3(3), 20
phase diagrams, 3(3), 20
physical properties, 3(4), 13–14
Carpenter-20, development for cladding, 3(3), 38
Carpenter-20 Cb, corrosion, 1(3), 34
Carpenter-20 Nb, oxidation, 2(4), 23
Ceramic coatings
See also Coatings
state of the art, 2(1), 50
Ceramics
See also specific ceramics
cladding by pressure bonding, 2(4), 42; 3(1), 50; 3(2), 44
coextrusion with stainless-steel cladding, 2(3), 51
corrosion, 1(3), 37; 2(1), 32; 3(4), 35–6

Ceramics (Continued)
densification, **2**(4), 42; **3**(1), 50; **3**(2), 44
electrophoretic coating with, **1**(1), 29
fission-gas release, **1**(1), 13
radiation effects, **3**(4), 40
Ceramics (irradiated), microstructure studies, **2**(2), 14
X-ray diffraction techniques, **2**(2), 14–15
Cerium, hydridation, **2**(2), 23
Cerium alloy hydrides, mechanical properties, **2**(4), 15
Cerium alloys, hydridation, **2**(4), 15
Cerium-cobalt-plutonium alloys, eutectic, **3**(2), 5
properties, **3**(3), 7
Cerium-copper-plutonium alloys, corrosiveness, **3**(3), 7
Cerium dioxide–plutonium dioxide system, X-ray diffraction studies, **2**(3), 15
Cerium dioxide–uranium dioxide ceramics, sintering, **1**(4), 10
Cerium dioxide–uranium dioxide pellets, reaction with Zircaloy-2, **1**(3), 19
Cerium hydrides, properties, **3**(1), 26
Cerium-magnesium-zinc-zirconium alloys, tensile properties, **3**(3), 46
Cerium-nickel-plutonium alloys, corrosiveness, **3**(3), 7
Cerium oxide–dysprosium oxide system, constitution, **3**(4), 28
Cerium-thorium alloys, constitution, **1**(3), 11
Cermets, cladding by pressure bonding, **2**(4), 42; **3**(1), 50; **3**(2), 44
coextrusion with stainless-steel cladding, **2**(3), 51
corrosion, **1**(3), 37; **3**(4), 35–6
densification, **2**(4), 42; **3**(1), 50; **3**(2), 44
electrophoretic coating with, **1**(1), 29
Cesium, properties, **3**(3), 40
Chromel, corrosion by Bi, Bi-Pb alloys, and Sn, **1**(2), 30
Chromium, corrosion, **1**(2), 33; **1**(3), 35
diffusion with Nb, **3**(4), 44
ductile-brittle transition, **2**(4), 37
oxidation, **1**(1), 33; **2**(4), 23–4; **3**(4), 34
radiation effects on crystal structure, **3**(3), 41
rare-earth addition effects on N_2 absorption, **3**(2), 34
scaling in O_2 and air, **2**(4), 24
Y addition effects on oxidation, **3**(1), 34
Chromium alloys, oxidation, **3**(4), 34
Chromium-base alloys, corrosion resistance, **1**(3), 35
Chromium-base binary alloys, corrosion resistance, **1**(3), 35–6
Chromium boride, properties, **3**(4), 34
Chromium carbide, corrosion resistance, **2**(1), 32
properties, **3**(4), 34
Chromium-cermet dispersions, development, **2**(3), 12
Chromium-cobalt-nickel alloys, oxidation resistance, **1**(4), 22
Chromium-cobalt-niobium alloys, oxidation, **3**(3), 37
Chromium–europium oxide–iron–nickel dispersions (clad with type 304L stainless steel), fabrication, **3**(1), 29–30
Chromium fluoride, activity coefficients in $NaF-ZrF_4$, **1**(4), 24
Chromium-germanium-nickel-silicon alloys, corrosion in Na, **3**(3), 40
Chromium-iron alloys, oxidation, **3**(4), 32
radiation effects on crystal structure, **3**(3), 41
rare-earth addition effects, **3**(2), 34
solid solubility of Y in, **3**(2), 32
transition temperatures, **3**(2), 31
Chromium-iron base alloys, oxidation, **3**(4), 32
Chromium-iron, manganese-nickel quadrupole system, phase diagrams and properties, **3**(2), 31
Chromium-iron-molybdenum-nickel alloys
See Hastelloys and INOR-8
Chromium-iron-nickel alloys
See also Inconel and Stainless steel
corrosion, **1**(2), 29; **3**(3), 38
Chromium-iron-nickel-silicon alloys, oxidation, **3**(2), 23
Chromium-iron-yttrium alloys, constitution, **3**(2), 32, 34
corrosion in H_2O, **3**(3), 39
grain size, **3**(2), 34
oxidation, **3**(2), 34
welding, **3**(2), 48
Chromium-iron-zirconium alloys, corrosion in steam, **3**(4), 31
Chromium-molybdenum alloys, corrosion, **1**(2), 33; **2**(3), 30
Chromium-molybdenum-nickel alloys, oxidation, **3**(1), 33
Chromium-molybdenum-uranium alloys, rolling, **3**(4), 5
Chromium-molybdenum-vanadium alloys, corrosion, **1**(2), 33
Chromium-nickel alloys, corrosion, **3**(4), 32
oxidation, **1**(1), 33; **1**(3), 34; **2**(2), 29
reactions with UN and U_3Si_2 in dispersions, **1**(4), 9
Chromium-nickel-niobium alloys, oxidation resistance, **2**(2), 29–30
Chromium-nickel-phosphorus alloys, corrosion in Na, **3**(3), 40
Chromium-nickel-silicon alloys, corrosion in Na, **3**(3), 40
Chromium-nickel-zirconium alloys, corrosion in steam, **3**(4), 31
Chromium-niobium alloys, strength, **3**(3), 46
Chromium-niobium-titanium alloys, corrosion, **2**(4), 21; **3**(4), 30
oxidation, **1**(3), 34; **3**(3), 37
tensile ductility, **3**(2), 30
Chromium-niobium-uranium-vanadium-zirconium alloys, corrosion in H_2O, **1**(4), 2–3
Chromium nitride, properties, **3**(4), 34

Chromium oxide, properties, **3**(4), 34
Chromium-thorium alloys, constitution, **1**(2), 11
Chromium-titanium ternary alloys, oxidation resistance, **1**(3), 35
Chromium-tungsten alloys, oxidation, **2**(3), 30
Chromium-tungsten-vanadium alloys, corrosion, **1**(2), 33
Chromium-uranium alloys, casting, **2**(1), 45
containment by Y, **2**(4), 22
heat-treatment effects on structure, **3**(4), 3
pin-cushion irradiation tests, **2**(1), 3–4
radiation-induced intergranular cracks, **3**(2), 7
rolling, **3**(4), 5
Chromium-uranium alloys (irradiated), alpha-beta cycling, **3**(2), 7
Chromium–uranium dioxide cermets, pressure bonding, **3**(4), 50
Chromium-uranium eutectic alloy (molten), containment, **1**(3), 48; **1**(4), 25
Chromium-uranium-zirconium alloys, corrosion in H_2O, **1**(4), 2–3
Chromium-vanadium alloys, constitution, **3**(2), 32
corrosion, **1**(2), 33; **1**(3), 36
hardness, **3**(2), 32
Chromium-yttrium alloys, phase diagram, **3**(2), 32
Chromium-zirconium alloys, oxidation, **1**(3), 34
Cladding
See also specific materials clad
coextrusion with fuel elements, **1**(1), 27–8
defects in coextrusion, **1**(1), 28
eddy-current thickness measurement, **1**(3), 54
summary, **3**(4), 2
Coatings
See also specific coatings
ceramic, **2**(1), 50
electrodeposited, **1**(1), 28–9
electrophoretic, **1**(1), 29
Cobalt, content control in stainless steel, **2**(3), 39
Cobalt-base alloy–stainless steel (type 410) (Cr-plated) couple, galvanic corrosion, **3**(2), 23
Cobalt-base alloys, chromizing effects on oxidation, **3**(3), 39
explosion forming, **3**(2), 49
Cobalt-niobium alloys, recrystallization, **2**(2), 35, 37
Cobalt-plutonium alloys, phase diagram, **3**(3), 7, 9
Coextrusion
See also specific materials coextruded
cladding defects, **1**(1), 28; **2**(3), 52
fuel elements with cladding, **1**(1), 27–8
tandem process, **1**(3), 51–2
Compaction, by explosion, **3**(1), 52
Compounds, radiation-induced displacement cascade, **3**(3), 42
Control materials, radiation effects, **3**(3), 1
summary, **3**(4), 2
Control rods
See also specific materials used in control rods
liquid metal, **3**(2), 24
Coolant materials, summary, **3**(4), 2
Coolants, properties, **3**(3), 40
Copper, Al gas plating on, **3**(2), 47
coextrusion with Zr cladding, **2**(3), 50
defect production by cold working, **2**(1), 40
defect production by radiation, **2**(1), 40
diffusion bonding in liquid salts, **2**(4), 43
diffusion of Fe in, **3**(2), 36
diffusion in Zircaloy-2, **3**(2), 34–5
explosion forming, **3**(4), 54
gas-bubble formation, **1**(3), 43
growth in corrosive gas, **3**(4), 16
metallographic effects of explosion shock, **3**(2), 49–50
pressure bonding with Zr, **2**(3), 50
radiation effects, **1**(1), 39; **1**(2), 33; **1**(3), 42–3; **3**(1), 37
crystal structure, **1**(3), 42–3; **2**(4), 25; **3**(3), 41
electrical resistivity, **2**(2), 33; **3**(3), 42; **3**(4), 37
internal friction, **3**(1), 37; **3**(3), 42; **3**(4), 37
mechanical properties, **2**(2), 33–4
stored energy release, **3**(1), 35
X-ray scattering, **3**(1), 36
Young's modulus, **3**(3), 42; **3**(4), 37
radiation-induced gas formation, **2**(1), 17; **3**(3), 23, 42
reaction with H_2O, **2**(1), 33
small-angle X-ray scattering studies in deformed, **3**(2), 26
Copper (Al-coated), radiation effects, **3**(4), 38–9
Copper (irradiated), annealing, **2**(1), 40; **3**(1), 36; **3**(2), 26; **3**(3), 41; **3**(4), 37
behavior of He injected into, **3**(3), 42
dislocation loops and reactions, **3**(4), 38
elastic-modulus measurements on annealing, **3**(1), 36
flow-stress, temperature dependence, **3**(1), 36
heating effects, **3**(3), 42
recovery, **3**(1), 35–6; **3**(2), 26; **3**(4), 41
small-angle X-ray scattering studies, **3**(2), 25–6
stored energy, **3**(2), 26; **3**(4), 37
vacancy formation, **2**(3), 32
Copper (OFHC), gas-pressure self-bonding, **3**(1), 49
solid-phase pressure bonding, **3**(2), 44
Copper eutectic fuel elements, diffusion bonding, **2**(3), 50
Copper films (irradiated), stored energy release, **3**(4), 39
Copper-iron alloys, radiation effects, **1**(1), 39
Copper-molybdenum-zirconium alloys, heat-treatment effects, **3**(4), 43
Copper-nickel alloys, corrosion resistance to NaOH, **1**(3), 36
radiation effects, **3**(2), 26–7; **3**(4), 38
Copper plating, measurement by eddy-current technique, **1**(4), 43
Copper-plutonium alloys, phase diagram, **3**(3), 8, 10
Copper tubing, coextrusion with Ti cladding, **2**(3), 50
Copper-uranium alloys, ignition in air and O_2, **2**(4), 9
Copper-yttrium alloys, structure, **3**(1), 41

Copper–Zircaloy-2 alloys, corrosion in H_2O and steam, **3**(1), 32–3
Corrosion
See also specific metals and alloys
experiment equipment, **3**(3), 40
Croloys
See also Steel
coating with Mo, **2**(1), 50; **2**(2), 55
coating with MoO_2, **2**(2), 55
corrosion, **2**(3), 29, 31–2; **3**(3), 39; **3**(4), 35
radiation effects, **1**(1), 39; **1**(2), 34; **2**(1), 43; **2**(2), 35–6
Crucibles, air cooling, **1**(1), 25
coating, **2**(3), 48; **2**(4), 41
Crystals, collisions in displacement spike, **3**(2), 27
defect effects, **3**(2), 35
dislocation sources, **3**(2), 27
radiation surface effects, **2**(4), 10
radiation-induced dimensional instability, **2**(4), 25
radiation-induced lattice displacement, **3**(4), 40
radiation lattice damage detection, **2**(4), 25
small-angle X-ray scattering studies, **3**(2), 25–6
Cutting, by explosion, **3**(2), 49
Cylinders, nondestructive testing, **1**(2), 42

D

Deuterium oxide, separation from H_2O, **3**(4), 1
Diamond, radiation effects, **2**(2), 33; **3**(2), 27
Diffusion
See also specific metals and alloys
bonding, **2**(3), 16
kinetics, **1**(2), 40–1
review, **2**(4), 33
tracer technique studies, **3**(2), 35
Dispersion-control materials, production, **3**(1), 29
summary, **1**(4), 18
Dispersion fuels
See also specific materials
cladding by pressure bonding, **2**(4), 42; **3**(1), 50; **3**(2), 44
densification, **2**(4), 42; **3**(1), 50; **3**(2), 44
radiation effects, **1**(3), 14
Duranickel
See also Nickel alloys
corrosion, **3**(4), 32
Dysprosium oxide ceramics, corrosion in H_2O, **3**(4), 28–9
thermal expansion, **3**(4), 28
Dysprosium oxide–niobium oxide system, constitution, **3**(4), 28
Dysprosium oxide–uranium dioxide system, constitution, **3**(4), 28
Dysprosium oxide–zirconium dioxide system, constitution, **3**(4), 28
Dysprosium-zirconium alloys, corrosion in H_2O, **2**(2), 25; **3**(1), 28–9
fabrication, **2**(2), 25
phase diagram, **3**(1), 28

E

Eddy-current testing
See also Nondestructive testing
applications, **2**(3), 53; **2**(4), 44
calibration, **1**(2), 42
development, **2**(1), 51; **2**(2), 56
electrical-conductivity measurement in metals, **3**(1), 54
jacket-to-core gap, **3**(3), 59
jacket thickness, **3**(3), 59
techniques, **3**(1), 54
Zr-cladding thickness, **3**(3), 59
Enamel, electrophoretic coating on U, **1**(1), 29
Erbium-zirconium alloys, corrosion in H_2O, **2**(2), 25
fabrication, **2**(2), 25
phase diagram, **3**(1), 28–9
Europium alloys, development, **1**(1), 23
Europium boride, radiation effects, **1**(2), 26
Europium oxide, neutron absorption, **3**(1), 30
Europium oxide–iron dispersions, development, **1**(2), 26
Europium oxide–iron–gadolinium oxide dispersions, neutron absorption, **3**(1), 30
Europium oxide–stainless steel dispersions, chemical reactions, **1**(2), 27
radiation effects, **1**(1), 24
Europium–stainless steel alloys, Eu vaporization, **1**(4), 19
Europium-titanium alloys, Eu vaporization, **1**(4), 19
Explosions, applications, **3**(1), 52–3; **3**(2), 49; **3**(4), 53–5
compaction, **3**(1), 52; **3**(2), 49
cutting, **3**(2), 49
extrusion, **3**(1), 52
forging, **3**(2), 49
forming, **3**(1), 52–3
pressure pulse, **3**(4), 54
sheet-metal critical impact velocities and strain rates, **3**(1), 52–3
surface hardening, **3**(2), 49
swaging, **3**(1), 52
tank stress insulation, **3**(3), 58
time-pressure profiles, **3**(4), 54
transfer media, **3**(3), 56; **3**(4), 54
welding, **3**(1), 52; **3**(2), 49; **3**(4), 55
Extrusion, by explosion, **3**(1), 52
Extrusion cladding
See specific materials

F

Fecral, oxidation resistance, **1**(3), 35
Ferrous materials
See also Metals
radiation effects, **3**(1), 37
Fiberglas fuel elements, development, **3**(4), 11
roll cladding with Al, **3**(4), 49

Fibers, applications of glass-clad U glass, **3**(3), 19
fabrication of Al containing Al-coated fueled, **3**(3), 19–20
Films
See also specific films
radiation effects on electron scattering and absorption, **2**(4), 11
Fission-gas bubbles
See also specific metals and alloys
electron microscopy study, **3**(1), 18
Fissium, diffusion, **2**(3), 17
Fissium-molybdenum-uranium alloys, radiation effects, **1**(3), 4
Fissium-plutonium-uranium alloys, compatibility with metals and alloys, **3**(4), 8–9
composition, **1**(1), 9
density, **3**(4), 8
development, **1**(3), 10
fabrication, **1**(2), 9–10
hardness, **3**(4), 8
radiation effects, **1**(1), 9; **3**(4), 9
solidus temperature, **3**(4), 8
thermal conductivity, **3**(1), 5–7
thermal expansion, **1**(1), 9; **3**(1), 5–7
Fissium-plutonium-uranium fuel pins, injection casting, **1**(3), 10
Fissium-uranium alloys, density, **3**(3), 3
hardness, **3**(3), 3
injection casting, **1**(3), 48
radiation effects, **1**(3), 4; **2**(2), 6
thermal expansion, **3**(3), 3
Fluorides, radiation damage, **2**(4), 11
Fluorides (molten), containment materials, **2**(1), 31
corrosion by, **1**(4), 24; **2**(1), 30; **2**(3), 31
Forging, by explosion, **3**(2), 49
Frost test
See also Nondestructive testing
characteristics, **1**(2), 42
Fuel, radiation effects, **2**(4), 9–10
summary, **3**(4), 2
Fuel billets (hollow), radiographic testing, **1**(3), 54
Fuel elements, bibliography on fabrication and properties, **1**(4), 1
cladding, **3**(1), 50
coextrusion with cladding, **1**(1), 27–8
fabrication, **1**(4), 1
gamma scanning, **3**(2), 51–2
hot swaging with Zircaloy cladding, **2**(4), 42
lead dip canning, **2**(4), 44
leak detection, **3**(1), 54
properties, **1**(4), 1
rare-gas concentration, **2**(1), 16–17
roll cladding, **1**(1), 26; **1**(4), 40
symposium, **3**(3), 1
technology, **3**(2), 1
Fuel elements (AlSi-bonded), U diffusion, **3**(3), 44
Fuel elements (AlSi-canned), bond testing by Lamb wave method, **3**(1), 54
Fuel elements (clad), bond testing, **1**(3), 54
Fuel elements (diffusion-bonded), examination, **2**(1), 46–7
fuel-cladding interaction, **2**(1), 46–7
Fuel elements (fused oxide), swaging with stainless-steel cladding, **3**(3), 53
Fuel elements (irradiated), gas-bubble effects, **3**(3), 23
ultrasonic bond testing, **2**(1), 51
Fuel elements (molten), reaction with steam, **1**(1), 35
Fuel elements (Ni-plated), blistering, **3**(4), 53
Fuel elements (oxide), bonding and swaging with cladding, **3**(3), 52–3
Fuel elements (pellet type), vacuum loading in canning, **2**(3), 52
Fuel elements (ribbed tubular), nondestructive testing, **1**(2), 42
Fuel elements (segmented), hot pressing with Al cladding, **3**(2), 46
Fuel materials, radiation effects, **1**(1), 37; **3**(1), 17–18; **3**(3), 1
vapor-phase plating, **3**(4), 52
Fuel materials (irradiated), fission-product effects on properties, **3**(1), 18
Fuel pins (Zr-clad), end capping, **2**(4), 44
Fuel plates, nondestructive testing, **1**(2), 42
resistance seam welding, **1**(3), 53
roll cladding, **1**(2), 40
X-ray photometry testing, **1**(3), 54
Fuel rods (Mg-clad), H_2 absorption in monoisopropylbiphenyl, **2**(2), 28
Fuel-slug jackets, eddy-current detection of Al-Si spikes, **1**(3), 54
Fuel slugs (cored), extrusion, **1**(1), 26
Fuel tubes, swaging with internal and external cladding, **3**(3), 52
Fused-salt systems, phase diagrams, **3**(2), 24–5
Fused salts, corrosion by, **1**(4), 23–4; **2**(1), 30

G

Gadolinium alloys, production, **1**(1), 23
Gadolinium oxide, neutron absorption, **3**(1), 30
Gadolinium oxide–nickel dispersions, neutron absorption, **3**(1), 30
Gadolinium oxide–nickel–samarium oxide dispersions, fabrication, **1**(2), 26
mechanical properties, **1**(2), 26
Gadolinium–stainless steel alloys, corrosion in H_2O and steam, **1**(4), 18–19
fabrication, **1**(1), 23; **1**(4), 18–19
segregation, **1**(4), 18
Gadolinium-titanium alloys, constitution, **3**(1), 28
corrosion in H_2O and steam, **1**(4), 18–19
fabrication data, **1**(4), 19
phase diagram, **3**(2), 20–1
segregation, **1**(4), 18

Gadolinium-zirconium alloys, constitution, **3**(1), 28
corrosion in H_2O, **3**(1), 29
phase diagram, **3**(2), 20–1
Gallium-plutonium alloys, preparation, **1**(4), 7
Gamma testing, applications, **2**(4), 44–5; **3**(3), 58
development, **2**(1), 51
Germanium, radiation effects, **2**(2), 33; **3**(1), 36; **3**(4), 39
Germanium (irradiated), damage annealing, **3**(4), 39
Germanium-uranium alloys, phase diagram, **3**(4), 4
Gold, pressure effects, **3**(2), 36
radiation effects on electrical resistivity, **2**(2), 33; **3**(3), 42; **3**(4), 37
vacuum deposition, **3**(3), 54
Graphite, annealing, **1**(1), 19
Bi penetration, **1**(3), 24; **2**(1), 22
brazing to Nilo-K, **3**(2), 47
canning, **2**(1), 49; **2**(2), 54–5
coating with carbides, **2**(1), 50; **2**(2), 55
compatibility with alloys, **1**(2), 20
compatibility with liquid Na, **2**(2), 20
creep properties, **2**(4), 14; **3**(3), 28–9
diffusion into Alnico, **1**(3), 24
Inconel X, **1**(3), 24
stainless steel (type 316), **1**(3), 24
diffusion of gases through, **1**(1), 19
electrophoretic coatings for, **1**(1), 29
imperviousness to H_2O, **1**(2), 20
molten-salt penetration into, **3**(1), 35
Na exposure effects, **1**(3), 37–8
permeability, **2**(1), 22–3; **3**(2), 24
properties, **3**(3), 47
purity, **1**(1), 19
radiation effects on, density, **3**(3), 28
dimensions, **2**(1), 22; **2**(4), 25; **3**(2), 12; **3**(3), 28
electrical resistivity, **2**(1), 22
oxidation, **2**(1), 22; **3**(1), 22
reaction with H_2, **2**(1), 22
thermal conductivity, **2**(1), 22
weight, **3**(3), 28
SiC coating, **2**(4), 44
thermal conductivity, **2**(3), 22
total capture cross section, **2**(1), 22
U absorption, **1**(3), 24
UO_2-containing, **1**(3), 24
vapor deposition of carbide coatings, **2**(3), 52
Graphite (annealed), radiation-induced dimensional changes, **3**(2), 12
Graphite (CO), oxidation, **3**(2), 12
Graphite (fueled), fabrication, **1**(1), 12
fission-product release, **2**(2), 15
Graphite (irradiated), thermal annealing, **2**(4), 14
total stored energy, **2**(4), 14
Graphite (pyrolytic), linear thermal-expansion coefficient, **3**(2), 12
oxidation, **3**(2), 12
Graphite (Si-coated), canning with type 316 stainless steel, **2**(1), 49
Graphite (SiC-coated), Bi absorption, **2**(3), 52
Graphite (SiC-Si-coated), heat effects, **3**(2), 12
internal pressure effects, **3**(2), 12–13
radiation effects on density, **3**(2), 13
Graphite (SiC-Si-coated) (irradiated), leakage and oxidation, **3**(2), 13
Graphite fibers, utilization in fuel elements, **3**(3), 52
Graphite fuels, coating, **3**(3), 55
radiation effects, **2**(2), 20
Graphite plates, vinyl coating, **2**(1), 51
Graphite tubes, vapor deposition of carbide coatings, **1**(1), 28
Graphite–uranium dicarbide dispersions, irradiation, **3**(1), 22
Graphite–uranium dioxide fuel elements, radiation effects, **2**(3), 22; **2**(4), 14
Graphite–uranium dioxide mixtures, physical properties, **2**(1), 23
Graphite–uranium monocarbide dispersions, irradiation, **3**(1), 22
Graphite–uranium monocarbide mixtures, physical properties, **2**(1), 23

H

Hafnium, corrosion, **3**(4), 30
ductility, **1**(3), 29
oxidation, **3**(4), 34
physical properties, **1**(2), 24
production, **1**(2), 24
properties, **1**(2), 24; **1**(4), 18; **3**(4), 30
radiation effects on corrosion, **3**(4), 33
radiation-induced transmutation, **3**(4), 33
radiographic testing, **1**(1), 30
reactor-control applications, **3**(2), 19
separation from Zr, **3**(4), 1
tensile properties, **1**(4), 18
wear factors, **1**(3), 31
welding, **3**(1), 53
Hafnium (crystal-bar), corrosion in steam, **1**(3), 29
tensile properties, **1**(3), 29
Hafnium (sponge), corrosion in steam, **1**(3), 29
tensile properties, **1**(3), 29
Hafnium alloys, oxidation, **3**(4), 34
Hafnium boride, properties, **3**(4), 34
radiation effects, **1**(2), 26
solubility in H_2O, **1**(3), 32
Hafnium carbide, properties, **3**(4), 34
Hafnium nitride, properties, **3**(4), 34
Hafnium oxide, arc spraying, **3**(2), 47
properties, **3**(4), 34
Hafnium strip, corrosion, fabricability, and tensile properties, **2**(3), 25
Hafnium-thorium alloys, constitution, **1**(2), 11
Hafnium-uranium alloys, equilibrium diagram, **3**(1), 2
Hafnium-yttrium alloys, constitution, **2**(3), 35

Hastelloys
See also INOR-8
B, carburization effects, **2**(4), 36
corrosion, **1**(2), 29; **1**(3), 37
high-temperature strength, **2**(4), 35–6; **3**(1), 45
mechanical properties, **2**(1), 37–8; **2**(2), 42, 44–5; **2**(3), 39–45
weldment properties, **3**(1), 53
corrosion in H_2O, **3**(3), 39
explosion forming, **3**(2), 49
R-235, corrosion, **3**(3), 39; **3**(4), 32
development for cladding, **3**(3), 38
oxidation, **1**(2), 32; **2**(2), 29; **2**(4), 23
thermal stability, **3**(3), 39
specifications, **2**(2), 40
W, corrosion, **1**(2), 29
mechanical properties, **2**(2), 42, 45; **2**(3), 39, 45
oxidation, **1**(2), 32; **2**(2), 29
weldment properties, **3**(1), 53
X, corrosion, **3**(3), 39; **3**(4), 32
oxidation, **2**(4), 23; **3**(2), 23
radiation effects, **1**(1), 39; **1**(2), 34; **2**(1), 43; **2**(2), 35–6
thermal stability, **3**(3), 39
Haynes 25, radiation effects on springs, **1**(3), 44; **3**(4), 41
Health and safety, summary, **3**(4), 1
Helium, properties, **3**(3), 40
Hydrogen, properties, **3**(3), 40
Hydrogen-niobium system, constitution, **1**(4), 16
equilibria, **1**(4), 15–16; **3**(1), 26
heats of solution, **1**(4), 16
phase diagram, **3**(1), 26
X-ray diffraction patterns, **2**(2), 23
Hydrogen–noble metal systems, electrochemical mechanisms, **3**(1), 15–16
Hydrogen-titanium-zirconium system, transformations, **3**(1), 25
Hydrogen-uranium-zirconium system, constitution, **3**(2), 17
corrosion in H_2O, **2**(1), 9
cracking, **2**(1), 9
dissociation pressure, **1**(2), 23
electrical resistivity, **2**(1), 9; **2**(2), 23
fabrication, **3**(1), 24
H_2 solubility, **1**(2), 23
mechanical properties, **2**(2), 23
phase boundaries, **2**(2), 23
phase diagram, **2**(3), 23–4
preparation, **2**(1), 9; **2**(2), 23
properties, **1**(1), 21; **3**(1), 24
radiation effects, **2**(2), 23; **2**(4), 16; **3**(2), 17
thermal conductivity, **2**(1), 9; **2**(2), 23
ultimate strength, **2**(1), 9
Hydrogen-zirconium system
See also Zirconium hydride
dilatometric study, **3**(2), 16
hydride precipitation habit plane, **3**(4), 23
phase boundaries, **3**(1), 24
phase diagram, **3**(1), 24–5; **3**(4), 23
pressure-composition isotherms, **3**(4), 23
transformation, **3**(1), 25–6

I

Inco 702, oxidation, **2**(4), 23
Inconel
See also Chromium-iron-nickel alloys and Stainless steel
arc spraying with Ca coating, **3**(1), 51
carburization, **1**(4), 24; **2**(3), 39, 44–5; **2**(4), 36
compatibility with UC, **3**(4), 13
corrosion in, fused salts, **1**(4), 24; **2**(3), 31; **3**(2), 24
H_2O, **1**(2), 32; **2**(2), 28–9; **2**(3), 30; **3**(3), 39
molten fluorides, **1**(3), 37; **2**(1), 31–2; **2**(2), 31–2; **3**(1), 35
N_2, **3**(3), 39
NaOH, **1**(3), 36–7
ductility, **2**(1), 37–8
high-temperature oxidation kinetics, **1**(3), 35
high-temperature strength, **2**(4), 35–6; **3**(1), 45
oxidation, **2**(2), 29; **2**(4), 23; **3**(4), 32
plastic-strain cycle effect in Ar, **1**(3), 41
properties, creep, **1**(2), 36–7; **1**(3), 41–2; **2**(3), 39
fatigue, **3**(1), 45
mechanical, **1**(3), 40–1
rupture, **1**(2), 37; **2**(3), 39
radiation effects, **2**(4), 22; **3**(3), 42–3
recrystallization, **2**(2), 37
specifications, **2**(2), 40
thermal fatigue, **2**(4), 36
thermal stability, **3**(3), 39
welding to Nb, **1**(3), 54
Inconel 550, thermal-fatigue effects, **2**(3), 39, 45
Inconel 600, corrosion, **3**(4), 32
Inconel 702, corrosion, **3**(3), 39; **3**(4), 32
development for cladding, **3**(3), 38
oxidation, **1**(1), 33
radiation effects, **1**(1), 39; **1**(2), 34; **2**(1), 43; **2**(2), 35–6
thermal stability, **3**(3), 39
Inconel X, corrosion, **1**(3), 35, 37; **3**(3), 39; **3**(4), 32
development for cladding, **3**(3), 38
ductility, **2**(1), 37–8
graphite diffusion, **1**(3), 24
oxidation, **1**(3), 35; **2**(4), 23
radiation effects, **2**(1), 43
impact properties, **2**(2), 36
mechanical properties, **1**(2), 34; **3**(3), 42–3
springs, **1**(3), 44; **3**(4), 41
tensile properties, **2**(2), 35
thermal stability, **3**(3), 39
Inconel–fluoride salt systems, corrosion, **1**(2), 28
Inconel-Inconel couples, galling, **3**(3), 39
Inconel-NaK loops, corrosion, **1**(2), 28
Inconel-sodium loops, corrosion, **1**(2), 28–9
Inconel-sodium system, corrosion inhibition, **1**(2), 28

Inconel–stainless steel couples, corrosion in H_2O, **2**(3), 30
Inconel tubing, radiation effects, **2**(4), 25–7
Indium-silver-tin alloys, mechanical properties, **1**(3), 30
Indium-thorium alloys, constitution, **3**(2), 5
Indium-thorium intermetallic compounds, crystal structure, **2**(3), 10
Ingots, ultrasonic testing, **1**(4), 43
INOR-8
See also Hastelloys
carburization effects, **2**(3), 39, 44–5; **2**(4), 36
corrosion in, molten fluorides, **2**(1), 31; 2(2), 31–2; **3**(1), 35
molten fluorides and graphite, **3**(2), 24
Na and graphite, **3**(2), 24
creep strength, **2**(3), 38, 42–3
fatigue studies, **2**(3), 38–9
heating effects, **2**(2), 43–5
high-temperature strength, **2**(4), 35–6; **3**(1), 45
notch effects, **2**(3), 38, 43
oxidation, **2**(4), 23; **3**(1), 33
physical properties, **1**(3), 40
welding, **1**(3), 53–4; **2**(3), 39, 45, 53; **3**(1), 53
Intermetallic compounds, properties, **3**(3), 47
Interstitials, diffusion, **2**(4), 33
Iridium-thorium system, compound formation, **1**(4), 8
Iron, corrosion in Li, **2**(1), 30–1
diffusion, **3**(2), 36; **3**(4), 44
explosion shock metallographic effects, **3**(2), 49–50
H absorption, **3**(4), 32
oxidation, **3**(2), 36
radiation effects, **2**(3), 33; **3**(1), 37; **3**(3), 41
self-diffusivity, **3**(2), 35
solid solubility in Be, **3**(3), 31
solution mass-transfer inhibition, **1**(4), 25
Iron (irradiated), damage recovery, **3**(3), 41; **3**(4), 41
Iron alloys, corrosion in liquid metals, **2**(2), 31–2
glass-bonded refractory coatings, **2**(4), 44
melting, **3**(2), 40
radiation effects, **2**(2), 35; **3**(1), 37–8, 41
rare-earth addition effects, **3**(2), 34
Iron–iron boride dispersions, corrosion in H_2O, **2**(2), 25
fabrication, **2**(2), 25
preparation, **2**(3), 26
Iron-manganese alloys, radiation effects, **3**(3), 41
Iron-molybdenum-nickel alloys, corrosion in NaOH, **1**(3), 36
Iron-molybdenum-nickel-niobium-tin-zirconium alloys, corrosion and strength, **3**(3), 45
Iron-molybdenum-nickel-tin-zirconium alloys, corrosion, **3**(3), 45
strength, **3**(3), 45
Iron-nickel alloys, corrosion in H_2O, **3**(3), 39
oxidation, **2**(1), 29; **3**(2), 35; **3**(3), 38
radiation effects, **3**(3), 41
Iron-nickel alloys (Zircaloy-2-clad), diffusion heat-treatment effects, **3**(2), 45
Iron-nickel-niobium-tin-zirconium alloys, corrosion and strength, **3**(3), 45
Iron-nickel-oxygen system, equilibria, **3**(2), 35
Iron-nickel-tin-zirconium alloys, corrosion and strength, **3**(3), 45
Iron-nickel-zirconium alloys, corrosion in steam, **3**(4), 31
Iron-niobium alloys, recrystallization, **2**(2), 35, 37
Iron oxide, H_2 reduction, **3**(2), 36
Iron-plutonium alloys, constitution, **1**(3), 10
cubic expansion, **3**(3), 12–13
hardness, **3**(3), 14
oxidation in air and CO_2, **3**(3), 14
properties, **3**(3), 14
thermal conductivity, **2**(3), 9
viscosity, **3**(3), 12
Iron-plutonium alloys (molten), corrosion of Ta, **2**(4), 22
density, **3**(2), 5
Iron-tin-zirconium alloys, constitution, **2**(3), 33–4; **2**(4), 30–1
Sn solubility in $ZrFe_2$, **2**(3), 33
Iron-tungsten alloys, radiation effects, **3**(3), 41
Iron-uranium alloys, equilibrium diagram, **3**(1), 4–5
properties, **3**(1), 2
Iron-uranium sandwich, diffusion, **2**(3), 17
Iron-yttrium alloys, constitution, **2**(3), 35; **3**(2), 32
effects of melting methods and impurities, **3**(2), 40–1
phase diagram, **3**(2), 32–3
Iron–Zircaloy-2 alloys, H_2 absorption in H_2O and steam, **2**(3), 28
Iron-zirconium alloys, oxidation, **1**(3), 34
Isotopes, gauging and nondestructive testing applications, **2**(1), 51

K

K-Monel, corrosion by He under irradiation, **3**(3), 40
radiation effects, **1**(1), 39; **1**(2), 34; **2**(1), 43; **2**(2), 35–6
Krypton, properties, **3**(3), 40

L

Lamb wave inspection, applications, **3**(4), 56
Lanthanum oxide–uranium dioxide compacts, CaO substitution effects on stability, **2**(4), 7
Lanthanum oxide–uranium dioxide solutions, structure, **1**(3), 17, 19
Lanthanum-plutonium alloys, phase diagram, **3**(3), 7, 9
Lanthanum-yttrium alloys, structure, **3**(1), 41
Lead–lead sulfide system, sulfide equilibria, **3**(2), 35

Lead-plutonium alloys, constitution, 1(3), 10
Lead-thorium alloys, constitution, 2(1), 11
solubility studies, 2(2), 10
Lead-thorium intermetallic compounds, crystal structure, 2(3), 10
Lead-uranium system, liquid immiscibility, 1(1), 3
Liquids, diffusion, 2(4), 33
Lithium, corrosion, 1(2), 30; 2(1), 30–1
radiation effects on stainless-steel corrosion, 2(4), 22
Lithium (molten), properties, 3(3), 40
Lithium fluoride, dislocation sources, 3(2), 27
radiation-damage etching, 2(1), 18–19
radiation effects, 1(2), 33; 2(2), 33; 2(4), 10; 3(4), 39
radiation-induced defects, 2(1), 40; 3(3), 41
gas formation, 3(3), 23
hardening, 3(3), 40–1; 3(4), 39
Lithium fluoride (irradiated), annealing, 2(1), 40, 42; 3(4), 39
Lithium-magnesium alloys, effects of He^4 and H^3 production, 2(2), 15–16
Lithium-magnesium mixtures, radiation-induced gas formation, 3(3), 23
Lithium uranate, preparation and properties, 2(4), 9
Lucite, radiation-induced gas formation, 3(3), 23

M

Magnesium, corrosion in, air, 1(3), 36
CO_2, 1(3), 36
H_2O, 1(3), 36; 2(2), 28; 3(1), 34
N_2, 2(4), 23
O_2, 1(3), 36
organic coolant, 3(1), 35
polyphenyl, 3(2), 23
SO_2, 1(3), 36
corrosion inhibition, 2(2), 28; 3(1), 34
H_2 absorption in monoisopropylbiphenyl, 2(2), 28
mechanical properties, 3(3), 32
nuclear properties, 3(3), 32
oxidation, 1(3), 36; 2(1), 30; 2(4), 23
pyrophoricity, 1(3), 36
radiation effects, 3(1), 37–8
reaction with H_2O vapor, 1(1), 35
Magnesium (sintered), radiation effects, 3(1), 38–9, 42
Magnesium (Zircaloy-2-clad), spontaneous ignition in steam, 3(2), 23–4
Magnesium alloy AZ 61
See Aluminum-magnesium-manganese-zirconium alloys
Magnesium alloys, Be addition effects on oxidation, 1(3), 36; 2(3), 30–1; 2(4), 23
Ca addition effects on oxidation, 2(4), 23
cladding applications, 1(3), 36
corrosion in H_2O, 1(3), 36; 3(1), 34
ignition temperatures, 2(4), 23
oxidation in CO_2, 1(3), 36; 2(1), 30
oxidation in SO_2, 1(3), 36
pyrophoricity, 1(3), 36
radiation effects, 1(2), 34–5; 3(1), 38, 42
Magnesium aluminate, corrosion resistance, 2(1), 32
Magnesium-base dispersions, radiation effects, 1(1), 15–16
Magnesium oxide, corrosion resistance to Li, Na, and Pb, 2(1), 32
reaction with PuO_2, 3(4), 15
Magnesium oxide ceramics (fueled), fission-product release, 2(2), 15
Magnesium oxide–plutonium dioxide mixture, reactions and sintering, 3(3), 21
Magnesium oxide–uranium dioxide system, fabrication, 3(1), 12
ultrahigh-pressure studies, 3(3), 18
Magnesium oxide–uranium dioxide–zirconium dioxide system, fabrication, 3(1), 12
Magnesium-plutonium alloys, preparation, 1(4), 7–8
Magnesium rods (Zircaloy-2-clad), corrosion in steam, 3(2), 23
Magnesium-thorium alloys, liquid immiscibility, 2(4), 6
Magnesium-thorium eutectic, corrosion of Nb and Ta, 2(4), 22
Magnesium-thorium-uranium alloys, constitution, 1(2), 11; 1(3), 11
Magnesium uranate, preparation and properties, 2(4), 9
Magnesium-uranium dispersions (Zircaloy-2-clad), radiation effects, 1(2), 12
Magnesium-zirconium alloys, radiation effects, 3(1), 38
Manganese, H_2 effect in oxide film on corrosion, 3(3), 21–2
Manganese-nickel alloys, radiation effects, 3(4), 38
Materials
See also Fuel materials, Metals, Refractory materials, and Shielding materials
radiation effects, 3(4), 40
Mercury, properties, 3(3), 40
solubility in Th, 2(2), 10
Metal coatings, scaleup and process improvement, 3(3), 55
Metal films, preparation, 3(4), 22
Metal fuels, preirradiation property effects on radiation-induced swelling, 3(3), 23
Metal hydrides, bibliography, 2(2), 22
fabrication, properties, reactions, and uses, 2(4), 15
Metal-hydrogen system, transformations, 3(1), 25
Metal hydroxide system, phase diagrams, 3(2), 24
Metallic fuels, fission damage, 3(2), 7
fission-gas bubble formation, 2(1), 18
radiation effects, 2(2), 15
Metallic fuels (irradiated), X-ray diffraction analysis, 2(2), 16

Metals
See also Alloys, Ferrous materials, Materials, Reactor materials, Refractory metals, Sheet metal, Solids, Structural materials, Transition metals, and specific metals and alloys
ceramic coating, **3**(4), 53
cladding, **3**(4), 52
coextrusion with cladding, **2**(3), 50
corrosion resistance to Li, **2**(1), 30–1
corrosion resistance to NaK, **1**(3), 37
diffusion, **2**(4), 33
diffusion bonding, **3**(4), 50
diffusion coating, **3**(4), 52
eddy-current measurement of electrical conductivity, **3**(1), 54
explosion forming, **3**(1), 51–2; **3**(3), 55–6; **3**(4), 54
explosion welding, **3**(3), 56
flame plating, **3**(4), 52
gas-bubble formation, **1**(3), 43
hard surfacing, **3**(4), 52
hot dipping, **3**(4), 52
inert-gas atom solution, **1**(3), 43
interdiffusion, **3**(4), 44
metallizing, **3**(4), 52
neutron-flux level effects on radiation damage accumulation, **3**(4), 41
oxidation, **3**(2), 35
pressure bonding, **1**(4), 41
pressure effects on diffusion kinetics, **1**(2), 40
radiation effects, **1**(3), 42–3; **2**(2), 35; **3**(1), 18, 37; **3**(2), 27; **3**(3), 1, 23, 42
critical shear stress, **2**(1), 40
defect production, **3**(4), 40
hardening, **3**(1), 37
heating, **3**(1), 18
lattices, **3**(3), 42
mechanical properties, **2**(3), 33
vacancy concentration, **3**(4), 38
radiation-induced changes, **3**(1), 37
reactions with H_2O, **1**(4), 25; **3**(4), 35–7
self-diffusion, **3**(2), 35
small-angle X-ray scattering studies, **3**(2), 25–6
surfacing, **3**(4), 52
temperature measurement by eddy-current methods, **3**(1), 54
thermal properties, **2**(3), 23
ultrasound attenuation, **2**(3), 53–4
volume measurement, **1**(4), 43
Metals (ceramic-coated), behavior under stress, **2**(3), 52
Metals (molten), corrosion, **1**(4), 23–4
reactions in Bi and Na, **2**(4), 22
reactions with H_2O vapor, **3**(2), 9
technology, **1**(3), 38; **3**(3), 40
Metals (noble), radiation effects, **2**(2), 33; **3**(4), 40
Metals (precious), resistance to corrosion by Li, **2**(1), 30–1
Metals (refractory), bibliography, **2**(3), 45
compatibility with UO_2, **3**(4), 12
corrosion resistance to Li, **2**(1), 30–1
ductile-brittle transition, **2**(4), 37
explosion forming, **3**(4), 54
melting method effects, **3**(2), 41
properties, **3**(3), 47
Metals (transition), radiation effects, **3**(4), 38
Moderator materials, radiation effects, **3**(3), 1
summary, **3**(4), 2
Molds, coating, **2**(2), 55; **3**(2), 39
Molybdenum, brazing, **2**(3), 53
casting, **3**(3), 51
cladding, **1**(3), 35; **2**(1), 46
coatings, **1**(2), 41; **2**(1), 29, 49; **2**(2), 30–1; **2**(3), 29–30; **2**(4), 21; **3**(4), 53
coextrusion with stainless-steel cladding, **2**(3), 50
compatibility with fissium-Pu-U alloys, **3**(4), 8–9
corrosion resistance to NaK, **1**(3), 37
creep-rupture properties, **3**(3), 46
diffusion bonding, **3**(3), 53
diffusion with, B, **2**(2), 37
C, **2**(2), 37
Nb, **3**(4), 44
Si, **3**(2), 36
U, **2**(2), 38
explosion welding, **3**(4), 55
fatigue properties, **3**(1), 45
forging, **2**(4), 41
oxidation, **1**(1), 33; **1**(3), 35; **2**(1), 29; **3**(4), 34
oxidation protection, **1**(2), 32; **1**(4), 22
pressure bonding, **2**(1), 46; **3**(2), 44; **3**(4), 50
pressure cladding, **2**(1), 46
pressure self-bonding, **2**(2), 49; **3**(1), 50
radiation effects, **1**(2), 33; **1**(4), 37; **2**(1), 40; **2**(2), 33; **3**(1), 37; **3**(2), 26
self-bonding by gas pressure, **2**(2), 49; **3**(1), 50
SiN deposition on, **3**(2), 47
solid-phase pressure bonding, **3**(2), 44; **3**(4), 50
tensile behavior, **3**(1), 45
welding, **1**(3), 54; **2**(3), 53; **3**(4), 55
Molybdenum (irradiated), annealing and damage recovery, **1**(2), 33; **2**(1), 40; **2**(2), 33–4; **2**(3), 32; **3**(3), 41; **3**(4), 38, 41
Molybdenum (type 310 stainless-steel-clad), welding, **3**(3), 53
Molybdenum alloys, compatibility with process equipment, **2**(4), 41
electroplated coatings, **3**(4), 53
fabrication, **2**(4), 41
oxidation, **3**(4), 34
properties, **2**(4), 41
recrystallization temperatures, **2**(4), 41
strength, **2**(4), 41
Molybdenum boride, properties, **3**(4), 34
Molybdenum carbide, properties, **3**(4), 34
Molybdenum-cermet dispersions, development, **2**(3), 12
Molybdenum fibers, utilization in fuel elements, **3**(3), 52
Molybdenum fuel systems, pressure bonding, **2**(4), 42

Molybdenum-nickel alloys, carburization, 1(4), 24
creep properties, 2(1), 36, 38
mechanical properties, 1(4), 32–5
oxidation, 1(4), 23
relaxation curves, 2(1), 36–7
tensile properties, 2(1), 36–8
weld cracking effects, 2(2), 55
Young's modulus temperature dependence, 2(1), 36–7
Molybdenum-nickel-titanium carbide cermets, electrodeposited Ni coating, 1(1), 28–9
Molybdenum-niobium alloys, tensile properties, 3(3), 46–7
Molybdenum-niobium-thorium alloys, oxidation weight gain, 1(3), 34
Molybdenum-niobium-thorium-titanium alloys, oxidation resistance, 1(3), 34
Molybdenum-niobium-titanium alloys, corrosion, 3(4), 32
tensile properties, 2(4), 38
Molybdenum-niobium-titanium-tungsten-zirconium alloys, composition, oxidation, and strength, 2(4), 21
Molybdenum-niobium-tungsten-zirconium alloys, composition, oxidation, and strength, 2(4), 21
Molybdenum-niobium-uranium alloys, corrosion, 3(2), 3–4; 3(4), 6
radiation effects, 3(4), 6
Molybdenum-niobium-uranium alloys (clad), corrosion, 3(4), 6
radiation effects, 3(4), 6
Molybdenum-niobium-uranium-zirconium alloys, corrosion in H_2O, 1(4), 2–3
Molybdenum-niobium-zirconium alloys, tensile properties, 3(3), 46–7
Molybdenum nitride, properties, 3(4), 34
Molybdenum oxide, properties, 3(4), 34
Molybdenum-plutonium-uranium alloys, compatibility with stainless steel, 3(3), 14
constitution, 3(3), 10–11
ductility, 3(3), 11
fabrication, 1(2), 10; 3(3), 10–11
hot hardness, 3(3), 14
metallurgical properties, 1(1), 9
oxidation in air and CO_2, 3(3), 14
phase-transformation kinetics, 3(3), 11
properties, 3(3), 14
radiation effects, 1(1), 9
reaction with stainless steels, 3(3), 12
thermal expansion, 1(2), 10
Molybdenum powder, vacuum evaporated, coatings, 2(3), 52
Molybdenum-ruthenium-uranium alloys, corrosion, 1(4), 5
Molybdenum silicide, corrosion resistance to Na, 2(1), 32
Molybdenum-silicon-uranium alloys, properties, as-cast, 2(4), 2
mechanical, 3(1), 2; 3(3), 3
metallurgical, 3(3), 3
Molybdenum-silicon-uranium alloys (Al-clad), radiation effects, 3(3), 3
Molybdenum-silicon-uranium-vanadium alloys, corrosion in H_2O, 1(4), 2–3
Molybdenum-silicon-uranium-vanadium-zirconium alloys, corrosion in H_2O, 1(4), 2–3
Molybdenum-thorium alloys, constitution, 1(2), 11
Molybdenum-tin-zirconium alloys, corrosion, 3(3), 45
strength, 3(3), 45
tensile properties, 2(2), 40
Molybdenum-uranium alloy fuel elements (Ta-clad), coextrusion and swaging, 2(1), 47
Molybdenum-uranium alloy fuel pellets, development, 3(4), 6
Molybdenum-uranium alloy fuel pins (Zr-clad), diffusion-layer growth, 2(1), 5
preparation, 2(2), 5–6
Molybdenum-uranium alloy fuel rods (Zircaloy-2-clad), coextrusion, 3(2), 3
Molybdenum-uranium alloy fuel rods (Zr-clad), specification conformance, 1(4), 5
Molybdenum-uranium alloy fuel slugs, coating with Cr and Mo, 3(3), 55
Molybdenum–uranium alloy–uranium dioxide dispersion, development, fabrication, and radiation effects, 2(3), 12
Molybdenum-uranium alloys, alpha-beta cycling, 1(3), 2–3
annealing effects, 3(4), 6
behavior summary, 2(4), 3
bibliography, 1(2), 5
burnup effects, 2(2), 5
casting, 1(1), 8; 1(2), 5
coextrusion with cladding, 2(2), 51; 2(3), 54; 3(2), 45
compatibility with stainless steel, 3(4), 6–7
constitution, 2(3), 4–5
corrosion, 1(2), 4–5; 1(3), 20; 1(4), 5; 3(4), 5–6
crystal structure, 3(4), 4
deformation effects, 3(4), 5
diffusion, 3(1), 3; 3(3), 44
elasticity modulus, 2(2), 5
electrical resistivity, 3(3), 3–4
enrichment effects, 2(1), 4–5
fabrication, 1(3), 5; 2(1), 5
fuel for CO_2-pressurized reactor, 2(2), 5
Hall effect, 3(3), 3
hardness, 1(4), 5
heating, 1(3), 5; 2(2), 5; 2(3), 4–5
interlamellar spacing effects, 2(1), 4–5
lattice parameters, 1(1), 6
magnetic susceptibility, 2(1), 5
melting, 1(3), 5
metallurgy, 1(3), 5
order-disorder reaction, 2(2), 5
oxidation, 2(4), 3; 3(1), 3
oxide orientation, 3(4), 6
phase transformation, 2(3), 2; 2(4), 3; 3(4), 4, 6
plastic reductions, 3(4), 4–5

Molybdenum-uranium alloys (Continued)
processing, 1(3), 5
properties, addition effects, 1(4), 5; 2(1), 6; 2(3), 6
as-cast, 2(4), 2
creep-rupture, 1(1), 5
mechanical, 1(3), 3; 1(4), 5; 2(1), 5; 2(3), 2; 3(2), 4–5; 3(3), 3
metallurgical, 3(3), 3
physical, 2(1), 5
summary, 2(3), 4–6
thermal, 1(1), 5; 1(3), 5; 1(4), 5
radiation effects, 1(1), 38; 1(2), 4–5; 1(3), 3, 5; 1(4), 4–5; 2(1), 4–5, 16–17; 2(2), 5; 3(1), 2–4; 3(2), 7; 3(4), 5–7
stability, 1(4), 5; 2(2), 5; 2(3), 6; 3(3), 3–5; 3(4), 6
strength, 2(3), 2
thermal-cycling effects, 3(3), 3
true stress–true strain curves, 2(2), 5
U_2Mo phase, 3(3), 4
vacancy agglomeration inhibition, 2(1), 16
Molybdenum-uranium alloys (Al-clad), radiation effects, 3(3), 3
Molybdenum-uranium alloys (clad), corrosion, 3(4), 6
Molybdenum-uranium alloys (irradiated), reversion, 2(4), 9
Molybdenum-uranium alloys (Zircaloy-2-clad), corrosion, 1(3), 4–5
Molybdenum-uranium alloys (Zr-clad), interdiffusion, 2(2), 39
Molybdenum-uranium compacts, radiation-induced dimensional changes, 3(2), 3
Molybdenum–uranium dioxide cermets, pressure bonding, 3(4), 50
Molybdenum–uranium dioxide dispersions, fabrication, 2(2), 11; 2(3), 11
properties, 2(2), 11
Molybdenum–uranium nitride dispersions, chemical reactions, 1(4), 9
fabrication, 2(2), 11
properties, 2(2), 11
Molybdenum-uranium powder compacts, radiation stability, 3(1), 3; 3(4), 5
Molybdenum–uranium silicide dispersions, chemical reactions, 1(4), 9
Molybdenum-uranium-zirconium alloys, alpha-beta thermal cycling, 1(1), 3
corrosion in H_2O, 1(4), 2–3
Monel, corrosion, 3(4), 32

N

NaK
See Potassium-sodium alloys (molten)
Neptenium-plutonium alloys, phase diagram, 3(3), 7–8
Nichrome cylinders, explosion forming, 3(2), 50–1
Nichrome-uranium eutectic alloy (molten), containment in oxidized Nb-U alloy crucible, 1(3), 48
Nichrome V
See Chromium-nickel alloys
Nickel, arc spraying with Ca coating, 3(1), 51
corrosion, 1(1), 34; 2(1), 30–1; 3(3), 40
creep-rupture properties, 1(4), 33, 35
defect production, 2(1), 40
diffusion with, Al, 3(2), 36
Mg, 3(2), 36
Nb, 3(4), 44
Si, 3(2), 36
U, 3(3), 44
Zr, 3(2), 36
eddy-current cold-work measurement, 1(3), 54
electrodeposited coating on cermet, 1(1), 28–9
H absorption, 3(4), 32
oxidation, 1(1), 33
radiation effects on, crystal structure, 3(3), 41
K absorption, 3(4), 38
magnetic properties, 3(4), 38
mechanical properties, 2(2), 33–4; 3(1), 39
vacancy clusters, 3(2), 27
reactions with Ni, 1(2), 32–3
solid solubility in Be, 3(3), 31
stress-rupture properties, 1(3), 35
Nickel (A), corrosion, 3(4), 32
properties, 2(3), 35
Nickel (A-286), 2(3), 35–6
Nickel (irradiated), annealing and damage recovery, 2(1), 40; 3(3), 41; 3(4), 41
electrical resistivity recovery, 3(2), 26
Nickel alloys, corrosion, 1(3), 36; 1(4), 23; 2(1), 30–1; 3(4), 32
electroless coatings, 2(3), 52; 3(4), 52
heat-treatment effects on microstructure and high-temperature properties, 2(3), 35
melting, 3(2), 40
oxidation, 1(2), 32; 3(3), 39
radiation effects, 2(2), 35; 3(1), 37–8
refractory coatings, 2(4), 44
Nickel films, radiation effects, 3(4), 39
Nickel-niobium alloys, recrystallization, 2(2), 35, 37
Nickel oxide, radiation effects, 2(2), 33
Nickel-plutonium alloys, crystal structure, 1(2), 9; 3(3), 7
Nickel-plutonium intermetallic compounds, crystal structure, 2(3), 9
Nickel–sodium hydroxide system, Ni mass transfer, 1(3), 35
stress corrosion, 1(3), 35
Nickel-uranium alloys, diffusion, 3(2), 3; 3(4), 43
Nickel–uranium dioxide dispersions, explosion compaction, 3(2), 51
Nickel-uranium-zirconium alloys, corrosion in H_2O, 1(4), 2–3
Nickel-yttrium alloys, constitution, 2(3), 35
phase diagram, 3(2), 32–3
Nickel-yttrium ternary alloys, eutectic, 2(1), 34
Nickel-zirconium alloy hydrides, structure, 3(1), 24

Nickel-zirconium alloys, constitution, **2**(4), 31
crystal structure, **2**(4), 31
hydriding, **1**(3), 27
lattice parameters, **2**(4), 31
Nicral D, oxidation, **3**(2), 23
Niobium, annealing, **1**(2), 37
cage zone melting, **2**(3), 48–9
coatings, Cr-Ni, **3**(3), 37
electroplated, **3**(4), 53
LM-5, **3**(3), 37
ZN, **3**(3), 37; **3**(4), 52
coextrusion with stainless-steel cladding, **2**(3), 50
compatibility with fissium-Pu-U alloys, **3**(4), 8–9
corrosion, **1**(2), 29; **2**(3), 29; **2**(4), 22, 33; **3**(1), 32; **3**(2), 22; **3**(3), 37; **3**(4), 30
creep rupture, **2**(3), 43, 45
development for cladding, **3**(3), 38
diffusion bonding, **2**(3), 17; **3**(3), 53
diffusion with, B, **2**(2), 37
C, **2**(2), 37
Cr, **3**(4), 44
Fe, **3**(4), 44
Mo, **3**(4), 44
Ni, **3**(4), 44
stainless steel, **3**(4), 44
U, **2**(2), 28
ductile-brittle transition, **2**(4), 37
ductility, **2**(3), 45
elastic modulus, **1**(3), 42; **2**(3), 43
electrical resistivity, **2**(4), 31–2
fabrication, **2**(3), 49; **3**(1), 48
H_2 diffusion coefficient, **1**(3), 35
H_2 solubility in, **2**(3), 24
ignition temperature, **3**(4), 30
ingot production, **2**(3), 49
mechanical properties, **2**(3), 43; **3**(2), 20; **3**(3), 47
melting, **2**(3), 48–9
N_2 diffusion, **2**(4), 33
N_2 solubility, **2**(4), 33; **3**(1), 32
oxidation, **1**(1), 33; **1**(2), 31–2; **1**(3), 34; **1**(4), 22; **2**(2), 30; **2**(3), 29; **3**(1), 32; **3**(3), 37; **3**(4), 30, 34
physical properties, **2**(3), 43; **3**(3), 47
preparation, **2**(3), 48–9; **3**(3), 54–5
pressure bonding, **3**(2), 44; **3**(4), 50
pressure self-bonding, **2**(2), 49; **3**(1), 50
protective coatings, **2**(1), 29; **2**(2), 55; **3**(3), 37
radiation effects, **2**(2), 33–4; **3**(2), 27; **3**(4), 38
reactions with CO and CO_2, **3**(4), 30
reaction with H_2, **1**(3), 35
reaction with N_2, **2**(4), 33; **3**(1), 32; **3**(2), 22
reaction with UC in Ar, **3**(3), 20
recrystallization, **2**(2), 35, 37; **2**(3), 43
rupture strength of annealed, **2**(1), 39
self-diffusion, **2**(1), 34; **3**(2), 35–6
tensile properties, **2**(3), 43, 46; **3**(2), 30
thermal conductivity, **2**(4), 31–2
thermal-expansion coefficient, **2**(4), 31
thermal properties, **3**(2), 32
utilization in fuel elements, **3**(3), 52
vacuum deposition, **3**(3), 54
vapor-deposited coating on stainless steel, **1**(1), 28
welding, **1**(3), 54
yield strength, **2**(3), 43
Zn coating, **3**(3), 37
Niobium (type 310 stainless-steel-clad), welding, **3**(3), 53
Niobium alloys, compatibility with UC, **3**(4), 13
corrosion, **2**(2), 30; **2**(4), 21; **3**(2), 22; **3**(3), 37
electroplated coatings, **3**(4), 53
fabrication, **3**(3), 51
mechanical properties, **1**(2), 37; **3**(3), 47
Nb oxide production, **3**(2), 22
oxidation, **1**(1), 33; **1**(2), 31–2; **1**(3), 34; **2**(1), 28–9; **3**(1), 32; **3**(4), 34
physical properties, **3**(3), 47
protective coatings, **3**(3), 37
recrystallization, **2**(2), 35, 37
strength, **3**(2), 30
tensile properties of annealed, **2**(1), 39
welding, **2**(3), 53; **3**(3), 58
Niobium alloys–Zircaloy-2 couples, diffusion, **2**(3), 17
Niobium boride, properties, **3**(4), 34
Niobium boride–stainless steel dispersions, preparation and properties, **2**(3), 26–7
Niobium carbide, properties, **3**(4), 34
vapor-deposited coating on graphite, **1**(1), 28
Niobium-carbon system, constitution, **3**(1), 39
Niobium-cermet dispersions, development, **2**(3), 12
Niobium crystals, cleavage and twinning, **3**(2), 32
Niobium fuel systems, pressure bonding and cladding, **2**(1), 46
pressure self-bonding, **2**(4), 42
Niobium hydride, activation energy, **1**(3), 27
H_2 diffusion coefficient, **1**(3), 27
phase studies, **1**(1), 21
properties, **1**(4), 15
Niobium hydride (annealed), martensitic phase transformation, **3**(2), 17
metallographic studies, **3**(2), 16–17
Niobium nitride, properties, **3**(4), 34
Niobium oxide, properties, **3**(4), 34
transformation, **2**(3), 29
Niobium-oxygen system, constitution, **3**(1), 39
Niobium pentoxide, transformation, **3**(3), 37
Niobium-rhenium alloys, recrystallization, **2**(2), 35, 37
Niobium-tantalum alloys, solid solutions, **2**(1), 34
Niobium-tin-uranium alloys, radiation effects on corrosion, **1**(3), 3; **3**(4), 5
Niobium-tin-zirconium alloys, corrosion in H_2O and steam, **3**(4), 31
mechanical properties, **3**(3), 45
tensile properties, **3**(4), 42
Niobium-titanium alloy–uranium nitride dispersions, chemical reactions, **1**(4), 9
Niobium-titanium alloy–uranium silicide dispersions, chemical reactions, **1**(4), 9

Niobium-titanium alloys, oxidation resistance, 2(1), 28–9
strength, 3(3), 46
Niobium-titanium-uranium alloys, corrosion in H_2O, 2(3), 3
Niobium-titanium-uranium diffusion couples, bonding effects on interaction, 2(4), 33–4
Niobium-titanium-vanadium alloys, oxidation, 1(3), 34
Niobium-titanium-zirconium alloys, oxidation resistance, 2(1), 29
tensile properties, 2(4), 38
Niobium-tungsten alloys, oxidation, 1(3), 34
recrystallization, 2(2), 35, 37
strength, 3(3), 46
Niobium-uranium alloy diffusion couples, phase study, 3(3), 4
Niobium-uranium alloy sheet, oxide orientation, 3(4), 6
Niobium-uranium alloys, age hardening, 2(3), 4
C removal, 1(1), 5
cast structure breakdown, 2(2), 8
constitution, 1(2), 4; 1(4), 3; 2(3), 16–17; 2(4), 3
corrosion, 1(1), 8, 25, 35; 1(4), 4; 2(1), 6, 9; 2(3), 4; 2(4), 5; 3(1), 3–4; 3(4), 5–8
diffusion, 2(3), 16–17; 3(3), 44
electrical resistivity, 3(3), 3–4; 3(4), 8
fabricability, mechanical and physical properties, 2(1), 9
fabrication, 1(1), 8; 1(2), 39–40; 1(4), 3; 2(3), 8
Hall effect, 3(3), 3
hardness, 1(4), 4; 2(2), 8
homogenization, 1(4), 3
melting, 1(4), 3
miscibility gap, 3(3), 4
oxidation, 1(4), 4; 2(3), 8
physical properties, 3(1), 3
preparation, 1(2), 4
processing, 1(3), 4
production, 1(1), 25
properties, 1(3), 4; 2(1), 6; 2(3), 6
radiation effects, 1(1), 3, 38; 2(1), 9; 3(1), 3; 3(4), 5–6
radiation-induced phase changes, 1(4), 4; 2(1), 4; 2(2), 5; 2(3), 3; 2(4), 3; 3(1), 3; 3(2), 7
radiation-induced swelling, 2(4), 10; 3(4), 5–6
segregation, 1(4), 3–4; 2(2), 47
stability, 1(3), 5; 2(3), 6
tensile properties, 2(4), 5; 3(3), 6; 3(4), 7–8
thermal cycling, 1(1), 3
thermal stability, 1(3), 5
U diffusion, 3(3), 44
X-ray diffraction studies, 2(2), 5
Niobium-uranium alloys (clad), corrosion and radiation effects, 3(4), 6
Niobium-uranium alloys (irradiated), electrical resistivity, 2(4), 3
transformation, 2(3), 3
X-ray diffraction studies, 2(4), 3
Niobium-uranium alloys (Mo-clad), fabrication, 1(4), 4
Niobium-uranium alloys (molten), effects of C and O_2 content, 1(3), 47–8
Niobium-uranium alloys (stainless-steel-clad), rolling, 1(4), 4
Niobium-uranium alloys (Zircaloy-2-clad), corrosion in H_2O, 2(1), 6
Niobium-uranium couples, concentration-penetration curves for diffusion, 2(4), 3
Niobium–uranium dioxide cermets, pressure bonding, 3(4), 50
Niobium–uranium dioxide dispersions, development, 2(3), 12
fabrication, 2(2), 11; 2(3), 11
properties, 2(2), 11
Niobium–uranium nitride dispersions, chemical reactions, 1(4), 9
fabrication, 2(2), 11
properties, 2(2), 11
Niobium–uranium silicide dispersions, chemical reactions, 1(4), 9
Niobium-uranium ternary alloys, corrosion in H_2O, 2(1), 6
transformation kinetics, 1(1), 5
Niobium-uranium ternary alloys (Zircaloy-2-clad), corrosion in H_2O, 2(1), 6
Niobium-uranium-vanadium diffusion couples, bonding effects on interaction, 2(4), 33–4
Niobium-uranium-vanadium sandwiches, bonding and diffusion, 2(3), 17
Niobium-uranium-zirconium alloy cores, roll cladding with Zircaloy-2, 1(3), 49–50
Niobium-uranium-zirconium alloy platelets (clad), corrosion in H_2O, 2(3), 4
Niobium-uranium-zirconium alloys, constitution, 1(2), 4
corrosion, 1(1), 35; 1(2), 5; 1(3), 3–4, 6; 1(4), 2–3; 2(3), 3–4; 3(1), 3
hot hardness, 1(3), 6
miscibility gap, 3(3), 4
physical properties, 3(1), 3
radiation effects, 1(3), 3; 2(2), 5; 2(3), 4–5; 3(1), 3
tensile properties, 2(2), 7–8
transformation, 2(2), 5; 2(3), 3–4; 3(1), 3
Niobium-uranium-zirconium alloys (irradiated), transformation, 2(3), 3
Niobium-uranium-zirconium alloys (Zircaloy-2-clad), corrosion in H_2O, 2(3), 4
Niobium-vanadium alloys, corrosion, 3(2), 22; 3(3), 37; 3(4), 30
properties, 3(2), 22, 30; 3(3), 46–7
UO_2 dispersion matrix properties, 3(1), 9
Niobium-vanadium-zirconium alloys, tensile properties, 3(2), 30; 3(3), 46–7
Niobium-zirconium alloy–uranium dioxide dispersions, development, 2(3), 12
Niobium-zirconium alloys, aging transformation, 3(2), 35
cold-rolling effects, 3(4), 43
corrosion, 2(4), 21; 3(3), 40; 3(4), 31

Niobium-zirconium alloys (Continued)
creep properties, **3**(3), 45
heat-treatment effects, **1**(4), 26; **3**(4), 43
mechanical properties, **2**(3), 39, 42
oxidation, **3**(1), 32; **3**(2), 22
radiation effects, **3**(1), 37
tensile properties, **2**(2), 40; **2**(4), 37–8; **3**(3), 46–7; **3**(4), 42
transformation, **3**(1), 39; **3**(2), 35
UO_2 dispersion matrix properties, **3**(1), 9
weldability, **2**(3), 53
Nitrides, compatibility with UO_2, **3**(4), 12
properties, **3**(3), 47
Nitrogen-thorium alloys, preparation, **3**(4), 9
Noble metals
See also Metals
radiation effects, **2**(2), 33; **3**(4), 40
Nondestructive testing
See also specific materials and methods
applications, **1**(2), 42; **3**(3), 58
bibliographies, **1**(2), 41
development, **3**(2), 51
equipment calibration, **1**(3), 54–5
limitations, **1**(2), 42
methods, **1**(3), 54–5
techniques, **1**(2), 42
Nonferrous alloys, rare-earth applications, **3**(2), 34

O

Organic materials, radiation effects, **3**(3), 1
Osmium-thorium system, compound formation, **1**(4), 8
Oxide fuel elements, bonding and swaging with cladding, **3**(3), 52–3
Oxides, compatibility with UO_2, **3**(4), 12
properties, **3**(3), 47
radiation damage, **2**(4), 11
Oxygen-plutonium system, heats of formation of oxides, **1**(3), 19
Oxygen-thorium system, Young's modulus, **2**(3), 10
Oxygen–uranium dioxide system, structure, **1**(3), 14
Oxygen-uranium system, diffusion, **3**(4), 43
electrical properties, **2**(2), 12
emissivity, **2**(2), 12
literature review, **3**(3), 17
melting points, **2**(2), 12
structure, **2**(2), 12
Oxygen-uranium-zirconium system, constitution, **1**(3), 9
Oxygen-vanadium system, stress relaxation, **3**(2), 36
Oxygen-zirconium alloys, deformation modes, **1**(3), 38

P

Palladium, solid solubility of U in, **1**(1), 7
Palladium-uranium alloys, phase diagrams, **2**(3), 9
Perspex, gas-bubble formation, **1**(2), 17
Phosphorus (liquid), properties, **3**(3), 40
Phosphorus-bearing materials, corrosion by Na, **3**(3), 40
Plastics, radiation effects, **2**(3), 33
radiation-induced gas formation, **3**(2), 7; **3**(3), 23
Plating, nonelectrolytic chemical techniques, **2**(3), 52
Platinum, defect production, **2**(1), 40
radiation effects, **2**(2), 33; **3**(4), 37
U solubility in, **2**(2), 8
vacuum deposition, **3**(3), 54
Platinum (irradiated), annealing, **2**(1), 40; **3**(2), 26
Platinum-uranium alloys, eutectics, **2**(2), 8
intermetallic compound formation, **2**(2), 8
Platinum-uranium-zirconium alloys, corrosion in H_2O, **1**(4), 2–3
Plutonium, alloying behavior, **3**(3), 8, 10
casting, **3**(3), 14–15
cathodic vacuum etching, **3**(3), 11
coatings, **1**(3), 10
conversion from Pu nitrate, **3**(3), 14
coreduction, **1**(4), 7
corrosion, **2**(2), 9
crystal properties, **2**(3), 9
cubic expansion, **3**(3), 12
data manual, **3**(2), 4
deformation during fracturing, **2**(2), 14
density, **2**(3), 9
distortion during cooling, **3**(3), 15
elastic constants, **3**(3), 13–14
electrical resistivity, **2**(2), 8
film production, **1**(1), 10
formability, **3**(3), 14
impurity removal, **3**(3), 14
mechanical properties, **3**(3), 14
melting, **3**(3), 14–15
oxidation, **3**(3), 12
phase transformation, **2**(1), 9–10; **2**(2), 8–9; **3**(3), 11
preparation of high-purity, **3**(3), 15
production, **3**(1), 5; **3**(3), 14
pyrophoricity, **1**(3), 20
radiation effects, **3**(1), 17
research, **3**(4), 8
rolling, **3**(3), 15
structure of alpha, **1**(3), 9
tensile properties, **3**(3), 15
thermal conductivity, **2**(2), 8–9
thermal-cycling effects, **3**(3), 6
X-ray mass-absorption coefficients, **1**(3), 9
zone refining, **1**(2), 8; **2**(1), 9
Plutonium (as-cast), tensile properties, **2**(2), 8
Plutonium (delta-annealed), tensile properties, **2**(2), 8
Plutonium (electrolytic), analyses, **3**(1), 5
Plutonium (molten), density, **3**(2), 5
Plutonium alloys, corrosion, **2**(2), 9
delta-phase retention, **3**(3), 11
radiation effects, **3**(1), 17

Plutonium alloys (Continued)
research, 1(1), 9
thermal-cycling effects in Na, 3(1), 5–6
thermal expansion, 3(3), 12, 14
Plutonium carbide–silicon carbide system, oxidation resistance, 2(3), 15
Plutonium carbides
See also Plutonium monocarbide
formation, 3(3), 21
hydrolyzation, 2(1), 15
melting point, 3(3), 21
preparation, 2(1), 15
published data, 3(4), 13
Plutonium carbides (diluted), physical and chemical stabilities, 2(3), 15
Plutonium dioxide, free energy of formation, 3(3), 16
melting, 3(4), 15
microstructure, 3(1), 12
reactions with, Al_2O_3, 3(4), 15
C, 3(3), 21; 3(4), 15
MgO, 3(4), 15
Ta, 3(3), 12
ZrO_2, 3(4), 15
stability in H_2, 3(4), 15
thermal expansion, 1(3), 19; 3(2), 7; 3(3), 12, 21
Plutonium dioxide (molten), lattice parameter, 3(3), 19
Plutonium dioxide ceramics, sintering in H_2, 3(1), 11
Plutonium dioxide–thorium dioxide system, X-ray diffraction studies, 2(3), 15
Plutonium dioxide–uranium dioxide ceramics, fabrication, 1(3), 14
Plutonium dioxide–uranium dioxide mixtures, radiation effects, 1(2), 15
sintering, 3(3), 16; 3(4), 13
Plutonium dioxide–uranium dioxide pellets, radiation effects, 1(3), 17
Plutonium dioxide–uranium dioxide powder (canned), radiation effects, 3(3), 19
Plutonium dioxide–uranium dioxide system, diffraction studies, 3(3), 19
phase studies, 3(3), 19
solid solubility, 2(3), 15
Plutonium dioxide–uranium dioxide system (Zircaloy-2 canned), radiation effects, 2(3), 14
Plutonium dioxide–zirconium dioxide mixture, reactions and sintering, 3(3), 21
Plutonium disks, canning in Ni, 3(3), 15
fabrication, 3(3), 14
Plutonium fission alloys, coefficient of expansion and phase transformation, 2(3), 9
Plutonium monocarbide
See also Plutonium carbides
crystal structure, 2(1), 15
fabrication, 3(4), 15
preparation, 3(4), 15
Plutonium monocarbide–uranium monocarbide mixed fuels, fabrication, 3(3), 21
Plutonium nitrate, conversion to Pu metal, 3(3), 14
Plutonium nitride, crystal structure and density, 3(1), 5
Plutonium oxides, crystal structures, 2(1), 15
formation, 1(3), 19
preparation, 2(1), 15
solubility in acids, 2(1), 15
volatility, 3(3), 12
Plutonium oxides (diluted), chemical and physical stabilities, 2(3), 15
Plutonium-ruthenium alloys, phase diagram, 3(3), 8
Plutonium salts, microscopic study, 3(1), 12
Plutonium-silicon alloys, preparation, 1(4), 7
Plutonium slugs, canning with type 304 stainless steel, 3(4), 52
Plutonium solid-solution alloys, thermal expansion, 3(3), 12, 14
Plutonium suboxide, preparation, 3(2), 7
Plutonium-thorium alloys, constitution, 1(2), 9, 11; 1(3), 10; 2(1), 10–11
hardness, 1(1), 10; 3(3), 14
oxidation, 3(3), 14
physical properties, 1(1), 9–10
preparation, 1(4), 7
properties, 3(3), 14
radiation effects, 1(1), 10
Plutonium-titanium alloys, constitution, 1(2), 9
phase diagram, 3(3), 7–8
Plutonium-uranium alloys, constitution, 2(1), 10
development, 1(3), 10
hardness, 3(3), 14
oxidation, 3(3), 14
preparation, 1(4), 7
properties, 3(3), 14
radiation effects, 2(1), 10
Plutonium-uranium alloys (Ni-plated), radiation dimensional stability, 2(2), 9
Plutonium-zinc alloys, constitution, 1(2), 9; 1(4), 8
phase diagram, 2(4), 5
Plutonium-zirconium alloys, corrosion, 2(2), 9
fabrication, 1(2), 9
hardness, 3(3), 14
oxidation, 1(3), 34; 3(3), 14
phase diagram, 3(3), 6–8
properties, 3(3), 14
radiation effects, 3(4), 9
Poison-containing materials, neutron absorption, 3(1), 29–30
Polymethyl methacrylate, gas-bubble formation, 1(2), 17
Potassium (liquid), properties, 3(3), 40
Potassium-sodium alloys (molten), corrosion of stainless steels, 2(3), 31
reaction with H_2O, 1(1), 35
UO_2 powder slurry behavior in, 2(3), 31
Potassium uranate, preparation and properties, 2(4), 9
Powder, explosion compaction, 3(2), 49
Precious metal alloys, corrosion by Na, 3(3), 40

Precious metals
See also Metals
corrosion resistance to Li, **2**(1), 30–1
Pressure bonding
See also Diffusion and specific materials bonded
applications, **2**(3), 49
description, **2**(3), 49
development, **1**(3), 50–1; **2**(1), 46
gold contacts, **1**(1), 27; **1**(2), 41; **1**(3), 51
interface formation, **2**(3), 50
kinetics, **2**(4), 42–3
Ni-plated U with Al, **1**(1), 26
Ni-plated U with Zr, **1**(1), 26–7
solid state, **2**(4), 42–3
stainless steel–UO_2 assemblies with stainless steel, **1**(1), 27
studies, **1**(2), 40; **1**(3), 51; **2**(1), 46
technique, **3**(2), 43–4
U fuel elements, **1**(1), 26
UO_2 with Zircaloy, **1**(1), 27
U-U-Zircaloy subassemblies, **1**(1), 27
Zircaloy methods, **1**(3), 50
Pulse type inspection units, applications, **3**(4), 56

Q

Quartz, radiation effects, **1**(3), 43; **2**(2), 33

R

Radiation-detection testing
See also Nondestructive testing
techniques, **3**(1), 54
Radiation effects, colloquium, **3**(3), 1
discussion, **1**(1), 37
production by imperfections in solids, **3**(1), 36
review, **3**(1), 36
theory, **1**(1), 38–9
Radiographic testing
See also Nondestructive testing
applications, **2**(3), 53; **2**(4), 44
development, **2**(2), 56
metals, **1**(1), 30
techniques, **3**(1), 54
Rare-earth borides, structure, **3**(3), 35
Rare-earth oxide dispersions, physical properties, **1**(1), 24
roll-cladding preparation, **1**(1), 24
sinterability, **1**(1), 24
Rare-earth oxide plates, pressing and sintering, **3**(3), 35
Rare-earth oxides, coating stainless-steel tubes with, **3**(3), 35
corrosion resistance to Na, **2**(1), 32
Rare-earth oxides–stainless steel dispersions, description, **1**(4), 18
extrusion, **1**(1), 24
Rare earth–uranium–Zircaloy-2 alloys, corrosion in H_2O, **3**(1), 29
Rare earth–yttrium alloys, delta-phase stabilization, **3**(3), 7
Rare earth–Zircaloy-2 alloys, corrosion in H_2O, **3**(1), 29
Rare earths, additions to ferrous and nonferrous alloys, **3**(2), 34
reactor-control applications, **3**(2), 19
Reactor-control materials, physics, metallurgy, and engineering aspects, **3**(2), 19
Reactor coolants, corrosion by, **3**(1), 34
Reactor materials
See also Metals
bibliography of properties, **2**(2), 39–40
diffusion, **2**(3), 17; **2**(4), 33
phase diagrams, **3**(2), 24–5
radiation effects, **3**(3), 1, 23
specifications, **2**(2), 40
technology, **3**(4), 1–2
Refractory materials, fabrication, **3**(3), 51
melting, **3**(2), 41; **3**(3), 51
properties, **3**(3), 46–7
Refractory metal alloys, bibliography, **2**(3), 45
Refractory metals
See Metals (refractory)
René 41, explosion forming, **3**(2), 49
Rhenium, vacuum deposition, **3**(3), 54
Rhenium-uranium alloys, constitution, **3**(4), 8
Rhodium–rhodium sulfide system, sulfide equilibria, **3**(2), 35
Rhodium-uranium alloys, constitution, **1**(3), 8
phase diagrams, **2**(3), 9
Rods
See also Control rods and Fuel rods (Mg-clad)
coextrusion-produced defects, **2**(3), 52
Roll cladding, development and evaluation, **1**(1), 26
Roto-arc welding, Al-clad fuel elements, **1**(1), 29
Rubidium (molten), properties, **3**(3), 40
Ruthenium-uranium alloys, composition, **1**(1), 7
constitution, **1**(2), 4
liquidus, **1**(3), 8
phase diagrams, **2**(3), 9
Ruthenium-uranium-zirconium alloys, corrosion in H_2O, **1**(4), 2–3

S

Safety and health, summary, **3**(4), 1
Samarium alloys, development, **1**(1), 23
Samarium oxide, corrosion resistance to Na, **2**(1), 32
Samarium oxide–stainless steel dispersions, coextrusion with stainless-steel cladding, **2**(3), 50–1
Sapphire (synthetic), radiation-induced expansion, **2**(3), 32
Segmented fuel elements, hot pressing with Al cladding, **3**(2), 46

Semiconductors, radiation effects, **3**(3), 1, 23; **3**(4), 38
Sheet metal
See also Metals
explosion forming, **3**(1), 52–3
Shielding materials, radiation effects, **3**(3), 1
summary, **3**(4), 2
Silica, radiation effects, **2**(2), 33
Silicides, properties, **3**(3), 47
Silicon, diffusion in metals, **3**(2), 36
Silicon carbide, corrosion resistance, **2**(1), 32
vapor deposition, **1**(3), 52–3
Silicon crystals, radiation-induced defects, **3**(3), 41
Silicon dioxide–thorium dioxide system, dissociation, **1**(2), 16
solid-state reaction study, **2**(4), 9
Silicon dioxide–uranium dioxide mixtures, radiation effects, **1**(2), 15
Silicon nitride, corrosion resistance, **2**(1), 32
Silicon-thorium alloys, corrosion in H_2O, **2**(3), 10
Silicon-uranium alloy rods, coextrusion with Cu cladding, **3**(2), 45
Silicon-uranium alloy tubes, coextrusion with Zircaloy cladding, **3**(2), 45
Silicon-uranium alloys, C content effects, **2**(1), 7
coextrusion with cladding, **2**(3), 51
corrosion, **1**(1), 6; **1**(3), 6; **2**(1), 7; **2**(2), 6; **3**(4), 7
development for power-reactor use, **3**(1), 4
electrical resistivity, **2**(1), 7
extrusion, **1**(3), 7
physical properties, **1**(3), 6; **2**(1), 7
processing, **1**(3), 6
radiation effects, **1**(1), 3, 6; **1**(2), 6; **2**(2), 6; **3**(1), 4; **3**(4), 5, 7
radiation stability, **2**(2), 6
strength, **1**(1), 5
Silicon-uranium alloys (irradiated), corrosion in H_2O, **2**(3), 6
Silicon-uranium alloys (Zircaloy-2-clad), corrosion in H_2O, **1**(3), 6
radiation dimensional stability, **2**(2), 6
Silicon-uranium alloys (Zircaloy-2-clad) (irradiated), corrosion in H_2O, **2**(3), 6; **3**(1), 4
Silicon-uranium-zirconium alloys, thermal stability, **1**(2), 16
Silver, diffusion of Fe in, **3**(2), 36
radiation effects on electrical resistivity, **2**(2), 33; **3**(3), 42; **3**(4), 37
reaction with H_2O, **2**(1), 33
reactor-control applications, **3**(2), 19
vacuum deposition, **3**(3), 54
Silver (irradiated), annealing kinetics, **3**(2), 26
Silver alloys, tensile properties, **1**(3), 30
Silver-zinc alloys, plastic deformation effects on diffusion, **3**(2), 36
Sodium, corrosion by, **2**(4), 22; **3**(1), 35
O_2 determination, **2**(1), 32–3
properties, **3**(3), 40
specific heat, **3**(2), 15
Sodium chloride, radiation effects, **3**(4), 39–40
Sodium hydroxide, corrosion of Ni, **1**(1), 34
Sodium uranate, preparation and properties, **2**(4), 9
Sodium-uranium-oxygen system, radiation effects, **3**(3), 21
Solids
See also Materials and Metals
radiation-damage studies, **2**(4), 10
radiation effects, **2**(2), 32; **2**(3), 45–6; **3**(4), 40
small-angle X-ray scattering studies, **3**(2), 25–6
Stainless steel
See also Chromium-iron-nickel alloys and Inconel
Co content control, **2**(3), 39
compatibility with B compounds, **3**(2), 19
compatibility with Mo-Pu-U alloys, **3**(3), 14
corrosion, **1**(2), 31; **1**(3), 34, 37; **1**(4), 22; **2**(1), 28; **2**(3), 29; **3**(1), 33; **3**(3), 38–9
creep-rupture strength, **3**(3), 45
diffusion with Nb, **3**(4), 44
fabricability, **3**(3), 45–6
pressure bonding to stainless steel–UO_2 assemblies, **1**(1), 27
radiation effects, **2**(1), 43; **3**(1), 37, 39
reaction with Mo-Pu-U alloys, **3**(3), 12
reaction with Th-U alloy, **2**(3), 10
specifications, **2**(2), 40
stress-corrosion cracking, **1**(3), 34; **1**(4), 22; **2**(1), 28; **3**(1), 33
tensile properties, **3**(3), 45–6
welding to Mo, **1**(3), 54
Stainless steel (17-7 PH), bonding with thermite type compositions, **3**(1), 51
Stainless steel (18-8–B^{10}), radiation effects, **2**(4), 26–7
Stainless steel (type 304), compatibility with UC, **3**(4), 13
corrosion, **1**(2), 29; **2**(3), 31; **2**(4), 21; **3**(1), 33–5; **3**(2), 23
creep properties, **3**(4), 42
diffusion, **2**(3), 17
ductility, **3**(2), 2
gaseous environment effects on properties, **3**(1), 45
radiation effects, **2**(3), 33; **3**(3), 43
stress-corrosion cracking, **2**(4), 21
tube burst testing, **2**(3), 43, 45; **3**(4), 42
tube creep buckling, **2**(3), 43
vapor deposition of Mo and Nb on, **1**(3), 53
welding, **2**(3), 39, 43
Stainless steel (type 304L), tensile properties, **2**(3), 39
Stainless steel (type 310), nitriding and oxidation, **1**(3), 34
Stainless steel (type 316), corrosion, **2**(3), 31; **2**(4), 22; **3**(1), 35; **3**(4), 35
diffusion with graphite, **1**(3), 24
nitriding, **1**(3), 34
oxidation, **1**(3), 34; **2**(2), 29
radiation effects on corrosion by Li, **2**(4), 22
welding, **2**(3), 39, 43

Stainless steel (type 318), oxidation, **2**(4), 23
Stainless steel (type 347), compatibility with fissium-Pu-U alloys, **3**(4), 8–9
corrosion, **1**(2), 29; **2**(3), 29
mechanical properties of nitrided, **2**(1), 38–9
strain-fatigue testing, **1**(2), 36
stress-corrosion cracking, **2**(3), 29
thermal fatigue properties, **3**(3), 45
Stainless steel (type 347) (irradiated), damage recovery, **3**(4), 41
Stainless steel (type 410), corrosion, **2**(3), 29; **2**(4), 21; **3**(1), 35; **3**(2), 23; **3**(3), 38; **3**(4), 34
radiation effects, **1**(1), 39; **1**(2), 34; **2**(2), 35–6
stress-corrosion cracking, **2**(3), 29; **2**(4), 21; **3**(3), 38
Stainless steel (type 410) (Cr-plated), stress corrosion, **3**(2), 23
Stainless steel (type 414), radiation effects, **2**(2), 35–6
Stainless steel (type 420), coating with ceramics, **2**(1), 50
Stainless steel (type 430), compatibility with fissium-Pu-U alloys, **3**(4), 8–9
stress-corrosion cracking, **2**(3), 29
Stainless steel (type 430T), aging temperature effects, **3**(4), 42
Stainless steel (type 446), Mo vapor deposition, **1**(3), 53
oxidation, **3**(2), 34
Stainless steel (type 4340), explosion welding, **3**(4), 55
Stainless steel (Alloy A286), nitriding and oxidation, **1**(3), 34
Stainless steel (AM-350), radiation effects, **2**(2), 35–6
Stainless steel (austenitic), brazing, **3**(4), 55
corrosion resistance to Li, **2**(1), 30–1
mechanical, **2**(4), 36–7; **3**(1), 45
physical properties, **2**(4), 36–7; **3**(1), 45
Y addition effects, **3**(2), 34
Stainless steel (Carpenter-20 Cb), nitriding and oxidation, **1**(3), 34
Stainless steel (ferritic), corrosion resistance to Li, **2**(1), 30–1
Stainless steel (martensitic), mechanical and physical properties, **2**(4), 36–7; **3**(1), 45
Stainless steel (molten), reaction with H_2O, **1**(1), 35
Stainless steel (semiaustenitic), mechanical and physical properties, **2**(4), 36–7; **3**(1), 45
Stainless-steel (type 316) powder, sintering, slip casting, and testing, **2**(3), 49
Stainless-steel tubing, bonded joints, **3**(3), 54
coating with rare-earth oxides, **3**(3), 35
injection casting in canning, **2**(3), 52
Nb vapor deposition, **1**(1), 28
Ni-P brazing alloy effects on ductility, **3**(2), 31
Stainless-steel (type 304) tubing, yield strength, **3**(2), 30–1
Stainless-steel (type 316) tubing, yield strength, **3**(2), 30–1
Stainless-steel (type 347) tubing, yield strength, **3**(2), 30–1
Stainless steel–uranium carbide dispersions, hot-cell evaluation, **2**(2), 11
physical properties, **1**(1), 15
radiation effects, **2**(3), 12–13
Stainless steel–uranium carbide dispersions (type 347 stainless-steel-clad), tensile properties, **1**(3), 13
Stainless steel (type 304)–uranium (molten) diffusion couples, interaction, **2**(4), 33
Stainless steel–uranium dioxide assemblies, annealing and pressure bonding with stainless steel, **1**(1), 27
Stainless steel–uranium dioxide cermets, electrical resistivity, **1**(3), 13
pressure bonding, **3**(4), 50
tensile strength, **1**(3), 13
Stainless steel–uranium dioxide dispersions, development, **2**(2), 11; **3**(4), 11
fabrication, **1**(1), 14; **1**(3), 14; **2**(2), 11; **2**(3), 11–14
mechanical properties, **2**(2), 11; **3**(1), 8; **3**(4), 10
physical properties, **1**(1), 14; **2**(2), 11
production, **1**(3), 13
properties, **1**(3), 14
radiation effects, **1**(1), 14–15; **1**(4), 9; **2**(1), 12
slip casting, **1**(4), 9
U variation determination, **1**(4), 8
Stainless steel (type 347)–uranium dioxide dispersions, explosion compaction, **3**(2), 51
radiation effects, **3**(4), 11
Stainless steel (ferritic)–uranium dioxide dispersions, operating temperature, **2**(1), 12
Stainless steel–uranium dioxide dispersions (stainless-steel-clad), preparation, **1**(2), 11–12
radiation effects, **2**(3), 12
slip casting, **3**(2), 5
tensile properties of annealed, **3**(2), 5
Stainless steel (type 304B)–uranium dioxide dispersions (type 304 stainless-steel-clad), development, **1**(3), 12–13
Stainless steel–uranium dioxide–zirconium boride dispersions, B sintering losses, **3**(2), 19, 21
Stainless steel–uranium nitride dispersions, chemical reactions, **1**(4), 9
fabrication, **2**(2), 11
hot-cell evaluation, **2**(2), 11
mechanical properties, **2**(2), 11
physical properties, **1**(1), 15; **2**(2), 11
radiation effects, **2**(3), 12–13
Stainless steel–uranium nitride dispersions (stainless-steel-clad), fabrication and properties, **3**(1), 8
Stainless steel–uranium nitride dispersions (type 347 stainless-steel-clad), tensile properties, **1**(3), 13
Stainless steel–uranium oxide dispersions, batch blending, **1**(4), 8–9

Stainless steel (type 304)–Zircaloy-2 couples, fretting corrosion, **2**(3), 28; **3**(2), 22
Stainless steel (austenitic)–Zircaloy-2 joints, brazing with Ag, **2**(1), 50
Stainless steel–zirconium boride dispersions, preparation and properties, **2**(3), 26–7
Stainless steel–zirconium joints, welding and brazing, **2**(3), 53
Steel
See also Croloys
chromizing effects on oxidation, **3**(3), 39
corrosion, **1**(4), 25; **3**(4), 32
explosion forming, **3**(3), 56–7
grain-size effects, **2**(1), 42–3
Na containment, **1**(4), 24
radiation effects, **1**(2), 35; **3**(1), 37, 40; **3**(2), 28
Steel (ASTM A201), radiation effects, **1**(1), 39
Steel (ASTM A302B), radiation effects, **1**(1), 39
Steel (AISI 310), corrosion, **3**(4), 32
Steel (AISI 1020), corrosion in polyphenyl, **3**(2), 23
explosion forming, **3**(3), 56–7
Steel (type 1020 carbon), corrosion in organic coolant, **3**(1), 35
Steel (AI 3301), corrosion in liquid Na, **3**(1), 34
Steel (AISI 4130), corrosion, **3**(1), 35; **3**(2), 23
explosion forming, **3**(3), 56–8
Steel (austenitic), radiation effects, **2**(3), 33
Steel (boron), neutron absorption, **3**(1), 30
Steel (carbon), corrosion in CO_2, **3**(3), 39
H absorption, **3**(4), 32
radiation effects, **2**(1), 43
Steel (construction), radiation effects, **1**(3), 43–4
Steel (Cr-Mo), corrosion in molten Bi-U alloys, **2**(2), 31
Steel (Ducol W.30), radiation effects, **2**(1), 42
Steel (En 2), radiation effects, **1**(4), 37
Steel (ferritic), corrosion, **2**(2), 31; **3**(4), 34
radiation effects, **2**(3), 33; **3**(1), 37–39, 41
Steel (high C), corrosion in molten Bi-U alloys, **3**(4), 34
Steel (high Cr), corrosion in molten Bi-U alloys, **3**(4), 34
Steel (HY-65), radiation effects, **2**(1), 42
Steel (low alloy), corrosion, **2**(1), 30–1; **3**(3), 39
Steel (low C), corrosion in molten Bi-U alloys, **3**(4), 34
radiation effects, **3**(1), 39
Steel (low Cr), corrosion in molten Bi-U alloys, **3**(4), 34
Steel (MBMC No. 1), explosion forming, **3**(3), 56–7
Steel (mild), compatibility with UC, **3**(4), 13
radiation effects, **1**(2), 35; **1**(4), 36–7; **2**(4), 25
Steel (Vascojet 1000), explosion forming, **3**(3), 56–7
Steel tubing, extrusion with Al cladding, **3**(3), 54
Strontium boride, compatibility with stainless steel, **3**(2), 19
Strontium uranate, preparation and properties, **2**(4), 9
Structural materials
See also Metals
corrosion in polyphenyl type coolant, **3**(1), 35
radiation effects, **3**(3), 1
summary, **3**(4), 2
Subassemblies, nondestructive testing, **2**(1), 51; **3**(2), 51
Sulfides, properties, **3**(3), 47
Sulfur, explosion compaction, **3**(2), 49
Sulfur (molten), properties, **3**(3), 40
Surfaces, diffusion, **2**(4), 33
explosion hardening, **3**(2), 49
Swaging, by explosion, **3**(1), 52

T

Tantalum, compatibility with Pu-U-fissium alloys, **3**(4), 8–9
corrosion, **1**(2), 29–30; **2**(4), 22; **3**(2), 24
creep properties of degassed sintered, **2**(1), 39
diffusion with, B, **2**(2), 37
C, **2**(2), 37
Si, **3**(2), 36
dissolution in molten Dy and Tm, **3**(1), 39, 41
ductile-brittle transition, **2**(4), 37
electrical resistivity, **2**(4), 31–2
electroplated coatings, **3**(4), 53
hardening, **2**(2), 30
mechanical properties, **2**(4), 31; **3**(1), 45
oxidation, **1**(4), 23; **2**(2), 30; **3**(4), 34
physical properties, **2**(4), 31; **3**(1), 45
Seebeck coefficient, **2**(4), 31, 33
thermal conductivity, **2**(4), 31, 33
thermal diffusivity, **2**(4), 31, 33
vapor-deposited coatings, **1**(2), 41
Tantalum (rare-earth oxide coated), high-temperature stability, **2**(4), 21–2
Tantalum (ZrO_2-coated), high-temperature stability, **2**(4), 21
Tantalum alloys, electroplated coatings, **3**(4), 53
oxidation, **3**(4), 34
Tantalum boride, properties, **3**(4), 34
Tantalum carbide, properties, **3**(4), 34
vapor-deposited coating on graphite, **1**(1), 28
Tantalum nitride, properties, **3**(4), 34
Tantalum oxide, properties, **3**(4), 34
Tantalum systems, corrosion, **2**(4), 22
Tantalum-thorium alloys, constitution, **2**(2), 10
eutectic, **2**(4), 6
Tantalum-tin-zirconium alloys, aging studies, **1**(3), 38
tensile properties, **1**(3), 38
Tantalum–uranium dioxide dispersion foils, fabrication, **2**(3), 11
Tantalum-uranium-zirconium alloys, corrosion in H_2O, **1**(2), 3–4
Tantalum-vanadium alloys, constitution, **2**(4), 31–2
Tantalum-zirconium alloys, constitution, **2**(2), 37; **2**(4), 31
radiation effects, **3**(1), 37, 39

Television, development of X-ray-sensitive Vidicon, **2**(2), 56
Thallium nitride, corrosion resistance, **2**(1), 32
Thallium-thorium intermetallic compounds, crystal structure, **2**(3), 10
Thermal-shock experiments, equipment, **3**(3), 40
Thermographic testing
See also Nondestructive testing
core-to-cladding bonds, **3**(3), 59
Thorium, anisotropy, **2**(3), 10
C solubility in, **3**(4), 9–10
chemical properties, **2**(4), 5–6
cladding, **1**(1), 10; **2**(2), 9
corrosion, **1**(2), 10; **1**(3), 3, 37; **1**(4), 8; **2**(2), 9; **2**(3), 10; **2**(4), 7; **3**(4), 10
data manual, **2**(3), 9–10; **2**(4), 5–6
decontamination, **1**(2), 10
diffusion, **1**(2), 10; **1**(3), 11–12
ductility, **2**(4), 6
dynamic modulus, **3**(4), 10
elastic constants, **2**(3), 10
entropy of sublimation, **3**(1), 7
fabrication, **2**(2), 9
H_2 diffusivity in, **3**(4), 9
H_2 solubility in, **1**(2), 11; **1**(3), 11; **2**(2), 10
heat of sublimation, **3**(1), 7
inclusions, **1**(2), 10; **2**(2), 9
lattice spacing, **3**(3), 16
mechanical properties, **2**(2), 9; **2**(4), 5–6; **3**(2), 4–5; **3**(3), 17
metallography, **2**(2), 9, 10
physical properties, **1**(2), 10; **2**(2), 9; **2**(4), 5–6
production technology, **2**(2), 9
pyrophoricity, **1**(3), 20
radiation effects, **1**(2), 11; **2**(2), 9; **2**(4), 5–6; **3**(4), 10
reactions with O_2 and ThO_2, **3**(1), 7
recrystallization, **2**(2), 9
solubility in Hg, **2**(2), 10
solubility in molten Zn, **3**(4), 9
specific heat, **3**(2), 15
strength, **2**(4), 6
technology, **2**(1), 11; **2**(2), 9
thermal-cycling properties, **2**(4), 5–6
vapor pressure, **3**(1), 7
Thorium (cold-reduced), preferred orientations, **3**(2), 5
Thorium (crystal-bar), electrical resistivity, **3**(3), 16
magnetic susceptibility, **2**(4), 6
specific heat, **3**(1), 7; **3**(3), 16
Thorium (iodide), grain-boundary relaxation, **1**(3), 11
shear modulus, **1**(3), 11
Thorium (irradiated), mechanical properties, **3**(3), 17
tensile properties, **2**(4), 7
Thorium (sintered), C, N_2, and O_2 effects on properties, **3**(4), 9
Thorium (Zircaloy-clad), corrosion in H_2O, **3**(4), 10
Thorium alloys, constitution, **2**(1), 11; **2**(2), 9
corrosion, **2**(2), 9; **2**(4), 6–7; **3**(4), 10
fabrication-technique effects, **2**(4), 6
heat-treating effects, **2**(4), 6
mechanical properties, **2**(2), 9
metallography, **2**(2), 10
oxidation, **1**(3), 12
precipitation hardening, **3**(1), 8
radiation effects, **1**(3), 12
technology, **2**(2), 9
Thorium beryllide, solubility studies, **2**(2), 10
Thorium carbide, fabrication, **2**(1), 14
published data, **3**(4), 13
Thorium carbide–uranium carbide mixtures, fabrication, **2**(1), 14
Thorium carbide–uranium carbide powder, coating with C, **3**(4), 53
Thorium compacts, preparation from Th powder, **2**(2), 10
properties, **2**(4), 6
Thorium dioxide, compressive strength, **3**(1), 10
corrosion, **2**(1), 32; **3**(1), 10
density, **1**(2), 16
elastic modulus, **3**(1), 10
radiation effects, **3**(4), 16
sintering, **2**(3), 15–16
structure, **3**(2), 7
surface chemistry, **3**(2), 7
thermal-shock resistance, **1**(2), 16; **2**(3), 16
Thorium dioxide ceramics, metal fiber reinforcement, **1**(1), 13
properties, **2**(2), 14
thermal-stress failure, **1**(1), 13
Thorium dioxide cermets, fabrication, **1**(1), 13
Thorium dioxide films, radiation effects, **3**(3), 22
Thorium dioxide–urania ceramics, fabrication and volatilization, **1**(1), 13
Thorium dioxide–uranium dioxide ceramic pellets, fabrication, **3**(1), 11
Thorium dioxide–uranium dioxide compacts, radiation effects, **1**(3), 17
Thorium dioxide–uranium dioxide mixtures, physical properties, **1**(2), 14
Thorium dioxide–uranium dioxide pellets, radiation effects, **1**(3), 16–17; **1**(4), 11
Thorium dioxide–uranium dioxide system, compressive strength, **3**(1), 10–11
corrosion in steam, **3**(1), 10–11
elastic modulus, **3**(1), 10–11
fission-gas release, **3**(2), 7
thermal expansion, **3**(1), 10–11
Thorium dioxide–uranium dioxide–yttrium oxide system, compressive strength, **3**(1), 10–11
corrosion in steam, **3**(1), 10–11
elastic modulus, **3**(1), 10–11
thermal expansion, **3**(1), 10–11
Thorium dioxide–zirconium dioxide system, physical properties, **1**(2), 16
Thorium monocarbide, reactions, **2**(2), 10

Thorium monocarbide ceramic fuels, properties, **2**(2), 14
Thorium monocarbide–zirconium monocarbide system, constitution, **2**(2), 10
Thorium-tin alloys, solubility studies, **2**(2), 10
Thorium-tin intermetallic compounds, crystal structure, **2**(3), 10
Thorium-uranium alloys, alloying effects, **3**(3), 16
annealing effects on hardness, **2**(1), 11
coextrusion with cladding, **2**(3), 51
constitution, **1**(3), 11; **2**(1), 11
corrosion in Na, NaK, and organics, **1**(4), 8
creep, **1**(4), 8; **3**(1), 18
creep strength, **3**(1), 7
density, **2**(4), 6
electrical resistivity, **1**(3), 11
fabrication effects, **3**(3), 16–17
fission-gas release, **2**(3), 10–11
grain-growth restriction, **2**(4), 6
hardness, **1**(1), 10; **2**(1), 11; **2**(4), 6
heat-treatment effects, **3**(3), 16
hot hardness, **2**(4), 6
mechanical properties, **3**(3), 16–17
metallurgy, **2**(4), 6
physical properties, **1**(3), 11; **3**(3), 16–17
radiation effects, **1**(1), 10; **1**(2), 11; **1**(3), 12; **1**(4), 8; **2**(1), 12; **2**(2), 10–11; **3**(1), 2–3, 8; **3**(4), 5
reaction with stainless steel, **2**(3), 10
segregation, **2**(2), 47
tensile properties, **1**(3), 11
thermal conductivities, **1**(3), 11
thermal-expansion coefficients, **2**(3), 10
U particle coarsening, **2**(4), 6
Thorium-uranium alloys (irradiated), thermal-expansion coefficients, **2**(3), 10
Thorium–uranium monocarbide–zirconium system, constitution, **2**(2), 10
Thorium-uranium-zirconium alloys, constitution, **2**(1), 11; **2**(2), 10
corrosion in H_2O, **2**(3), 10; **2**(4), 6, 7
Th detection, **2**(4), 6
Thorium-yttrium alloys, constitution, **1**(3), 11; **2**(2), 10; **3**(1), 5, 7
eutectic, **2**(4), 6
solidus, **2**(2), 10
Thorium-zinc alloys, constitution, **2**(4), 6
Thorium-zirconium alloys, corrosion in H_2O, **2**(3), 10; **2**(4), 7; **3**(1), 8; **3**(4), 10
cubic-phase stability, **3**(3), 16
hot hardness, **2**(4), 6
metallography, **2**(4), 6
miscibility gap, **3**(3), 16
Thorium-zirconium alloys (Zircaloy-clad), corrosion in H_2O, **3**(4), 10
Through-transmission testing
See also Nondestructive testing
applications, **3**(4), 56
plates and tubes, **3**(3), 58
Tin, reaction with H_2O, **2**(1), 33
solubility in $ZrFe_2$, **2**(3), 33
Tin-zirconium alloys, oxidation, **1**(3), 34
Titanium, compatibility with fissium-Pu-U alloys, **3**(4), 8–9
diffusion, **2**(3), 17
diffusion with, B, **2**(2), 37
C, **2**(2), 37
Si, **3**(2), 36
U, **2**(2), 38
electroplated coatings, **3**(4), 53
forging, **2**(4), 41
joining to Ag-Cd-In alloys, **1**(3), 31
lattice stability, **3**(2), 35
oxidation, **2**(3), 28; **3**(4), 34
radiation effects, **3**(1), 37
spontaneous ignition in O_2, **2**(3), 28
Titanium (B-120VCA), explosion welding, **3**(4), 55
Titanium (irradiated), damage recovery, **3**(4), 41
Titanium alloys, electroplated coatings, **3**(4), 53
explosion forming, **3**(2), 49
lattice stability, **3**(2), 35
oxidation, **3**(4), 34
radiation effects, **2**(2), 33–4
Titanium borides, corrosion in H_2O, **1**(2), 26
properties, **3**(4), 34
solubility in H_2O, **1**(3), 32
Titanium carbide, corrosion resistance, **1**(3), 37; **2**(1), 32
melting effects, **3**(2), 41
properties, **3**(4), 34
Titanium carbide cermets, corrosion resistance to NaK, **1**(3), 37
Titanium dispersions, roll cladding with Hf, Ti, and Zircaloy-2, **2**(2), 48
Titanium nitride, properties, **3**(4), 34
Titanium oxide, properties, **3**(4), 34
Titanium–titanium diboride dispersions (Zircaloy-2-clad), radiation effects, **3**(2), 19
Titanium-uranium alloys, corrosion, **1**(1), 3–4
diffusion, **3**(3), 44; **3**(4), 43
Titanium-uranium alloys, corrosion in H_2O, **2**(3), 2–3
diffusion, **3**(3), 4
phase diagrams, **2**(3), 3
quenching-induced decomposition, **2**(4), 3
transformation, **2**(3), 2
Titanium-uranium-zirconium alloys, constitution, **1**(2), 6
corrosion in H_2O, **1**(4), 2–3; **2**(3), 3
phase diagrams, **2**(3), 3
Titanium-uranium-zirconium diffusion couples, bonding effects on interaction, **2**(4), 33–4
Titanium-vanadium alloys, oxidation resistance, **1**(3), 35
Titanium-yttrium alloys, eutectic, **3**(1), 42
Titanium-zirconium alloys, lattice stability, **3**(2), 35
Transition metals
See also Metals
radiation effects, **3**(4), 38

Tubing
See also specific tubing
coextrusion-produced defects, **2**(3), 52
development, **1**(3), 1
radiation effects, **1**(3), 1
Tungsten, creep-rupture properties, **3**(3), 46
diffusion of B and C in, **2**(2), 37
ductile-brittle transition, **2**(4), 37
ductility, **3**(4), 49
electroplated coatings, **3**(1), 51; **3**(4), 53
extrusion, **3**(4), 48–9
oxidation, **3**(4), 33–4
radiation effects, **1**(4), 37
self-bonding by roll cladding, **3**(4), 49
tensile properties, **3**(2), 31; **3**(4), 49
vacuum arc melting, **3**(4), 48–9
vapor-deposited coatings, **1**(2), 41
Tungsten (irradiated), annealing, **2**(1), 40
damage recovery, **3**(4), 37–8
electrical resistivity of annealed, **2**(1), 40
stored energy of annealed, **2**(1), 40
Tungsten alloys, electroplated coatings, **3**(4), 53
oxidation, **3**(4), 34
Tungsten binary alloys, oxidation resistance, **1**(3), 35
Tungsten boride, properties, **3**(4), 34
Tungsten carbide, corrosion resistance to NaK, **1**(3), 37
electroplating with Ni, **3**(2), 47
properties, **3**(4), 34
Tungsten carbide cermets, corrosion resistance to NaK, **1**(3), 37
Tungsten nitride, properties, **3**(4), 34
Tungsten oxide, properties, **3**(4), 34
Tungsten powder, explosion compaction, **3**(2), 51
Tungsten–tungsten sulfide system, sulfide equilibria, **3**(2), 35
Tungsten–uranium dioxide dispersion foils, fabrication, **2**(3), 11

U

Ultrasonic testing
See also Nondestructive testing
applications, **1**(1), 30; **1**(2), 42; **2**(3), 53; **2**(4), 44
calibration, **1**(2), 42
development, **1**(1), 30; **1**(2), 42; **1**(4), 43; **2**(1), 51; **2**(2), 56
energy losses in metals, **2**(3), 53–4
fluoroscope development, **2**(2), 56
plates, **3**(3), 58–9
techniques, **3**(1), 54
tubing, **3**(3), 58; **3**(4), 56
Ultrasonic welding
See also Welding
development, **1**(3), 54
Uranium, anodic treatment, **3**(2), 47
bulk modulus, **2**(2), 1
burnup determination, **2**(1), 4
canning, **3**(2), 46
casting, **1**(1), 25; **1**(2), 39; **1**(3), 47, 54; **2**(2), 47, 54; **3**(1), 48
chemistry, **2**(4), 2
cladding, **2**(1), 4
bonding with, **1**(2), 40; **3**(3), 54
coextrusion with, **2**(2), 51; **2**(3), 51; **3**(2), 45; **3**(4), 51
extrusion, **2**(2), 40; **3**(1), 50–1
coatings, **1**(1), 29; **2**(2), 5; **3**(1), 51; **3**(3), 55; **3**(4), 53
corrosion, **1**(3), 3; **1**(4), 2–3; **2**(1), 4; **2**(3), 17; **3**(3), 21–2
corrosion in, H_2O, **1**(1), 34; **1**(4), 11–12; **2**(1), 15; **2**(3), 1; **3**(4), 4
Na, **1**(3), 37
organics, **1**(3), 37
steam, **1**(4), 11–12; **2**(4), 2
creep, **1**(1), 1; **2**(2), 16; **2**(3), 19; **3**(2), 3; **3**(4), 3
crucible mold coating, **2**(3), 48
crystal growth, **2**(2), 1
data manual, **3**(2), 3
deformation, **2**(2), 14; **2**(4), 1–2; **3**(3), 2; **3**(4), 3
density, **1**(1), 1–3
determination, **2**(3), 54
diffusion, **1**(1), 37; **2**(2), 1, 16, 38; **2**(3), 1–2, 17; **2**(4), 2; **3**(1), 3, 13–14; **3**(2), 1; **3**(3), 1; **3**(4), 13
diffusion bonding, **2**(1), 46; **3**(4), 51
diffusion welding, **3**(4), 50
grain-size effects, **3**(1), 2
elastic moduli, **2**(4), 2
elastic parameters, **2**(2), 1–2
electric conductivity, **1**(1), 1–2
electronic microdiffraction, **3**(1), 2
electroplating on, **3**(2), 47
elongation, **1**(1), 1
enamel coating, **1**(1), 29
end-quench tests, **2**(2), 1
expansion, **2**(2), 1–2
extrusion, **1**(1), 26; **2**(2), 48
fabrication, **2**(1), 4; **2**(3), 1, 48; **3**(1), 48
forging, **1**(1), 26
forming, **2**(2), 47
grain size, **1**(1), 1–3; **1**(2), 1–2; **2**(3), 1, 48; **2**(4), 2; **3**(4), 4, 48
growth in corrosive gas, **3**(4), 16
H_2, content of dingot, **1**(2), 39
effects, **1**(1), 1; **2**(2), 47; **3**(3), 21–2
reduction, **2**(4), 41
solubility, **2**(4), 2
vacuum outgassing, **2**(3), 48
heat-treatment, **1**(2), 1; **1**(4), 1; **2**(3), 1, 18; **3**(4), 3
heating history determination, **3**(2), 42
ignition, **1**(3), 20; **2**(4), 9; **3**(1), 17
impurities, **1**(4), 39; **2**(3), 48
lattice constants, **1**(1), 1–3, 6
literature, **3**(2), 3
melting, **1**(1), 25; **1**(2), 39; **3**(1), 48; **3**(2), 39
metallography, **2**(1), 3–4
metallurgy, **2**(1), 4; **2**(2), 1; **2**(4), 2; **3**(3), 3

Uranium (Continued)
micrography, **3**(1), 2
nonelectrolytic chemical plating, **3**(4), 52
oxidation, **1**(1), 34–5; **1**(2), 16; **2**(1), 15; **3**(2), 1; **3**(3), 2
pin-cushion irradiation, **2**(1), 3–4
plating, **3**(2), 47; **3**(4), 52
preferred orientation, **2**(4), 1; **3**(4), 3–4
production, **2**(1), 4; **3**(1), 2
properties, **3**(3), 1
fatigue, **3**(2), 3
mechanical, **2**(1), 4; **3**(2), 4–5; **3**(3), 3
physical, **2**(1), 4
tensile, **1**(1), 1; **3**(1), 2
pyrophoricity, **1**(3), 20
quenching media, **3**(2), 42
radiation effects, **1**(1), 37; **1**(2), 2–3; **2**(3), 18; **2**(4), 10; **3**(1), 2–3, 17–18; **3**(2), 3; **3**(4), 3–4
radiation effects on, chemical properties, **2**(2), 3, 5
creep strength, **2**(4), 10
density, **3**(1), 2–3, 19
dimensions, **2**(1), 1, 3–4, 16; **2**(2), 16; **2**(4), 1; **3**(1), 2–3
gas diffusion, **2**(2), 15
hardness, **3**(1), 18–19
mechanical properties, **1**(4), 1; **2**(2), 3, 5; **2**(4), 10
physical properties, **2**(1), 2–3; **2**(2), 3, 5
surfaces, **2**(1), 3–4
tensile properties, **1**(4), 1; **3**(1), 18
radiation-induced, cracking, **3**(2), 2, 7
displacement spikes, **3**(1), 17
Frenkel pairs, **3**(1), 17
gas-bubble formation, **1**(2), 17; **2**(1), 17; **3**(1), 18
lattice defects, **3**(1), 18
microstress recovery, **3**(1), 18–19
swelling, **2**(1), 16; **2**(2), 15; **2**(3), 18; **2**(4), 10; **3**(1), 17; **3**(2), 2; **3**(3), 23; **3**(4), 15–16
twinning, **2**(3), 18–19
radiographic testing, **1**(1), 30
reactions with, air, **3**(1), 17
alkanes, **3**(2), 6
CO_2, **1**(4), 12; **3**(1), 17
H_2O, **2**(1), 33; **3**(2), 8–9; **3**(4), 37
H_2O vapor, **3**(2), 8–9
N_2, **1**(2), 16
O_2, **3**(1), 16–17
steam, **1**(1), 35; **1**(2), 3
recrystallization, **2**(4), 1
reduction of area, **1**(1), 1
rolling, **2**(2), 48; **3**(3), 51
scrap recovery, **2**(1), 45
self-diffusion, **1**(1), 37; **2**(2), 1; **2**(3), 1–2; **3**(1), 3, 13–14; **3**(2), 1; **3**(3), 1
shot preparation, **1**(1), 25
soldering, **1**(4), 42
solubility in, Pd, **1**(1), 7
Pt, **2**(2), 8
UAl_3, **3**(1), 15
Zn, **2**(2), 8
specific heat, **3**(2), 15
stability, **1**(3), 1
strain-rate sensitivity, **3**(1), 1–2
stress relaxation, **2**(4), 10
stress-strain curves, **1**(1), 1
structure, **2**(4), 2
technology, **2**(2), 1, 3; **3**(1), 2
tensile properties, **1**(1), 1
thermal conductivity, **1**(1), 1
thermal cycling, **1**(3), 2, 38; **2**(2), 3, 5, 16; **2**(4), 10; **3**(2), 3; **3**(3), 2–3
thermal expansion, **3**(2), 3
transformations, **1**(1), 1, 3; **1**(2), 1; **3**(2), 41–2; **3**(4), 3–4
tube fabrication, **2**(3), 48
twinning, **2**(4), 1–2
ultrasonic soldering, **1**(4), 42
vacuum deposition, **3**(3), 54
vacuum melting, **1**(2), 39; **3**(2), 39
vacuum outgassing of H_2, **2**(3), 48
volumes, **1**(1), 1–3
welding, **1**(2), 41; **1**(4), 42; **3**(4), 50
yield strength, **1**(1), 1
Young's modulus, **1**(1), 1
Uranium (depleted), nonnuclear uses, **3**(3), 1
radiation effects, **1**(3), 1–2
Uranium (irradiated), annealing, **1**(1), 3–4; **1**(3), 2; **2**(2), 1, 3; **2**(3), 2, 19; **2**(4), 10; **3**(1), 18–19; **3**(3), 1–2
creep testing, **2**(2), 1; **2**(3), 19
damage recovery, **3**(1), 18
dimensional instability, **2**(3), 18
electropolishing, **2**(3), 18
filamentary growth, **2**(2), 16
fracture surfaces, **3**(3), 23
gases, bubble formation, **1**(4), 2
mobility, **2**(3), 18; **3**(2), 7
release, **2**(3), 18; **3**(3), 2; **3**(4), 4
voids, **2**(3), 18
hardness, **2**(3), 19
inclusions, **3**(2), 3
metallography, **2**(1), 3; **2**(3), 18
preferred orientation, **2**(3), 18
quench cracking, **3**(2), 2
swelling, **1**(4), 2; **2**(1), 17
tensile properties, **2**(1), 1–2; **2**(3), 19; **3**(4), 4
thermal conductivity, **3**(2), 2
thermal-cycling effects, **3**(4), 4
twinning, **2**(4), 10
Xe^{133} diffusion, **1**(4), 2; **2**(1), 17
X-ray diffraction studies, **2**(2), 16
Uranium (molten), C pickup, **2**(4), 41
reactions with, ceramics, **1**(3), 48
H_2O, **1**(1), 35
O_2, **1**(3), 47
Uranium (Mo-Sn-Zr-clad), bonding, **2**(2), 40
thermal-cycling effects, **1**(3), 38
Uranium (Nb-Sn-Zr-clad), thermal-cycling effects, **1**(3), 38

Uranium (Ni-plated), pressure bonding with Al and Zr, **1**(1), 26–27
Uranium (nontextured), radiation effects, **2**(3), 18
Uranium (sponge), evaluation for fuel usage, **3**(3), 2
Uranium (textured), radiation effects, **2**(3), 18
Uranium (Zircaloy-2-clad), corrosion in H_2O, **3**(3), 3
Uranium (Zr-clad), cladding-thickness determination, **3**(2), 52
thermal-cycling effects, **1**(3), 38

Uranium-235, radiation effects, **2**(1), 2–3
Uranium alloy fuels, coextrusion with cladding, **1**(3), 52; **3**(2), 45–6
pressure bonding with Al cladding, **3**(2), 44
radiation effects, **2**(2), 5

Uranium alloy powder compacts, thermal cycling, **1**(3), 3
Uranium alloy–zirconium hydride system, phase boundaries, **2**(1), 24

Uranium alloys, casting, **3**(1), 48
cladding, **2**(1), 4
coating, **3**(4), 53
constitution diagrams, **2**(1), 11
corrosion, **1**(3), 3, 6, 19–20, 37; **1**(4), 2–3; **2**(1), 4; **2**(2), 5; **2**(3), 1, 6; **3**(4), 4
creep, **3**(1), 18
fabrication, **2**(1), 4; **2**(3), 6; **3**(1), 48
failure, **1**(3), 20
hydride formation, **1**(3), 20
ignition, **3**(1), 17
mechanical properties, **2**(1), 4
melting, **3**(1), 48
metallography, **2**(1), 4
phase studies, **2**(3), 6
physical metallurgy, **2**(1), 4
physical properties, **2**(1), 4
powder metallurgy, **2**(1), 4; **2**(2), 5
production, **2**(1), 4; **3**(1), 2
properties, **3**(2), 3
radiation effects, **1**(1), 5; **1**(3), 3; **2**(1), 4, 17–18; **2**(2), 3, 5; **3**(1), 17; **3**(4), 5
radiation-induced, gas-bubble formation, **3**(1), 18
phase changes, **2**(1), 4, 17
swelling, **2**(1), 16; **2**(3), 18
reactions with air and O_2, **3**(1), 17
stability, **1**(3), 6; **1**(4), 3, 5
stress relaxation, **2**(4), 10
thermal cycling, **1**(1), 5; **2**(2), 3, 5; **3**(2), 3
transformation, **2**(3), 2, 6; **2**(4), 3
Uranium alloys (molten), quality, **1**(3), 48
Uranium aluminide, development, **3**(1), 13
growth kinetics, **3**(1), 15
oxidation, **1**(1), 14; **1**(2), 16
physical properties, **1**(3), 18
properties, **3**(4), 13–15
reaction with N_2, **1**(1), 14; **1**(2), 16
thermal expansion, **1**(2), 16
U solubility in, **3**(1), 15
Uranium aluminide–uranium silicide system, constitution, **3**(1), 12

Uranium beryllide, heat of formation, **3**(2), 7
oxidation, **1**(1), 14; **1**(2), 16
physical properties, **1**(3), 18
preparation, **3**(2), 7
radiation effects, **1**(1), 14
reactions with H_2O vapor, **1**(2), 16
solubility, **2**(2), 10

Uranium beryllide compacts, preparation, **2**(3), 16
Uranium binary alloys, high-temperature properties, **2**(1), 4
phase diagrams, **3**(2), 3
strength, **1**(3), 3
transformation, **2**(1), 4

Uranium boride compacts, preparation, **2**(3), 16
Uranium borides, oxidation, **1**(2), 16
physical properties, **1**(3), 18
properties, **3**(4), 13–15
reactions with N_2 and H_2O vapor, **1**(2), 16
Uranium carbide ceramics, fabrication, **1**(1), 13
Uranium carbide cermets, thermal cycling, **1**(3), 2
Uranium carbide compacts, fabrication, **2**(2), 13
preparation, **2**(3), 16

Uranium carbide fuels, technology, **3**(4), 13
Uranium carbide–metal dispersions, development, **2**(3), 11–12
Uranium carbide–metallic monocarbide mixtures, hot pressing, **2**(1), 14
Uranium carbide powders, sintering, **2**(4), 9
Uranium carbide–Zircaloy-2 cermets, corrosion and fabrication, **1**(1), 13
Uranium carbide–zirconium alloy dispersions, radiation effects, **1**(2), 12
Uranium carbide–zirconium carbide system, solid solubility, **1**(3), 19
Uranium carbides
See also Uranium dicarbide and Uranium monocarbide
casting, **2**(2), 13
chemical reactions, **1**(1), 14; **1**(2), 16; **3**(4), 13
compatibility with Al, **3**(2), 6
compatibility with Nb-base alloys, **3**(4), 13
corrosion, **1**(3), 19; **3**(2), 6
density, **3**(1), 13
fabrication, **1**(2), 15; **2**(1), 14; **3**(1), 13
literature reviews, **3**(4), 13
microstructure, **3**(1), 13
oxidation, **1**(1), 14; **1**(2), 16
phase diagrams, **3**(2), 6
physical properties, **1**(3), 18
preparation, **2**(2), 13; **3**(2), 5–6
structural properties, **3**(2), 6
thermal expansion, **1**(1), 14
U_2C_3 formation, **2**(3), 15
Uranium ceramic fuels, properties, **3**(4), 6
Uranium cermets, cladding and densification by pressure bonding, **2**(2), 49
properties, **3**(4), 6
Uranium composite billets, coextrusion with Zircaloy cladding, **2**(1), 48

Uranium compounds, properties, 1(3), 18–19; 3(4), 13–15
radiation-induced gas formation, 3(3), 23
review, 3(4), 13–15
sintering, 1(1), 13–14
Uranium cores, Ni plating before cladding, 2(1), 49
Uranium crystals, plastic slip, 3(1), 1
preparation, 3(2), 2
recrystallization of deformed, 3(1), 1
self-diffusion, 3(1), 13
thermal expansion, 3(1), 1
Uranium diboride, development, 3(1), 13
Uranium dicarbide
See also Uranium carbides and Uranium monocarbide
C coating, 3(4), 53
hot pressing, 2(4), 8
metallography, 2(4), 8
reactions with heat-transfer liquids, 3(4), 13
structure transformation, 3(4), 13
Uranium dicarbide–uranium monocarbide system, interdiffusion, 2(4), 8
Uranium dingots, H_2 reduction, 2(4), 41
Uranium dioxide
See also Uranium oxide
bibliography, 2(4), 7
coating with Al_2O_3, 2(3), 15
coextrusion with cladding, 2(4), 43; 3(4), 51
compaction, 2(4), 42; 3(2), 43
compatibility with, Al_2O_3, 1(3), 15
borides, 3(3), 17; 3(4), 12
carbides, 3(3), 17; 3(4), 12
Nb, 1(3), 15
nitrides, 3(3), 17; 3(4), 12
oxides, 3(3), 17; 3(4), 12
refractory metals, 3(3), 17; 3(4), 12
ZrC, 1(3), 15
ZrO_2, 1(3), 15
corrosion in steam, 3(3), 19
deformation, 2(2), 12
density, 1(2), 13
detection in fuel elements, 1(4), 43
diffusion with, He, 1(3), 15
I, 3(4), 16
O_2, 1(1), 12
rare gases, 2(1), 13
U(IV), 1(1), 12
electrical conductivity, 1(1), 11
electrical properties, 1(2), 14
etching, 3(1), 11
extrusion, 1(3), 14
fabrication, 1(1), 10–11; 1(3), 14
failure, 1(2), 14
fracture, 1(3), 15
He density, 1(3), 15
He diffusion, 1(3), 15
He release, 1(1), 38
impact failure, 1(2), 14
melting, 1(1), 11; 1(4), 11; 3(1), 9, 12
nonstoichiometry, 2(2), 12
NRX fuel studies, 1(3), 15
O/U ratio determination, 3(1), 9
oxidation, 1(1), 11–12; 1(2), 14
physical properties, 1(3), 18; 3(3), 17
polishing, 3(1), 11
preparation, 1(2), 13; 1(4), 11
properties, 1(2), 14; 1(3), 14
radiation effects, 1(1), 11–12; 1(2), 14; 1(3), 14, 17; 3(1), 19
radiation effects on structure, 2(4), 11; 3(4), 16
radiation effects on thermal conductivity, 1(3), 15; 3(4), 12
radiation-induced gas, bubble formation, 2(1), 18
diffusion, 1(1), 38; 1(2), 16–17
release, 1(1), 12, 37; 1(2), 14; 1(3), 14–15; 2(4), 11; 3(2), 8
retention, 1(3), 15
radiation-induced sublimation, 3(3), 22
radiation-induced void formation, 2(4), 11
reactions at high temperatures and pressures, 2(4), 7
reactions with Zircaloy-2 and Zr, 1(1), 11
reduction by C, 3(2), 6
sintering, 1(1), 10–11; 1(2), 13; 3(4), 13
stabilization, 2(4), 7; 3(1), 11
strength, 1(2), 14
structure, 3(3), 17
swaging, 1(1), 11; 1(3), 14
technology, 2(2), 12
thermal properties, conductivity, 1(1), 11; 1(2), 14; 1(4), 10–11; 2(1), 12–13; 2(3), 14–15; 3(3), 18–19; 3(4), 12
expansion, 1(1), 11; 2(1), 13
fracture, 1(1), 11
shock, 1(2), 14
stability, 1(4), 11
UF_6 conversion to, 3(1), 51
volatility, 1(4), 11
Uranium dioxide (Al_2O_3-coated) (irradiated), fission-product retention, 1(3), 15; 2(3), 15; 3(4), 52
Uranium dioxide (irradiated), diffusion with, fission gas, 2(1), 18
Kr^{85}, 3(3), 18
U, 3(3), 18
Xe, 2(4), 11; 3(4), 16
electron diffraction patterns, 3(4), 16
fission-gas, diffusion coefficients, 2(1), 18
reentry, 3(4), 16
release, 2(2), 12–13; 3(3), 22; 3(4), 16
Mo^{99} chemical behavior, 3(1), 19
Uranium dioxide (Ni-plated), brazing and pressure bonding, 1(2), 40
Uranium dioxide (pressure-bonded), He permeability, 3(4), 50
Uranium dioxide (sintered), coating with Be, 3(4), 52
radiation effects, 2(4), 11
radiation-induced melting and grain growth, 2(4), 11

Uranium dioxide (sintered) (Continued)
reaction with CO_2, **2**(4), 7
thermal conductivity, **2**(4), 7, 11
Uranium dioxide (type 304 stainless-steel-clad), swaged density, **3**(2), 42
Uranium dioxide (swaged), processing effects on density, **2**(1), 12
Uranium dioxide blanket rods, failure in PWR and thermal performance, **1**(3), 17
Uranium dioxide blanket rods (Zircaloy-2-clad), radiation effects, **3**(4), 11–12
Uranium dioxide ceramic dispersions, fuel loss, **3**(4), 12
Uranium dioxide ceramic fuels (irradiated), annealing effects, **2**(2), 15
Uranium dioxide ceramic fuels (Zircaloy-canned), vibratory packing, **3**(1), 11
Uranium dioxide ceramics, burnable-poison additives, **3**(1), 11
C addition effects, **1**(4), 9–10
chemical properties, **2**(2), 14
extrusion, **1**(3), 14
fabrication, **1**(3), 14; **3**(1), 11; **3**(2), 7
hot isostatic pressing, **2**(2), 12
Kr^{85} release, **2**(2), 15
mechanical properties, **2**(2), 14
physical properties, **2**(2), 14
pressure bonding with stainless-steel cladding, **2**(4), 42
properties, **3**(1), 11
radiation effects, **3**(1), 19
swaging, **3**(1), 11
thoron release, **2**(2), 15
Uranium dioxide cermets, thermal conductivity, **3**(3), 17
Uranium dioxide compacts (Al-clad), fabrication and irradiation testing, **2**(4), 7
Uranium dioxide crystals, growth from vapor, **3**(3), 20
high-temperature growth, **3**(1), 11
preparation by hydrolysis of UF_4, **3**(3), 55
Uranium dioxide dispersions, radiation effects, **1**(3), 13–14
ultrasonic welding, **3**(3), 53
Uranium dioxide films, radiation effects, **3**(3), 22
Uranium dioxide fuel elements (stainless-steel-clad), annulus filling with Pb, **3**(4), 51–2
fabrication, **2**(4), 8
mechanical twisting, **3**(3), 53
Uranium dioxide (ceramic and fused powder) fuel elements, densification and cladding by pressure bonding, **3**(2), 44
Uranium dioxide (fused) fuel elements, swaging with cladding, **3**(2), 43
Uranium dioxide fuel particles, cladding with Al_2O_3, **3**(1), 51; **3**(4), 52–3
cladding with graphite, **3**(4), 53
electroless Ni coating, **3**(1), 51
sintered cladding, **3**(3), 55
Zr vapor deposition, **3**(1), 51
Uranium dioxide fuel rods (mild-steel-clad), explosion forming, **3**(3), 20
Uranium dioxide fuel rods (sintered), stretch forming and swaging with cladding, **3**(2), 43
Uranium dioxide fuel rods (stainless-steel-clad), explosion compaction, **3**(4), 55
explosion forming, **3**(3), 20
Uranium dioxide fuel rods (Zircaloy-clad), explosion forming, **3**(3), 20
Uranium dioxide fuel rods (Zircaloy-2-clad), explosion compaction, **3**(4), 55
Uranium dioxide fuels, Canadian program, **1**(3), 15; **3**(1), 9
coating with C and Cr, **2**(4), 44
coextrusion with cladding, **3**(1), 50; **3**(2), 45; **3**(4), 51
compressive strength, **3**(1), 10–11
corrosion in steam, **3**(1), 10–11
densification, **3**(4), 50
development, **2**(3), 14
diffusion bonding with cladding, **2**(1), 46–7; **2**(2), 49–53; **2**(4), 43; **3**(2), 45
elastic modulus, **3**(1), 10–11
fabrication, **3**(4), 12–13
NRX, **1**(3), 15
performance, **3**(3), 17
pressure bonding with cladding, **1**(1), 27; **1**(2), 40; **1**(3), 51; **1**(4), 41; **2**(1), 46; **2**(2), 49; **2**(3), 49–50; **2**(4), 42; **3**(1), 49–50; **3**(2), 44; **3**(4), 50
properties, **3**(1), 10–11
radiation effects, **2**(1), 12; **3**(1), 9
rolling with cladding, **3**(3), 53
summary, **2**(4), 7
swaging with cladding, **3**(1), 49; **3**(2), 42–3; **3**(3), 52–3; **3**(4), 49
technology, **3**(1), 9
thermal conductivity, **3**(1), 10–11
thermal expansion, **3**(1), 10–11
Uranium dioxide–metal dispersions, development, **2**(3), 11–12
Uranium dioxide–metal fiber fuel elements, swaging with cladding, **3**(3), 52
Uranium dioxide–metal fiber fuel elements (swaged), mechanical and thermal properties, **3**(2), 43
Uranium dioxide pellets, cladding with Al_2O_3, **2**(3), 52–3
compatibility with Al, **3**(3), 17
densification, **3**(1), 49–50
development, **1**(4), 9
fabrication, **1**(3), 14; **2**(3), 14–15
pressure bonding with cladding, **3**(1), 49–50
thermal conductivity, **1**(3), 15; **3**(1), 11
Uranium dioxide pellets (irradiated), solid fission-product mobility, **3**(3), 17–18
Uranium dioxide pellets (stainless-steel-clad), thermal conductivity, **3**(1), 11
Uranium dioxide pellets (Zircaloy-2-clad), in-pile loop experiment, **1**(3), 15, 17
Uranium dioxide powder, annealing effects, **3**(3), 17
coating with metallic films, **2**(1), 49–50

Uranium dioxide powder (Continued)
comminution effects, **3**(3), 17
densification, **3**(1), 50
fluidized-bed coating, **3**(4), 53
metallurgy, **2**(1), 12
oxidation, **2**(2), 12; **3**(3), 17
physical properties, **2**(4), 7
preparation, **1**(3), 14; **2**(4), 7
sintering, **1**(4), 9; **3**(3), 20
vibratory compaction in Zircaloy tubes, **2**(4), 44
X-ray diffraction, **1**(3), 17
Uranium dioxide powder (canned), radiation effects, **2**(2), 12–13
Uranium dioxide powder (Zircaloy-2-canned), radiation effects and sintering, **3**(3), 19
Uranium dioxide powder (Zircaloy-3-canned), radiation effects, **2**(3), 14
Uranium dioxide powder slurries, behavior in NaK, **2**(3), 31
Uranium dioxide slugs (sintered), thermal conductivity, **2**(2), 12
Uranium dioxide spheres, metallic coatings, **3**(4), 52
Uranium dioxide system, phase diagrams with oxide additives, **2**(2), 12
Uranium dioxide–yttrium oxide mixtures, constitution, **1**(2), 14–15
Uranium dioxide–yttrium oxide system, phase studies, **2**(3), 14
Uranium dioxide–zirconium alloy dispersions, radiation effects, **1**(2), 12
Uranium dioxide–zirconium boride dispersions, development, **2**(4), 19
fabrication, **2**(3), 26
Uranium dioxide–zirconium dioxide ceramics, properties, **3**(1), 11–12
Uranium dioxide–zirconium dioxide system, constitution, **1**(3), 19
fabrication, **3**(1), 12
phase studies, **2**(3), 14
Uranium dioxide–zirconium oxide solid solution, radiation effects, **3**(3), 22
Uranium dioxide–zirconium silicate dispersion ceramic, radiation effects, **3**(1), 19
Uranium eutectic alloys (molten), containment in oxidized crucibles, **1**(3), 48
Uranium fuel cylinders, internal canning with Zircaloy-2, **2**(1), 49
Uranium fuel elements, coextrusion with cladding, **1**(3), 51–2; **1**(4), 14, 41; **3**(1), 50; **3**(3), 54
drawing with Zircaloy-2 cladding, **3**(4), 49
extrusion with Al cladding, **1**(3), 52
pressure-bonding production, **1**(1), 26
radiation effects, **2**(2), 1; **3**(4), 4
technology, **2**(2), 1, 3
Uranium fuel elements (Al-clad), radiation effects and thermal transmission, **1**(3), 52
Uranium fuel elements (Al-clad, Ni-bonded), corrosion in H_2O, **1**(4), 11
Uranium fuel elements (AlSi-coated), canning with X-8001, **2**(2), 54
Uranium fuel elements (Ni-plated), extrusion with Al cladding, **2**(2), 53–4
Uranium fuel elements (Ni-plated, Al-clad), radiation effects and thermal transmission, **1**(3), 52
Uranium fuel elements (stainless-steel-clad), radiation effects, **3**(2), 2
Uranium fuel elements (Zircaloy-2-clad), corrosion in H_2O, end capping, and H_2 release, **3**(2), 8
Uranium fuel plates, canning with Al, **3**(4), 51
extrusion with Al cladding, **2**(1), 48–9; **3**(4), 51
machining, **2**(1), 48–9
preferred orientation, **1**(4), 1–2
rolling with Zircaloy cladding, **1**(4), 39–40
Uranium fuel plates (Ni-coated), pressure bonding with Al cladding, **1**(3), 50–1
Uranium fuel plates (Ni-plated, Al-clad), interdiffusion, **1**(1), 26
Uranium fuel rods, coextrusion with cladding, **1**(4), 41–2; **2**(1), 48; **2**(2), 53; **2**(3), 51; **3**(2), 46; **3**(3), 54
radiation effects, **1**(4), 2
Uranium fuel rods (Zircaloy-2-clad), etching, swaging, and testing, **2**(1), 48
Uranium fuel slugs, ceramic coating, **1**(3), 53
evaluation, **3**(2), 39
Mo jacketing, **3**(4), 51
nondestructive testing, **1**(2), 42
pressure bonding with Zircaloy-2 cladding, **3**(2), 44
Uranium fuel slugs (AlSi-bonded, X-8001-clad), diffusion, **2**(3), 16
Uranium fuel slugs (AlSi-coated), canning with Al, **2**(2), 54
Uranium fuel slugs (Ni-plated), pressure bonding with Al cladding, **1**(4), 40–1
Uranium fuel slugs (Zircaloy-clad), fabrication, **3**(2), 39–40
Uranium glass fibers (glass-clad), applications, **3**(3), 19
Uranium hexafluoride, conversion to UO_2, **3**(1), 51
Uranium hydride, effects on tensile properties of U, **1**(1), 1
Uranium ingots, alpha extrusion, **2**(2), 48
furnace pressure effects, **3**(4), 48
mold heating effects, **3**(2), 39
solidification, **2**(4), 41
soundness, **3**(2), 39
Uranium monocarbide
See also Uranium carbides and Uranium dicarbide
annealing effects, **3**(1), 12
casting, **2**(3), 15; **3**(3), 21
chemical reactivities, **3**(3), 20
compatibility with, Be, **2**(2), 13
container materials, **3**(1), 12
Inconel, **3**(4), 13
mild steel, **3**(4), 13
Na, **2**(2), 13
NaK, **2**(1), 14
type 304 stainless steel, **3**(4), 13
Zr, **2**(2), 13; **3**(4), 13

Uranium monocarbide (Continued)
evaluation as fuel material, 3(3), 20
fabrication, 3(1), 13; 3(4), 15
fission-gas release, 2(2), 13–14; 2(4), 8
green density, 2(1), 14
handling, 3(4), 15
hot pressing, 3(3), 21
Kr^{85} release, 2(2), 14
lattice parameter, 3(4), 13
melting, 2(1), 14; 3(1), 12; 3(3), 21
physical properties, 2(4), 8
preparation, 2(1), 14; 3(1), 12–13; 3(2), 5–6; 3(3), 55; 3(4), 15
production by C reduction of U oxides or ammonium diuranate, 3(3), 21
properties of sintered bodies, 2(2), 13
radiation effects, 2(1), 14; 2(3), 15; 2(4), 8; 3(1), 19; 3(2), 6; 3(3), 20; 3(4), 13
reaction with, CO_2, 2(2), 13; 2(4), 8
H_2, 2(2), 13
Nb in Ar, 3(3), 20
sintering, 2(3), 15; 3(3), 21; 3(4), 15
storage, 3(4), 15
strength, 3(3), 20
thermal conductivity, 2(4), 8
thermal expansion, 2(4), 8
U diffusion into, 3(3), 20; 3(4), 13
Xe^{133} release, 2(2), 14
Uranium monocarbide (cast), irradiation behavior, 2(3), 15
physical properties, 2(3), 15
Uranium monocarbide (sintered), properties, 2(2), 13; 3(3), 21
Uranium monocarbide fuels, C diffusion, 3(1), 12
C effects on density and electrical resistivity, 3(1), 12
corrosion in H_2O, 3(1), 12
development, 3(1), 12
fabrication, 2(4), 9
hot pressing, 2(4), 8
mechanical properties, 3(1), 12
metallography, 2(4), 8
physical properties, 3(1), 12
properties, 2(2), 14; 3(4), 13–15
thermal conductivity, 3(1), 12
U diffusion, 3(1), 12
Uranium monocarbide–graphite fuel elements, preparation, 2(2), 13
Uranium monocarbide powder, production, 3(3), 21
Uranium monocarbide–uranium mononitride system, cold pressing and melting, 2(2), 13
Uranium monocarbide–uranium nitride system, constitution, 3(1), 12
Uranium mononitride, compatibility with metallic matrices, 2(2), 11
fabrication, 3(4), 15
preparation, 2(2), 11
properties, 3(4), 13–15
Uranium nitride, crystal structure, 3(1), 12
density, 2(4), 8–9; 3(1), 13
development, 3(1), 13
fabrication effects, 3(1), 13
melting point, 3(1), 12
physical properties, 1(3), 18
preparation, 2(4), 8; 3(1), 8; 3(3), 21
sintering, 2(3), 15
structure, 2(4), 8; 3(1), 13
Uranium nitride compacts, preparation, 2(3), 16
Uranium nitride–metal dispersions, development, 2(3), 11–12
Uranium nitride–vanadium dispersions, chemical reactions, 1(4), 9
Uranium oxide
See also Uranium dioxide
CO decomposition on, 2(2), 14
composition, 1(2), 14
flow behavior, 2(2), 12
interstitial O_2, 1(3), 15
O_2 self-diffusion, 1(3), 15
oxidation, 3(3), 18–19
properties, 2(1), 12
radiation effects, 1(2), 17; 2(1), 12; 2(4), 11; 3(3), 22
sintering, 1(2), 13; 1(3), 14
stability, 3(4), 12
structure, 1(2), 14; 1(3), 15
technology, 2(1), 12
thermal conductivity, 2(1), 2
thermodynamic properties, 2(3), 14
volatilization, 3(3), 18–19
Uranium oxide ceramics, sintering, 2(2), 12
Uranium oxide dispersion ceramics, radiation effects, 3(1), 19
Uranium oxide (fused) fuel elements, swaging with Zircaloy cladding, 3(2), 43
Uranium oxide powders, Kr^{85} diffusion from, 3(4), 11
Uranium oxides (active), oxidation, 1(3), 15
preparation, 1(3), 15
structural behavior, 1(3), 15
Uranium oxides (inactive), oxidation, 1(3), 15
preparation, 1(3), 15
structural behavior, 1(3), 15
Uranium oxides (irradiated), differential calorimetry, 3(3), 17
Mo^{99} chemical behavior, 3(1), 19
Xe^{133} diffusion, 3(3), 18
Uranium phosphide, development, 3(1), 13
properties, 3(4), 13–15
Uranium powder, metallurgy, 2(1), 4; 2(2), 5
preparation, 3(1), 2
Uranium powder compacts, radiation effects, 2(1), 2
sintering, 3(1), 2
Uranium powder compacts (irradiated), fission-gas escape, 2(1), 2
Uranium powder products (dispersion-hardened), preparation and properties, 3(4), 10–11
Uranium refractories, fabrication, 2(1), 14
Uranium selenide, evaluation as fuel material, 3(3), 20–1
Uranium sheet, annealing effects and rolling, 1(3), 49

Uranium sheet (cold-rolled), recrystallization, **3**(1), 48
Uranium silicide (Zircaloy-2-clad), preparation and radiation effects, **3**(3), 5
Uranium silicide ceramic fuels, properties, **2**(2), 14
Uranium silicide dispersant, preparation and compatibility with metallic matrices, **2**(2), 11
Uranium silicide–vanadium dispersions, chemical reactions, **1**(4), 9
Uranium silicides, corrosion, **1**(3), 20
development, **3**(1), 13
fabrication, **3**(4), 7
heat-treatment, **3**(4), 7
high-temperature stabilization, **1**(3), 19
microhardness, **1**(2), 16
oxidation, **1**(1), 14; **1**(2), 16
preparation, **1**(3), 19; **3**(3), 21; **3**(4), 15
properties, **1**(3), 18–19; **3**(4), 7, 13–15
radiation effects, **1**(1), 38; **1**(3), 19; **3**(4), 7
reaction with N_2, **1**(1), 14; **1**(2), 16
specific heat, **1**(2), 16
thermal expansion, **1**(1), 14; **1**(2), 16
Uranium sulfide, development, **3**(1), 13
evaluation as fuel material, **3**(3), 20–1
physical properties, **1**(3), 18
Uranium sulfide fuel, properties, **3**(4), 13–15
Uranium-sulfur compounds, preparation, properties, and X-ray diffraction, **2**(2), 14
Uranium telluride, evaluation as fuel material, **3**(3), 20–1
Uranium ternary alloys, hot hardness, **1**(3), 6
Uranium trioxide, properties, **1**(4), 11
Uranium tubing, cable cladding with Al, **2**(1), 45
casting, **3**(4), 8
coextrusion, **2**(3), 50
coextrusion with Zircaloy cladding, **3**(4), 51
development, **1**(3), 1
external extrusion cladding with Al, **3**(2), 46
extrusion, **3**(2), 41
fabrication, **1**(3), 48–9
internal extrusion cladding with Al, **3**(2), 46
pressure bonding with cladding, **3**(4), 50
radiation effects, **1**(3), 1
Uranium tubing (Al-clad), multitemperature coextrusion, **2**(1), 48
Uranium tubing (Al-Mg alloy clad), multitemperature coextrusion and cracking of cladding, **2**(1), 48
Uranium tubing (Ni-plated), external and internal extrusion cladding with Al, **3**(3), 54
Uranium tubing (Zircaloy-2-clad), coextrusion, **1**(4), 41
Uranium tubular fuel elements (Zircaloy-2-clad) (pressure-bonded), diffusion, **3**(2), 44–5
Uranium–uranium aluminide diffusion couple, UAl_2 growth kinetics, **3**(1), 15
Uranium-vanadium alloys, metallic addition effects on eutectic temperature, **1**(4), 2
Uranium-vanadium-zirconium alloys, corrosion in H_2O, **1**(4), 2–3
Uranium washers, production, **1**(1), 26
Uranium wires, vapor deposition with Be-Mg alloy coating, **2**(3), 52
Uranium-yttrium dispersions, density, **3**(1), 9
distortion, **2**(4), 5
fabrication, **3**(1), 8–9
hardness, **2**(4), 5
tensile properties, **2**(4), 5; **3**(1), 9
thermal conductivity, **3**(1), 9
thermal cycling, **3**(1), 9
Uranium-yttrium-zirconium alloys, phase diagram, **1**(4), 36
Uranium-Zircaloy alloys, corrosion in H_2O, **1**(4), 7
Uranium–Zircaloy-2 alloys, corrosion in H_2O, **1**(4), 7
Uranium–Zircaloy-3 alloys, corrosion in H_2O, **1**(4), 7
swelling, **2**(3), 7
Uranium–Zircaloy-3 alloys (irradiated), annealing effects, **2**(3), 8
swelling, **2**(3), 7
Uranium-Zircaloy-Zircaloy subassemblies, pressure bonding, **1**(1), 27
Uranium zirconide, crystal structure, **3**(4), 8
Uranium-zirconium alloy dispersions, radiation effects, **1**(2), 12
Uranium-zirconium alloy hydride
See Hydrogen-uranium-zirconium system
Uranium-zirconium alloys, behavior summary, **2**(1), 6; **3**(2), 3
coating with Zr, **2**(2), 55
coextrusion with cladding, **2**(3), 51; **2**(4), 43
coextrusion with cladding and thermocouple, **2**(2), 53
constitution, **2**(2), 8; **3**(3), 5
corrosion, **1**(1), 4–5, 7–8; **1**(2), 6; **1**(3), 20; **1**(4), 2–3, 5–7; **2**(1), 7, 15; **2**(2), 14; **2**(3), 8; **3**(3), 6, 22
development for power-reactor use, **3**(1), 4
diffusion, **2**(2), 37; **2**(4), 4; **3**(2), 3; **3**(3), 44; **3**(4), 43
electrical resistivity, **2**(1), 7
fabrication, **3**(3), 6
hardness, **1**(4), 5; **2**(1), 7
heat-treatment effects, **3**(3), 5–6
hydrogen, heats of solution, **3**(1), 25
migration, **1**(2), 23
reaction with, **3**(1), 24–5
solubility, **3**(3), 22
interdiffusion, **2**(3), 16
Kr^{85} diffusion coefficient in, **2**(4), 4
magnetic susceptibility, **2**(1), 7
modulus of elasticity, **1**(1), 8
oxidation, **1**(1), 6, 35
phase diagrams, **2**(3), 3; **3**(3), 5
phase transformation, **3**(3), 5
physical properties, **2**(2), 6, 8
pressure-weld bond strengths, **2**(4), 43
processing, **1**(3), 6
production, **2**(1), 9
properties, **1**(3), 6; **2**(1), 6; **2**(3), 6; **3**(2), 3

Uranium-zirconium alloys (Continued)
radiation effects, 1(1), 8; 1(2), 6–8, 12; 1(3), 8–9; 2(1), 3–4, 7–8; 2(2), 8; 2(3), 8; 3(1), 2–3; 3(3), 2–3, 6; 3(4), 5
scrap recycling, 1(3), 9
sintering, 2(1), 9
stability, 1(4), 5; 2(3), 6
strain at fracture, 1(1), 8
structure, 1(1), 6; 1(3), 6; 2(2), 6
technology, 3(3), 5
tensile strength, 1(1), 8
thermal stability, 1(3), 5–6
transformation, 1(1), 6; 1(4), 7; 2(2), 8; 2(3), 2
U diffusion, 3(3), 44
Xe^{133} and Xe^{135} diffusion coefficients in, 2(4), 4
yield strength, 1(1), 8
Uranium-zirconium alloys (extrusion-clad), radiation effects, 3(3), 2–3
Uranium-zirconium alloys (irradiated), annealing, 1(3), 8; 2(1), 8, 17; 2(2), 7; 2(4), 4, 9
bend testing, 2(1), 8–9
corrosion in H_2O, 2(2), 7
effects of transients, 2(1), 17; 2(2), 7; 2(4), 9
fission-gas release, 2(3), 19; 2(4), 4
heating effects on swelling, 2(2), 7
Uranium-zirconium alloys (Zircaloy-clad), corrosion detection, 1(2), 3
fabrication yield evaluation, 1(1), 26
radiation effects on corrosion, 1(3), 3–4
resistance bonding, 1(4), 42
Uranium-zirconium alloys (Zircaloy-2-clad), corrosion, 1(2), 6; 2(2), 3; 3(2), 8; 3(3), 3
heat-treatment, 2(2), 3
melting, 2(4), 24–5
radiation effects, 1(2), 8; 2(1), 8; 2(2), 3, 15; 2(4), 4; 3(4), 5, 15
reaction with H_2O, 2(4), 24–5
thermal cycling, 1(3), 6; 3(2), 3
Uranium-zirconium alloys (Zircaloy-2-clad) (irradiated), heating effects on swelling, 1(4), 7
Uranium-zirconium alloys (Zircaloy-3-clad), radiation effects, 1(2), 7–8
Uranium-zirconium ceramics, fabrication, 1(1), 13
Uranium (molten)–zirconium diffusion couples, interaction, 2(4), 33
Uranium–zirconium hydride alloys, radiation effects, 2(4), 16
Uranium-zirconium subassemblies, pressure bonding with Zircaloy cladding, 2(3), 50
Uranium-zirconium tubing, coextrusion with Zircaloy-2 cladding, 2(1), 47–8
Uranyl hexahydrate, thermal-decomposition products, 1(4), 11

V

Vanadium, brittleness, 2(4), 37
chemical behavior, 2(3), 31
compatibility with fissium-Pu-U alloys, 3(4), 8–9
corrosion, 2(3), 31
diffusion, 2(3), 17
electroplated coatings, 3(4), 53
fabricability, 3(2), 34
oxidation, 3(4), 34
radiation effects on thermal conductivity, 3(4), 38
relaxation time, 3(2), 36
Vanadium alloys, electroplated coatings, 3(4), 53
oxidation, 3(4), 34
Vanadium boride, properties, 3(4), 34
Vanadium carbide, properties, 3(4), 34
Vanadium nitride, properties, 3(4), 34
Vanadium oxide, properties, 3(4), 34
Vanadium-yttrium alloys, constitution, 2(3), 35
Vapor-deposited coatings, graphite tubes with metallic carbides, 1(1), 28
stainless-steel tubing with Nb, 1(1), 28

W

Washers, production of U, 1(1), 26
Water, separation from D_2O, 3(4), 1
Welding
See also specific metals and alloys
age hardening, 2(3), 53
bibliographies, 3(4), 55
corrosion, 3(4), 34
electrical potential testing, 1(3), 54
electron beam, 2(2), 55
explosion, 3(1), 52; 3(2), 49
nondestructive testing, 1(2), 42
stainless steels, 2(3), 39, 43
technical report catalog, 3(3), 58
ultrasonic, 1(3), 54
Zr, Zircaloy-2, and Zircaloy-3, 1(1), 29

X

X-ray testing
See also Nondestructive testing
applications, 2(3), 53; 2(4), 44–5; 3(3), 58
development, 2(1), 51
fuel-element U content determination, 2(3), 54

Y

Yttrium, addition effects on oxidation resistance of metals and alloys, 3(1), 34
canning in Cu, 3(1), 34
chemistry, 3(1), 48
containment by Cr-U alloy, 2(4), 22
corrosion in H_2O vapor, 2(4), 23
fabrication, 3(1), 48; 3(3), 43–4, 51
melting, 3(1), 48

Yttrium (Continued)
metallurgy, **3**(1), 48
O content effects on H absorption, **3**(2), 16
O removal, **3**(2), 46
oxidation, **3**(4), 33
physical constants, **3**(1), 42–3
porcelain-enamel coating, **2**(4), 44
properties, **3**(1), 48
solid solubility in Cr-Fe alloys, **3**(2), 32
solid-state reactions with metals and alloys, **3**(1), 15–16
welding, **3**(4), 55
Yttrium alloys, phase diagrams, **3**(1), 48
Yttrium hydrides, density, **3**(2), 16
dissociation pressures, **3**(2), 16
electrical resistivity, **3**(4), 25
fabrication, **3**(2), 16
hardness, **3**(4), 24
H content effect on N_H, **3**(2), 16
H content reduction, **3**(2), 16
lattice constant, **3**(2), 16
linear thermal expansion, **3**(4), 24–5
magnetic susceptibility, **3**(4), 25
N_H, **3**(2), 16
properties, **3**(2), 16; **3**(4), 23–4
radiation effects, **3**(2), 16
specific heat, **3**(4), 25
stress-rupture data, **3**(2), 16–17
technology, **3**(3), 32
thermal conductivities, **3**(4), 24
transformation, **3**(4), 25
ultimate tensile strength, **3**(4), 23–4
Yttrium-zirconium alloys, eutectic, **3**(1), 42
phase diagram, **1**(4), 36

Z

Zinc, radiation effects on resistivity, **2**(2), 33
reaction with H_2O, **2**(1), 33
U solubility in, **2**(2), 8
Zinc (irradiated), annealing kinetics, **3**(2), 26
Zinc (molten), solubility of Th in, **3**(4), 9
Zircaloy, chemical plating with Cu, **2**(4), 43
corrosion, **1**(2), 30–1; **1**(3), 33; **1**(4), 21, 35–6; **2**(2), 27
electron-beam welding, **2**(1), 51
fabrication, **2**(2), 47; **3**(1), 48
H_2 diffusion, **1**(3), 26–7
H_2 pickup, **1**(4), 21
hardness, **2**(4), 35
hydriding, **1**(3), 33; **3**(4), 26
melting, **2**(2), 47
metallurgically bonded joints with stainless-steel tubes, **3**(3), 54
pressure bonding, **1**(1), 27; **1**(2), 40; **1**(3), 50; **1**(4), 41
production cost reduction, **1**(3), 49
properties, **2**(4), 35
quality, **1**(2), 39; **1**(3), 49
radiation effects, **2**(1), 41–2
reaction with steam, **3**(4), 36
salt bonding, **2**(4), 43
stringer occurrence, **1**(3), 49
welding, **1**(3), 53; **2**(1), 51
Zircaloy (irradiated), annealing effects, **2**(1), 41–2
Zircaloy fuel assemblies, ceramic-coated weld backing, **2**(4), 44
Zircaloy fuel-element components, forge rolling, **2**(3), 48
Zircaloy ingots, ultrasonic testing, **1**(3), 54
Zircaloy sheets, diffusion bonding, **2**(1), 51
Zircaloy tubing, cold working of extruded, **2**(1), 45
injection casting in canning, **2**(3), 52
Zircaloy-2, annealing, **2**(3), 35–6; **3**(3), 51
brazing, **3**(2), 48
burst strength, **1**(2), 35
cold-work effects, **3**(3), 44
compatibility with fissium-Pu-U alloys, **3**(4), 8–9
corrosion, **1**(1), 32, 35; **1**(3), 49; **1**(4), 21–2, 39; **2**(1), 28, 34; **2**(2), 27; **2**(3), 28; **2**(4), 20; **3**(2), 22; **3**(3), 22, 37; **3**(4), 8, 31, 35
corrosion under irradiation, **3**(1), 32
creep properties, **1**(2), 35–6; **1**(3), 39; **1**(4), 27–8, 30; **2**(1), 34, 36; **2**(2), 41; **2**(4), 35; **3**(1), 42–3; **3**(2), 30; **3**(4), 42
creep-rupture properties, **3**(1), 43
crystal properties, **1**(2), 35
D heat of transport, **3**(4), 26
diffusion bonding, **3**(2), 45
diffusion with Th, **1**(2), 10
ductility, **1**(3), 39
dynamic modulus of elasticity, **2**(3), 37
explosion forming, **3**(1), 52
flow-stress recovery, **1**(3), 40
fretting corrosion, **2**(3), 28; **3**(2), 22; **3**(4), 31
grain growth, **2**(3), 35
grain size, **2**(2), 40; **2**(3), 38, 40–1
heat-treatment effects, **1**(3), 38–9; **1**(4), 39; **2**(1), 34; **2**(2), 27, 40; **2**(3), 38, 40–1
hydridation, **1**(3), 33; **1**(4), 15, 21; **2**(1), 24; **2**(3), 23, 28; **2**(4), 20; **3**(3), 37–8; **3**(4), 26, 30–1
hydrogen, absorption in H_2O and steam, **2**(3), 28
effects, **1**(3), 39–40; **2**(1), 34–36; **3**(2), 29
pickup, **3**(3), 33
thermal diffusion, **3**(3), 33, 44
immersion plating, **3**(2), 47
inclusions, **2**(4), 30
joining to Ag-Cd-In alloys, **1**(3), 31
mechanical properties, **1**(3), 38–9; **1**(4), 26, 30, 32; **2**(1), 34, 36; **2**(3), 36–7; **3**(3), 44; **3**(4), 42
metallic coatings, **1**(3), 53; **2**(2), 55
physical metallurgy, **2**(3), 37
precipitates, **2**(4), 30
production, **2**(1), 28
properties, **3**(2), 40; **3**(3), 46
quality control, **1**(4), 22

Zircaloy-2 (Continued)
radiation effects on, H_2 absorption, **2**(2), 22; **2**(3), 28
impact properties, **2**(2), 36; **3**(1), 37
mechanical properties, **1**(2), 33–4; **2**(4), 27, 29–30; **3**(2), 28; **3**(3), 43
tensile properties, **1**(1), 39; **2**(2), 35; **2**(3), 32–3; **3**(4), 40–1
reactions with H_2O and steam, **1**(1), 35; **3**(4), 35
relaxation, **2**(3), 36
residual work effects, **3**(1), 42–3
rolling, **3**(3), 51
soaking effects, **2**(4), 35
strain-fatigue testing, **1**(2), 36
strain-rate effects, **2**(3), 36–8, 40–1
stress effects, **1**(3), 39
stress-fatigue properties, **2**(3), 36–7
stress-relaxation characteristics, **3**(4), 42
stress-rupture properties, **2**(3), 36
stringers, **2**(2), 47; **3**(3), 51
structural anisotropy effects, **2**(3), 38
surface O_2 effects, **2**(3), 36
tensile properties, **1**(4), 27, 30, 32, 39; **2**(2), 40–2; **2**(3), 36, 38, 40–1; **2**(4), 35; **3**(2), 29
thermal expansion, **2**(3), 37–8
transformation temperatures, **1**(4), 35
wear factors against stainless steel 347, **1**(3), 31
welding, **1**(1), 29; **1**(2), 41; **2**(2), 25; **3**(4), 55
yield strength, **1**(2), 35
Zircaloy-2 (annealed), creep properties, **3**(1), 42; **3**(2), 30
Zircaloy-2 (cast), impact and tensile properties, **2**(1), 34–5
Zircaloy-2 (cold-worked), properties, **3**(1), 42–3; **3**(2), 30; **3**(3), 44
Zircaloy-2 (Cu diffusion-bonded), H_2 absorption in H_2O, **2**(1), 28
Zircaloy-2 (Cu-jacketed), Cu diffusion, **3**(2), 34–5
Zircaloy-2 (Fe diffusion-bonded), H_2 absorption in H_2O, **2**(1), 28
Zircaloy-2 (fusion-welded), ultimate and yield strengths, **2**(1), 34–5
Zircaloy-2 (irradiated), damage annealing, **3**(4), 40
hardening recovery, **1**(3), 44
oxide weight gains in H_2O, **2**(3), 28
Zircaloy-2 (molten), reaction with H_2O, **1**(1), 35; **2**(1), 33–4
reaction with uranyl sulfate solution, **2**(1), 33–4
Zircaloy-2 (vacuum-melted), impact properties, **3**(1), 43
low-cycle strain-fatigue properties, **3**(1), 43
Zircaloy-2 (wrought), impact and tensile properties, **2**(1), 34–5
Zircaloy-2 diaphragms, creep and deflection testing, **3**(2), 30
Zircaloy-2 module boxes, explosion sizing, **3**(2), 51
Zircaloy-2 receptacle plates, fabrication, **2**(3), 50
Zircaloy-2 strip, tensile properties, **2**(3), 36
Zircaloy-2 tubing, fabrication, **1**(4), 39
hydrostatic destructive testing, **3**(2), 29–30
pressure testing, **3**(2), 29
Zircaloy-2 welds, backup contamination, **3**(2), 48
corrosion in H_2O, **2**(1), 50; **2**(4), 20
properties, **2**(4), 34–5
Zircaloy-2–Zircaloy-2 sheet, fretting corrosion in H_2O, **2**(3), 28
Zircaloy-2–zirconium alloy couples, diffusion, **2**(3), 17
Zircaloy-3, corrosion, **1**(1), 32
creep properties, **1**(2), 36; **1**(4), 27, 29
crystal properties, **1**(2), 35
heat-treatment effects, **1**(3), 38–9
mechanical properties, **1**(3), 38–9; **1**(4), 26
radiation effects, **2**(1), 41–2; **2**(3), 32–3; **2**(4), 26–8
strain-fatigue testing, **1**(2), 36
stress-rupture properties, **2**(3), 36
tensile properties, **1**(2), 35–6; **1**(4), 27, 30–1; **2**(3), 36
welding, **1**(1), 29; **2**(3), 53
Zircaloy-3 welds, corrosion resistance in H_2O, **2**(1), 50
Zircaloy-4, creep properties, **3**(3), 44–5
hydriding, **3**(2), 17; **3**(3), 37–8
mechanical properties, **3**(4), 42
Zircaloy-B, reactions with H_2O and steam, **1**(1), 35
Zirconium, arc cutting, **3**(2), 47
brazing, **1**(1), 29–30
compatibility with fissium-Pu-U alloys, **3**(4), 8–9
compatibility with UC, **3**(4), 13
corrosion, **1**(3), 33, 37; **1**(4), 21, 24–5; **3**(1), 34
cracking in hydridation, **2**(4), 15
creep properties, **3**(2), 29
crystal production, **2**(3), 34–5
deformation, **1**(4), 26; **2**(4), 20
density, **2**(2), 22
diffusion, **2**(2), 37–8; **2**(3), 17; **3**(2), 36
diffusion welding, **3**(4), 50
dimensional changes, **2**(2), 20
electron-beam welding, **3**(1), 53
forging, **2**(4), 41
hot hardness, **3**(2), 29
hydridation, **1**(4), 15, 21; **2**(1), 24; **2**(2), 22; **2**(4), 15; **3**(3), 37; **3**(4), 30
hydrogen, content adjustment, **2**(3), 23
diffusion, **1**(2), 23; **2**(4), 15–16; **3**(1), 24
distribution, **3**(2), 34
role in corrosion, **1**(4), 21
ignition, **1**(3), 20; **2**(3), 28; **2**(4), 20
lattice stability, **3**(2), 35
mechanical properties, **3**(3), 32
metallic coating, **1**(3), 53
nuclear properties, **3**(3), 32
oxidation, **1**(2), 31; **1**(3), 34; **2**(4), 20; **3**(2), 22; **3**(4), 34
pressure bonding with metals, **1**(1), 26–7; **2**(3), 50
properties, **3**(3), 46; **3**(4), 30
published data, **2**(3), 45
pyrophoricity, **1**(3), 20; **2**(3), 28

Zirconium (Continued)
radiation effects on, gaseous oxidation, 3(2), 27
impact strength, 3(1), 37
lattice, 1(1), 39; 3(1), 37
mechanical properties, 3(1), 39
radiographic testing, 1(1), 30
reaction with H_2O, 1(1), 35; 1(2), 30; 1(4), 25; 2(1), 33; 2(4), 24–5; 3(2), 8; 3(4), 35
recovery kinetics, 3(2), 35
scaling, 1(2), 31; 1(4), 21–2; 2(2), 27; 2(4), 20
separation from Hf, 3(4), 1
solubility in Y, 3(1), 42
stringers, 1(3), 33; 1(4), 35
technology, 1(3), 49
thermal-gradient effects, 3(2), 34
welding, 1(1), 29; 3(1), 53
Zirconium (cold-worked), hardness, recovery, and recrystallization, 2(3), 34
Zirconium (irradiated), damage recovery, 3(3), 41; 3(4), 41
fission-fragment recoil range, 3(2), 26
Zirconium (molten), reaction with H_2O, 1(1), 35; 3(2), 25
Zirconium alloy hydrides, dissociation pressures, 1(2), 23
mechanical properties, 2(4), 15
Zirconium alloy ingot, piercing, 3(1), 48
Zirconium alloys, annealing, 3(3), 51
corrosion, 2(1), 28; 3(3), 38, 45
deformation modes, 1(3), 38
fabrication, 3(1), 48
H_2 pickup, 3(3), 32–3
hardness, 2(1), 28
hydridation, 1(3), 33; 1(4), 21; 2(4), 15
mechanical properties, 3(1), 37–8, 43–5
oxidation, 1(2), 31; 1(3), 33–4; 3(2), 22; 3(4), 34
pickling, 2(1), 28
published data, 2(3), 45
radiation effects, 2(2), 33–4; 3(1), 37–8
rolling, 3(3), 51
scaling, 1(2), 31; 2(2), 27
strength, 3(3), 38, 45
stringer-formation prevention, 3(3), 51
Zirconium boride
See also Zirconium diboride
compatibility with stainless steel, 3(2), 19
corrosion resistance to Na, 2(1), 32
properties, 3(4), 34
radiation effects, 1(2), 26
solubility in H_2O, 1(3), 32
Zirconium boride–stainless steel dispersions, fabrication, 2(2), 26
Zirconium carbide, corrosion resistance, 2(1), 32
properties, 3(4), 34
vapor-deposited coating on graphite, 1(1), 28
Zirconium cladding, diffusion with Mo-U alloys, 2(2), 39
thickness determination, 3(2), 52
Zirconium diboride
See also Zirconium boride
chemical reactions, 3(4), 29
melting effects, 3(2), 41
oxidation, 3(4), 53
radiation-induced He release, 3(3), 35–6
thermal-shock resistance, 3(4), 53
vapor pressure, 3(4), 28–9
Zirconium diboride powder, coating with Nb, 3(2), 47
radiation effects, 2(4), 19
Zirconium diboride powder (irradiated), annealing effects, lattice constant changes, and line broadening, 2(4), 19
Zirconium dioxide, arc spraying, 3(2), 47
corrosion resistance, 2(1), 32
properties, 3(4), 34
protective effects against H_2, 2(3), 28
radiation effects, 2(4), 11; 3(2), 27; 3(3), 22; 3(4), 39
radiation-induced phase transformation, 3(3), 41
reaction with PuO_2, 3(4), 15
Zirconium dioxide (irradiated), phase changes, 3(4), 40
Zirconium dioxide film breakdown, 3(1), 32
Zirconium dispersions, radiation effects, 1(1), 15
Zirconium hydride
See also Hydrogen-zirconium system
cladding, 1(3), 26; 2(4), 15
compatibility with CO_2, 3(3), 33
crystal structure, 1(2), 23
electrical resistivity, 3(2), 15; 3(3), 32
fabrication, 2(4), 15
H_2 diffusion in, 1(2), 23; 3(2), 16; 3(3), 32–3
Hall coefficients, 3(2), 15; 3(3), 32
heat content, 1(3), 26
mechanical properties, 2(4), 15
moderator uses, 3(1), 24
preparation, 1(3), 26
pressure bonding with stainless-steel cladding, 1(3), 51
properties, 1(1), 21; 1(3), 26; 1(4), 15; 2(4), 15
reactions with N_2 and NaK, 1(3), 26
specific heat, 3(3), 32
structure, 1(4), 15
technology, 3(3), 32
tensile properties, 2(4), 15
thermal conductivity, 2(4), 15
thermal expansion, 1(3), 26
vapor deposition of Mo, 1(3), 53
Zirconium nitride, properties, 3(4), 34
Zirconium silicate, oxidation, 3(4), 53
radiation effects, 3(3), 22; 3(4), 20
thermal-shock resistance, 3(4), 53
Zirconium tubing, fabrication, 1(4), 39
ZW1, radiation effects, 3(1), 38–9

LEGAL NOTICE

This document was prepared under the sponsorship of the U. S. Atomic Energy Commission. Neither the United States, nor the Commission, nor any person acting on behalf of the Commission:

A. Makes any warranty or representation, expressed or implied, with respect to the accuracy, completeness, or usefulness of the information contained in this report, or that the use of any information, apparatus, method, or process disclosed in this report may not infringe privately owned rights; or

B. Assumes any liabilities with respect to the use of, or for damages resulting from the use of any information, apparatus, method, or process disclosed in this report.

As used in the above, "person acting on behalf of the Commission" includes any employee or contractor of the Commission, or employee of such contractor, to the extent that such employee or contractor of the Commission, or employee of such contractor prepares, disseminates, or provides access to, any information pursuant to his employment or contract with the Commission, or his employment with such contractor.

NUCLEAR SCIENCE ABSTRACTS

The U. S. Atomic Energy Commission, Office of Technical Information, publishes *Nuclear Science Abstracts (NSA)*, a semimonthly journal containing abstracts of the literature of nuclear science and engineering.

NSA covers (1) research reports of the U. S. Atomic Energy Commission and its contractors; (2) research reports of government agencies, universities, and industrial research organizations on a world-wide basis; and (3) translations, patents, books, and articles appearing in technical and scientific journals.

Complete indexes covering subject, author, source, and report number are included in each issue. These are cumulated quarterly, semiannually, and annually providing a detailed and convenient key to the literature.

Availability of *NSA*

SALE *NSA* is available on subscription from the Superintendent of Documents, U. S. Government Printing Office, Washington 25, D. C., at $18.00 per year for the semimonthly abstract issues and $15.00 per year for the four cumulated-index issues. Subscriptions are postpaid within the United States, Canada, Mexico, and all Central and South American countries, except Argentina, Brazil, British and French Guiana, Surinam, and British Honduras. Subscribers in these Central and South American countries, and in all other countries throughout the world, should remit $22.50 per year for subscriptions to semimonthly abstract issues and $17.50 per year for the four cumulated-index issues.

EXCHANGE *NSA* is also available on an exchange basis to universities, research institutions, industrial firms, and publishers of scientific information. Inquiries should be directed to the Office of Technical Information Extension, U. S. Atomic Energy Commission, P. O. Box 62, Oak Ridge, Tennessee.

TECHNICAL PROGRESS REVIEWS may be purchased from Superintendent of Documents, U. S. Government Printing Office, Washington 25, D. C. for $2.00 per year for each subscription or for $0.55 per issue. The use of the coupon below will facilitate the handling of your order.

POSTAGE AND REMITTANCE: Postpaid within the United States, Canada, Mexico, and all Central and South American countries except as hereinafter noted. Add $0.50 per year, or $0.15 per single issue, for postage to all other countries, including Argentina, Brazil, British and French Guiana, Surinam, and British Honduras. Payment should be by check, money order, or document coupons, and MUST accompany order. Remittances from foreign countries should be made by international money order, or draft on an American bank, payable to the Superintendent of Documents, or by UNESCO book coupons.

order form

SUPERINTENDENT OF DOCUMENTS
U. S. GOVERNMENT PRINTING OFFICE
WASHINGTON 25, D. C.

Enclosed:
document coupons ☐ check ☐ money order ☐

Charge to Superintendent of Documents No. _____

Please send a one-year subscription to

☐ REACTOR CORE MATERIALS
☐ POWER REACTOR TECHNOLOGY
☐ NUCLEAR SAFETY
☐ REACTOR FUEL PROCESSING

(Each subscription $2.00 a year; $0.55 per issue.)

SUPERINTENDENT OF DOCUMENTS
U. S. GOVERNMENT PRINTING OFFICE
WASHINGTON 25, D. C.

(Print clearly)

Name _____

Street _____

City _____ Zone ____ State _____